

CRANFIELD UNIVERSITY

SCHOOL OF MECHANICAL ENGINEERING

DEPARTMENT OF POWER ENGINEERING AND PROPULSION

I.M. SALAMA

HIGH TEMPERATURE PARTICLE-TO-METAL INTERACTION IN A SIMULATED GAS TURBINE ENVIRONMENT

Ph. D. Thesis

CRANFIELD UNIVERSITY

SCHOOL OF MECHANICAL ENGINEERING

DEPARTMENT OF POWER ENGINEERING AND PROPULSION

Ph. D. Thesis

Academic Year 2001/2002

I.M. SALAMA

HIGH TEMPERATURE PARTICLE-TO-METAL INTERACTION IN A SIMULATED GAS TURBINE ENVIRONMENT

Supervisors: Prof. R.L. Elder and Dr. S.C. Tan

May 2002

A thesis submitted in partial fulfillment
of the requirements for the degree of

Doctor of Philosophy

ABSTRACT

An experimental study of the particle-to-metal interaction during high temperatures and velocity impact conditions is presented. A novel continuous erosion testing facility have been used to study the effect of particle and metal target temperatures as well as impact particle velocity on the erosion/deposition behaviour of the stainless steel 321, Nimonic 75, and aluminium target materials. The study was carried out to provide database information on the behaviour of those metals under simulated gas turbine conditions. The erosive particles used were quartz sand with diameters ranging from 20-30 μm. The erosion characteristics of stainless steel 321 were recorded at target surface temperature of 285°C, 415°C, 570°C and 715°C. The tests were carried out at two different impingement angles of 30° and 60° and at particle impact velocities of up to 300m/s. The effects of particle temperatures of 550°C, 750°C and 950°C on erosion/deposition rates were examined. The Nimonic 75 target temperatures were slightly modified to give a similar surface to melting point ratio as the stainless steel. The Nimonic 75 was tested at 545°C, 685°C, 825°C and 965°C surface temperatures and at the same particle velocities and temperature used for the stainless steel tests. The Nimonic targets were only tested at one impact angle of 30°. The aluminium targets were only tested at an impact angle of 60° and particle impact velocity of 100 m/s. The surface temperature was modified to give a ratio up to 0.8 of the melting point temperature, where the particle temperature was set to be 350°C, 550°C and 750°C.

Abstract

It was found that particle and target temperatures, impact velocity and angle have a significant effect on the erosion/deposition characteristics. There is a threshold target and particle temperature for which deposition begins, and it depends on impact velocity and angle. The Nimonic 75 targets exhibit a better resistance to particle deposition over the stainless steel 321 at high impact velocity and temperatures. Simple models of the erosion/deposition were established to describe the conditions of particle deposition on the stainless steel and Nimonic targets. The aluminium targets show an increase in the erosion rate as target temperature reaches certain level, which then drops as target temperature continues to increase beyond this point.

ACKNOWLEDGEMENTS

First, I must tank Allah for his blessing and bounties.

I am indebted to my supervisor, Prof. Robin Elder and Dr. S. C. Tan for their invaluable and patient guidance and support during the course of my research. This thesis would never see the light without their encouragement.

My thanks for Mr. R. Luttly for his technical support and bright ideas in building and running the test rig.

Also I would like to thank my wife for here continues support and encouragement during the research time.

TABLE OF CONTENT

ABSTRACT I

ACKNOWLEDGEMENTS III

TABLE OF CONTENT IV

CHAPTER 1 1

INTRODUCTION AND BACKGROUND 1
1.1 OVERVIEW 1
1.2 SCOPE OF THESIS 2
1.3 GAS TURBINE SOLID PARTICLE INGESTION DAMAGE 3
1.4 EROSION OF TURBOMACHINERY 4
1.5 ALLEVIATING ENGINE COMPONENT EROSION 5
1.6 LIST OF FIGURES FOR CHAPTER 1 10

2 CHAPTER 2 12

LITERATURE REVIEW 12
2.1 EROSION OF METALS 12
2.1.1 INTRODUCTION 12
2.1.2 EROSION PARAMETERS 13
2.2 MATERIAL REMOVAL MECHANISMS 17
2.3 PARTICLE DEPOSITION 18
2.3.1 INTRODUCTION: 18
2.3.2 DEPOSITION MECHANISMS: 20
2.3.3 FACTORS AFFECTING DEPOSITION 25
2.4 EROSION EXPERIMENTAL TECHNIQUES 28
2.5 CURRENT WORK 31
LIST OF FIGURES FOR CHAPTER 2 33

3 CHAPTER 3 40

EXPERIMENTAL INVESTIGATION OF EROSION 40
3.1 INTRODUCTION 40
3.2 EXPERIMENTAL TEST RIG 42
3.2.1 ACCELERATION AND HEATING TUBE 43
3.2.2 PARTICLE FEEDER 46
3.2.3 TARGET HOLDER AND HEATER: 46

Table of Contents

3.2.4 SAMPLE SHAPE.....47
3.3 TEST MATERIALS:.....47
3.3.1 EROSIVE PARTICLES:.....47
3.3.2 TARGET MATERIAL:.....48
3.3.3 CALIBRATION.....49
3.4 TEST PROCEDURES.....51
3.5 TEST PROGRAM AND TEST MATRIX.....52
3.6 SUMMARY.....53
LIST OF FIGURES FOR CHAPTER 3.....59
CFD RESULTS FOR 1400K TUBE WALL TEMPERATURE. 63

4 CHAPTER 4.....69

RESULTS AND DISCUSSIONS.....69
4.1 INTRODUCTION.....69
4.2 FINDINGS FOR STAINLESS STEEL 321.....73
4.2.1 SUMMARY.....73
4.2.2 TARGET HT RATIO (TEMPERATURE) EFFECT ON THE EROSION RATE.....76
4.2.3 PARTICLE TEMPERATURE EFFECT ON THE EROSION RATE.....78
4.2.4 PARTICLE VELOCITY EFFECT ON THE EROSION RATE.....80
4.2.5 COMPARISON BETWEEN THE EFFECT OF TARGET AND PARTICLE TEMPERATURE ON THE EROSION BEHAVIOUR.....82
4.2.6 TARGET SURFACE EXAMINATION.....84
4.2.7 EROSION MODEL.....87
4.2.8 CONCLUDING REMARKS.....88
4.3 FINDINGS FOR NIMONIC 75.....89
4.3.1 SUMMARY.....89
4.3.2 TARGET HT RATIO (TEMPERATURE) EFFECT ON THE EROSION RATE.....90
4.3.3 PARTICLE TEMPERATURE EFFECT ON EROSION RATE.....91
4.3.4 PARTICLE VELOCITY EFFECT ON EROSION RATE.....92
4.3.5 COMPARISON BETWEEN THE EFFECT OF TARGET AND PARTICLE TEMPERATURE ON THE EROSION RATE.....94
4.3.6 SURFACE EXAMINATION USING SEM.....96
4.3.7 EROSION MODEL.....97
4.3.8 CONCLUDING REMARKS.....98
4.4 COMPARISON BETWEEN THE EROSION BEHAVIOUR OF STAINLESS STEEL 321 AND NIMONIC 75 AT 30°.....99
4.4.1 INTRODUCTION.....99
4.4.2 RESULTS AND DISCUSSIONS.....99
4.4.3 CONCLUDING REMARKS.....102
4.5 FINDINGS FOR ALUMINIUM.....103
4.5.1 INTRODUCTION.....103
4.5.2 RESULTS AND DISCUSSIONS.....103
4.5.3 SURFACE EXAMINATION USING SEM.....105
4.5.4 CONCLUDING REMARKS.....107

List of Figures for Stainless Steel 321. 109
List of Figures for Nimonic 75 131
List of Figures for the Comparison between the Stainless Steel 321 and Nimonic 75 at 30° Impact Angle 145
List of figures for Surface Examination Results For Aluminium at 30° Impact Angle. 151

5 CHAPTER 5 156

REVIEW, CONCLUSIONS, AND RECOMMENDATIONS FOR FUTURE WORK 156
5.1 REVIEW 156
5.2 CONCLUSIONS 158
5.3 RECOMMENDATIONS FOR FUTURE WORK 163
5.3.1 FEASIBLE IMPROVEMENTS TO THE TEST FACILITIES. 163
5.3.2 EXPANDING THE TEST CONDITIONS 163
REFERENCES 165

1 APPENDIX 1 171

1.1 LASER TWO-SPOT ANEMOMETER (L2F) 171

2 APPENDIX 2 175

2.1 CFD SIMULATION RESULTS OF PARTICLE AND GAS TEMPERATURE AND VELOCITY 175
2.1.1 CFD RESULTS FOR 550°C GAS TEMPERATURE. 178
2.1.2 CFD RESULTS FOR 750°C GAS TEMPERATURE 182
2.1.3 CFD RESULTS FOR 950°C GAS TEMPERATURE. 186

3 APPENDIX 3 190

1.1 MECHANICAL PROPERTIES OF STAINLESS STEEL 190

CHAPTER 1

INTRODUCTION AND BACKGROUND

1.1 Overview

The operation of gas turbine engines in an environment laden with particles, such as helicopters operating close to ground and aircraft flying in dust storms or over volcanic mountains, are always accompanied with potentially hazardous problems such as erosion, corrosion and particle deposition. There are two main sources of particles in the gas turbine engine, viz.

- Dust found in the main gas stream. This is due to external effects such as sand storms, volcanic clouds and sand vortices during landing and taking off.
- Particles located within the engine itself that could be products of wear and/or combustion products.

This thesis focused on category 1 (ingested particles) although much of study has reduced to the second category.

These ingested particles can cause severe damages to the engine which can take the form of one or a combination of erosion, corrosion or deposition on the engine depending on the particle composition, component position and engine operating condition, [1]. For example the erosion is most likely to effect the fan and compressor blades, while the corrosion is usually limited to the hot part of the engine, i.e. turbine blades. There is a link between these damages; for example, the deposition of particles

with highly sulphur and/or chloride content will increase the tendency of corrosion.

Particles, which have been ingested into the engine, can progress throughout the whole engine stages. As particles enter the compressor stages, the erosion damage to the first stage reflects an even distribution of particles whereas later blades are subjected to particle bunching caused by upstream blade rows. In compressors, there is generally an overall reduction in blade chord caused by material removal from the pressure side of the leading edge and thinning of the trailing edge. Particles are centrifuged out towards the blade tips in the rotors of the compressor causing a severe damage to those areas. The compressor also causes fragmentation of the particles reducing the after average size significantly.

As the particles enter the combustion chamber, their temperature are raised to the local temperature and carried out in the hot gas stream into the turbine blades. At this stage they impinged and can solidify on turbine blade surfaces, which are relatively cool, [1]. Sand deposition can cause engine shutdown due to particle blocking the turbine cooling holes thus causing localised overheating or melting. On the other hand, if the particle has enough energy they may rebound and erode some of the material. For example, small particles, which deposit on the surface of turbine blade can disturb the local flow field characteristics and affect the local heat transfer rate causing local overheating [2].

1.2 Scope of Thesis

Chapter 1 gives a general background on the damage caused by the ingested particles in gas turbine engines and

highlights the problem of erosion in turbomachinery and details some methods used to minimise the effect. Chapter 2 reviews the published literature in the field of erosion and deposition in gas turbine and discusses research work carried out in the field. A comparison between different erosion testing techniques is also highlighted in the chapter. Chapter 3 details the erosion/deposition test rig and describes test procedures and calibrations. Chapter 4 discusses the erosion/deposition results for the tested materials, i.e. stainless steel 321, Nimonic 75 and aluminium. The chapter also represents the comparison between the erosion behaviour and characteristics of the stainless steel 321 and Nimonic 75. Chapter 5 was assigned for the review and conclusions, which also includes recommendation and future work suggestions.

1.3 Gas Turbine Solid Particle Ingestion Damage

Gas turbine most often operates in environments laden with particles. Typical situations are;

- Helicopters operating close to the ground.
- Aircraft flying in dust storms.
- Turbine powered vehicles and auxiliary power units operating in dusty or desert regions.

Under these operating conditions, the most common particles ingested are sand and dust. These particulates can cause engine damage in several ways;

- Erosion of compressor and turbine blades
- Glassification (deposition) on hot section components.
- Blockage of cooling channels.
- Contamination of lubrication and air supply systems.

Erosion is the biggest cause of engine deterioration in non-marine environment, whereas corrosion in the largest problem in the marine environment.

Erosion is a phenomenon defined as the wear process that occurs when solid particles or liquid droplets impact against a target at speed. Particles ingested into the engine erode the compressor and turbine components by impacting with them which can significantly change the shape of the aerofoil sections and their performance including:

- Reducing pumping and suction efficiency as well as power output,
- Increasing specific fuel consumption,
- Reducing stall margin (and compressor surge), which sequentially degrades the operational safety.

The problem is particularly acute in helicopter gas turbines for the following reasons;

- Helicopters usually operate close to ground; the rotor downdraft can lift huge quantities of loose material (including sand dust) into the engine, especially on desert environments. Sand particles as large as 200 μm are raised sufficiently far off the ground to be ingested by helicopters engines, [3,4].

1.4 Erosion of Turbomachinery

Erosion changes the aerodynamic characteristics of the stationary and rotating blades by preferentially removing material, figure 1-1, which can change the blade geometry by blunting the leading edge, thinning the trailing edge, and/or increasing the surface roughness. These changes to the profile and surface finish increase the total

pressure loss across the blade row, degrading stage efficiency.

The motion and distribution of particulates within the compressor cascade changes as particles progress through the cascade. Particles ingested at a gas turbine inlet tend to be evenly distributed as evident by the uniform erosion pattern along almost the entire blade length in the first stage of the compressor cascade. There is an overall reduction in blade chord caused by material removal from the pressure side of the leading edge and thinning of trailing edge. Particles are also centrifuged out towards the blade tip and shroud and continued till the last stages of the cascade causing an increase in the tip clearance, thus degrade aerodynamic performance [5]. As particles leave the compressor section, their sizes are usually reduced to a fine dust and passes to the combustor where they tend to melt in the hot gas stream. In the molten stage, they impinge and condense or solidify on blade surface of the turbine. Some particles are transported in the cooling air stream as bleed air for the turbine blades.

1.5 Alleviating Engine Component Erosion

The level of particulate in country, coastal and industrial areas is usually 0.01 to 0.1 ppm (part per million). In desert regions, particle concentrations tend to be much higher; 0.1 to 700 ppm [6]. A gas turbine requires an air flow of half a ton of air per hour for every horsepower it outputs; if particles are present at only 1 ppm, an 11,000-hp engine will ingest 1/2 kg of solids every hour. Furthermore dust storms are capable of

lifting sand to several thousand feet of altitude which can potentially cause damage at altitude.
There are two ways that engine components can be protected from erosion damage:

- Prevention

  To date there is no practical means for totally preventing the ingestion of particles into a gas turbine. Some reduction in particle ingestion can be achieved by careful location of the intake ducts, but relocating engine position would not reduce particle intake in conditions such a sandstorm.
  Many air-cleaning systems have been tried, [7], especially on helicopters, including barrier filters, vortex tube panels and inertial particle separators (IPS). Barrier filters required a high level of maintenance due to the need to clean the filter in order to prevent pressure losses. Furthermore, engine vibration tends to dislodge particles from the filters, which can then be ingested into the engine. The vortex tube provides high separation efficiency but requires a large intake area and has a large installed volume. Inertial particle separators are regarded as the most effective air cleaning systems, being both compact and effective. Several IPS techniques, figure 1-2, have been used; these include centrifugally swirling particles outward, rebounding particles off specially contoured internal surfaces and contouring the airflow so the particle's linear momentum can be utilised to improve separation. An experimental high efficiency separator design for the General Electric T700 was able to remove 85% of the sand for less than a 1% total pressure loss, [8].

Nevertheless 15% of the sand passed into the engine which still can cause considerable damage to the engine components.

- Increase Resistance to Particle Impact

If the component of the turbine engine were able to withstand particle impacts without damage, particle ingestion would be of only minor consequence, as there would be only a temporary loss of performance due to ingestion, [9].

Several technologies have been used to increase component erosion resistance, and these include:

i. Ceramic components, [10],
ii. Erosion resistant inserts for most heavily eroded regions of the compressor, [11],
iii. Coatings, [11-13].

Ceramic materials have the future to replace the usage of the conventional metal alloys currently used in the gas turbine engines such as compressor and turbine blades. Ceramic materials are more resistant to erosion than titanium, steel or nickel alloys. In addition, ceramic materials are generally lighter than metal alloys which can reduce engine's weight, hence specific fuel consumption (SFC), but more importantly, tensile loading on the rotor blades. Furthermore, ceramic can withstand a higher gas temperature than other alloys, which can allow a higher turbine inlet temperature (TIT) that can increase the engine thermal efficiency. However the current lack of reliability from ceramic components,

and their manufacturing difficulties limits their use at this stage of gas turbine life, [10].

Erosion resistant inserts have been used in blades susceptible to erosion but with only limited success. It is an expensive solution in terms of manufacture and quality control.

Coatings provide protection for the substrate which may be protection from corrosion, erosion, or excessive heat. The brief discussion here relates to the protection from erosion. There are, in general, two types of coatings; overlay and diffusion. In overlay coatings material is deposited onto a substrate surface to form a distinctly separate layer. Diffusion coatings are formed when extrinsic species enter a substrate surface to shallow depth modifying materials properties. Coatings can be produced from the gaseous, liquid or solid phase. Figure 1-3 shows the erosion response of WC substrate material compared to three different types of coating at an impact angle of 90° and temperature of 260°C at different impact velocities. The figure shows that the coated samples exhibit better erosion resistance than the than the pure metal. The figure, also, shows the variation of the erosion response of different types of coating.

In its simplest form, the erosion resistance of a coating is created when a sufficiently hard and continuous layer defeats the impacting erodent particles by causing them to shutter or slide across

the target surface without indention or scratching [14].

List of Figures for Chapter 1

Figure 1-1. Typical sites for erosive material removed on turbine blades. [5]

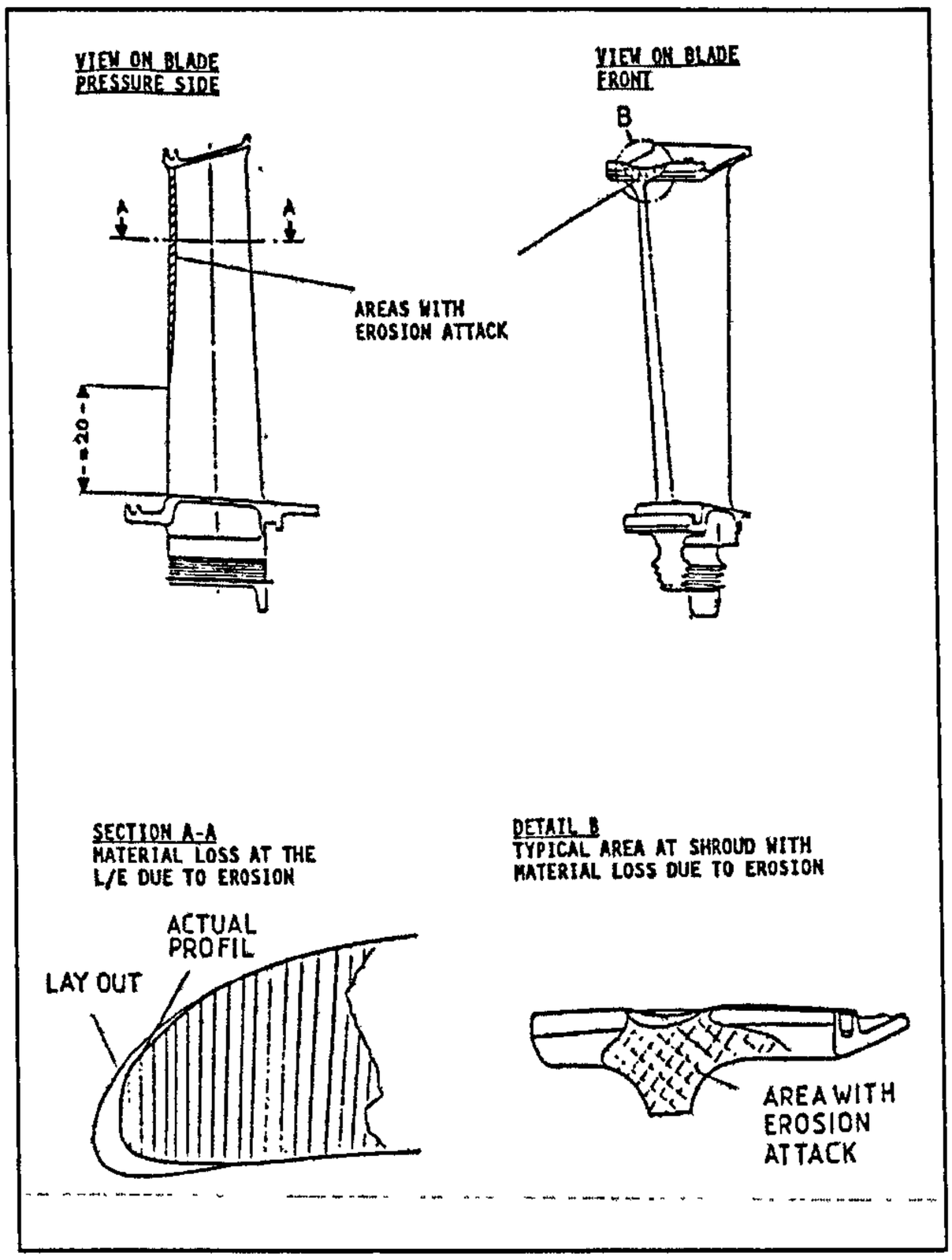


Figure 1-2. An inertial Particle Separate (ISP). [8]

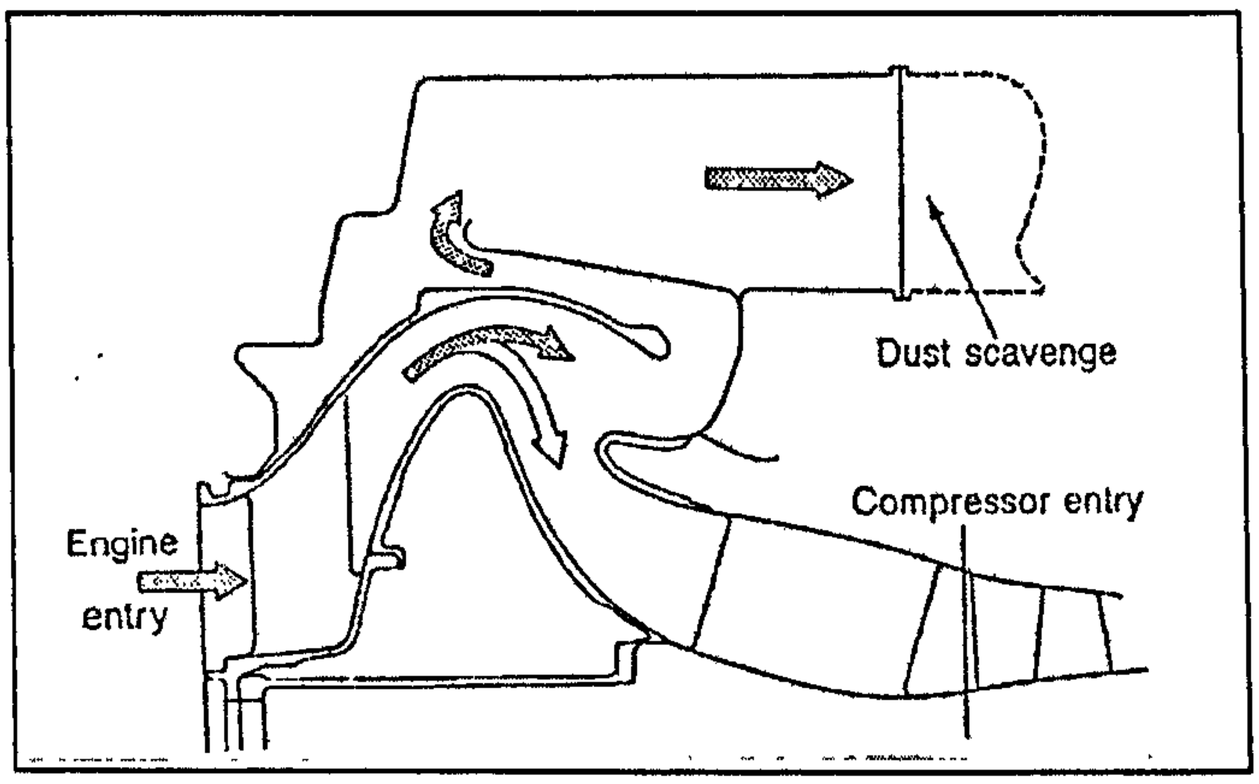
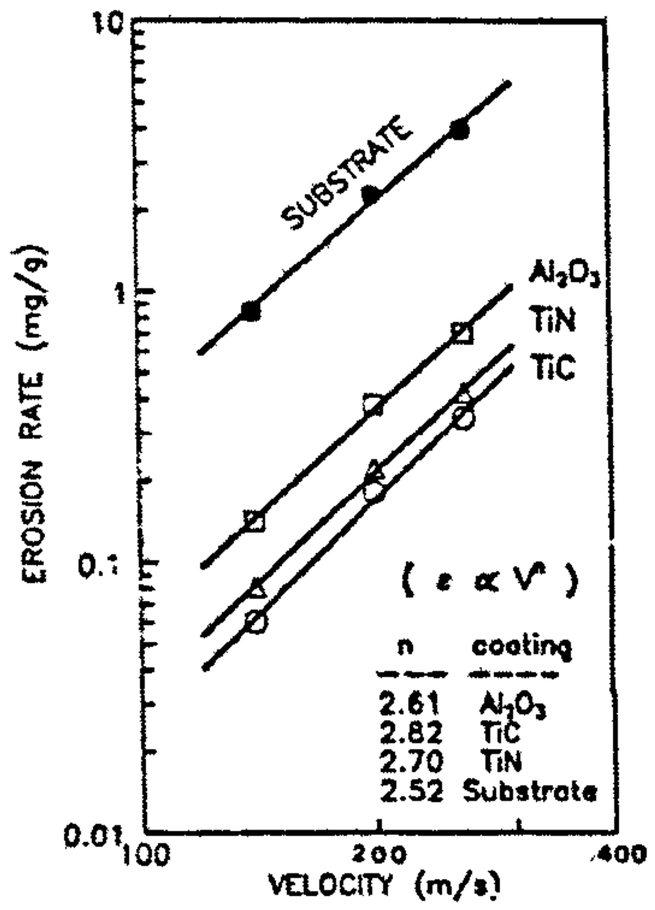


Figure 1-3. Comparison between the erosion behaviour of the pure and coated metal. [14]



CHAPTER 2

LITERATURE REVIEW

2.1 Erosion of Metals

2.1.1 Introduction

Erosion is the term used to describe the process of the material loss or removal as a result of particle impact on the original material surface.

In general the amount of erosion can be quantified as the erosion rate; the ratio of amount of material removed for a known mass of erodent. The amount of material removed can be expressed in terms of mass (g/mg) or volume (mm^3/mg). This second form is more applicable to changes in blade shape, which was first introduced by Tilly and Sage [15] and some other workers. In general, erosion characteristics can be categorised into two distinct types; ductile and brittle, [16]. Most metals, alloys and resilient plastics show a ductile behaviour. Ceramics and glasses on the other hand generally exhibit a brittle response. The mechanisms by which ductile and brittle materials erode are quite different. In general, ductile materials show a maximum erosion response at shallow angles between 15°-25°, while brittle materials show that occur at about 90°. In ductile erosion the removal mechanisms are known as ploughing, cutting type I and cutting type II, figure 2-1. On the other hand brittle erosion involves the loss of target material through the propagation of cracks, figure 2-2. However, the

discussion will be restricted to the ductile behaviour throughout this chapter.

There are several factors and parameters such as particle velocity and size, impingement angle, particle and target temperature, and target properties, which affecting erosion behaviour. The effects of these parameters are not entirely independent of each other. For example, there is a strong link between particle size and velocity effect on erosion rate. Numerous studies on the effect of these parameters on material erosion has been carried out due to their importance to the field of gas turbine engine industries [17] A general discussion of the effect of each of the above mentioned parameters follows.

2.1.2 Erosion Parameters

Particle size is one of the most important parameters effects erosion characteristics which had been the first to be considered by many workers. Sage and Tilly [15,18] made early attempts to quantify the erosion effects in turbine engines. They examined the effect of different parameters on erosion rate, including particle size. They found that the erosion rate for a given particle velocity increased with increasing particle diameter up to onset of saturation plateau, beyond which no further increase in erosion rate occurred. They also reported that erosion was negligibly small for particles below 5μm in diameter. Goodwin et al. [4], Yarranaveddy and Bahadur [19] have reported the similar 'particle size effect' on erosion rate of ductile materials, where erosion rate initially increases with increasing particle size until a critical size is reached when the erosion rate becomes size independent, figure 2-3.

The critical size at which saturation erosion rates are reached varies with impact velocity. Several explanations for this behaviour have been made. Goodwin et al. suggested that particle fragmentation increases with particle size initially, which then remains constant with the onset of saturation erosion [4]. They found there is also a particle size below which a target was undamaged by impact. They reported that particle size less than 5μm produces no discernible erosion to steel at velocity up to 300m/s. Tilly reported that this threshold size is dependent upon velocity [20]. Actual engine testing carried out by Montgomery and Clark [21] also seems to support these findings. Hutchings claimed that the particle size effect is due to changes in target yield strength as a result of change in strain rate with particle size [22]. Tan et al. [23] concluded that as particle impact velocity and size increase, the amount of fragmented dust also increases. For larger particles, fragmentation occurs at the lower end of the dust size spectrum whereas for smaller particles, it is across the whole size bandwidth.

Particle velocity was also found to be an important parameter affecting erosion rate. Several workers have presented a relation between erosion rate and particle velocity using the power law form [4, 24, 25]

$$\varepsilon = Const.V^n \qquad (2\text{-}1)$$

where ε is the erosion rate, V is the particle impact velocity, and n is the velocity exponent. They found that for ductile materials the velocity exponent n generally

has a value between 2.0 and 2.5. Goodwin et al. [4] found that velocity exponent was dependant upon particle size; the exponent *n* tends toward 2.0 with decreasing size. They also reported that when test conditions are totally identical a range of materials would often have the same velocity exponent. Scattergood and Routbort [26] also found similar findings. Tabakoff et al. [27] reported a dependency of *n* on the impact angle during erosion tests with coated materials. Ives and Ruff [28] however, also, reported the velocity exponent for copper to be dependant on impact angle rather than particle size.

The effect of temperature on erosion rate is of twofold, both particle and target material temperatures influence the erosion rate. Stephenson et al. [29], found that at certain atmospheres and high temperature, oxidation of the surface can modify the rate of erosion. For example, if the oxide scales are thin and at sufficiently high temperature, the strains produced by particle impingement can be accommodated by plastic deformation and under these conditions scale remains protective. Yee et al. [30] investigated the effect of surface temperature on erosion rate of HE30 aluminium and BG303 stainless steel targets using 42-66μm fly ash particles. They reported that the erosion rate initially increases to its maximum at HT ratio of 0.4, (HT refers to the ratio of surface temperature to the melting point temperature), for aluminium targets. Then it decreases as the target temperature is increased further. This characteristic behaviour, however, varies from material to material depending on its properties and composition. They also concluded that the reduction in erosion rate at higher temperatures indicates a change in the erosion mechanism

(at the higher temperature). Hockey et al. [31] reported an increased in plastic flow with temperature in erosion tests on glass, silicon nitride, and aluminium oxide. Tabakoff et al. [27] have reported an increased in erosion rate of the 304 stainless steel targets with temperature at different particle impact velocities and impingement angles when they examined the effect of target temperature of 304 stainless steel using fly ash of 38.4μm diameter. In general, ductile materials show an increase in erosion rate with temperature, [27,32,33,34].

The effect of impact angle on erosion behaviour was studied by many researchers, Tabakoff [27], Finnie [24], Hutchings [22]. It was concluded that ductile materials exhibit maximum erosion at an angle of about 15°-30°, while brittle material exhibits a maximum erosion loss near normal incidence [24,35,36]. Although this is true in majority of cases, the exact angular response of both ductile and brittle materials is dependent on other parameters as well. For example, in some cases of ductile materials, when particle roundness increases, the angle of maximum erosion tends to be steeper [16,37,38]. On the other hand, particle size was found to have an effect on the angle where maximum erosion of brittle materials occurs [39], as small particles of 9μm caused a ductile response for brittle materials like glass and magnesia, figure 2-4.

Material, ductile and brittle, properties have been reported as influencing erosion response. This includes mechanical properties such as material hardness, thermal properties such as heat treatment of material,

microstructure and even chemical properties. Finnie et al. [25] found a relationship of the form $1/\varepsilon \propto H_v^{0.66}$, where ε is the erosion rate and H_v is the Vickers hardness, between hardness and erosion resistance for pure metals. He has examined number of different pure metals, which vary in their hardness such as lead, aluminium, iron, and many others, figure 2-5. Oka et al. [40] took the idea of representative hardness further and found excellent correlation, figure 2-6, between erosion rate and surface hardness for all ductile materials. They examined a number of alloys having different hardness values at 30° and 90° using silicon quartz particle of 215μm at impact velocity of 100 m/s, and concluded that erosion rate increase linearly with material hardness value. Tilly [41] proposed a relationship between erosion rate and material hardness which takes the form of $\varepsilon = K.H^{2.3}$, where H is the material hardness and K is a constant. Zhu and Moa [42] claimed that the relative hardness of erodent and target material have a profound effect on erosion response, where the angle where the maximum erosion response occurs is being a fraction of relative hardness.

2.2 Material Removal Mechanisms

The erosion damage morphology, and the mechanisms behind its formation, has yet to be fully understood. [41,43,44,45,46].

Hutchings et al. [17,47], however, established that three types of erosion damage could be produced during oblique impact. These are known as ploughing, cutting type I and cutting type II as shown in figure 2-1. During ploughing,

which causes most of the impact damage; target material is displaced by plastic deformation at the exit of the contact. The fraction of the displaced material that forms the lip is dependent upon impact velocity. Cutting types I and II are both produced by angular particles, with an impacting edge dividing the target material during contact. Soderberg et al. [48] found this to be true at all impact angles with a wide range of ductile materials, figure 2-7.

2.3 Particle Deposition

2.3.1 Introduction:

Fouling and particulate deposition is a term commonly used for the formation of undesirable deposition on surfaces. There are many engineering, technological and environmental situations where the deposition of particulate and aerosol particles on surfaces is of prime importance in solid-vapour-gas mixture. Deposit can be, generally, classified into many groups, [50], but the one of particular interest to the present study is the particlulate deposition; which is defined as the accumulation of finely suspended solids on the target surface (e.g. as in the gas turbine blades, heat exchanger, etc.). The interaction between various types of deposition is poorly understood and for the purposes of the present work the discussion is primarily restricted to particulate that are deposited on exchange surfaces at finite temperature difference between the surface and the main flowing stream.

Particles from a high temperature gas-particle flow into an adjacent cooled surface is of great interest to various engineering applications such as the fabrication of optical wave guide and semiconductor devices, corrosion/deposition/erosion of turbine blades or heat transfer surfaces [51-54]. For example, small particles deposited on the wall of turbine blades can disturb the flow field characteristics and affects the local heat transfer rate. For an air-cooled blade, particle deposition can block cooling holes or pores in the surface of the turbine blade, [51]. This reduces the airfoil permeability resulting in a reduced coolant flow to the surface with an increase in blade metal temperature, which can lead to oxidation, corrosion and strength limitation. Particle deposition, particularly due to unusually high particle loading, can reduce the aerodynamic passage resulting in a reduced power output and possibly causes compressor surge. Gas turbine manufacturers generally stipulate a limit of 5% to 10% reduction in power, at which point cleaning of the blading is required, [51].

The understanding of the physical effects that occur in the process of particle deposition from non-isothermal flow is, therefore, of major importance. The deposition process has to be fully understood, and although experimentation has made a significant progress, the predictive capability, however, has not been able to accurately simulate deposition rate with any degree of confidence. Particle deposition in gas turbines depends on the particle migration to the blade surface and the most known mechanisms of deposition include inertial impaction, thermophoresis, diffusion (both Brownian and Eddy), and electrophoresis. One or more mechanisms may

dominate the deposition process depending on particle size and flow field characteristics. For example, suspended particles can migrate in a flow with large temperature gradient, by the action of thermophoresis, or in combination with other mechanisms such as Brownian diffusion and inertial effects, [52,53]. Many different mechanisms have been proposed to explain how particles in the main gas stream deposit onto a surface. Richards et al. [55] have reported that three main mechanisms are involved in deposition process, figure 2-8:

- Particle/surface molten phase adhesion, where particles will stick to the surface if the adhesion force is sufficiently strong to overcome the energy remaining from impact, which would otherwise allow the particle to rebound. For this to occur the deposit surface must be cooler than the particles as in the case of the gas turbine blades, figure 2-8a.
- Deposit erosion, where particles may have sufficient energy to rebound and, in addition, erode some of the existing deposit, figure 2-8b.
- Deposit spallation, as particles may adhere to the deposit surface, due to their molten phase and the relative coldness of the surface, but the deposit strength is so low that part of the deposit may occasionally spall off the surface because of the aerodynamic forces, vibration or abrasive injection cleaning, figure 2-8c.

2.3.2 Deposition Mechanisms:

The detailed study of the deposition mechanisms is beyond the scope of this project, hence only, a brief discussion of the most important mechanisms, related to gas turbine

engine, will be presented here. The phenomenon of deposition relies upon complex and possibly multiple mechanisms, these mechanisms surface are summarised on table 2-1, [56].

Table 2-1. Mechanisms for deposition phenomenon.

Particles migration	Particles on Blade Surface
Direct impingement (Inertia)	Physical/Mechanical
Thermophoresis	Physical/Chemical
Electrophoresis	Electrical
Diffusionphoresis	Physical/Mechanical

The main and most important deposition mechanisms are discussed briefly as follows:

- Direct impingement (or inertial impaction), the mechanisms where large particles deviate from the gas streamline due to their high inertia, [50,52,53], figure 2-9. This mechanism is believed to be the most important one in bringing particle into the blade surface. The sensitivity of deposition rate by inertial impaction to the system parameters such as the flow velocity, particle mass loading, rebound velocity, mean particle size, target diameter, impact angle have been discussed in details and given in references, [57-65].

To the author's knowledge, there is a very little research on particle inertial impaction relevant to the gas turbine engine environment, [3,4,19]. Most of the available literatures are based on the

investigation of the phenomena related to the impaction of aerosol particles on spherical targets and air filters. Smith [66], reported that, for typical gas turbine conditions, particles diameter of 10μm or greater will reach the blade leading edge, by impact and the pressure side by centrifuging. He also concluded that the major deposition and fouling threats is posed by inertial impaction due to the associated high deposition velocities, and the particles reach is expected to have mass mean diameter greater than 5μm, due to size reduction as they pass through the compressor stages. The accumulative particle size distribution found on the HP turbine blade cooling system of the Tornado fighters, operating in Dhahran, Saudi Arabia, during the 1991 Gulf War, was found to contain about 30% less than 4μm, and 90% less than 20μm, [67].

In general, the main mechanism affecting particle deposition due to inertial impaction is the particle velocity [66], which is size dependence. Particles smaller than certain sizes will not be able to reach the surface and deposit due to their inertia. This size is experimentally determined, but generally it could be around 1-5 μm, depending on particle characteristics and flow field, [68].

- Thermophoresis is the phenomenon where particles suspended in a gas stream are subjected to a temperature gradient, migrate from the hot zone (gas) to the relatively cold zones (eg. blade surface), [69-71]. This movement is believed to be

due to a differential molecular bombardment gives rise to radiomatic forces. Particles sizes large as 5μm (radii) are affected by this phenomenon. The thermophoretic force is caused by the difference in heat absorption and subsequent re-radiation on the hot and cold sides of the particle. This according to Newton's third law would result in the particles moving away from the heat source. He also developed the governing equation of thermophoresis velocity, which is given by

$$V_t = -K\frac{\nu}{T}\frac{dT}{dX} \qquad (2\text{-}2)$$

The thermophoresis velocity V_t, depends on gas properties, the kinematic viscosity ν, and the temperature T. The temperature gradient ΔT far from the particle, and the thermophoretic coefficient K, are both important parameters. The coefficient K, depends on particle size (d_p), ratio of the thermal conductivity of the gas (k_g) and particle (k_p), and upon the Knudsen number.

Montassir [69] has concluded that as particle diameter increases the thermophoresis velocity decreases, and the commutative efficiency for sub-micron particles (<1μm) is much higher than that for the larger particles (≥1μm), i.e smaller particles are more likely to deposit by the mean of temperature gradient mechanism (thermophorasis effect). Also he concluded that as the ratio of wall temperature to the gas temperature rise, ΔT, the number of deposited small particles decreases

rapidly which indicates that the thermophoresis is the dominant mechanism of small particle deposition and it depends, also, on the temperature gradient. For more detailed theoretical analysis of the thermophoresis effects the reader is referred to Goren [70], and Pratsinis and Kim [54].

- Diffusionphoresis: Sub-micron particles suspended in a non-uniform but isothermal conditions of particle and gas mixture move due to concentration gradients. The botanist Robert Brown first observed this motion in 1827 who noticed pollen grains, when suspended in water, exhibited a continual and haphazard motion in all directions. This erratic motion, now called Brownian movement, has been observed with suspended particles of all kinds and is quite independent of the medium in which they are suspended, whether liquid or gaseous. The effect of this movement on particles of less than about 0.5μm diameter will cause them to deviate from the streamlines, particularly if the airstream velocity is low, and may cause them to be deposited on the catchment surface from the velocity boundary layer. Deposition by particle diffusion is directly proportional to diffusivity, which in turn inversely proportional to particle size. Thus, the smaller the particles in the gas stream, the more important particle diffusion becomes as a mean of deposition.

- Electrophoresis: Charged aerosol particles suspended in Particle-gas mixture migrate due to the electric field and charge on the particles. The significant

of electrophoresis was studied by Raj [17]. The charge of particles, in general, can be due to one or more of the following reasons:

- Injecting a mixture of contaminants and fuel through a burner nozzle and subsequent combustion.
- Ionic exchange between solid contaminants and the gas.
- Particle friction with solid boundaries such as turbine casing.
- Relative motion between the dry gas and solid particles.

The significant of electrophoresis is thought to be the retainment of particles to the blade surface.

2.3.3 Factors Affecting Deposition

The severity of deposition can be quantified as the sticking coefficient (capture fraction), which is defined as the mass fraction of incident particles that are retained on that surface expressed as (mg/g). This coefficient is affected by different factors such as particle impact velocity. Since the kinetic energy gained by the accelerated particle is a direct function of the particle velocity ($k=mv^2$), the energy that remains after the impact will determine whether or not the particle adherence will take place. If the particle kinetic energy is high enough to overcome the adhesive force the particle will rebound, otherwise the particle will adhere to the surface (provide that the threshold deposition temperature is exceeded). Anderson et al. [72] have showed an interesting dependence of sticking coefficient on the velocity. They reported that at low velocities, the sticking coefficient decreases with impact velocity

until it reaches a minimum at about 50 m/s, and then increases as the velocity is increased.

Duration of particles exposed to the hot target material is another significant factor affecting both the deposition amount and the adhesion strength of the deposited particles. Kim et al. [74] have reported that the capture ratio increases with time, implying that the target surface becomes a better captor of material as the deposit on the surface increase, which could be due to the increased roughness of the target surface.

Surface temperature, onto which the particles impact, must be above a certain threshold temperature for the deposition to occur, varies depending on the type of particles, [74]. Ahluwalia et al. [56] in the study of the effect of gas temperature on the deposition rate of combustion products on turbine blades, have shown that ash deposition rate increases by a factor of 2.5 as the surface temperature increases from 900°C to 1050°C at gas temperature of 1050°C. They proposed a relationship that gives particle temperature as a function of turbine residence time τ and particulate thermal relaxation time τ_t. Particle temperature can be written as:

$$T_p = \exp(-\tau/\tau_t)\left(T_{in} + \int_0^{\tau/\tau_t} T\exp(t)dt\right) \qquad (2\text{-}3)$$

where

$$\tau_t = 1/12(k_p/k_g)(d_p^2/\alpha_p) \qquad (2\text{-}4)$$

The above equation states that the relaxation time of particle temperature from the inlet temperature T_{in} to the local gas temperature T is govern by the parameter τ/τ_t. For $\tau << \tau_t$, T_P approaches T, and for $\tau >> \tau_t$, T_P retains the inlet temperature. Thus one can determine the critical

size corresponding to $\tau_t = \tau$. Particles larger than the critical size have temperature intermediate between T_{in} and T, whereas the smaller particles have temperatures closer to the local gas temperature T. Kim and Kim. [74] have found that the deposition rate increases with increasing gas temperature, once the threshold temperature for deposition is exceeded, since increasing number of particles melt during their traverse through the hot section of the combustor at the higher temperature. On the other hand, if the gas temperature is increased to above the condensation (solidify) temperature (which is higher than the deposition threshold temperature) of the deposited particles, the condensed particles will re-evaporate and the particulate matter may be swept away by aerodynamic forces, i.e. the deposition rate will decrease [50]. Richards et al. [55] studied the effect of gas temperature on the deposition behaviour of combustion residuals on turbine blade and found that at low combustion temperature (1100°C and 1200°C) surface cooling had no effect on the deposition rate; while at higher combustion temperature (1300°C) surface cooling reduces the deposition rate significantly. That is thought to be due the quenching effect on the boundary layers and the small size of the soot particles associated with high combustion temperature.

Particle size also has an effect on the position and where the deposition may take place, for example, large particles tend to hit the leading and trailing edges of the stators and rotors as well as suction and pressure surfaces. Conversely, small particles tend to hit the

leading edge and pressure surfaces more frequently than that of trailing edge and suction surfaces but less frequent than the larger particles.

Kim and Kim [74] had also carried out a deposition test using different types of volcanic ashes. They noted that for some type of ashes (call it type I), the deposition started at a threshold temperature of between 1060°C and 1120°C and the capture ratio is smaller than a different type of ash (type II) at a given temperature. For both of the types (I & II) the resulted deposits were ranged from grainy agglomerate to a glasslike deposit (depending on the temperature) and were easily removed from the surface. For a third type of volcanic material (type III) deposition was first observed at gas temperature of 1120°C. The deposits were observed to have a greenish-black coloration and the physical appearance of a relatively thin glaze applied to the total surface.

2.4 Erosion Experimental Techniques

There are three basic types of erosion experimental techniques:

i. air-blast, is the most widespread technique used in the erosion tests. Particles are introduced into a constant flow of gas travelling down a tube, where the faster moving gas accelerates the particle by fluid drag. Particle velocity can be controlled by the variation of the gas velocity. Particle outlet velocity can be measured in different ways such as the rotating slit disc method introduced by Ives and Ruff [28], but using the laser anemometer is more accurate. Particles may be introduced to the

propellant gas in a mixing chamber and particles feed rate can be controlled in several ways such as the rotational speed of an archimedian spiral, [75,76], vibration of a hopper, [77] or the speed of a conveyor belt or turntable [42,78]. Angle of impingement is usually controlled with a variable angle specimen holder [79]. Figure 2-10 shows a schematic drawing of the air blast test rig. The air blasting testers are potentially very simple, however, they tend to have some disadvantages which can be summarised as:

- The maximum possible gas velocity with the majority of gas gun testers is $(RT)^{1/2}$. For air at room temperature this is ~ 290 m/s [80]. This limitation is due to unfavourable aerodynamic interaction between the moving gas and the tube wall.
- Unless a very long acceleration tube is used, particle velocity is only a fraction of the gas velocity as particles may require a considerable length in which to accelerate. The extent to which particles accelerate over a fixed distance depends mainly on the particle size.
- Most erodents are a distribution of particle sizes. Different size particles, and indeed differently shaped particles, are accelerated to different velocities. This distribution in both particle size and velocity can greatly complicate the analysis of impact behaviour.

Tabakoff and co-worker [81] have developed an air blast erosion rig tester, figure 2-11, that is capable of particle velocities up to 450 m/s at a

temperature over 1000°C. This rig uses an acceleration tube with a large cross section of 2250 mm^2. Tube wall friction is much less of a problem with such a large cross section. The acceleration tube is 3.7 m long, which not only allows particle to attain a greater proportion of gas velocity but also to reduce the range of particle velocities, figure 2-12. The rig was designed for erosion testing compressor and turbine stage materials under conditions representative of a real operating environment. From the above description it is clear that this rig is enormous, costing a great sum to build and operate.

ii. whirling arm; in this erosion experimental technique the desired particle impact velocity is achieved by the rotation of the target material fixed on a rotating disc where targets rotate in a path of free falling particles. The rig, figure 2-13, consists of two highly evacuated interconnected, upper and lower, chambers. The upper chamber contains a vibratory feeder, which dispenses the erosive particles through a hole into the lower chamber which houses the rotor arm to which the targets are attached. When the arm rotates, particles dropping from the vibratory feeding chamber, impact onto the samples (targets) at the desired velocity obtained by the rotating arm, which could be as high as 550 m/s. The impact angle variation can be obtained by the targets inclination.

iii. erofuge; in this technique the erodent is accelerated prior to impact by its passage through a

rotor, figure 2-14, particles fed into a collection cup pass into adjoining radial tubes. Erodent is accelerated down these tubes by centrifugal force. The tested target are arranged circumferentially

iv. round, and a short distance from the rotor's edge. Particles impact and erode in a band across the circle of targets. Particle dynamics and sample orientation are functions of both radial and tangential motion. The erofuge tester has been used in several erosion testers [48,82,83]. The main disadvantage upon using this type of erodent tester is the temperature limitation, where the testing temperature is limited to 700°C only. This temperature range does not represent the actual in-service environment of gas turbine engine.

Full description of the test rig used in the current work is given on chapter3 "*Experimental Investigation of Erosion*".

2.5 Current Work

The literature review shows little progress in the erosion/deposition in gas turbine and the effect of target and particle temperature. The objective of the present study is to investigate the relationship between different parameters and erosion/deposition phenomena and to study the effect of the target and particle temperature on the erosion/depositon behaviour. The project aimed to cover the following areas:

- To study the influence of target temperature on both erosion and deposition of sand particles.

- The effect of particle temperature on erosion/deposition behaviour.
- The effect of particle impact velocity on the erosion/deposition rate. High velocities up to 300m/s were considered.
- The effect of impingement angle on erosion/deposition was also examined.
- To discuss the experimental results of the above effects on erosion and deposition.

List of Figures for Chapter 2

Figure 2-1. The three types of ductile impact damage reported by Hutchings and co-workers are all observed on actual impacted surface: a) Ploughing, b) Type I cutting, c) Type II cutting, [63].

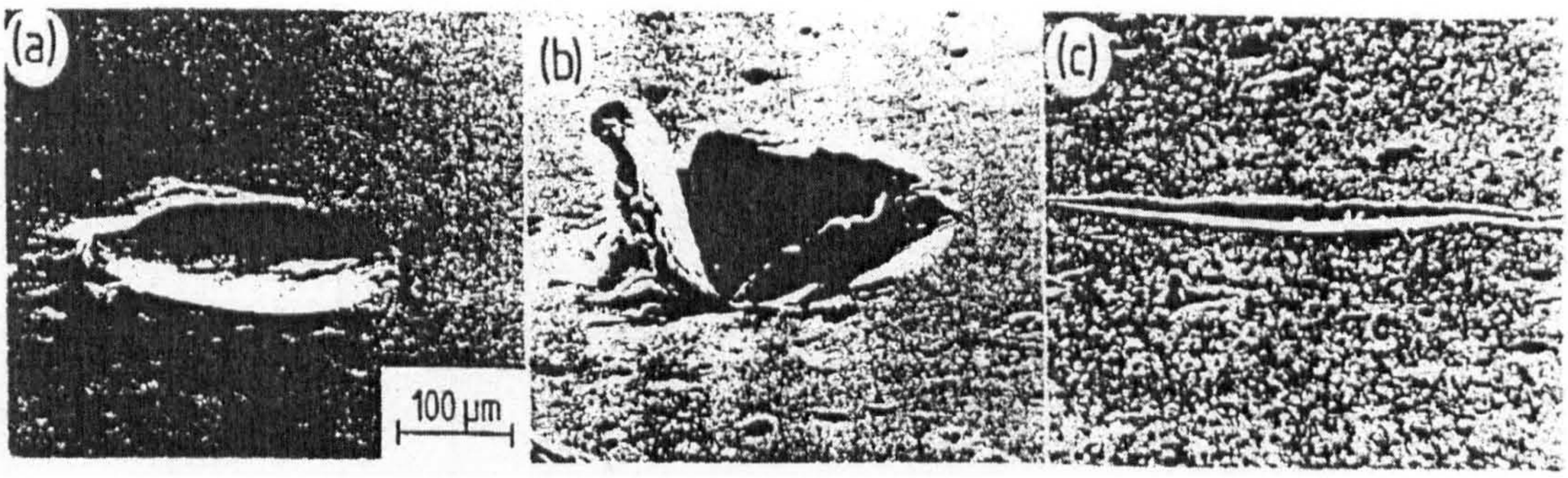


Figure 2-2. Radial fracture in soda-lime silica glass formed by a conical indentor [17].

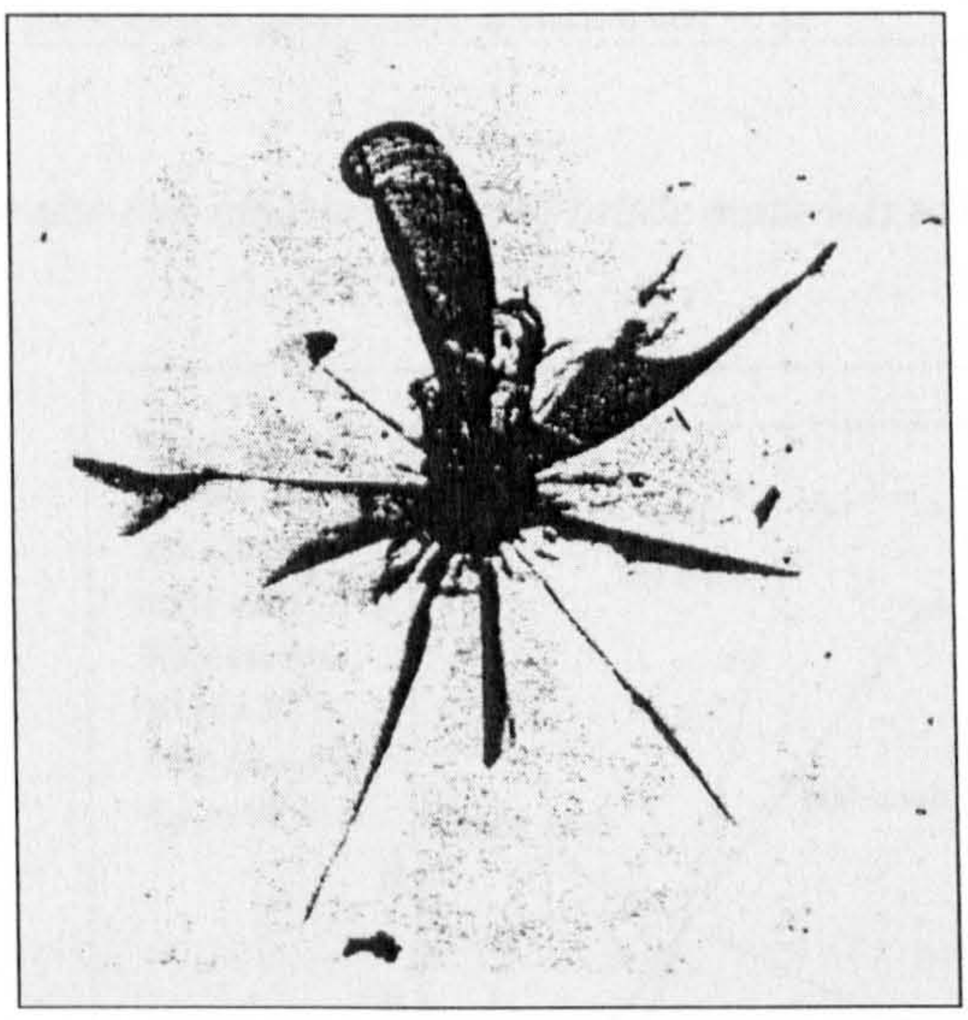


Figure 2-3. The influence of particle size on the erosion rate of 11% chromium steel, Goodwin [4].

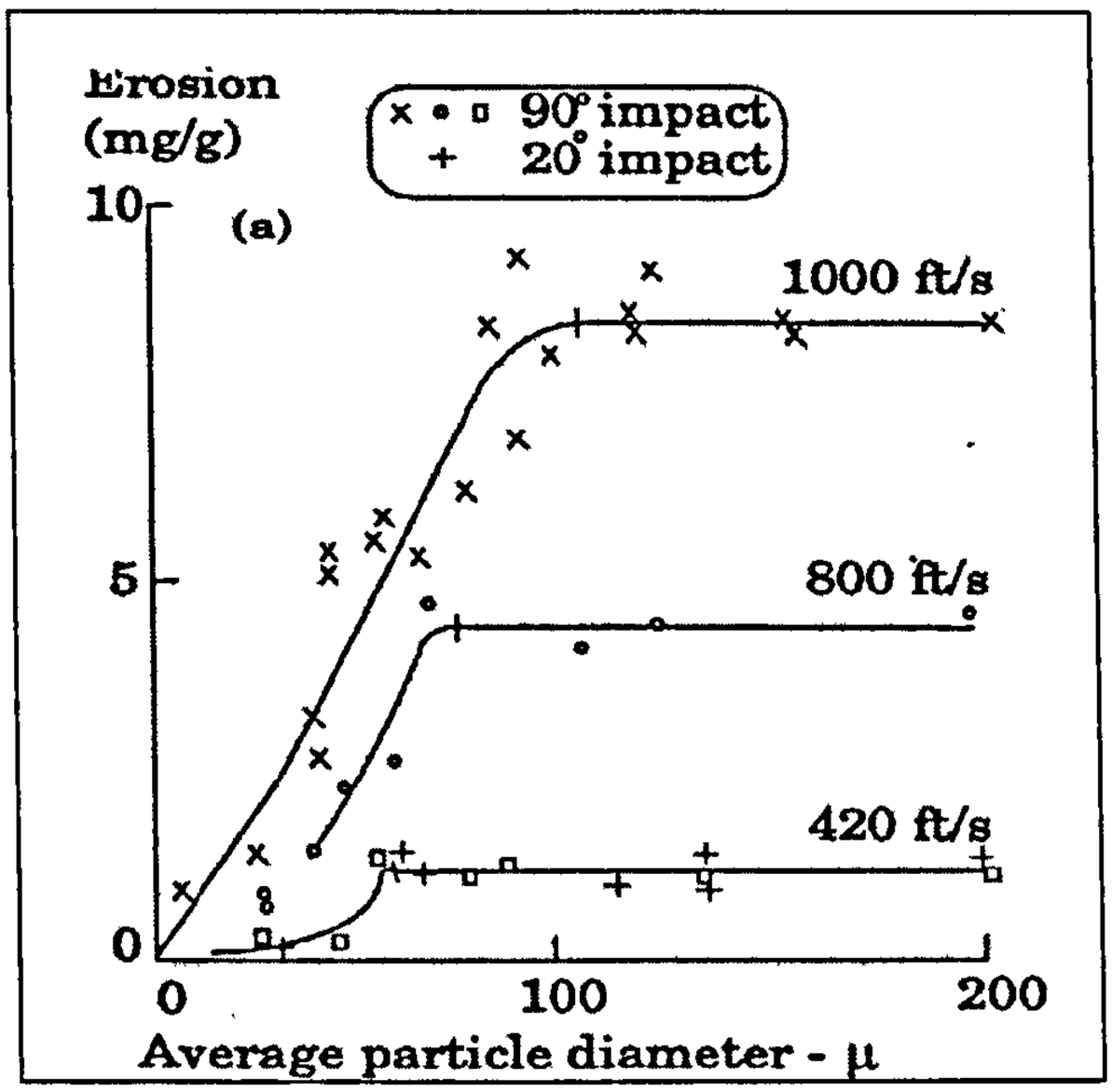


Figure 2-4. Particle size can alter response of brittle materials to that typical of ductile material [39].

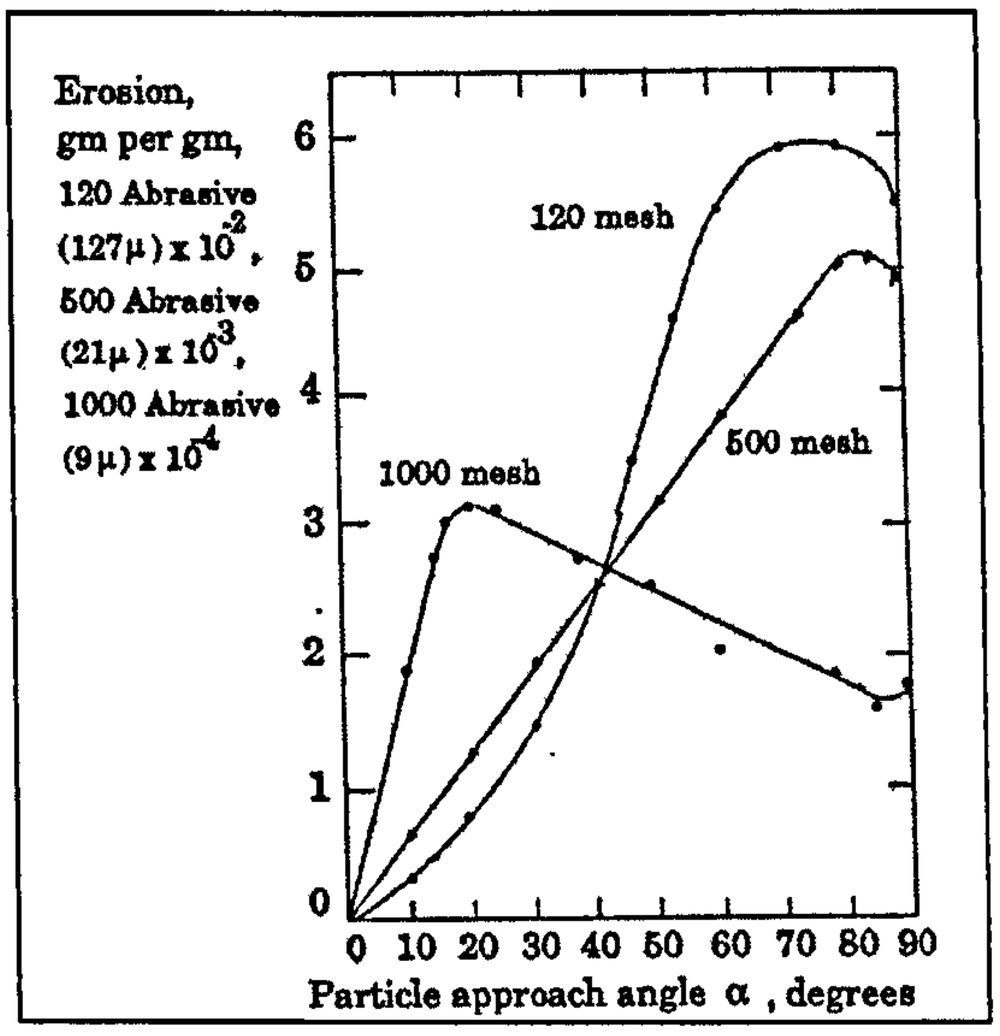


Figure 2-5. The erosion rate resistance of steels is insensitive to quench and tempered hardness [25].

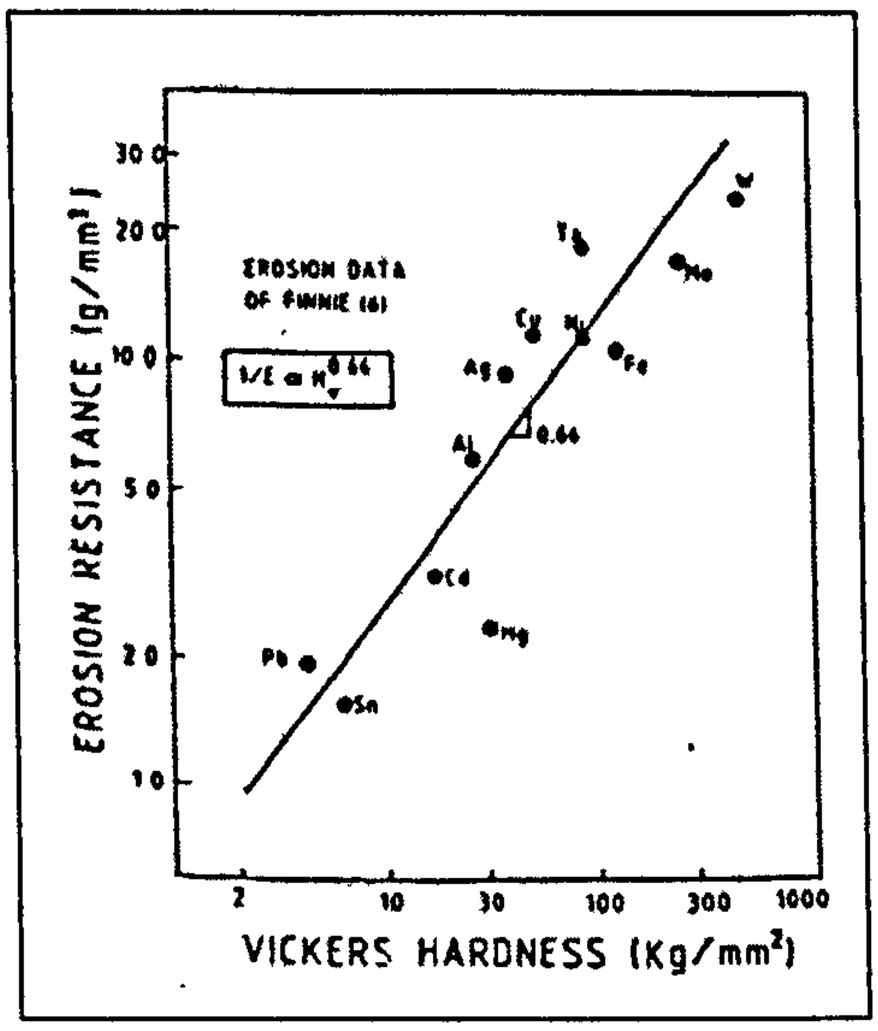


Figure 2-6. The erosion efficiency-hardness map indicates regimes corresponding to metals, alloys, ceramic and coatings. The slanting parallel lines represent erosion rate [40].

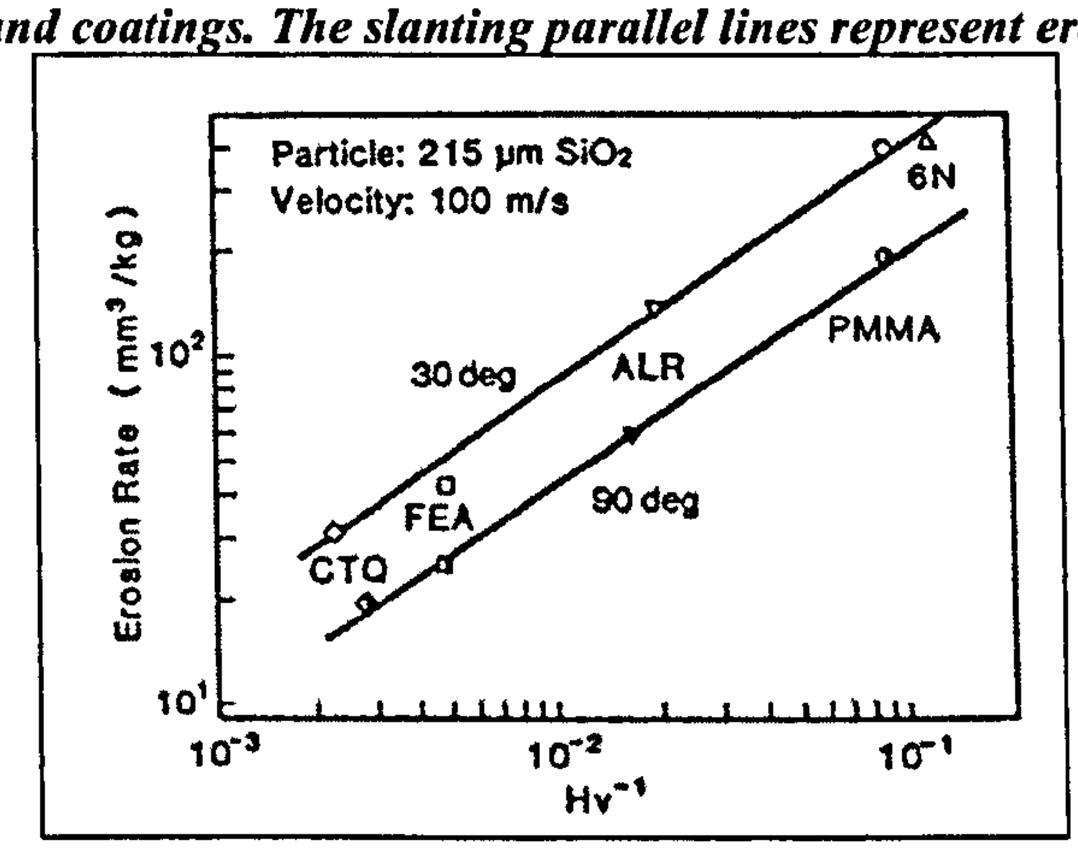


Figure 2-7. Ploughing is by far the most common ductile damage type; it is observed over a wide range of impact angles, Soderberg [47].

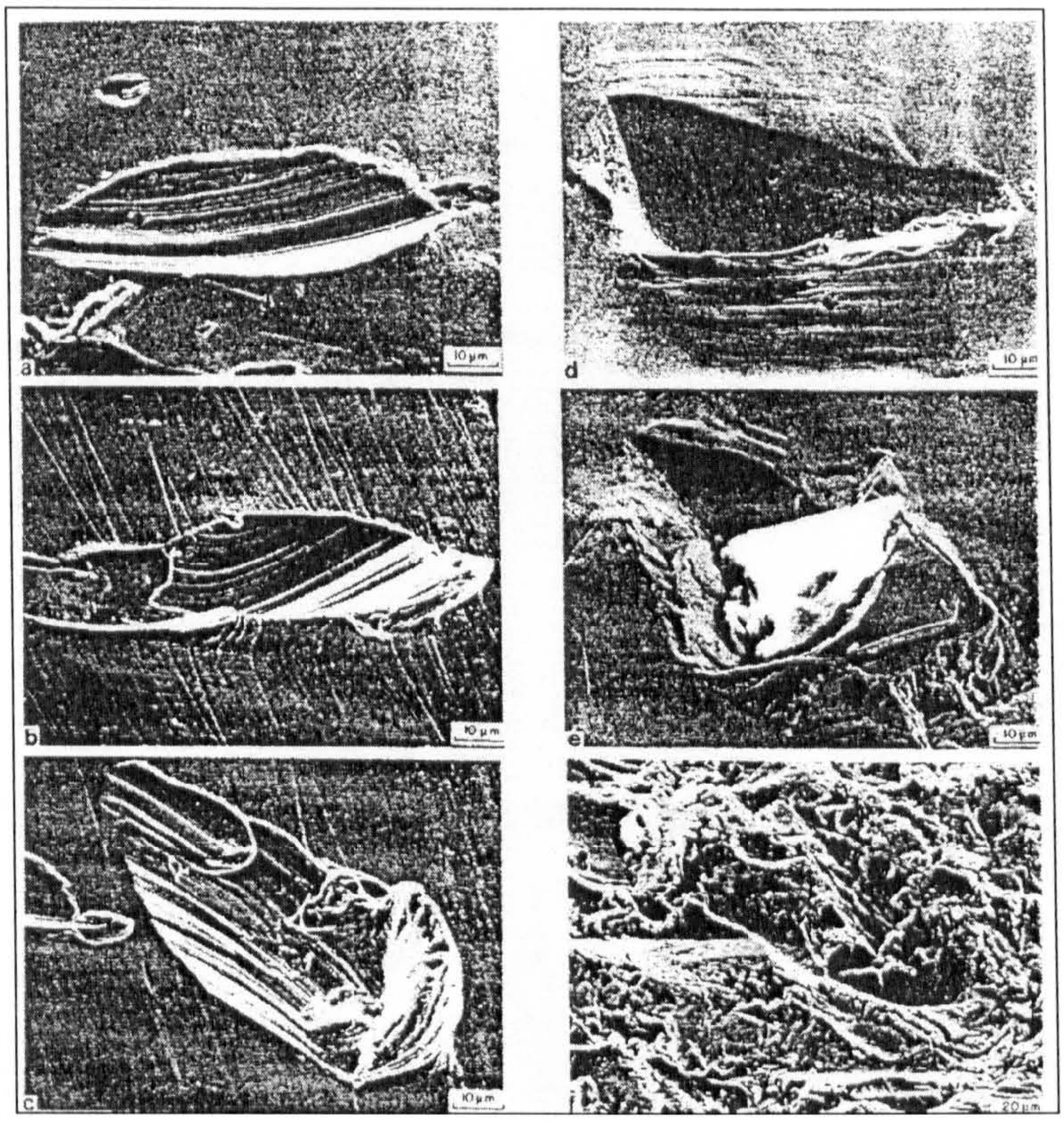


Figure 2-8 Mechanisms of deposition [55].

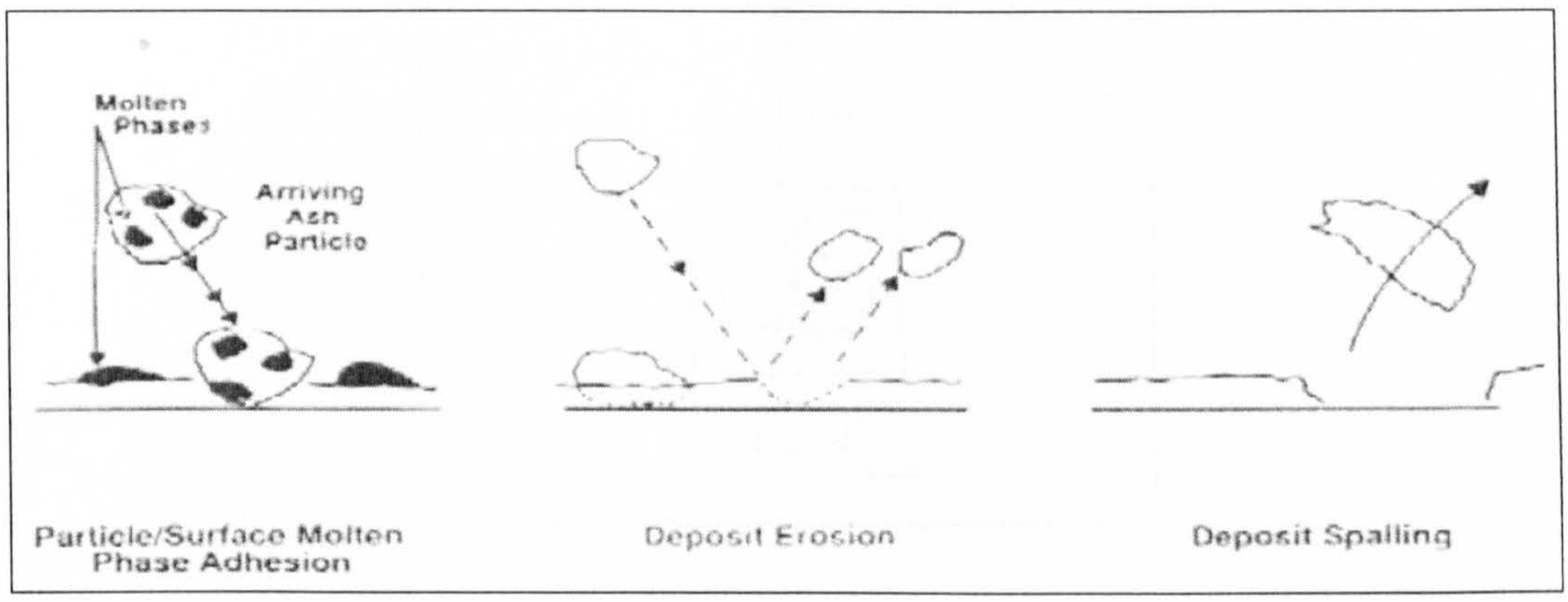


Figure 2-9. Flow lines of large and small particles [57].

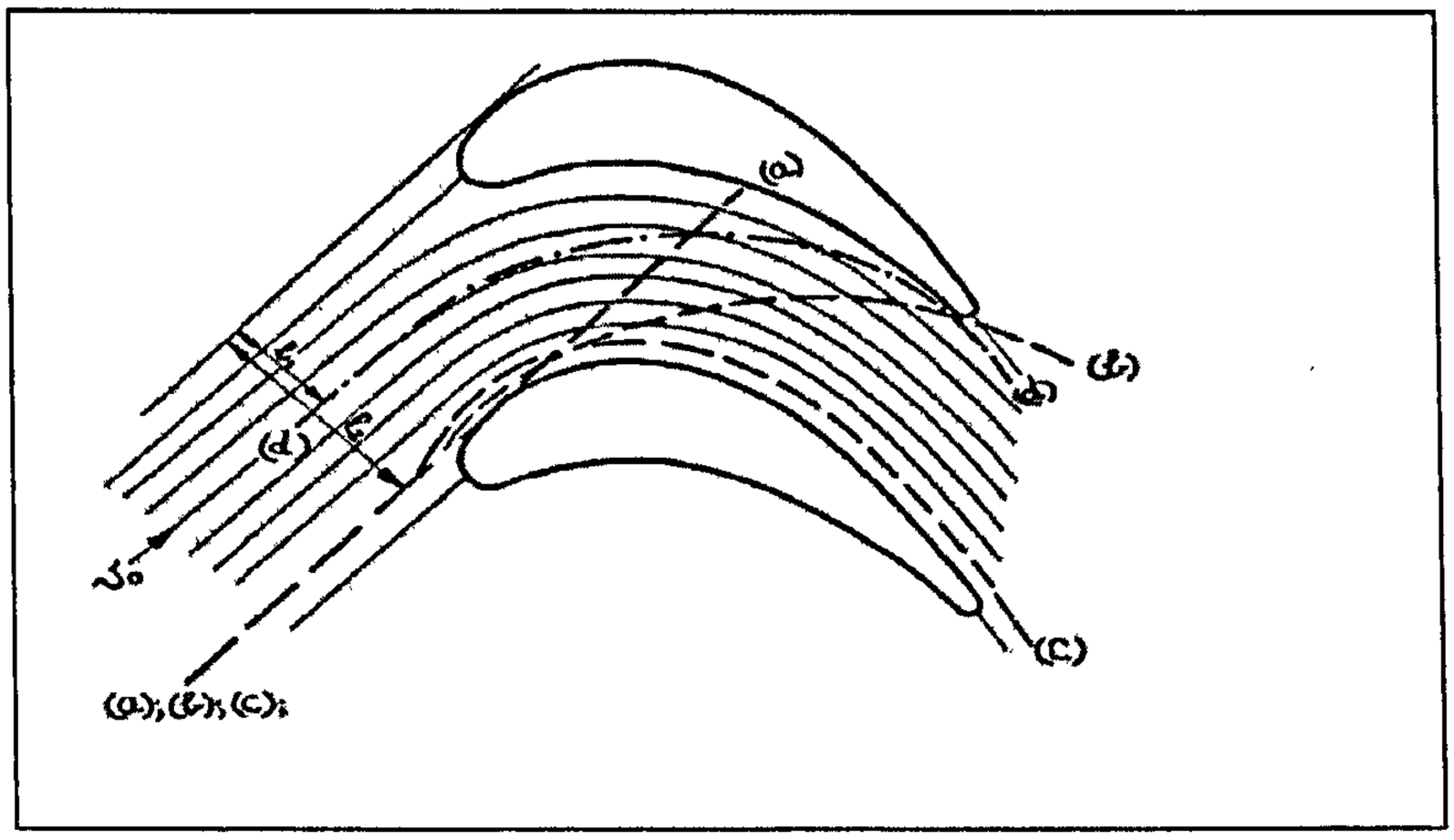


Figure 2-10. A schematic drawing of an air blast erosion tester [79].

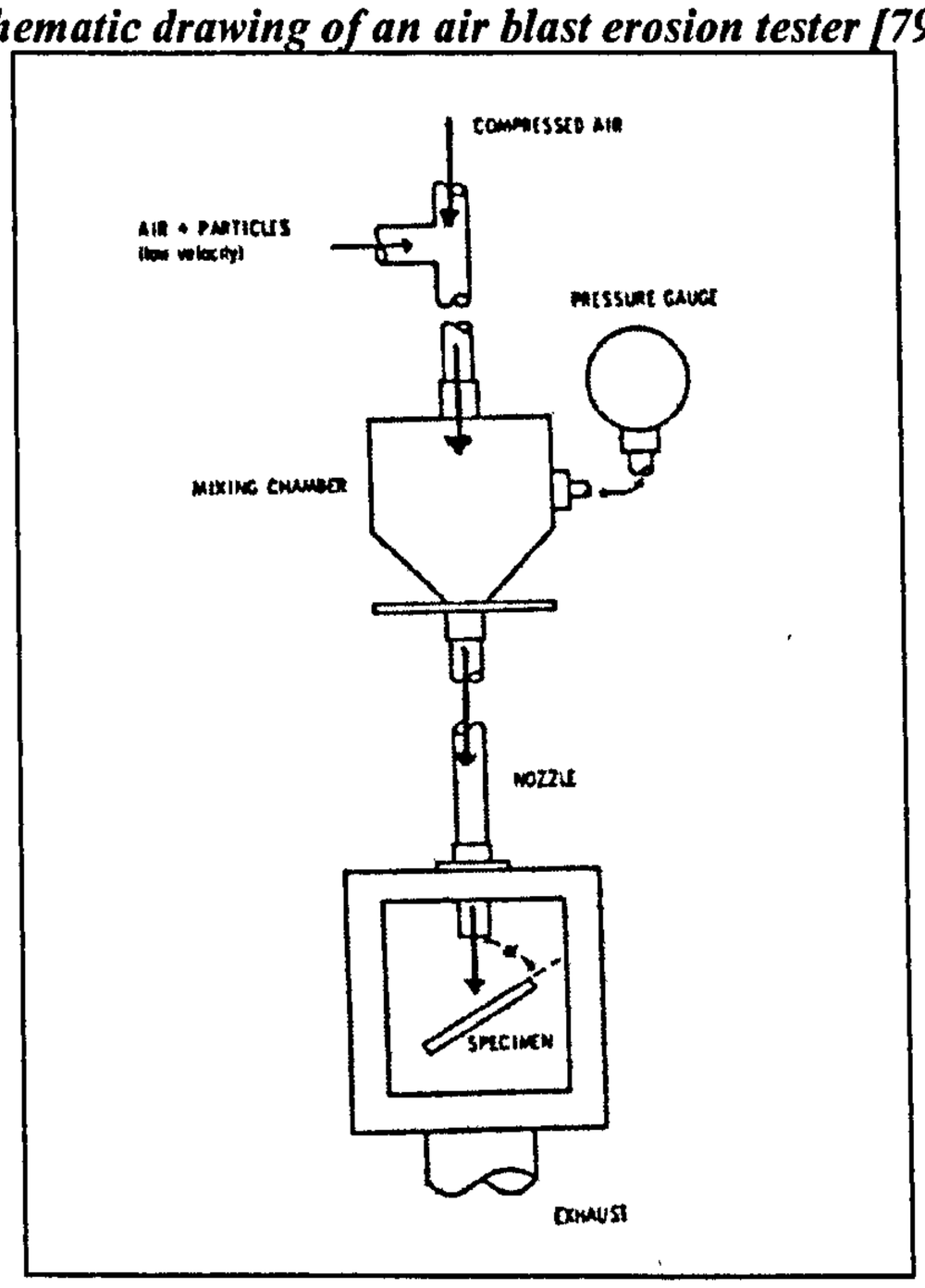


Figure 2-11. The erosion test rig built by Tabakoff group [81].

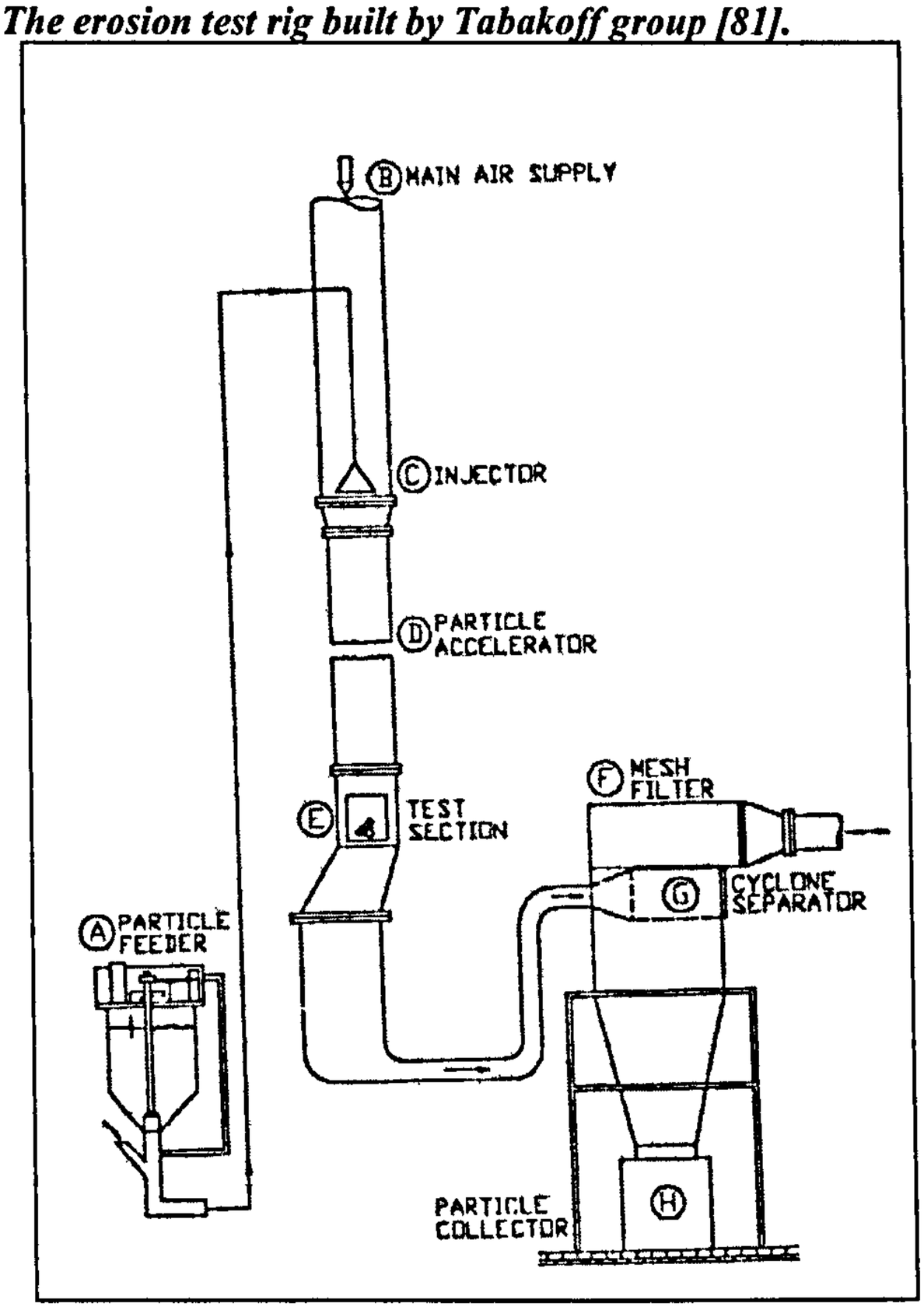


Figure 2-12. The effect of acceleration tube length on particle dynamics [81].

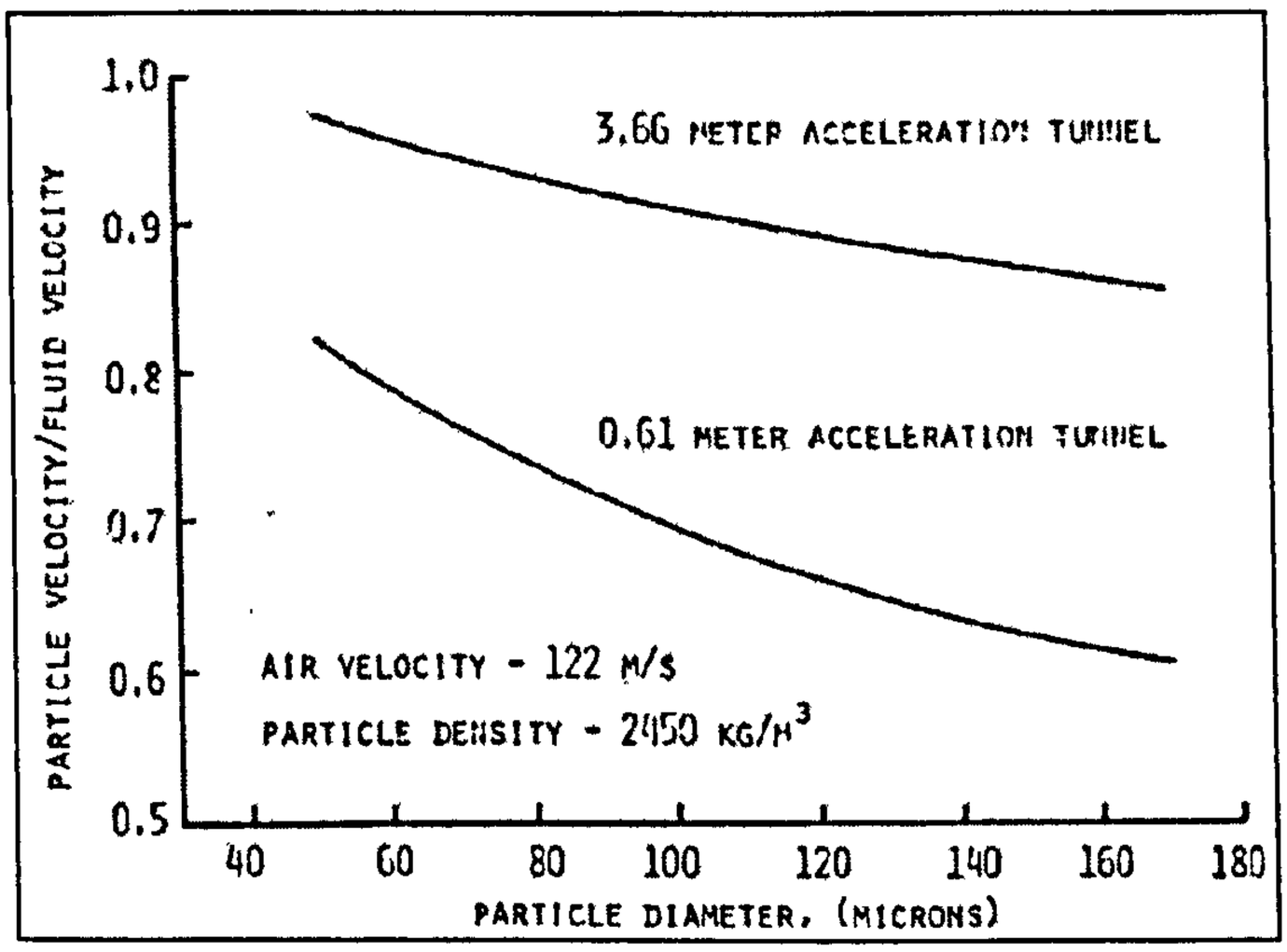


Figure 2-13. A whirling arm erosion rig [49].

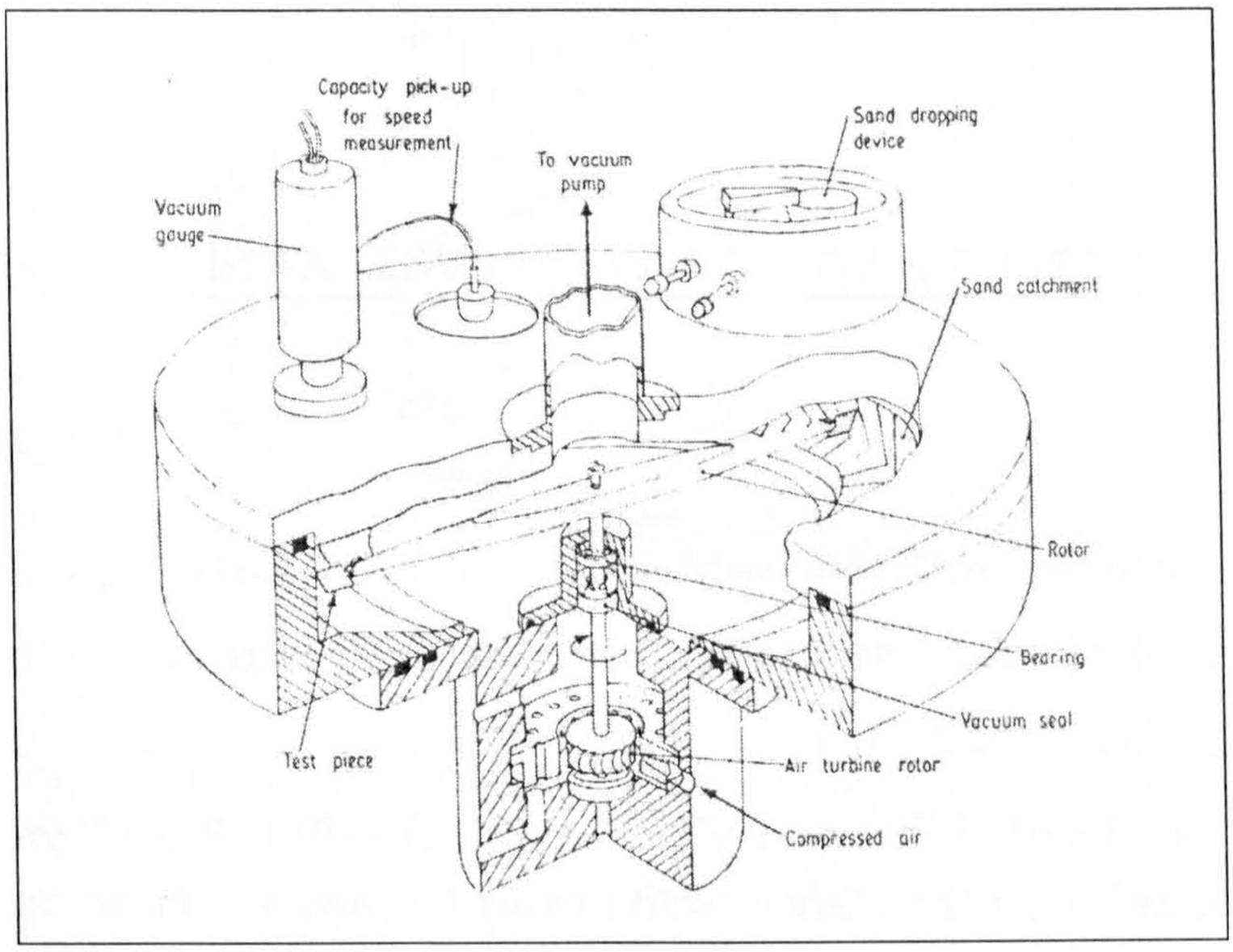
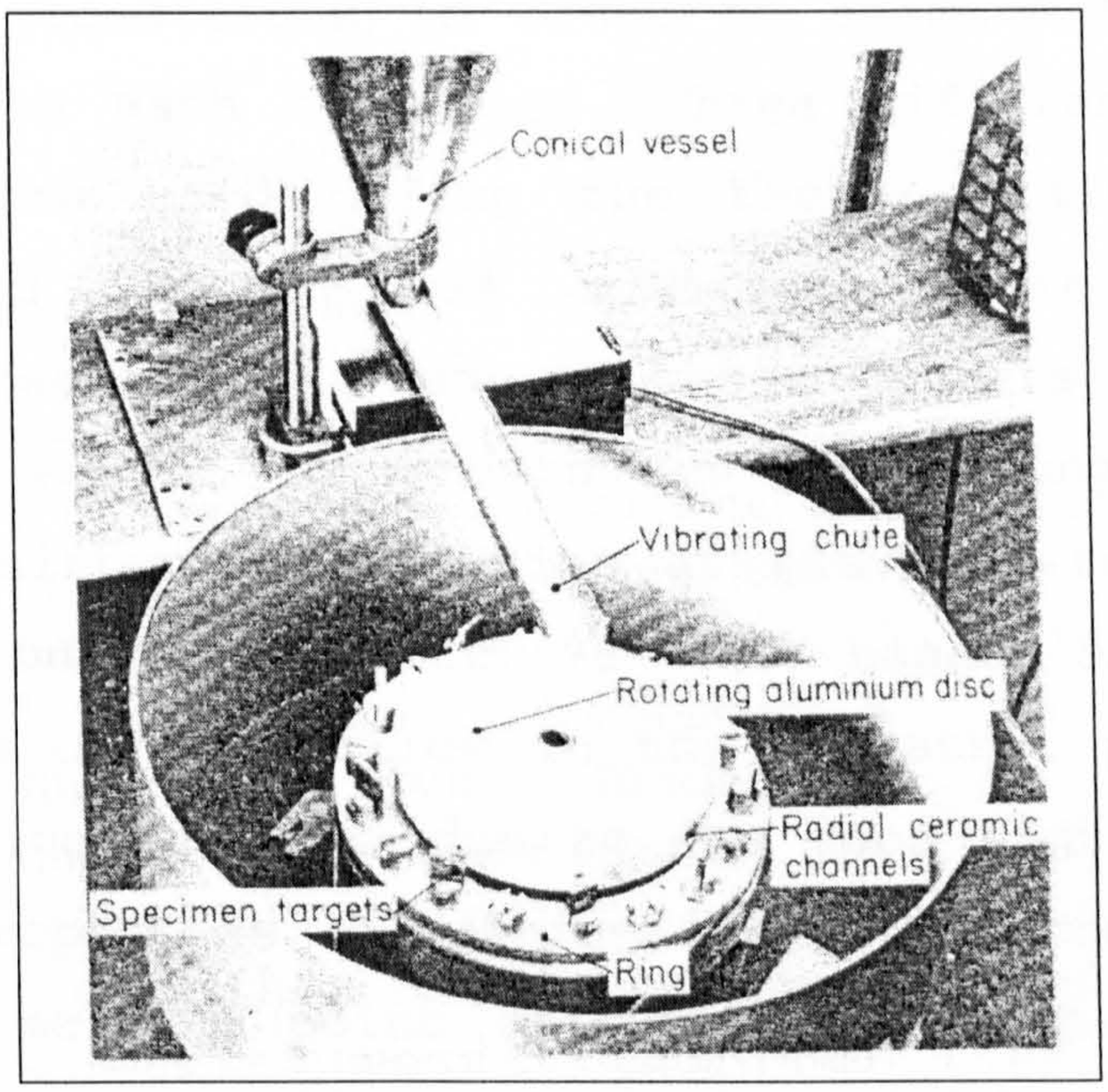


Figure 2-14. A centrifugal erosion tester or erofuge [48].



CHAPTER 3

EXPERIMENTAL INVESTIGATION OF EROSION

3.1 Introduction

In order to examine the erosion/deposition phenomena at elevated temperatures, a series of test conditions were carried out. The parameters that can effect changes in material behaviour under impact conditions are; material temperature and type, particle velocity, size and temperature, and angle of impact, as well as gas temperature. Erosion/deposition rates were examined at each of the conditions in order to examine the rate of change due to each condition. Three different types of materials were used during the tests; stainless steel 321, Nimonic 75 and 99% commercial pure aluminium. Stainless steel 321 is one of the materials widely used in aircraft engine components due its strong mechanical and heat resistance properties at elevated temperatures. The selection of Nimonic 75 was based on the wide applications of this alloy in the industry, particularly in gas turbine engines, due to its good high-temperature corrosion properties. Aluminium target was chosen because of its low melting point temperature, which allowed the examination of the effect of the target temperature close to the melting point. Experimental tests were carried out at different target and particle temperatures. The term 'homologous temperature (HT) ratio', was used to describe the ratio of target temperature to that of its melting point. The target is directly heated using an electrical heater where the temperature can be controlled by varying

the voltage supplied to the heater. On the other hand, the main air stream heated the particles as they pass through the 4m long acceleration tube described later in this chapter. For stainless steel and Nimonic 75, the maximum target HT ratio was HT=0.5, which represents target temperatures of 715°C and 690°C for stainless steel 321 and Nimonic 75 respectively. These temperatures are fairly representative to those found in gas turbine engine. Aluminium targets were tested at higher HT ratios of up to 0.8 times its melting point in order to predict the material response to erosion/deposition at such high temperature.

Silicon quartz, SiO_2, particle with a size range of 20-30μm was used as the erosive material since it is the most commonly found deposits and particles in gas turbine engines, for example, those engines operated in the Gulf war [1992]. previous conclusions revealed that more than 90% of the deposits were less than 30μm in size, with 30% being less than 4μm [1]. Particles temperature up to 950°C was achieved during the tests that is close to that found at the entrance to the HP turbine section. The impact angles where chosen to be at 30° and 60°, which are similar to the angles that the impact most occurs within the turbine engine.

The test program was organised in the following manner;

1. The effect of target temperature on erosion/deposition rate was considered. Tests were carried out at different target temperature, which is represented in term of the homologous temperature ratio (HT ratio) defined as *the ratio of material temperature to its melting point temperature*, while particle's velocity,

impingement angle and temperature were kept constant during each run.

2. the influence of particle temperature on the erosion behaviour was considered for the three tested materials. During the testes, three different particle temperatures were used while the other variables were kept unchanged.
3. Also the effect of impingement angle was investigated for stainless steel 321 at different impact velocities. This gives a relation between erosion/deposition rate and impingement angle at different target and particle temperatures.
4. To investigate the effect of impact velocity on erosion/deposition rate, tests were carried out at different particle velocities while other parameters were kept constant

3.2 Experimental Test Rig

The test rig was built to simulate the conditions in the turbine section of the gas turbine engine where the blade tip speed and temperature exceeds 300m/s and 950°C respectively. The test rig, figure 3-1 had been fabricated and set up in such a way to give a maximum outlet gas temperature of 1100°C and a particle velocity of 370 m/s for 20-30μm particle size. The test rig was operated as a sandblaster where particles were accelerated by compressed air. The air and particles were heated along a 4m long tube by applying a voltage difference between the two ends. The amount of heat input can be varied to the required exit gas temperature and velocity. The rig consists of three main parts, namely;

accelerating and heating tube, particle feeder, and target heater and holder.

3.2.1 Acceleration and Heating Tube

The acceleration and heating tube is made out of a heat resistance tube commercially known as KANTHAL™ tube which is normally used for furnace purposes. A 4.0m long by 0.004m inner and 0.006m outer diameters tube was chosen to provide the required temperature and velocity of the gas and particles at the tube outlet. Figure 3-2 shows a 3-D drawing of the tube assembly. A throttle valve and pressure gauge were used to control the flow rate of compressed air entering the tube which was measured during each run and set accordingly to give the desired outlet velocity and temperature. The tube was heated by applying voltage difference between the two ends with a high alternative current, which is adjustable to obtain the suitable heat input. The tube was then inserted into an outer ceramic tube which provides electrical insulation. This arrangement also allows tube expansion both the axial and tangential directions. To minimise heat loss, the tube was further insulated using two different types of high grade insulating materials. Figures 3-3 and 3-4 show a prediction of the temperature and velocity distribution at different test conditions obtained from a CFD code. Detailed CFD set up results are given on appendix 2.

Figure 3-3 and 3-4 shows the gas temperature distribution at a maximum wall temperature of 1100°C, for gas inlet velocity (flow rate) of 40 m/s (0.703 kg/hr) and 140 m/s (2.46 kg/hr) respectively. The predicted maximum outlet gas temperature at the mean exit area is about 1010°C and

that is around 980°C correspondingly. Figure 3-5 and 3-6 shows the gas velocity distribution at wall temperature of 1100°C and gas inlet velocity (flow rate) of 40 m/s (0.703 kg/hr) and 140 m/s (2.46 kg/hr) respectively. The former shows a predicted mean outlet gas velocity of 120 m/s while the later is about 320 m/s. this implies that by increasing the inlet air flow rate (inlet velocity) 40 m/s to 140 m/s, only results a small change in gas outlet temperature (from 1010°C to 980°C), and a great change in the gas outlet velocity (from 120 m/s to 320 m/s). So the gas velocity is controlled by changing mass flow rate without significantly changing the gas outlet temperature. For the purpose of comparison, table 3-1 represents a sample of experimental and theoretical (obtained from CFD simulations) results of particle velocity and gas (particle) temperature at the two fore mentioned settings.

Table 3-1 Experimental and calculated gas and particle velocity and temperature.

Stagnant Tube Wall Temperature		1100°C	
Gas Inlet Velocity (Flow Rate)		40 m/s (0.703 kg/hr)	140 m/s (2.46 kg/hr)
Mean outlet Gas Temperature °C	Experimental	1100	1050
	Calculated (CFD)	1010	980
Mean Outlet Particle Velocity (m/s)	Experimental	110	300
	Calculated (CFD)	120	320

Experimental values of the gas temperature were obtained by placing a thermocouple at a distance of 20mm from the tube exit. The gas outlet velocity was taken as the velocity of particles (20-30 μm), which was measured with a laser transit anemometer. It is expected that the true gas velocity will be slightly higher than the particles

velocity due to the slip velocity (between the particles and the gas). The results in table 3-1 show good agreement between the calculated and measured values.
Thermocouples were also used to measure the temperature distribution along the tube; 0.2 m from the inlet end, the second at the middle of the tube, and the last one at 0.1 m away from the outlet end, as shown in figure 3-2. Figure 3-7 shows the thermocouples reading during stagnant and running conditions.
Particles were fed in the tube, under gravitational forces at room temperature and gained their velocity and temperature from the compressed air. The particle exit velocity and temperature depend on the acceleration gas flow rate (velocity) and tube wall temperature.
It was deemed difficult to practically measure particle temperature due to the small quantity of particles involved (≈1gm/sec) and the high temperatures involved, hence they were estimated from the measured gas temperature. Sample results of particle velocity and temperature obtained from a FLUENT CFD package show particle temperature distribution at tube wall temperature of 1100°C and gas inlet velocities (flow rate) of 40 m/s (0.703 kg/hr) and 140 m/s (2.46 kg/hr). The former shows an average outlet particle temperature of 1000°C, while the later shows an average particle temperature of 950°C, as presented in by figures 3-8 and 3-9 respectively. Figure 3-10 and 3-11 represents particle velocity distribution at the same fore mentioned wall temperature and inlet velocities.

3.2.2 Particle Feeder

The Particle feeder consists of a pressurised particle container and a mechanical vibrator. Compressed air is supplied to the pressurised container at the same pressure to that of the acceleration tube to ensure a constant particles delivery rate and to equalise the pressure preventing back-flow. Varying the pressure of compressed air supplied to the mechanical vibrator controls particle delivery rate. Figures 3-12 and 3-13 show the pressurised particle container and mechanical vibrator.

3.2.3 Target Holder and Heater:

The target holder, figure 3-14, consists of a vertical rectangular bracket to hold the target plate and electrical heater assembly. It is attached to the base by a mean of rotating disk, which allows an angle change between 0° to 90° with respect to air stream.

A commercial strip electrical heater was used to heat up the target plate to the required temperatures. Fast Heat's Better Strip Heater was used as the standard heater through out the experiments. The heater has a maximum sheath temperature of 815°C. A variable voltage control was used to control heater temperature. The heater WAS sandwiched between the target holder and target specimen in such a way to ensure maximum heat transfer between the heater and the target. The heater was thermally insulated from the target holder with a fibre insulator to minimise the heat loss. The whole assembly is thermally insulated from the surrounding ambient region except for a hole of 25x25 mm which allows particles to strike the target specimen. Three

thermocouples were used to measure target temperature and to ensure an even temperature distribution on the target surface as shown in figure 3-15. K-type thermocouples have been inserted in a 1.0 x 1.0 mm groves were machined in the back of one target piece of each different material tested, and surface temperature readings were reported at every different test condition. Table 3-6 gives the thermocouples readings at for four settings and shows the temperature at the three points.

3.2.4 Sample Shape

Tested samples have a dimension of 40 x 30mm and 1.0 - 3mm thick. The heater element is made of a high-grade nickel chromium resistance wire and a stainless steel sheath. Both heater and target are thermally insulated from the surrounding ambient region except for the hole where the target is exposed to the erodent particles. Each sample is fitted with an erosion shield which is made of stainless steel 320 sheet with a 25 x 25 mm-exposure window centred along the major axis of the tested material face. The shield is about 6.0mm thick with insulation filling to reduce heat loss from target and heater assembly. The shield also provides protection for the insulator and heater surfaces.

3.3 Test materials:

3.3.1 Erosive Particles:

The particles used in the experiment are silica sand and its chemical composition is shown on table 3-2. The density of the particle is between 2600-2700 kg/m^3 and moisture content is less than 1.0% by weight. The particle size distribution is shown in figure 3-16 which

was obtained using COULTER electronic multisizer fitted with AccuComp software (Particle Technology Ltd, UK).

Table 3-2. Chemical analysis of silica sand- wt %.

Substance	Amount (mass%)
Silica SiO_2	98.0-98.5
Ferric oxide Fe_2O_3	0.03-0.06
Alumina Al_2O_3	0.6-1.0
Chromium oxide Cr_2O_3	0.0007-0.0015
Na + K Oxide	0.15-0.4

Particle size of 20-30μm was chosen as a result of the work done by Rolls-Royce who had gathered considerable data on their engines performance in desert conditions. From figure 3-16, obtained from COULTER analyser, the particle size distribution shows that about 80% of particles are smaller than 29.61 μm and 25% are smaller than 20μm, i.e. 55% falls on the range of 20 - 30 μm.

3.3.2 Target Material:

Three different target materials were used during the erosion/deposition testing. All tested materials are listed in table 3-3 below with their composition and major physical and mechanical properties.

Table 3-3. Physical constants and mechanical properties of alloys used in the erosion/deposition tests.

Property	Material		
	Nimonic 75 80Ni-20Cr	Commercial Pure Aluminium	Stainless steel 321
Composition % wt	0.08-0.15C, 1.0 max. Si, 5.0Cu, 5.0Mn, 18Cr, 0.2Ti, Ni Bal.	99% Purity	0.08C, 1.0Si, 0.04P, 0.025S, 17Cr, 0.8Ti
Density (kgm^{-3})	8.37	2.71	7.9
Melting Temperature °C	1380	643-657	1430
Young's modulus (GPa at 20°C)	221	69	278
Thermal conductivity (wmk^{-1} at 20°C)	11.7	209	
Tensile Strength (MPa)	745	125	510-710
Hardness (max) (HV)			200

3.3.3 Calibration

The dust used in the tests was composed of 20-30 μm crushed quartz particles. They were specially graded to give a small size distribution as described in section 3.3.1.

The laser two-spot (L2f) anemometer, described in appendix 1, was used to determine the particle velocity. A series of repeated measurements at different velocities were carried out in order to check the measurement accuracy. At higher velocities, there were some

difficulties in measuring the velocity due to the flow turbulence near the tube exit. However, the correct distance from the tube exit was chosen to eliminate this effect and the velocity was measured 20 mm from the tube exit. In addition, the laser beam was centred at the mean tube exit area to measure the mean velocity and to avoid the boundary layer effects. Table 3-4 shows the statistics of repeated measurements at particle velocity of 100 m/s. From the results, the laser anemometer has proven to be very accurate in measuring particle velocities.

Table 3-4. Statistics for laser anemometer (L2F) measurement.

	Particle Velocity of 100 m/s
Mean Value	100.55
Median Value	100.47
Standard Deviation	0.45
Lower 95%	99.48
Upper 95%	101.75

The measurement of gas temperature at the tube exit was affected by the position of the thermocouple bead; figure 3-17 shows the sensitivity of the gas temperature to the thermocouple position.

The accuracy of the erosion data were examined at different test conditions as a series of runs were carried out to ensure the repeatability of the results. Table 3-6 shows a sample statistics of repeated measurements at impact velocity of 250 m/s, particle temperature of 750 and target HT ratio of 0.4 at impact angle of 30° C. From the sample results, the erosion tests were proven to be at high level of accuracy.

Table 3-5. Statistics for a sample erosion test.

	Erosion Rate of 21.2 mg/g
Mean Value	21.19
Median Value	21.2
Standard Deviation	0.18
Lower 95%	21.24
Upper 95%	20.74

3.4 Test Procedures

A measured amount of sand, usually about 20 gm, was fed into the particle feeder. The acceleration tube is heated to the required temperature and the compressed air flow rate was set to give the desired outlet velocity and temperature. The target is placed at about 20 - 40 mm away from the tube exit, depends on the required particle temperature. The particle exit velocity was measured at a distance of 20 mm from the tube exit using a laser two-spots (L2F) anemometer. Each target plate was weighed before and after each run using a balance accurate to ±0.001gm. Erosion/deposition rate is deduced from loss/gain in the weight of the target plate and Scanning Electron Microscope SEM analysis. The erosion/deposition rate is defined as *the ratio between the change in target mass and the mass of the impacting particles*, which is given in

$$\text{Erosion rate} = \frac{\text{change in sample weight}}{\text{mass of impacting particles}} \qquad (3\text{-}1)$$

At the end of each test, the target surface was examined using the SEM to assess the damage incurred by the particles.

3.5 Test Program and Test Matrix

The complete test programme is shown in table 3-6. They are divided into the following conditions:

i) Particle impact velocity;

- V: 100 m/s (for Aluminium targets only)
- V: 200 m/s
- V: 250 m/s
- V: 300 m/s

ii) Particle Impact Angle;

- 30° (Stainless steel, Nimonic 75 and Aluminium)
- 60° (Stainless steel only)

iii) Particle Temperature;

- Tp: 350°C (Aluminium only)
- Tp: 550°C
- Tp: 750°C
- Tp: 950 (Stainless steel and Nimonic75 only)

iv) Target Materials;

- Stainless steel 321
- Nimonic 75
- Commercially pure Aluminium (99%)

v) Target Temperatures, (HT Ratios);

a) Stainless steel

- 285°C (0.2)
- 430°C (.03)
- 570°C (0.4)
- 715°C (0.5)

b) Nimonic 75

- 275°C (0.2)
- 415°C 0.3)

- 550°C (0.4)
- 690°C (0.5)

c) Aluminium

- 195°C (0.3)
- 260°C (0.4)
- 325°C (0.5)
- 390°C (0.6)
- 455°C (0.7)
- 520°C (0.8)

3.6 Summary

The test programme was selected to provide a better understanding of the erosion/deposition phenomena for the stainless steel 321, Nimonic 75 and aluminium targets where targets were tested at different conditions. Tests for stainless steel were carried out at 30 and 60° impact angles and at HT ratios of HT=0.2 to HT=0.5 at three particle temperatures of 500°C, 750°C and 950°C. All tests were carried out at 200, 250, and 300 m/s incident velocity as listed in table 4-1 and 4-2 in chapter 4 *"Results and Discussions"*, which shows the tests results of the stainless steel targets at 30° and 60° respectively. For the purpose of comparison, the erosion tests for Nimonic 75 targets were carried out at the same test conditions to that of the stainless steel and at one impact angle of 30°. The Nimonic results are tabulated in table 4-4 listed in chapter 4. The aluminium targets were subjected to one impact velocity tests of 100 m/s at 30° impact angle. The particle temperature was set at 350°C, 550°C, and 750°C and target HT ratio was chosen to at

HT=0.3 to 0.8 which are listed in table 4-6. The previously described test programme was mainly designed to establish a full view of the effect of the main parameters influencing the material erosion, i.e. target temperature, particle temperature and impact velocity.

Table 3-6 Erosion Test Conditions.

Test No.	Material Type	Impact Angle (deg)	Impact Velocity (m/s)	Particle Temperature°C	Target Temperature °C (HT Ratio)
1	**Stainless steel**	**30**	**200**	500	285 (0.2)
2	Stainless steel	30	200	500	430 (0.3)
3	Stainless steel	30	200	500	570 (0.4)
4	Stainless steel	30	200	500	715 (0.5)
5	Stainless steel	30	200	750	285 (0.2)
6	Stainless steel	30	200	750	430 (0.3)
7	Stainless steel	30	200	750	570 (0.4)
8	Stainless steel	30	200	750	715 (0.5)
9	Stainless steel	30	200	950	285 (0.2)
10	Stainless steel	30	200	950	430 (0.3)
11	Stainless steel	30	200	950	570 (0.4)
12	Stainless steel	30	200	950	715 (0.5)
13	Stainless steel	30	**250**	500	285 (0.2)
14	Stainless steel	30	250	500	430 (0.3)
15	Stainless steel	30	250	500	570 (0.4)
16	Stainless steel	30	250	500	715 (0.5)
17	Stainless steel	30	250	750	285 (0.2)
18	Stainless steel	30	250	750	430 (0.3)
19	Stainless steel	30	250	750	570 (0.4)
20	Stainless steel	30	250	750	715 (0.5)
21	Stainless steel	30	250	950	285 (0.2)
22	Stainless steel	30	250	950	430 (0.3)
23	Stainless steel	30	250	950	570 (0.4)
24	Stainless steel	30	250	950	715 (0.5)
25	Stainless steel	30	**300**	500	285 (0.2)
26	Stainless steel	30	300	500	430 (0.3)

Test No.	Material Type	Impact Angle (deg)	Impact Velocity (m/s)	Particle Temperature°C	Target Temperature °C (HT Ratio)
27	Stainless steel	30	300	500	570 (0.4)
28	Stainless steel	30	300	500	715 (0.5)
29	Stainless steel	30	300	750	285 (0.2)
30	Stainless steel	30	300	750	430 (0.3)
31	Stainless steel	30	300	750	570 (0.4)
32	Stainless steel	30	300	750	715 (0.5)
33	Stainless steel	30	300	950	285 (0.2)
34	Stainless steel	30	300	950	430 (0.3)
35	Stainless steel	30	300	950	570 (0.4)
36	Stainless steel	30	300	950	715 (0.5)
37	**Stainless steel**	**60**	**200**	500	285 (0.2)
38	Stainless steel	60	200	500	430 (0.3)
39	Stainless steel	60	200	500	570 (0.4)
40	Stainless steel	60	200	500	715 (0.5)
41	Stainless steel	60	200	750	285 (0.2)
42	Stainless steel	60	200	750	430 (0.3)
43	Stainless steel	60	200	750	570 (0.4)
44	Stainless steel	60	200	750	715 (0.5)
45	Stainless steel	60	200	950	285 (0.2)
46	Stainless steel	60	200	950	430 (0.3)
47	Stainless steel	60	200	950	570 (0.4)
48	Stainless steel	60	200	950	715 (0.5)
49	Stainless steel	60	**250**	500	285 (0.2)
50	Stainless steel	60	250	500	430 (0.3)
51	Stainless steel	60	250	500	570 (0.4)
52	Stainless steel	60	250	500	715 (0.5)

Test No.	Material Type	Impact Angle (deg)	Impact Velocity (m/s)	Particle Temperature°C	Target Temperature °C (HT Ratio)
53	Stainless steel	60	250	750	285 (0.2)
54	Stainless steel	60	250	750	430 (0.3)
55	Stainless steel	60	250	750	570 (0.4)
56	Stainless steel	60	250	750	715 (0.5)
57	Stainless steel	60	250	950	285 (0.2)
58	Stainless steel	60	250	950	430 (0.3)
59	Stainless steel	60	250	950	570 (0.4)
60	Stainless steel	60	250	950	715 (0.5)
61	Stainless steel	60	300	500	285 (0.2)
62	Stainless steel	60	300	500	430 (0.3)
63	Stainless steel	60	300	500	570 (0.4)
64	Stainless steel	60	300	500	715 (0.5)
65	Stainless steel	60	300	750	285 (0.2)
66	Stainless steel	60	300	750	430 (0.3)
67	Stainless steel	60	300	750	570 (0.4)
68	Stainless steel	60	300	750	715 (0.5)
69	Stainless steel	60	300	950	285 (0.2)
70	Stainless steel	60	300	950	430 (0.3)
71	Stainless steel	60	300	950	570 (0.4)
72	Stainless steel	60	300	950	715 (0.5)
73	Nimonic 75	30	200	500	275 (0.2)
74	Nimonic 75	30	200	500	451 (0.3)
75	Nimonic 75	30	200	500	550 (0.4)
76	Nimonic 75	30	200	500	690 (0.5)
77	Nimonic 75	30	200	750	275 (0.2)
78	Nimonic 75	30	200	750	451 (0.3)
79	Nimonic 75	30	200	750	550 (0.4)
80	Nimonic 75	30	200	750	690 (0.5)
81	Nimonic 75	30	200	950	275 (0.2)
82	Nimonic 75	30	200	950	451 (0.3)

Test No.	Material Type	Impact Angle (deg)	Impact Velocity (m/s)	Particle Temperature°C	Target Temperature °C (HT Ratio)
83	Nimonic 75	30	200	950	550 (0.4)
84	Nimonic 75	30	200	950	690 (0.5)
85	Nimonic 75	30	**250**	500	275 (0.2)
86	Nimonic 75	30	250	500	451 (0.3)
87	Nimonic 75	30	250	500	550 (0.4)
88	Nimonic 75	30	250	500	690 (0.5)
89	Nimonic 75	30	250	750	275 (0.2)
90	Nimonic 75	30	250	750	451 (0.3)
91	Nimonic 75	30	250	750	550 (0.4)
92	Nimonic 75	30	250	750	690 (0.5)
93	Nimonic 75	30	250	950	275 (0.2)
94	Nimonic 75	30	250	950	451 (0.3)
95	Nimonic 75	30	250	950	550 (0.4)
96	Nimonic 75	30	250	950	690 (0.5)
97	Nimonic 75	30	**300**	500	275 (0.2)
98	Nimonic 75	30	300	500	451 (0.3)
99	Nimonic 75	30	300	500	550 (0.4)
100	Nimonic 75	30	300	500	690 (0.5)
101	Nimonic 75	30	300	750	275 (0.2)
102	Nimonic 75	30	300	750	451 (0.3)
103	Nimonic 75	30	300	750	550 (0.4)
104	Nimonic 75	30	300	750	690 (0.5)
105	Nimonic 75	30	300	950	275 (0.2)
106	Nimonic 75	30	300	950	451 (0.3)
107	Nimonic 75	30	300	950	550 (0.4)
108	Nimonic 75	30	300	950	690 (0.5)
109	**Aluminium**	**30**	**100**	350	195 (0.3)
110	Aluminium	30	100	350	260 (0.4)
111	Aluminium	30	100	350	325 (0.5)
112	Aluminium	30	100	350	390 (0.6)
113	Aluminium	30	100	350	455 (0.7
114	Aluminium	30	100	350	520 (0.8)
115	Aluminium	30	100	500	195 (0.3)
116	Aluminium	30	100	500	260 (0.4)
117	Aluminium	30	100	500	325 (0.5)
118	Aluminium	30	100	500	390 (0.6)
119	Aluminium	30	100	500	455 (0.7
120	Aluminium	30	100	500	520 (0.8)
121	Aluminium	30	100	750	195 (0.3)
122	Aluminium	30	100	750	260 (0.4)
123	Aluminium	30	100	750	325 (0.5)
124	Aluminium	30	100	750	390 (0.6)
125	Aluminium	30	100	750	455 (0.7
126	Aluminium	30	100	750	520 (0.8)

List of Figures for Chapter 3

Figure 3-1. General layout of the test rig assembly.

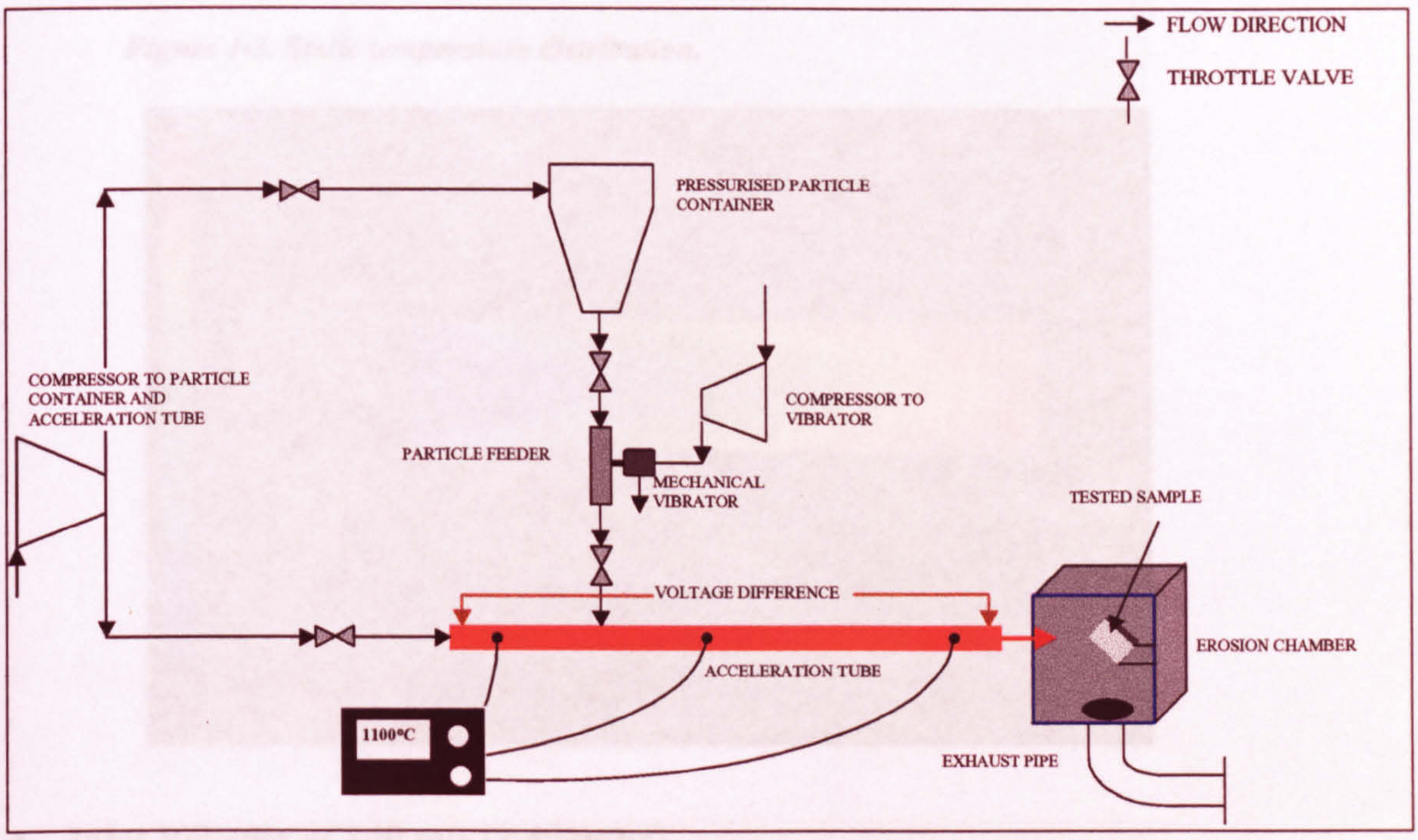
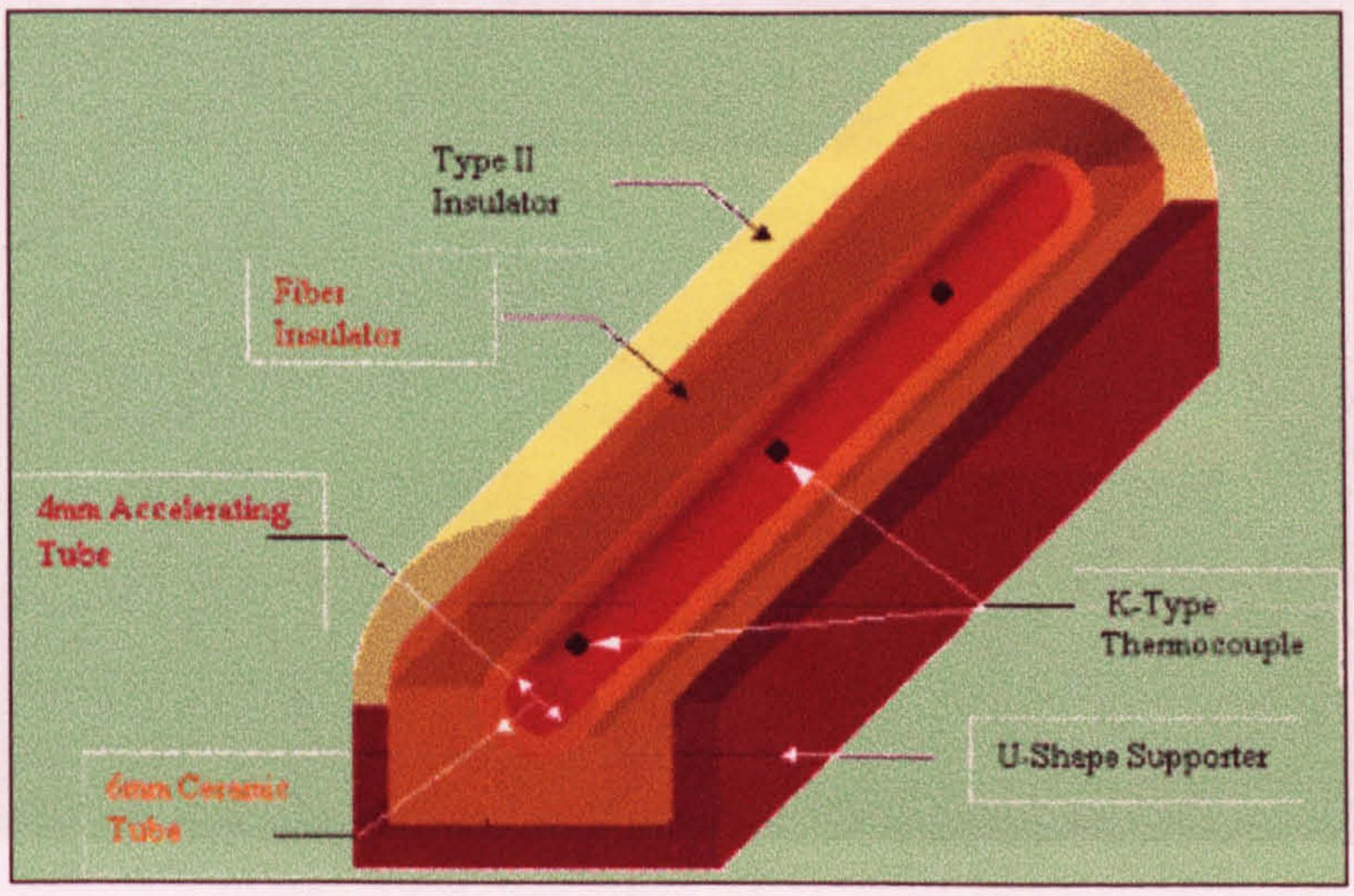


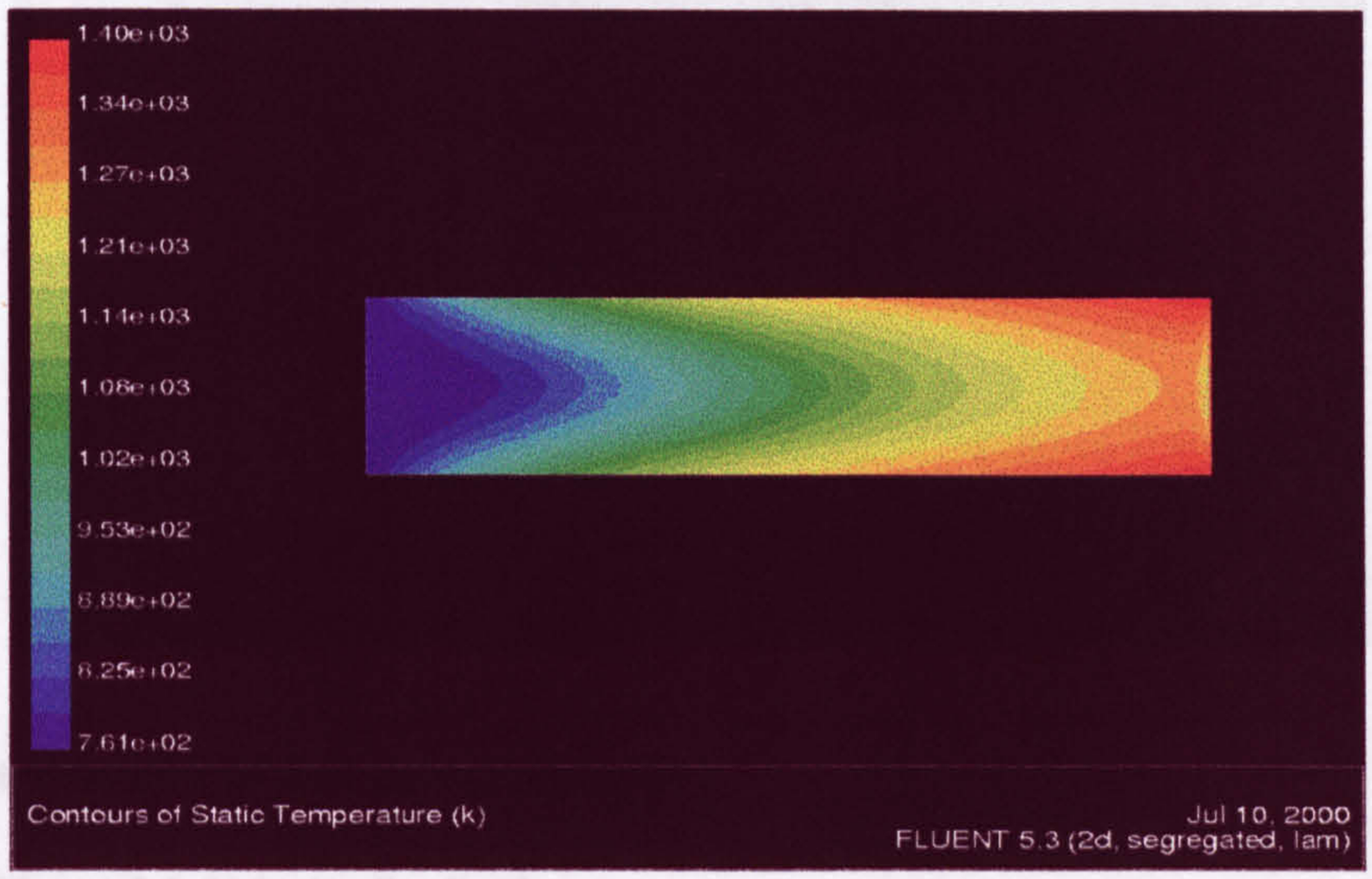
Figure 3-2. Acceleration and heating tube assembly.



CFD Results for 1100°C Tube Wall Temperature.

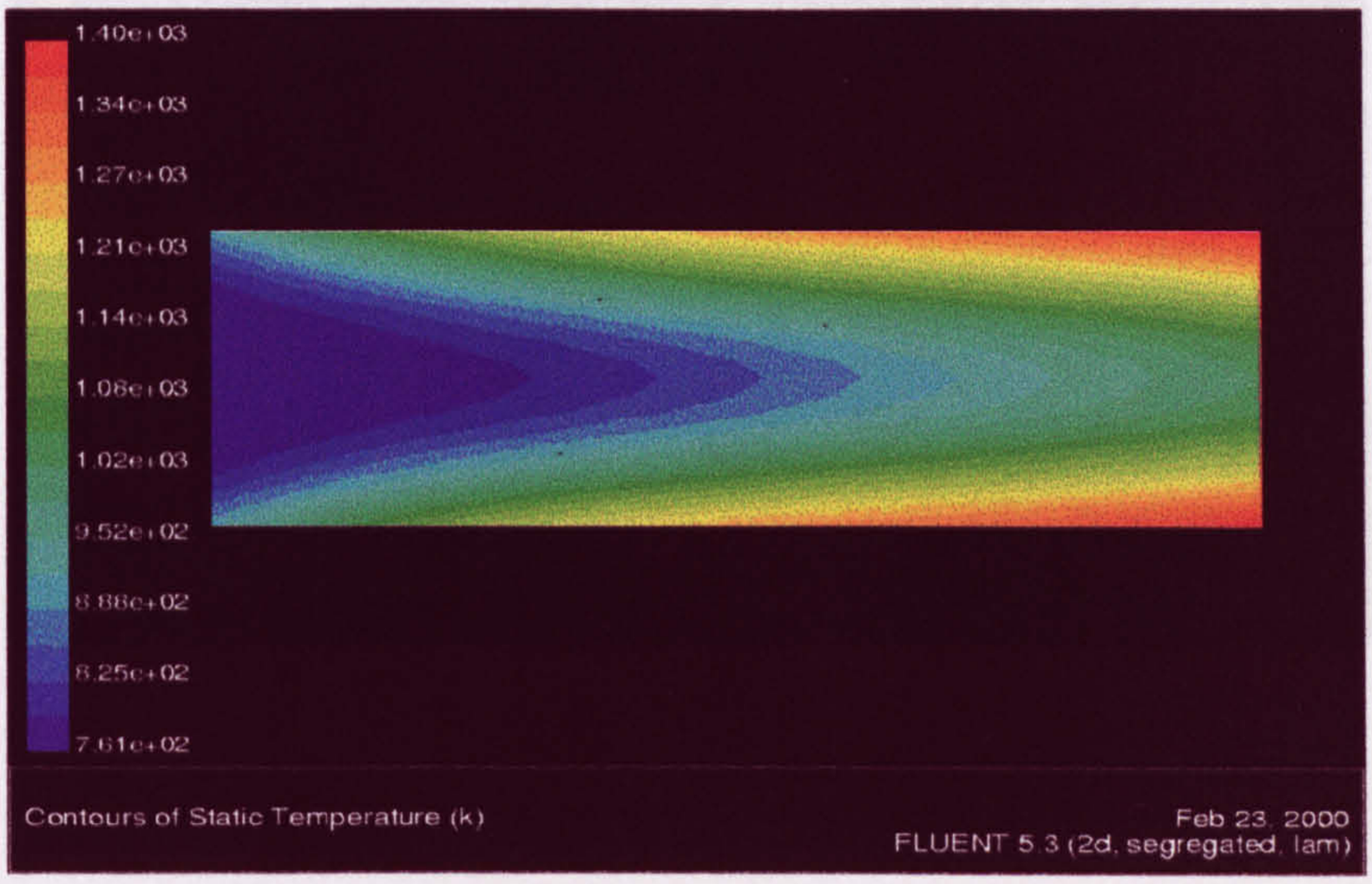
- **Inlet Velocity of 40 m/s (0.703kg/hr)**

Figure 3-3. Static temperature distribution.



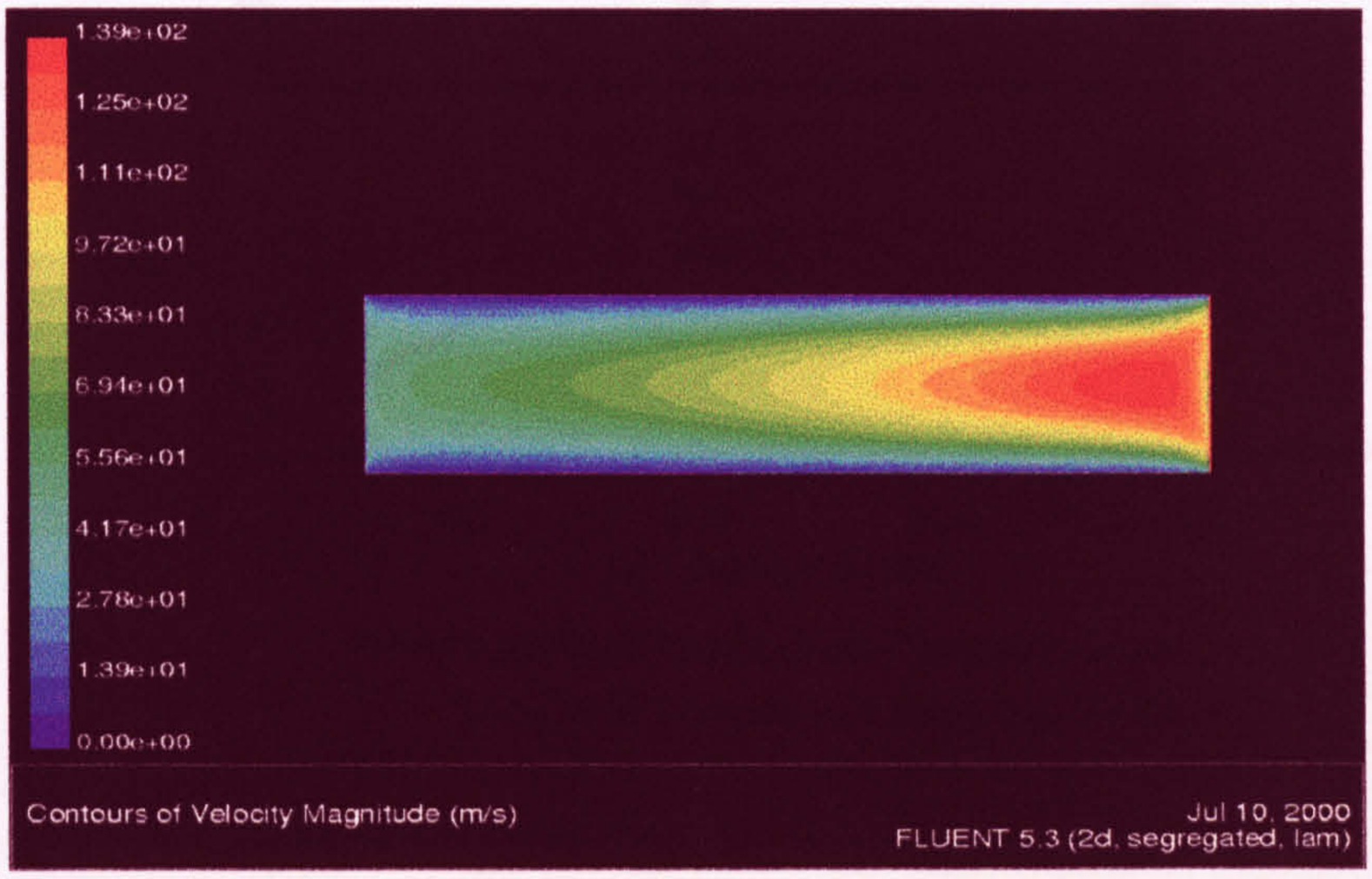
- **Inlet Velocity of 140 m/s (2.46kg/hr)**

Figure 3-4. Static temperature distribution.



- **Inlet Velocity of 40 m/s (0.703kg/hr)**

Figure 3-5. Flow velocity distribution.



- **Inlet Velocity of 140 m/s (2.46kg/hr)**

Figure 3-6. Velocity distribution

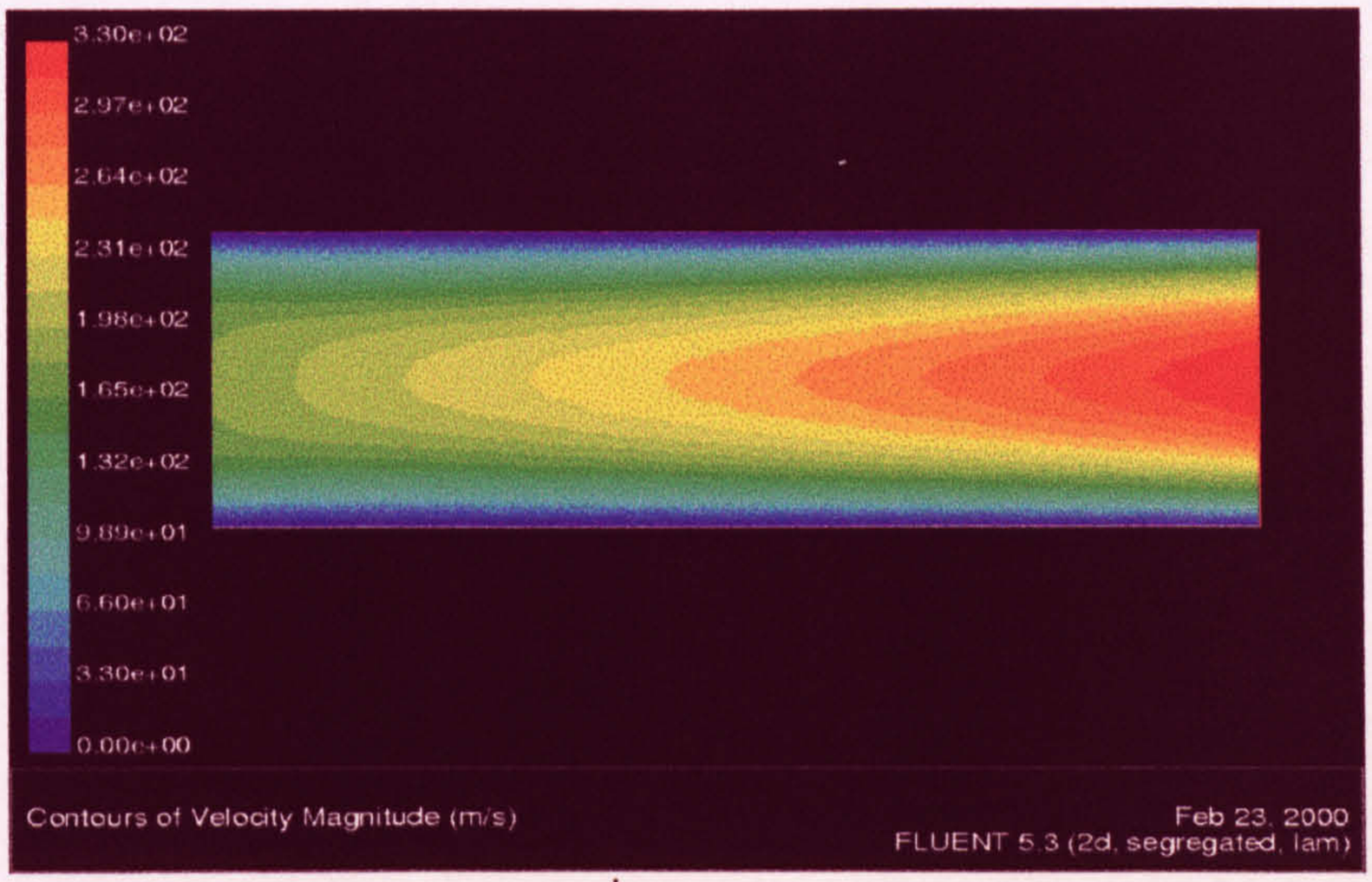
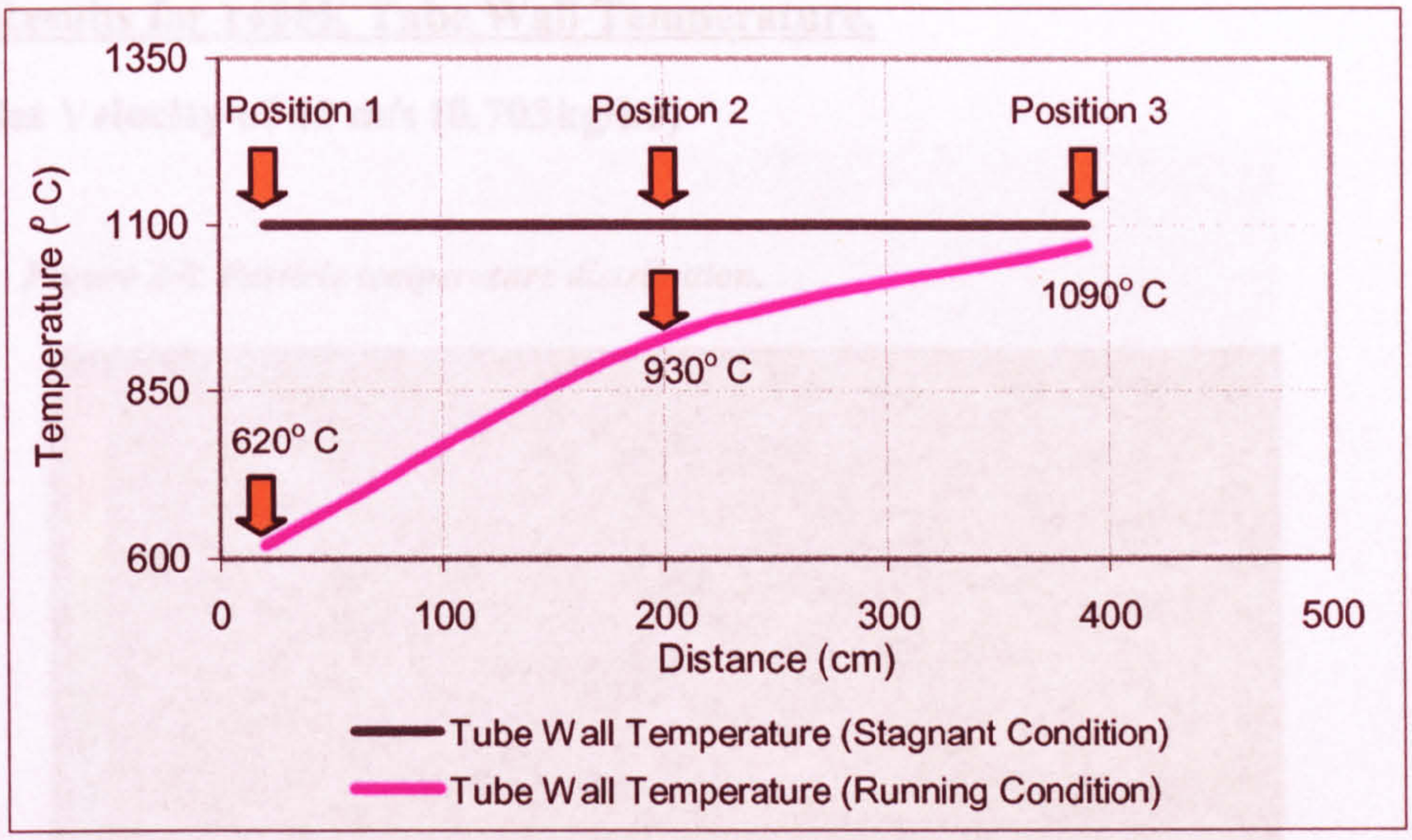


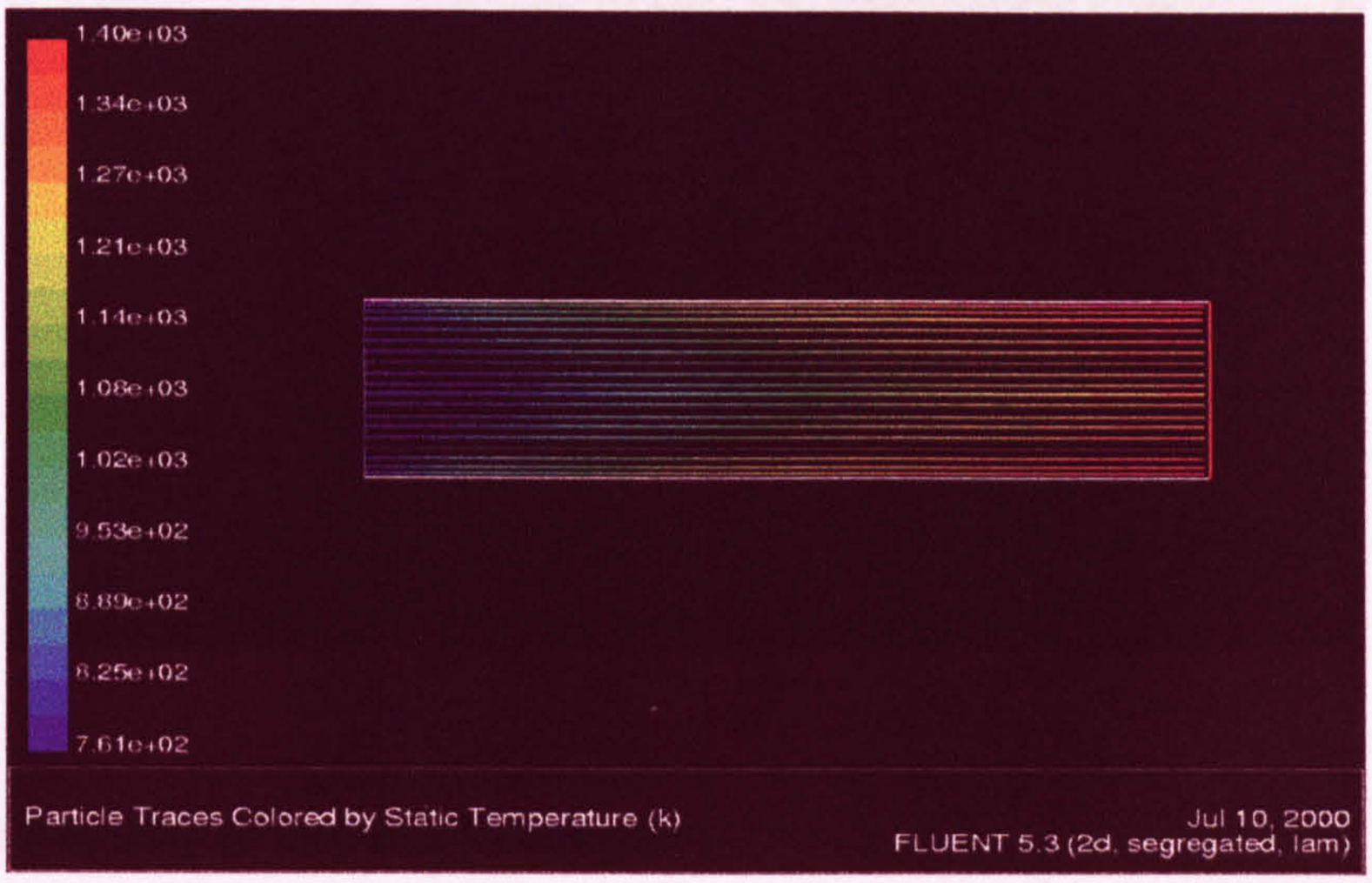
Figure 3-7. Thermocouples reading.



CFD Results for 1400K Tube Wall Temperature.

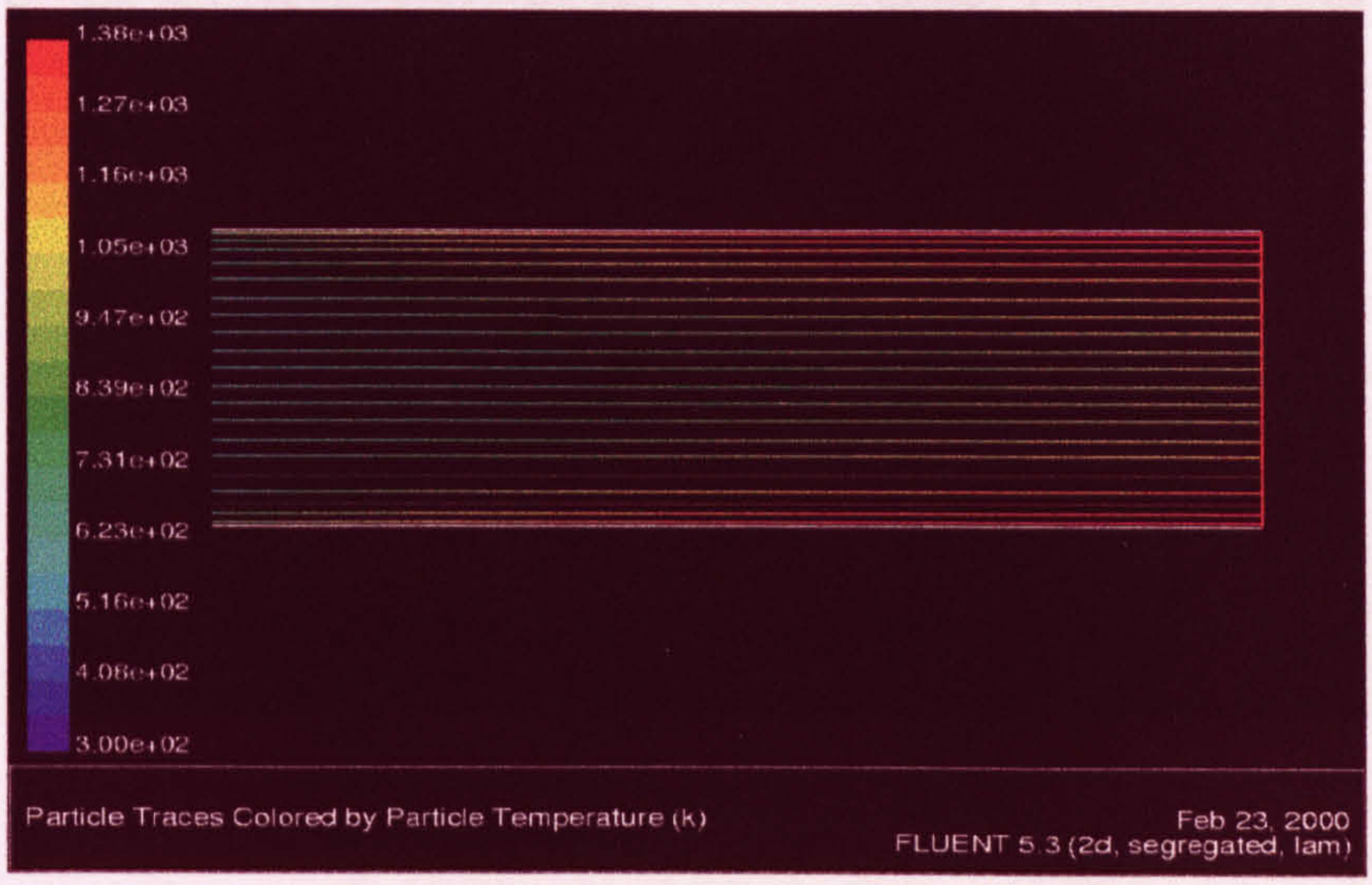
- **Inlet Velocity of 40 m/s (0.703kg/hr)**

Figure 3-8. Particle temperature distribution.



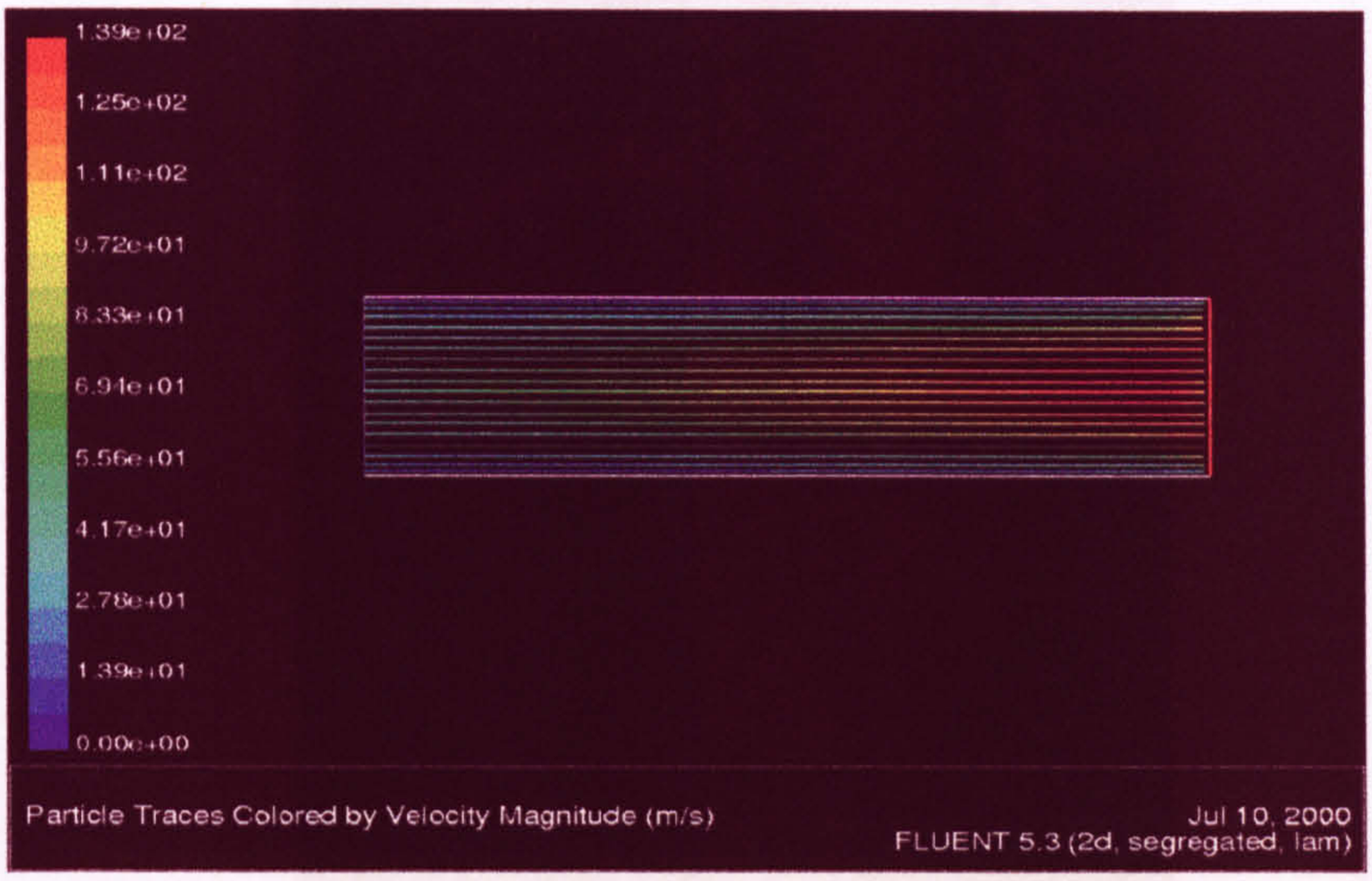
Inlet Velocity of 140 m/s (2.46kg/hr)

Figure 3-9. Particle temperature distribution.



- **Inlet Velocity of 40 m/s (0.703kg/hr)**

Figure 3-10. Particle velocity distribution.



- **Inlet Velocity of 140 m/s (2.46kg/hr)**

Figure 3-11. Particle velocity distribution.

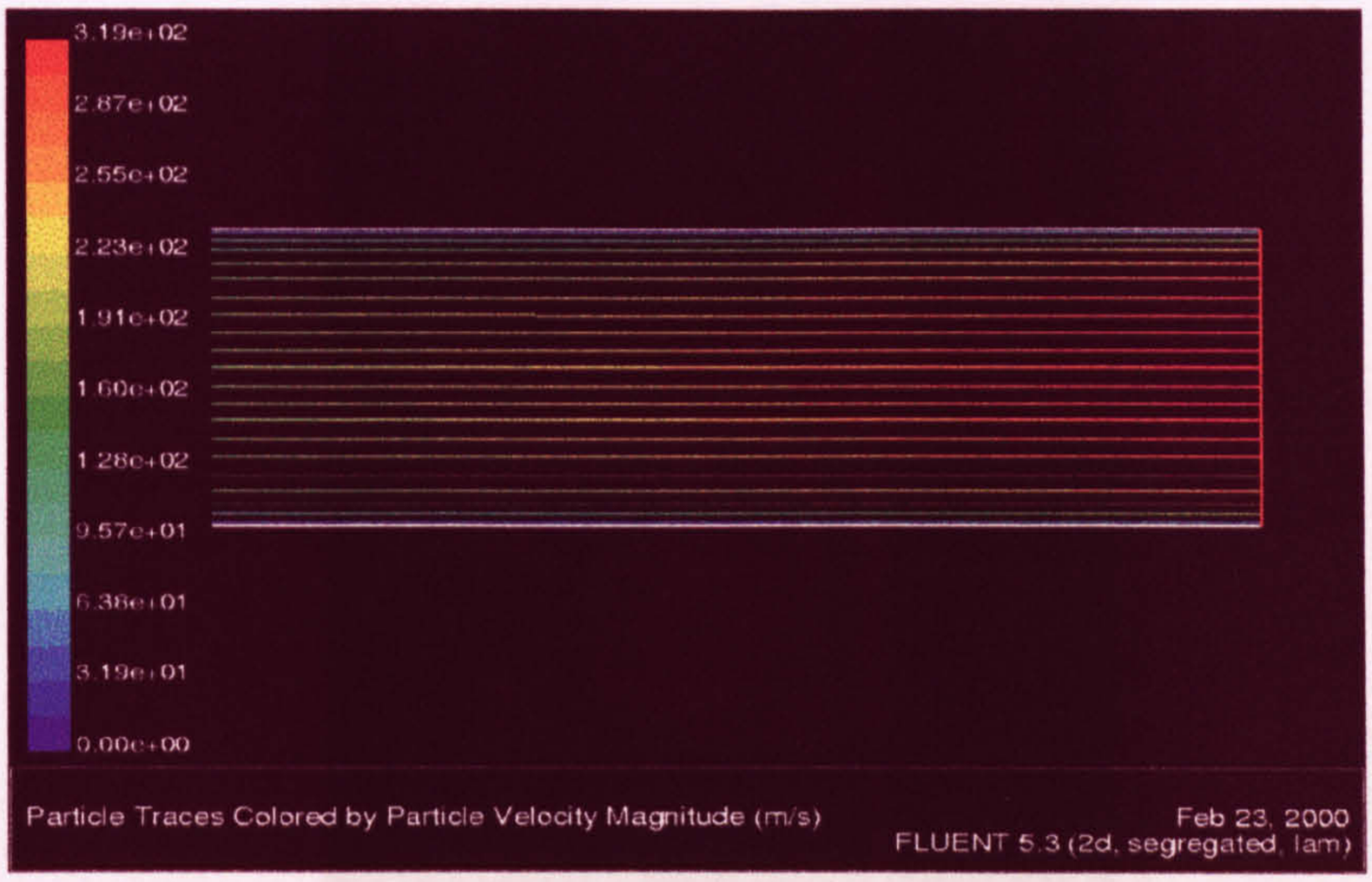


Figure 3-12. The Pressurised Particles Container.

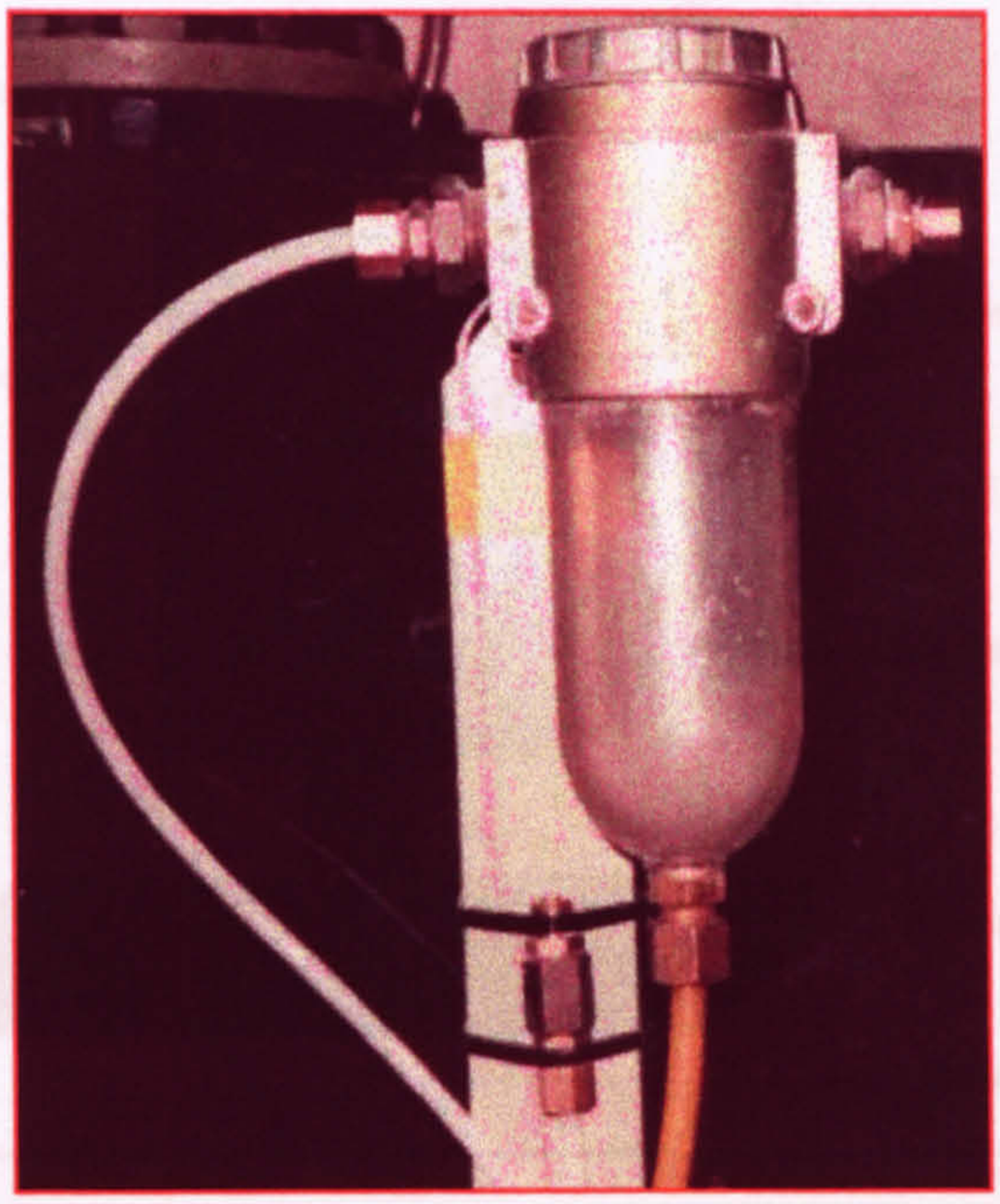


Figure 3-13. The Mechanical Vibrator.

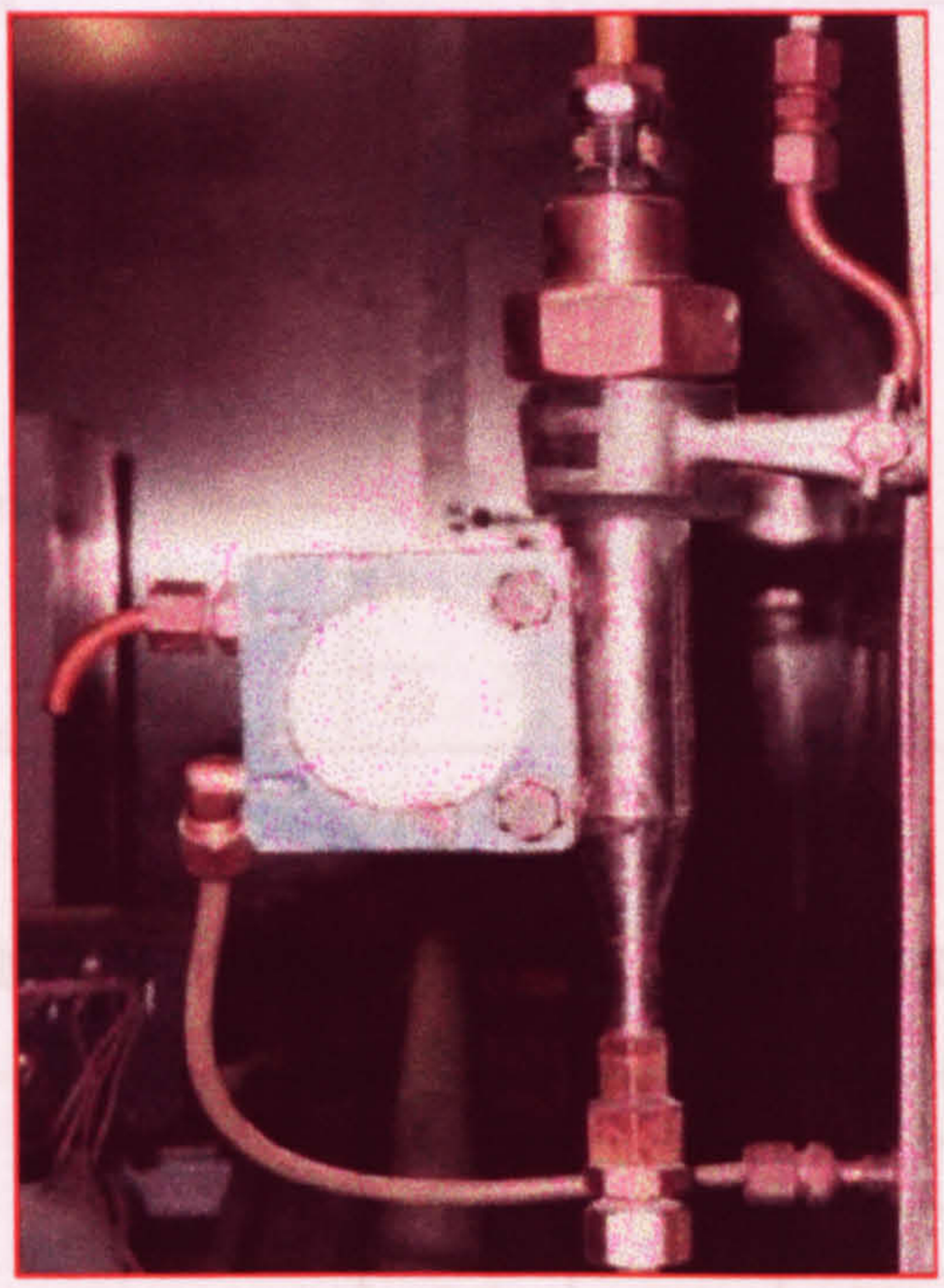


Figure 3-14. Target and Heater Holder assembly diagram.

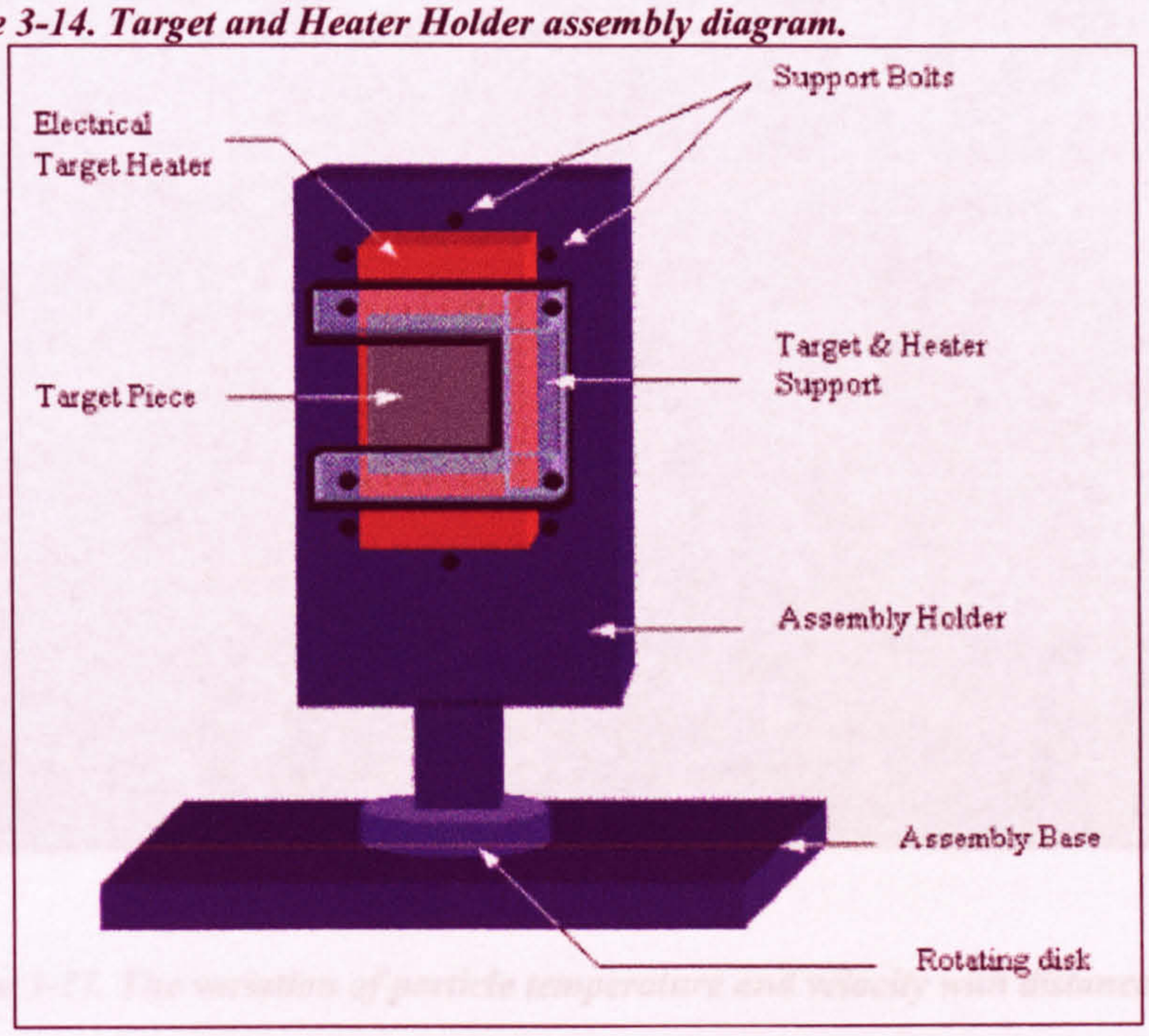


Figure 3-15. Target shape and thermocouples arrangement.

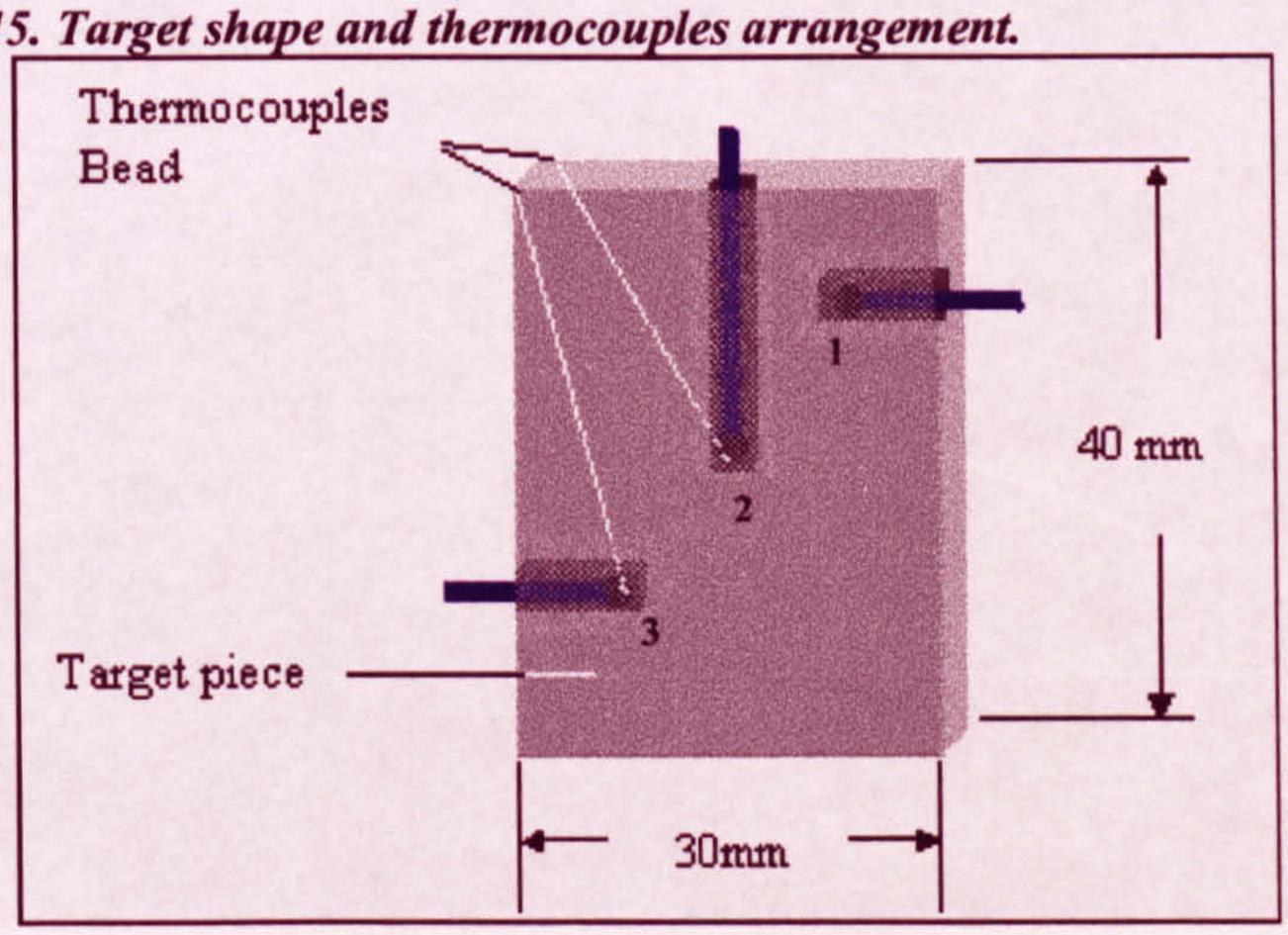


Table 3-7. Thermocouples readings at different points of the target surface.

Position	1	2	3
Thermocouples Reading	73.0	73.2	72.1
	285	289	283
	410	418	406
	710	719	703

Figure 3-16. Particle size distribution for 20-30 μm diameter

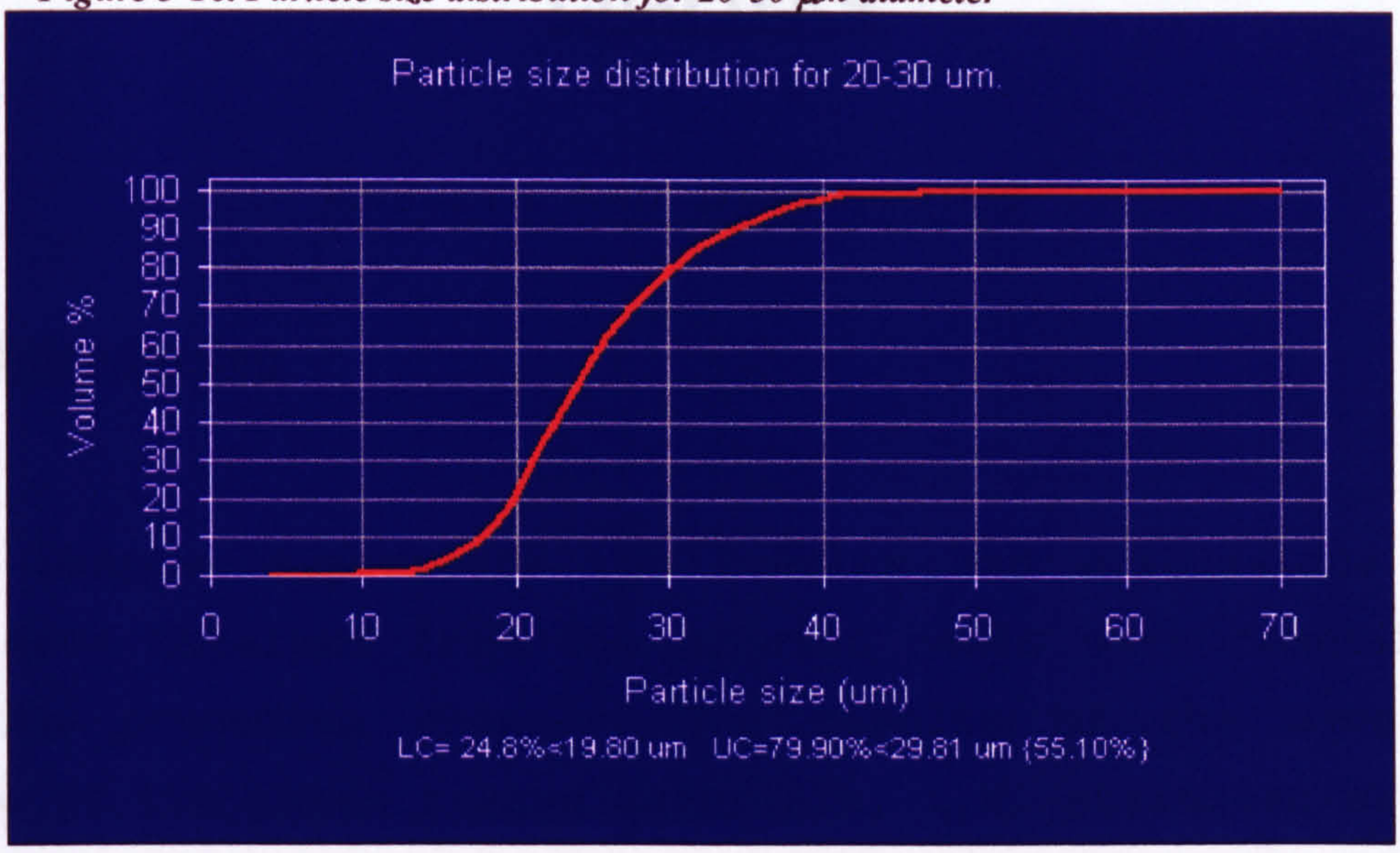
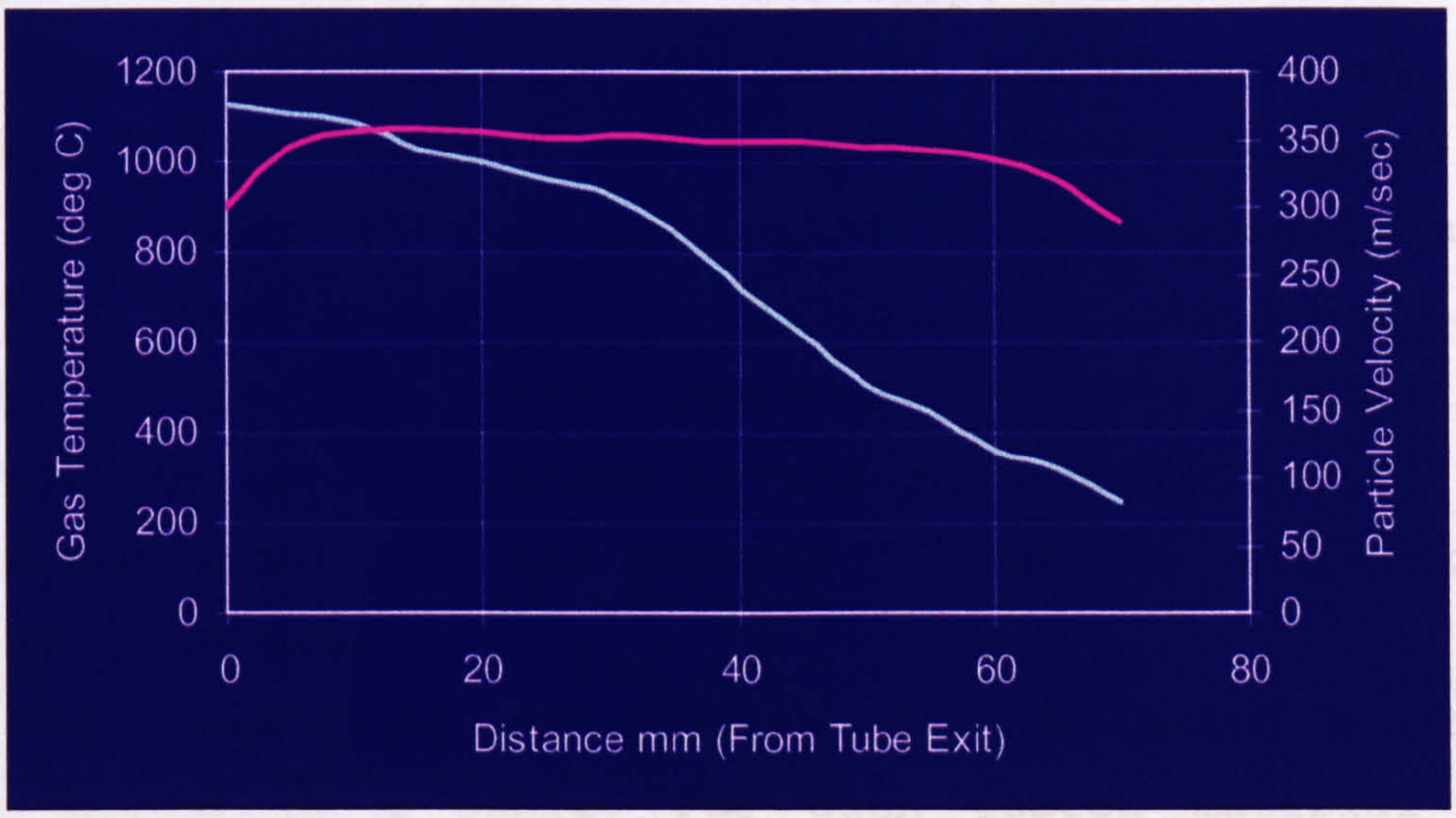


Figure 3-17. The variation of particle temperature and velocity with distance from the tube exit.



CHAPTER 4

RESULTS AND DISCUSSIONS

4.1 Introduction

This chapter represents the results and discussions of the data obtained from the erosion tests were described in the preceding chapter. The results of the erosion tests of the three tested materials, i.e. stainless steel 321, Nimonic 75 and aluminium were represented throughout this chapter associated by the illustration of mass loss graphs and Scanning Electron Microscope (SEM) figures.

The erosion behaviour of the tested stainless steel 321 targets was considered and discussed first, followed by the discussion of the Nimonic 75 erosion results and, finally, the results of the erosion tests of the aluminium targets were examined. Also a comparison between the erosion behaviour and characteristics of the stainless steel 321 and Nimonic 75 targets was carried out and discussed.

The test conditions and results of each tested material were listed in a table. For each tested material the discussions were organised in the following approach:

- the effect of target temperature on the erosion rate,
- the effect of particle temperature on the erosion rate,
- the effect of particle velocity on the erosion rate.

This was followed by the consideration of the surface examination of the tested samples. Each section was forwarded by a summary and closed with a conclusion.

The stainless steel targets were tested at different surface temperatures (HT ratios) of 285°C (HT=0.2), 415°C (HT=0.3), 570°C (HT=0.4), and 715°C (HT=0.5) and at particle temperatures of 500°C, 750°C and 950°C. The term Homologous Temperature ratio (HT ratio) is defined as the ratio of target surface temperature to its melting temperature, was used to represent the target temperature throughout this chapter. All tests were carried out at particle velocities of 200m/s, 250m/s, and 300m/s, and at two impact angles of 30° and 60°. The erosion test results were represented in the form of the mass loss curves, which gives the erosion rate as a function of one of the variables i.e target temperature, particle temperature or particle impact velocity. The effect of the target temperature (HT ratio) on the erosion rate is summarised in figure 4-1 and shown in details in figures 4-5 to 4-7 at particle temperature of 500°C, 750°C and 950°C respectively and at two impact angles of 30° and 60°. Figures 4-9 to 4-12 show the effect of particle temperature on the erosion rate at target HT ratios of HT=0.2 (285°C), HT=0.3 (415°C), HT=0.4 (570°C), and HT=0.5 (715°C) ratios respectively. The effect of the particle impact velocity on the erosion rate was considered and plotted in figures 4-13 to 4-15, which show the variation of the erosion rate with particle impact velocity at particle temperatures of 500°C, 750°C and 950°C. For the purpose of comparison between the effect of the target HT ratio and particle temperature on the erosion rate, the results from the two tests were combined in one chart at different impact velocities. Figures 4-16 to 4-18

represent the results at 30° impact angle whereas figures 4-19 to 4-21 shows the results at 60°.

The eroded surfaces of the tested samples were examined by the Scanning Electron Microscope (SEM) to give details on target surface damage morphology and to reveal the deposits amount and characteristics. The SEM output for a number of the tested samples is given in figures 4-22 to 4-35.

The Nimonic 75 targets were, similar to the stainless steel, tested at four target HT ratios (temperatures) of HT=0.2 (275°C), HT=0.3 (415°C), HT=0.4 (550°C), and HT=0.5 (690°C), and at three particle temperatures of 500°C, 750°C and 950°C. All tests were carried out at 200, 250, and 300 m/s particle velocity and at one incident angle of 30°. The resulted data were represented in the form of the mass loss curves. The effects of target HT ratio (temperature) was considered first and summarised in figure 4-36 at different test conditions, where the detailed effect is shown in figures 4-40 to 4-42. This was followed by the examination of the effect of the particle temperature which is briefed in figure 4-37 and thoroughly represented in figures 4-43 to 4-46, furthermore, the effect of particle velocity was, also, considered at different target HT ratios and particle temperatures and represented in figures 4-38 and also in figures 4-47 to 4-50. In order to determine the predominant parameter affecting the erosion behaviour of the Nimonic 75 material, a comparison between the effect of the target and particle temperature was carried out, where the results from the two parameters were combined in a single chart at different particle velocity as shown

in figures 4-51 to 4-53. Finally, the eroded surface of the tested samples was examined using the SEM to define the erosion characteristics and verify any particle deposition, is represented in figures 4-54 to 4-59.

The results of the tested aluminium targets were, also, represent and discussed in this chapter. The aluminium targets were tested at high target HT ratios of up to HT=0.8 (520°C). The tests were carried out at particle impact velocity of 100 m/s and at an incident angle of 30° and at three particle temperatures of 350°C, 550°C. Figure 4-69 shows the variation of the erosion rate of the aluminium targets with the change in the target HT ratio (temperature) at three different particle temperatures. The figure, also, shows the effect of particle temperature on the erosion rate. However, figure 4-70 shows a better presentation of this effect, on the erosion rate of the tested aluminium targets. The examination of the eroded surfaces of the tested samples was carried out using the SEM and sample results are shown in figures 4-72 to 4-76.

The unit of the erosion rate for the impact data are given in milligrams of material removed per gram of particles used (mg/g).

PAGE

NUMBERING

AS ORIGINAL

4.2 Findings for stainless steel 321

4.2.1 Summary

Stainless steel 321 is one of the materials widely used in many high temperature engineering applications including the gas turbine engines. The operation of these engines involved temperatures of about 1100°C and velocities of about 300 m/s. The current study of the erosion/deposition involved tests being conducted to simulate the effects of the target temperature, particle temperature, particle impact velocity, and impact angle on the erosion/deposition behaviour under a simulated gas turbine environment. In order to achieve this, several erosion tests were carried out at different conditions as elaborated in section 4-1 and listed in table 3-5.

Throughout this section, the effects of each tested parameter were summarised to give an overall view, while the full consideration of the results is given in separate sections. Figure 4-1 summarises the effects of the target HT ratio (temperature) on the erosion rate at particle temperatures of 500°C, 750° C, and 950°C and at particle impact velocities of 200, 250 and 300 m/s. In the figure, the solid lines represents the erosion curves at 60° impact angle while the dashed ones stand for the 30° results. In general, the stainless steel 321 targets show an increasing rate of erosion with increasing HT ratio, and that the erosion rate is greater at impact angle of 30° than at 60°. As particle temperature increases, however, the erosion rate at 30° is less affected by the change of the target HT ratio

(temperature) than that at 60°. More reference will be made to this figure when considering detailed discussion on the next few sections.

Figure 4-2 is a re-plot of the figure above to highlight the effect of particle temperatures on the erosion rate at target HT ratios of HT=0.2 (285°C), HT=0.3 (415°C), HT=0.4 (570°C) and HT=0.5 (715°C) and at different particle impact velocities. The figure shows discrete effects of particle temperature at different target HT ratios (temperatures). Generally, the erosion characteristic trends with increasing particle temperature is similar, regardless of the target HT ratio, and that the erosion rate is higher at impact angle of 30° than at 60°. Also, The pattern of the change in erosion rate as particle temperature increases is comparable at particle impact velocities of 250 and 300 m/s. In addition, the erosion rate at 60° impact angle is more affected by the change of particle temperature than at 30°.

The effects of particle impact velocity on the erosion rate at 30° and 60° were plotted on figure 4-3 at target HT ratios of HT=0.2, HT=0.3, HT=0.4 and HT=0.5. The effect of the particle impact velocity on the erosion rate is, usually, measured by the value of the velocity exponent, n, calculated from the power law equation of the form $\dot{\varepsilon}=c.V^n$, where $\dot{\varepsilon}$ is the erosion rate, c is a constant and V is the particle impact velocity. Table 4-1 lists the n values at different test conditions. With the reference to the figure and the table, the erosion rate at 30° impact angle is less affected by the change in the

particle impact velocity than at 60° at all target HT ratios (temperatures) and particle temperatures which is manifested by the values of the velocity exponent, *n*, where higher values reflect higher effects. The general trend is that the effect of particle impact velocity tends to decrease as target HT ratio increases at 30° impact angle, though, the particle impact velocity has a greater effect on the erosion rate at high target HT ratio than at impact angle of 60°.

Table 4-1. Velocity exponent, n, values at different test conditions.

			Target HT Ratio			
Particle Temperature	Impact Angle		0.2	0.3	0.4	0.5
500°C	30°	Velocity exponent *n*	1.0	0.8	1.0	1.23
	60°		3.1	2.56	2.25	2.78
750°C	30°		1.0	0.5	1.0	1.0
	60°		2.7	1.54	1.46	1.85
950°C	30°		0.68	0.95	0.52	0.5
	60°		2.04	2.45	2.33	2.64

The results from the SME generally show that there is an increasing amount of particle deposits when target HT ratio reaches HT=0.4 (=570°C) at an impact angle of 30°. The results, also, show no conclusive evidence of particle deposition at 60° impact angle for all tested target HT ratios, particle temperatures, and particle velocities.

Detailed discussion of the effect of target HT ratio, particle temperature and particle impact velocity follows. In the discussions, in addition to the above summary figures, the reference is also made to additional illustration figures to highlight the effect of each parameter.

4.2.2 Target HT Ratio (Temperature) Effect on the Erosion Rate

Target HT ratio has a conspicuous effect on the erosion/deposition behaviour of the tested stainless steel 321 targets, however, this effect depends on the other test conditions of particle temperature, impact velocity, and incident angle. Therefore the data were represented at different groups of test conditions. Figure 4-1 and figures 4-5 to 4-7 (listed at the back of the chapter) show the variation of the erosion rate with target HT ratio (temperature) at particle temperatures of 500°C, 750°C, and 950°C, respectively, and particle impact velocities of 200, 250, and 300m/s. In the figures, the dashed lines represent results at 30° impact angle, wile the solid ones stands for the results at 60°. At 500°C particle temperature the erosion rate at 30° is much higher than at 60°, however, the erosion rate at 30° is slightly less affected by the change of the target HT ratio (temperature) than at 60° at all particle impact velocities as in figure 4-5. The figures also show that the increase in the erosion rate at 30° with target HT ratio is more significant at particle impact velocity of 300m/s, while at 60° angle, the effect of target HT ratio is almost of the same order at all particle impact velocities. As particle impact velocity increases, the differences in the rate of erosion at impact angle of 30° and 60° become smaller. For example, the erosion rate at 30° impact angle is three times that at 60° when impact

velocity is 200 m/s and only two times at 300 m/s. As particle temperature increases to 750°C, figure 4-6, the effect of target HT ratio on the erosion characteristics remains almost as same as that observed at 500°C. At higher particle temperature of 950°C, target HT ratio shows different effect on the erosion trend at different velocities than at lower particle temperatures. Figure 4-7 show that the erosion rate at 30° is still higher than at 60° at all HT ratios and particle impact velocities. However, the rate of erosion at 60° (250 and 300 m/s) overlaps that at 30° (200 and 250 m/s) at target HT ratio ≥0.3. Furthermore, the gap in the erosion rate between the two angles became very much smaller at particle impact velocities of 250 and 300 m/s compared to that at 200m/s, as the rate of erosion at 30° is comparable to that at 60° at HT=0.5 at particle velocities of 300 m/s. It is clearly observed that the erosion rate at 30° increases at lower rate than at 60°, especially at high particle velocity of 250 and 300m/s.

The above-observed behaviour (the increase in the erosion rate with target HT ratio) was also observed by Tabakoff [27] and Yee [30], though the ash erosive particles were used at lower impact velocities. Figure 4-8 shows a comparison between the results obtained by Tabakoff and Yee, plotted to different scale. They have carried out the study on the effect of target temperature on the erosion rate of stainless steel 304 using similar target temperature to those considered in the present study. The erosive particles were fly ash and particle size and velocities were different from the current work. From the figure one can draw the following; the erosion rate trend

for the present work and the others' work appears very similar, where the erosion rate increases in a steady rate at low impact velocities. Despite the great differences on the erosion rate magnitude between the present work and the others' work (they used ash particles), the general trend of erosion rate with HT ratio in very similar.

The effect of particle temperature on the erosion behaviour, discussed on the next section, is not well defined in the above-considered figures and discussion, thus the data were re-arranged to show the effects and were plotted at different target HT ratios and particle impact velocities as in figure 4-2 and figures 4-10 to 4-12.

4.2.3 Particle Temperature Effect on the Erosion Rate

The effects of particle temperature on the erosion rate and behaviour of the stainless steel 321 targets were considered at target HT ratios of HT=0.2, HT=0.3, HT=0.4, and HT=0.5, and at particle velocities of 200, 250, and 300m/s. The experimental data at 30° and 60° impact angles were plotted on the same graph to compare the effect at different impact angles. During the discussion, in addition to figure 4-2 presented in section 4.2.1, the reference is also made to additional illustration figure to highlight the effect of particle temperature. Figure 4-9 shows the erosion behaviour with the change in particle temperature at target HT ratio of HT=0.2 and at different velocities. The figure shows similar erosion behaviour at 30° impact angle for all impact velocities, that is the erosion rate increases in a steady rate with the change in particle temperature, where it reaches the

maximum at particle temperature of 950°C, which is the same at all particle impact velocities. At 60° impact angle, the rate of erosion increases at an accelerated rate with particle temperature which is more rapidly than that at 30° impact angle. It was clearly observed that the gap between the erosion rate at 30° and 60° becomes smaller as particle temperature increased to 950°C and when particle velocity reached 250m/s. As target HT ratio increases to HT= 0.3, figure 4-10, the rate of erosion at 30° impact angle increases at a lower rate compared to that at 60°, however the growth at 30° tends to be more stable that at 60°. On the other hand, the rate of erosion at 60° start to increase very slowly as particle temperature increases from 500°C to 750°C, at particle velocity of 250 and 300 m/s but once the particle temperature exceeded 750°C, the erosion rate encountered a sudden augment compared to that observed at 30°. Therefore the erosion of the stainless steel 321 targets tend to be more severe as particle temperature exceeds certain limit at large impact angle of 60°. This severity depends on the target HT ratio and particle impact velocity where higher HT ratios and velocities result higher augmentation in erosion rate. When target HT ratio increases further to HT=0.4 and HT=0.5, figures 4-11 and 4-12, particle temperature effect on the erosion rate shows a distinct features than that observed at lower HT ratios. That is the erosion rate at 30° impact angle is nearly constant over the range of particle temperatures when particle velocity is 250 and 300 m/s, while at 60° impact angle, the rate of erosion continues to increase in an accelerated rate as particle temperature reaches 750°C.

Also the rate of erosion at 60° starts to overlap that at 30° impact angle when particle temperature is at 950° and at particle impact velocities of 250 and 300 m/s. Therefore, the erosion of the target material continues to increase in magnitude at high particle temperatures when the impact angle is at 60°, which is not the case at 30°, where the erosion rate tends to almost remain constant over a range of particle temperatures.

It is obvious that the particle velocity has a great influence on the erosion rate as treated on the above two sections, however, the effect has not been fully articulated, therefore the results were represented on different way to highlight the velocity effects.

4.2.4 Particle Velocity Effect on the Erosion Rate

The effect of particle impact velocity on the erosion of metals was a centre of attraction for many workers on the field of power turbines. This effect is usually manifested by the use velocity exponent *n*, which calculated from the least squares fit through the data points using $\dot{\varepsilon} = c.V^n$, which previously defined. The effect of particle impact velocity was considered and represented at different test conditions of target HT ratio and particle temperature as in figures 4-13 to 4-15. At particle temperature of 500°C, figure 4-13, particle impact velocity has approximately an even effect on the rate of erosion at 30° impact angle and at all target HT ratios (temperatures), at which the velocity exponents have almost the same magnitude of unity. Whereas at 60° impact angle, the erosion rate is very

responsive to the particle impact velocity as manifested by the high values of the velocity exponents *n*, which are in addition far greater than those at 30°. Therefore, the particle impact velocity has more significant effect on the propagation of the erosion of the stainless steel 321 targets at 60° impact angle than at 30° at all target HT ratios. The effect of particle impact velocity on erosion behaviour at 750° particle temperature is presented in figure 4-14, and shows different characteristics than those observed at lower particle temperature of 500°C. At 30° impact angle, the average change on the rate of erosion with particle velocity, manifested by the values of the velocity exponents, *n*, tends to decrease as target HT ratio increases and reaches its minimum at HT=0.5. In contrary, at 60° impact angle, particle impact velocity has an increasing effect on erosion rate at higher target HT ratios, as it attains the highest effect at HT ratio of HT=0.5 which attributed by the *n* values. Similar observations were noticed at 950°C particle temperature, figure 4-15, where the magnitude of the velocity exponent drops with the increase in target HT ratio at 30° impact angle, and increases at 60°. Hence, from the previous discussions, the dependency of erosion rate on incident velocity becomes less significant at higher target HT ratio and particle temperatures of 750°C and 950°C when the impact angle is 30° (near the angle associated with maximum erosion), while at 60° impingement angle, the dependency of the erosion on the particle impact velocity increases with target HT ratio at all particle temperatures. These observations contrast with those found by Tabakoff, et al. [27], who observed that the

erosion rate became less reliant on the impact velocity at higher impact angles when they carried out the tests using the ash particles at ambient temperature and at HT=0.3, HT=0.4, and HT=0.5. This growing discrepancy between the two observations confirms the great effect of particle temperature on the erosion behaviour.

The earlier discussion of the effects of target and particle temperature on the erosion behaviour of the stainless steel 321 did not provide the full picture of the superior parameter dominating the effect on erosion characteristics at different impact angles and velocities. Therefore, the results were reorganised in such a way to compare the predominant of the two variables and considered in the following section.

4.2.5 Comparison Between the Effect of Target and Particle Temperature on the Erosion Behaviour

To compare the influences of particle and target temperature on the erosion rate, the resulted data were combined in a single chart at 200, 250 and 300 m/s incident velocity and at 30° and 60° impact angles. At particle impact velocity of 200 and 250 m/s and at 30° impact angle, figure 4-16 and 4-17, the erosion rate tends to increase steadily with target HT ratio (temperature) at all particle temperatures, while the effect of particle temperature becomes less important at target HT=0.4 and HT=0.5, as increasing particle temperature from 750°C to 950°C resulted only a minor increase in erosion rate. This erosion characteristics also observed at 300 m/s, figure 4-18, as the erosion rate becomes less sensitive to change in the particle

temperature at target HT ratios of HT=0.4 and HT=0.5, where changing particle temperature from 500°C to 750°C and from 750°C to 950°C resulting a small change the erosion rate compared to the change with target HT ratio. Hence, in general, the erosion rate is less affected by the change in the particle temperature, especially, at HT≥0.4, than that compared with the change in target HT ratio (or temperature), therefore, at 30° impact angle, target HT ratio may be regarded as the key parameter affecting the erosion rate of the stainless steel 321 at all tested velocities. Figure 4-19 to 4-21 illustrate the compared effect of particle and target temperature on the erosion behaviour at 60° impact angle and particle velocities of 200, 250, and 300 m/s respectively. The erosion rate increases at a constant rate with the change in target and particle temperature at particle velocity of 200 m/s, figure 4-19. At 250 and 300 m/s particle impact velocities, it is clear that the erosion rate increases quite rapidly as particle temperature exceeds 750°C at all target HT ratios, while the change in erosion rate with target HT ratio remains stable at all particle temperatures as in figures 4-20 and 4-21. Hence, at 60° impact angle, particle temperature is the major parameter affecting the erosion behaviour at 250 and 300 m/s impact velocities, while target HT ratio (temperature) has a lesser effect.

The distinctive erosion characteristics observed (above) at different test conditions could be explained on the light of the results obtained from the scanning electron microscope (SEM) of the eroded surface of the tested

targets, as it will be considered in the following section.

4.2.6 Target Surface Examination

The examinations of the eroded surface of the tested samples were carried out using the scanning electron microscope (SEM) to assess the damage caused by the impacting particles and to determine any signs of deposition. The results were divided into two groups, as the erosion characteristics are different at 30° (figures 4-22 to 4-32) and at 60° (figures 4-33 to 4-35) impact angles. Figures 4-22 to 4-25 show the SEM output for the tested samples at 30° impact angle and at 200m/s. The typical ductile material 'beach wave' erosion pattern at shallow impact angles is presented in figure 4-22, where figure 4-23 and 4-24 shows a ploughing cut and cut type (I) respectively. At this impact velocity (200 m/s) there was no conclusive deposition at all particle and target temperatures, however few particles, especially of small sizes (≤5μm), were been able to deposit on the target surface as those presented in figure 4-25 which shows the deposited particles at HT=0.5 and particle temperature of 950°C with no evidence of deep cutting occurred on the eroded surface. This deposition was believed to be due to the effect of temperature grandniece in the flow field, which is known as the thermophoresis effect, or it could be as a result of electrophoresis forces. Hence smaller particles have had a greater chance to deposit on the target surface as a result of the fore-mentioned mechanisms, which usually dominate the deposition mechanism of small particles. The resulted surface

examination at 250 and 300 m/s impact velocity has, in general, shown a quite similar erosion pattern, material removal mechanisms, and particle deposition characteristics which is different from that at 200 m/s. Figures 4-26 and 4-27 shows a typical SEM output for two different types of ploughing cuts different from that observed at 200 m/s, while figure 4-28 represents type (I) cut at 250 m/s, HT=0.5 and 750°C particle temperature. Also cut type (II) was observed at these two sets of impact velocity, a typical presentation of what was observed all over the target surface is shown on by figure 4-29. However at 300 m/s particle impact velocity, the deposition is more acute especially at high particle and target temperatures than that observed at 250 m/s. Figure 4-30 shows a typical area of heavily deposited particles at target HT=0.5, 300 m/s particle velocity, and particle temperature of 950°C and areas of similar deposition concentration were observed all over the target surface. The figure shows the size of deposited particles to be varying from very small ones, circa 2.5 microns, to larger ones, ≥20 microns which have more availability. Further magnification of area with deposited particles reveals how deep particles have penetrated the hot target surface. Figures 4-31 and 4-32 shows deep embedding of small particle into the target surface at high target and particle temperatures, where particles are fully embedded into the surface causing a permanent deposit, that is different from what observed at 200 m/s impact velocity where the deposition was only superficial.

Particle deposition at high HT ratios of 0.4 (570°C) and 0.5 (715°C) when particle temperature and velocity exceed

750°C and 250 m/s respectively is believed to be due the change in target material properties at high temperatures. In general, all types of stainless steel experience a very steep drop in material hardness as surface temperature exceeds 500°C, which is below the 0.4 HT ratio for stainless steel 321 used in the currant tests. More details on material properties are given in appendix 3. When particles impinge on the hot target surface at such high velocities (≥250 m/s) and temperatures (≥750°C), causing local softening to the surface due to the elevated temperature and high impact energy, and gives the following particles a greater chance for deposition which explains the increased amount of deposition at these conditions.

At 60° impact angle, surface examination has revealed a very diverse erosion and deposition characteristics than that been found at 30°. The erosion morphology at this impact angle was of pitting type, where particles hit the target surface at large angles and rebound, leaving the surface with sharp edge holes corresponding to particle size, figure 4-33. The surface examination at this impact angle has proven only a very minor amount of deposited particles. Figure 4-34 shows the deposited particles, as white and black spots, at the central area of the eroded surface at particle impact velocity of 200 m/s, HT=0.5, and particle temperature of 950°C, which shows a very little amount of deposited particles. The same behaviour was also found at higher impact velocities of 250 and 300 m/s and the deposited particles at these settings were found to have a size range less than 10μm in diameter as shown by the figure 4-35.

The above discussions of the eroded surface may possibly put forward an explanation for the erosion behaviour at different impact conditions been seen earlier. At 30° impact angle, at high particle velocities and temperatures and at high target HT ratios, the large amount of deposited particles on the target surface over the test duration alters the variation of the sample mass and therefore, the erosion rate which is purely relates the target mass prior and after the erosion test. Hence any change in the target mass, even minor, will result a change in the erosion rate. This offers a clarification for the reduction in the increase rate of the erosion as particle temperature exceeds 750°C and at target HT ratios over 0.4 when impact angle is 30° compared to the continual growth of the erosion rate at 60°.

4.2.7 Erosion Model

In order to summarise the previous observations and discussions of the erosion behaviour of the stainless steel 321 at various test conditions, the erosion/deposition trends were moulded in a single diagram to stand as an erosion model. Figure 4-4 represents the erosion model at 30° impact angle, which shows the areas of possible deposition hatched at different directions. The inclination of the solid lines shows the degree of change in the propagation of the erosion rate with target HT ratio, while the dashed ones represent the constant velocity lines.

4.2.8 Concluding Remarks

The erosion tests of the stainless steel targets at different impact conditions has demonstrated variance erosion and deposition characteristics, depends on the impact angle, particle velocity, target temperature, and particle temperature.

The erosion rate, in general, increases at an accelerated rate as target HT ratio reaches 0.4, however, it was observed (the erosion rate) to be less affected by the change in the target HT ratio at particle impact velocity of 250 and 300 m/s when particle temperature ≥ 750°C compared to that at 200 m/s. This characteristic was only seen at 30° impact angle and not at 60° as the erosion rate continued to increase with target temperature at all impact velocities and particle temperatures. The rate of erosion was found to be less sensitive to the change in particle temperature at 30° than at 60°, when the target HT ratio reaches the value of HT=0.4 and HT=0.5. The influence of particle impact velocity on the erosion rate was found to be different at the two impact angles, where at 60° impact angle, particle velocity showed a greater effect on the variation of the erosion than at 30° impact angle. On the other hand, the effect of particle velocity becomes smaller at higher HT ratios, while it becomes more responsive at 60° as target HT ratio increases.

The target surface examinations have revealed that particles were been able to form a considerable amount of deposition only at 30° impact angle and when particle temperature is at 750°C and 950°C and at target HT ratios over 0.4.

4.3 Findings for Nimonic 75

4.3.1 Summary

The requirement for the high temperature and corrosion resistance components in the gas turbine industry is very high where the use of the engineering alloys becomes essential. One of the common alloys widely used in the high temperature applications is the 80Ni-20Cr, which has good high-temperature corrosion properties. The Nimonic 75 represents a typical example for this type of alloys, and was considered for the high temperature erosion test program to establish a good understanding of the influence of the particle and target temperature on the erosion characteristics of this type of alloys at high impact velocities. The test results and conditions, were detailed in section 4-1, are represented in table 3-5 and summarised in figures 4-36 to 4-38.

The effect of the target HT ratio on the erosion rate is presented in figure 4-36, which summarises the effect at different test conditions. In general, Nimonic 75 targets show an increasing rate of erosion with increasing HT ratio at all particle temperatures and velocities and the erosion rate is higher at higher HT ratios. However, this increase rate varies at different settings as will be discussed later in this chapter.

The summary of the effect of particle temperature on the erosion rate is shown in figure 4-37 and represented in details in figures 4-43 to 4-46. From the figure, there are distinctive effects of particle temperature at different target HT ratios but in general, the erosion rate is higher at higher particle temperature; however,

erosion rate becomes less affected by the change in particle temperature at higher target HT ratios especially at high impact velocity.

Also the effects of particle impact velocity were considered and plotted in figure 4-38. Similar to the stainless steel, the effect of impact velocity is measured by the velocity exponent *n*, as defined before, and listed in table 4-2. The general trend is that the particle impact velocity at low target HT ratios of HT=0.2 and HT=0.3, has a greater influence on the rate of erosion when particle temperature is high. Conversely, at higher target HT ratio, this effect becomes less important as particle temperature increases, which manifested by the velocity exponent.

Table 4-2. Velocity exponent, n, at different test conditions.

		Target HT Ratio			
Particle Temperature		0.2	0.3	0.4	0.5
500°C	Velocity exponent *n*	1.45	0.84	1.32	1.48
750°C		1.0	1.23	1.1	1.0
950°C		1.75	1.34	1.0	0.9

The above considerations are only a general view of the effect of the different parameters on the erosion rate and the full discussions follow in the next few sections.

4.3.2 Target HT Ratio (Temperature) Effect on the Erosion Rate

The effects of target HT ratio on the rate of erosion of the nimonic targets are fully represented in figures 4-40 to 4-42. The average increase trend of the erosion rate with target HT ratio is almost similar at all tested

particle temperatures of 500°C, 750°C and 950°C and that is the erosion rate at HT=0.5 is almost twice that at HT=0.2. However, at 500°C particle temperature, figure 4-40, the rate of erosion increases in an accelerated rate at all particle impact velocities compared to that at higher particle temperatures of 750°C and 950°C. On the other hand the erosion rate at 250 and 300 m/s impact velocity is very comparable at all particle temperatures, and that is higher than the rate at 200 m/s, specially as target HT ratio exceeds 0.3.

The effect of particle temperature on the erosion rate is not clearly defined at the above discussion; therefore the figures were re-plotted and discussed, in the next section, to highlight this effect.

4.3.3 Particle Temperature Effect on Erosion Rate

Figures 4-43 to 4-46 represent the change in the rate of erosion of the Nimonic 75 targets with particle temperature at different HT ratios. At target HT ratio of HT=0.2, figure 4-43, the erosion rate at 200 m/s, initially increases at a high rate compared to that at 250 m/s and 300 m/s, which then becomes fairly-stable, whereas at 250 and 300 m/s impact velocity the erosion rate continues to increase at constant rate. At target HT ratio of HT=0.3, figure 4-44, the erosion rate at 200 and 250 m/s becomes less affected by the change in particle temperature than at 300 m/s where the erosion rate increases continually with particle temperature. At higher target HT ratio of HT=0.4, figure 4-45, the rate of erosion at 300 m/s is still the highest, though, the erosion rate at 200 and 250 m/s increases in an accelerated rate compared to that at 300 m/s. Similar

situation was also observed at target HT ratio of HT=0.5 (690°C), where the change in the rate of erosion at 300 m/s becomes minimal, while at 200 and 250 m/s becomes higher than before, figure 4-46. Therefore, the rate of erosion becomes less affected by the change in particle temperature at high target HT ratios (HT≥ 0.4) and when the impact velocity is at 300 m/s. This diverse erosion behaviour of the Nimonic 75 targets suggests that the target material experiences certain types of property changes which effect the erosion rate. More insight into these changes will be considered when discussing the surface examination later in this chapter.

From the above discussions, the effect of particle impact velocity on the erosion behaviour cannot be ignored; nevertheless, it is not fully defined in the considered figures and discussions. Therefore the data was rearranged and re-plotted to highlight this effect which is discussed in the next section.

4.3.4 Particle velocity Effect on Erosion Rate

The discussion of particle impact velocity effect on the erosion rate is usually carried out by considering the velocity exponent *n*, previously defined. Figure 4-47 to 4-50 represent the influence of the particle impact velocity on the erosion rate at HT=0.2 (275°C), HT=0.3 (415°C), HT=0.4 (550°C) and HT=0.5 (690°C) respectively.

Figure 4-47 represents the data at HT=0.2 and shows that the rate of erosion increases at higher rate with particle impact velocity, manifested by the higher velocity exponent *n*, at particle temperature of 950°C compared to that at 500°C, while the velocity exponent at

750°C particle temperature does not follow this pattern and suggests experimental errors. Figure 4-48 shows the impact velocity effect at target HT ratio of HT=0.3 (415°C), and evidences that the rate of erosion increases at higher rate as particle temperature increases which is clearly manifested by the magnitudes of the velocity exponent *n*. In opposition, as HT ratio increases to HT=0.4 (550°C) and HT=0.5 (690°C), the effect of impact velocity becomes more significant at lower particle temperature of 500°C. Figure 4-49 shows the results at target HT ratio of HT=0.4 (550°C) where the highest effect of particle impact velocity is found to be at 500°C particle temperature followed by that at 750°C and finally at 950°C particle temperatures. Similarly, at higher target HT ratio of HT=0.5 (690°C), figure 4-50, the velocity exponent, *n*, at 500°C is higher that at 750°C and 950°C, and that also greater than what measured at HT=0.4. The preliminary conclusion, on the effect of particle impact velocity on the erosion behaviour of the nimonic 75, is; the impact velocity has various effects depending on the other impact parameters, i.e. particle and target temperatures, and as target HT ratio exceeds 0.4 (550°C), the influence of impact velocity starts to step-down at higher particle temperatures over 750°C.

As seen from the foregoing discussions of the effects of target temperature, particle temperature and impact velocity, the erosion characteristics vary at different settings. Therefore, the requirement to examine the eroded surface microscopically, which is discussed later on this chapter, was essential in order to draw a clearer picture on the damage caused to the target surface, which

caused this erosion behaviour. Also the effect of particle and target temperature on the erosion behaviour was considered previously, though the need for a comparison between the weight of the effect of the two parameters on the erosion rate at different particle velocity is necessary and is considered on the next section.

4.3.5 Comparison between the Effect of Target and Particle Temperature on the Erosion Rate.

The comparison between the effect of the target HT ratio (temperature) and the particle temperature on the erosion rate gives an overall picture for the critical parameter dominating the erosion process. To accomplish the task, data from the two variables were plotted on a single chart at different impact velocity as in figures 4-51 to 4-53. At an impact velocity of 200 m/s, figure 4-51, target HT ratio (temperature) has a greater effect on the erosion rate at 500°C particle temperature compared to that at 750°C and 950°C, where the rate of erosion increases at higher rate with target HT ratio. On the other hand, the effect of particle temperature seems to be approximately similar at all target HT ratio (temperatures), except at HT=0.2 where the erosion rate start to increase at an accelerated pace as particle temperature changes. Furthermore, at 200 m/s impact velocity, the change in the rate of erosion is more affected by the change in target HT ratio (temperature) than the change in particle temperature. Hence at this impact velocity of 200 m/s, the change in target HT ratio (temperature) may be considered as the controlling parameter affecting the erosion behaviour of the tested Nimonic 75 targets. At particle impact velocity of 250

m/s, figure 4-52, the rate of increase in erosion with target HT ratio is approximately constant at all particle temperatures, however, this (the rate of increase) is higher than that increase rate with particle temperature which is minimal at all HT ratios. Hence, target HT ratio (temperature) has more considerable effect on erosion rate than the effect of particle temperature at 250 m/s impact velocity. At higher impact velocity of 300 m/s, figure 4-53 the erosion rate is more affected by the change in target HT ratio at 500°C than that at 750°C and 950°C and the least effect was seen to be at 950°C. Also the effect of particle temperature on erosion rate varies with HT ratio, where the highest rate of increase in erosion as particle temperature changes was observed at HT=0.2 and HT=0.3, and the lowest to be at HT=0.5. It is clear, at this impact velocity of 300 m/s, that the change in the erosion rate with particle temperature is almost negligible at target HT ratios of HT=0.4 and HT=0.5, thus, particle temperature has a very minor effect on the erosion rate when target HT ratio exceeds 0.4, while target HT ratio (temperature) still the controlling parameter on the change of erosion rate. The above observations suggests that the erosion characteristics change with both target and particle temperature, especially at high impact velocities like that seen at 300 m/s. The rational explanation of this behaviour at 300 m/s impact velocity and when target HT ratio ≥0.4 is that the target has experienced smaller change in the after test weight, which appeared as a reduction in the erosion rate, which could be due to particle deposition. The surface examination using the

scanning electron microscope (SEM) can give a clear picture of the causes.

4.3.6 Surface Examination using SEM

The eroded surface of the Nimonic 75 target material was examined using the scanning electron microscope (SEM) in order to explore the damage morphology caused by the impacting particles and to determine the conditions of particle deposition which can give an explanation to the erosion behaviour observed earlier in this chapter. The surface examination has revealed comparable results at impact velocities of 200 and 250 m/s, which is different from that at 300 m/s. The erosion pattern seen at all velocities was of 'beach wave' type, similar to that found in the stainless steel at 30° impact angle, as presented in figure 4-54. The general material removal mechanism found at all impact velocities was of type (I) cut similar to that presented in figure 4-55. The surface examination has revealed only a trivial amount of deposited particle at 200 and 250 m/s impact velocities at all particle and target temperatures. Figure 4-56 shows a sample of the few particles deposited on the target surface at impact velocity of 250 m/s, target HT ratio of HT=0.4 and particle temperature of 750°C, where the size of deposited particles ranged between 5μm to 20μm in diameter. The SEM examination of the target surface at 300 m/s has shown an excessive signs of deposition as particle temperature reaches 750°C at target HT ratio ≥0.4. A typical SEM results at 300 m/s impact velocity are presented by figures 4-57 to 4-59. Figure 4-57 and 4-58 shows a sample SEM output at the 300 m/s

impact particle velocity, target HT=0.5 and particle temperature of 950°C where different sizes of the deposited particles were spread all over the target surface, as the figures only show an example of the observed deposition. At lower particle temperature of 750°C, the deposited particles tend to be less concentrated and smaller in size than that at 950°C temperature as shown in figure 4-59, which shows the deposited particles at 750°C particle temperature, HT=0.5 and 300 m/s impact velocity. The deposition of particles at these conditions reveals that the nimonic 75 target material behaves differently at high temperatures as the Nimonic alloys experience a steep reduction in hardness and stress as their temperature reaches 500°C (≅0.4 HT), as shown in figure 3-2 in Appendix 3. Therefore, the surface examination together with the material properties can offer a clarification for the erosion behaviour at different test conditions; the target sample becomes softer as its temperature exceeds 500°C (HT≅0.4), and under this condition, more particles were able to embed in the target surface as particle temperature reaches 750°C. This high particle temperature causes more softening as impacting the surface at high velocity of 300 m/s, which increases the chance of deposition and explains the small changes in the erosion rate at high particle temperatures over 750°C and high target HT ratio ≥0.4 (≥500°C).

4.3.7 Erosion Model

In order to summarise the previous observations and discussions of the erosion behaviour of the Nimonic 75 at various test conditions, the erosion/deposition trends

were moulded in a single diagram to stand as an erosion model. Figure 4-39 represents the erosion model at 30° impact angle, which shows the areas of possible deposition hatched at different directions. The inclination of the solid lines shows the degree of change in the propagation of the erosion rate with target HT ratio, while the dotted ones represent the constant velocity lines.

4.3.8 Concluding Remarks

The experimental examination of the erosion/deposition of the Nimonic 75 targets at 30° impact angle has revealed different erosion characteristics depending on test conditions of particle temperature, target HT ratio and particle impact velocity. The change in target HT ratio (temperature) was found to be influencing the rate of erosion more than the change in particle temperature at all impact velocities. Also the erosion rate found to be increasing in an accelerated rate with particle temperature at low HT target ratios of HT=0.2 and HT=0.3, which becomes smaller at HT≥0.4. Furthermore, the effect of particle velocity depends on target and particle temperature, where the impact velocity at low target HT ratios (HT=0.2 and HT=0.3) tends to have a greater effect on erosion at high particle temperature of 950°C but gradually becomes smaller as target HT ratio exceeds 0.4. The target surface examination revealed that the erosion characteristics at 200 and 250 m/s are similar and particle deposition starts as particle temperature reaches 750°C and target HT ratio ≥0.4 and at particle impact velocity of 300m/s.

4.4 Comparison Between the Erosion Behaviour of Stainless Steel 321 and Nimonic 75 at 30°

4.4.1 Introduction

It is well known that the erosion characteristics for certain material depends on several parameters such as impact velocity, target temperature, impact angle, etc, and material properties, which varies (the erosion behaviour) with accordance to these variables and the erosion characteristics vary from one material to another. In the current study, it was clear that the stainless steel has exhibited different erosion characteristics from the Nimonic 75 at 30° impact angle and at same test conditions of impact velocities, target HT ratios and particle temperatures. This variation in the erosion/deposition behaviour depends mainly on the mechanical and thermal properties of the two materials. Some of these properties were listed in chapter 3. This section is about a comparison between the effects of the parameters under consideration, i.e. target temperature, particle temperature, and impact velocity, on the erosion rate of the stainless steel 321 and Nimonic 75 target materials. To accomplish this task, the data collected from the tests of both materials were combined in a single chart to highlight the effect of each single parameter on the erosion rate.

4.4.2 Results and Discussions

The general observation is that the erosion rate of the stainless steel is higher than that of the nimonic 75 at all impact velocities and temperatures. However the gap

in erosion rate changes at different impact conditions, and the growth rate of erosion also varies depending on test conditions.

At 200 m/s impact velocity, the erosion rate of the stainless steel target is greater than the erosion rate of the Nimonic at all particle and target temperatures as shown in figure 4-60 and the gap in erosion rate between the two materials seems to be constant at different particle and target temperatures. Figures 4-61 and 4-62 show the effect of the target HT ratio on the erosion rate of the two materials at 250 and 300 m/s impact velocity respectively and show that the erosion rate of the stainless steel is still higher than that of the Nimonic, but the difference between the two rates is smaller than that at 200 m/s impact velocity. Figures 4-63 to 4-65 show the effect of particle temperature on the erosion rate of the two materials at particle velocity of 200, 250, and 300 m/s respectively. Figure 4-63 shows that the erosion rate of the stainless steel is far higher than the Nimonic at all target and particle temperatures. At impact velocity of 250 and 300 m/s, figures 4-64 and 4-65, the gap of erosion, again, becomes smaller particularly at target HT ratios of HT=0.4 and HT=0.5 as particle temperature exceeds 750°C.

The effect of particle impact velocity on the erosion rate is shown in figures 4-66 to 4-68 at different particle temperatures. In general the increase in the rate of erosion of the Nimonic 75 with impact velocity is faster than that of the stainless steel which is manifested by the velocity exponent, n, listed in table 4-3.

Table 4-3. Velocity exponent, n, of stainless steel 321 and Nimonic 75 at 30° impact angle and at different test conditions.

			Target HT Ratio			
Particle Temperature	Impact Angle		0.2	0.3	0.4	0.5
500°C	St St 321	Velocity exponent n	1.0	0.8	1.0	1.23
	NI 75		1.45	0.84	1.32	1.48
750°C	St St 321		1.0	0.5	1.0	1.0
	NI 75		1.0	1.23	1.1	1.1
950°C	St St 321		0.68	0.95	0.52	0.5
	NI 75		1.75	1.34	1.0	0.9

Hence, for an instant, stainless steel shows better erosion resistance than Nimonic 75 at particle impact velocity of 250 and 300 m/s and at all target HT ratios and particle temperatures. But the Nimonic 75 shows better thermal properties than stainless steel 321, as the former is able to operate normally at temperature range of 600-1100°C and is able to retain its hardness over a higher range of temperature than stainless steel. Then the possible cause of this behaviour is that particles start to form deposition on the stainless steel targets as impact velocity reaches 250 m/s at target HT≥0.4 (where the reduction of hardness starts) and particle temperature of 750°C, which is not observed in Nimonic targets. This deposition can give the explanation of the reduction in the erosion rate of the stainless steel at higher velocity and temperature compared to the erosion rate of the Nimonic targets, which only encountered particle deposition at 300 m/s impact velocity, target HT≥0.4 as particle temperature exceeds 750°C, which was revealed from the target surface examination. The surface examination, also, shown similar

erosion pattern i.e. 'beach wave' pattern, but different material removal mechanisms as only type (I) cut was seen on the Nimonic surface, while different types of ploughing and type (I) and (II) cuts on the stainless steel surface.

4.4.3 Concluding Remarks

The above considerations of the erosion characteristics of the Nimonic 75 and stainless steel 321 targets have led to the following conclusions; the nimonic 75 target has shown a better erosion resistance over a wide range of particle and target temperatures and shown different material removal mechanisms. On the other hand, particle deposition started to form on the stainless steel target at lower particle temperatures and impact velocities. Hence Nimonic 75 can be considered of having a better ability to resist erosion and particle deposition than stainless steel 321 at elevated operating temperatures.

4.5 Findings for Aluminium

4.5.1 Introduction

The examination of the erosion behaviour of metal at near the melting temperature is one of the objectives of the current work. Aluminium target was chosen to be examined at high target HT ratios up to HT=0.8, since it has low melting temperature which is achievable using the current test facilities. The choice of this target HT ratio was required in order to establish better understanding of the effect of target and particle temperatures at such conditions which could be experienced during the operation of the gas turbine engine. Though the aluminium is not used in the gas turbine engines, it still represents an example of the ductile materials behaviour. Hence the results found in this study can give a general sought of material behaviour under these severe operating conditions (high HT ratio and high particle temperature compared to the target melting temperature). The aluminium targets used in the tests have a melting temperature of 650°C and targets were tested at HT ratios (temperature) between HT=0.3 (195°C) and HT=0.8 (520°C) and at particle temperatures of 350°C, 550°C and 750°C while the impact angle was set at 30° and at 100 m/s particle impact velocity. The test conditions and results are listed in table 3-5.

4.5.2 Results and Discussions

The examination of the effect of target HT ratio (temperature) on the erosion behaviour of the aluminium

targets was carried out at six different HT ratios, ranging from HT=0.3 to HT=0.8, and at three particle temperatures of 350°C, 550°C and 750°C. The aluminium has shown diverse erosion characteristics to stainless steel 321 and Nimonic 75 targets as shown in figure 4-69, which represents the results of erosion rate versus target HT ratios at different particle temperatures. From the figure, the maximum erosion rate was at particle temperature of 350°C and the erosion rates at particle temperatures of 550°C and 750°C are almost identical as the curves seem to be overlapped, i.e. both particle temperatures have, virtually, the same influence on the erosion of the aluminium targets as target HT ratio changes. The erosion rate starts at low values at HT=0.3 for all particle temperatures and as target HT ratio increases, the erosion rate increases in an accelerated rate at particle temperature of 350°C, while it increases (the erosion rate) at lower rate at 550°C and 750°C particle temperatures until it reaches the maximum at target HT=0.6 (390°C). In the same way, erosion rate drops to lower values as target temperature increases to 520°C (HT=0.8). This erosion characteristic of the aluminium target as HT ratio changes consists with the results found by Yee [30], where he found that the erosion rate of the tested aluminium targets starts to increase in an accelerated rate and reaches its maximum at target HT ratio of HT=0.45 which then drops again to its minimum, though he used ash particle at slightly higher impact velocity of 130 m/s and impact angle of 35°, his results are shown in figure 4-70. He found that the maximum erosion rate occurred at target HT ratio of HT=0.45 compared to HT=0.6 for the current study which may be

attributed to the fact that he used different erosive material at ambient temperature only.

It is clear that the particle temperature has a great influence on the erosion behaviour of the aluminium targets but this effect is still not clearly defined in figure 4-69; hence the results were re-plotted to highlight this effect as in figure 4-71. The erosion rate was found to be maximum at the lowest tested particle temperature of 350°C when target HT ratio is at HT>0.4 and it (erosion rate) starts to fall abruptly as particle temperature increases to 550°C, which is close to the target melting point of 650°C where the steepest drop in the erosion rate was found to at target HT ratios of HT=0.7 and HT=0.8 as particle temperature changes from 350°C to 550°C. In general, increasing particle temperature further causing a negligible change in erosion rate when particle temperature exceeds 550°C, where the curves become almost flat. At target HT ratios of HT=0.3 and HT=0.4, the target material responses differently to that seen at higher HT ratios; that is the erosion rate continually increases with particle temperature and reaches the maximum at 750°C. The above observed erosion behaviour could be explained on the light of the microscopic surface examination carried out using the SEM and discussed in the following section.

4.5.3 Surface Examination using SEM

The eroded surfaces of the tested aluminium targets were examined using the scanning electron microscope (SEM) and the results have exposed important features of the particle-target interaction during the impact at particle temperature exceeds the target melting point and target

temperatures near the melting point (HT=0.8). The presentation of the SEM output will focus on the target tested at high particle temperatures in order to find out what caused the erosion rate to drop as particle temperature reaches or exceeds the target melting point and to identify the conditions of particle deposition. Figure 4-72 shows a typical view of erosion pattern at 350°C particle temperature, which is of ploughing type while figure 4-73 and 4-74 shows different material removal mechanisms at particle temperatures of 550°C and 750°C respectively which involved a local melting process due to the high particle temperature (compared to target melting temperature). Deposited particles, like that shown in figure 4-75, were intensely seen all over the target surface at 350°C particle temperature settings as target HT ratio exceeds 0.6 (390°C), which explains the reduction in the apparent erosion rate occurred as target HT ratio go beyond 0.6, where the deposited particles reduce the change in target weight after impact which directly reduces the erosion rate. Figure 4-76 shows one area of heavily deposited particles at particle temperature of 550°C and target HT=0.8 (520°C) where the deposited particles have sizes as large as 20-30μm, which is shown in the enlarged figure. Surface examination has shown that the particle deposition is, in general, more significant at particle temperatures of 550°C and 750°C and there is more deposited particles at target HT ratios over 0.6 (390°C) at all particle temperatures. Owing to the properties of the aluminium material, i.e. low melting point and low hardness value, the hot particles were able to cause local melting in the target surface,

especially at high surface temperatures (HT≥0.6). Once the local melting occurred, particle would tend not to rebound after impact, leaving the surface with a substantial amount of deposition.

4.5.4 Concluding Remarks

The aluminium targets have shown different erosion characteristics than the stainless steel and the Nimonic 75 targets, where the erosion rate is higher at lower particle temperature. The aluminium has exhibited different material removal mechanisms at different particle temperatures which also different from those seen on the stainless steel and Nimonic targets. The particle deposition on the aluminium targets surface had occurred over a wide range of particle and material temperatures and it is more severe at target HT≥0.6 (390°C) and as particle temperature exceeds 550°C. Hence particles at high temperature, which exceeds target melting temperature, impact the target surface at relatively low velocity (100 m/s) tend to form significant deposits on the surface when the target HT ratio exceeds the value of 0.6 and when particle temperature reaches or exceeds the target melting temperature

List of Figures for Stainless Steel 321.

Effect of Target HT Ratio (Temperature)

Figure 4-1. The erosion rate verses target HT ratio at different particle temperatures and impact velocities.

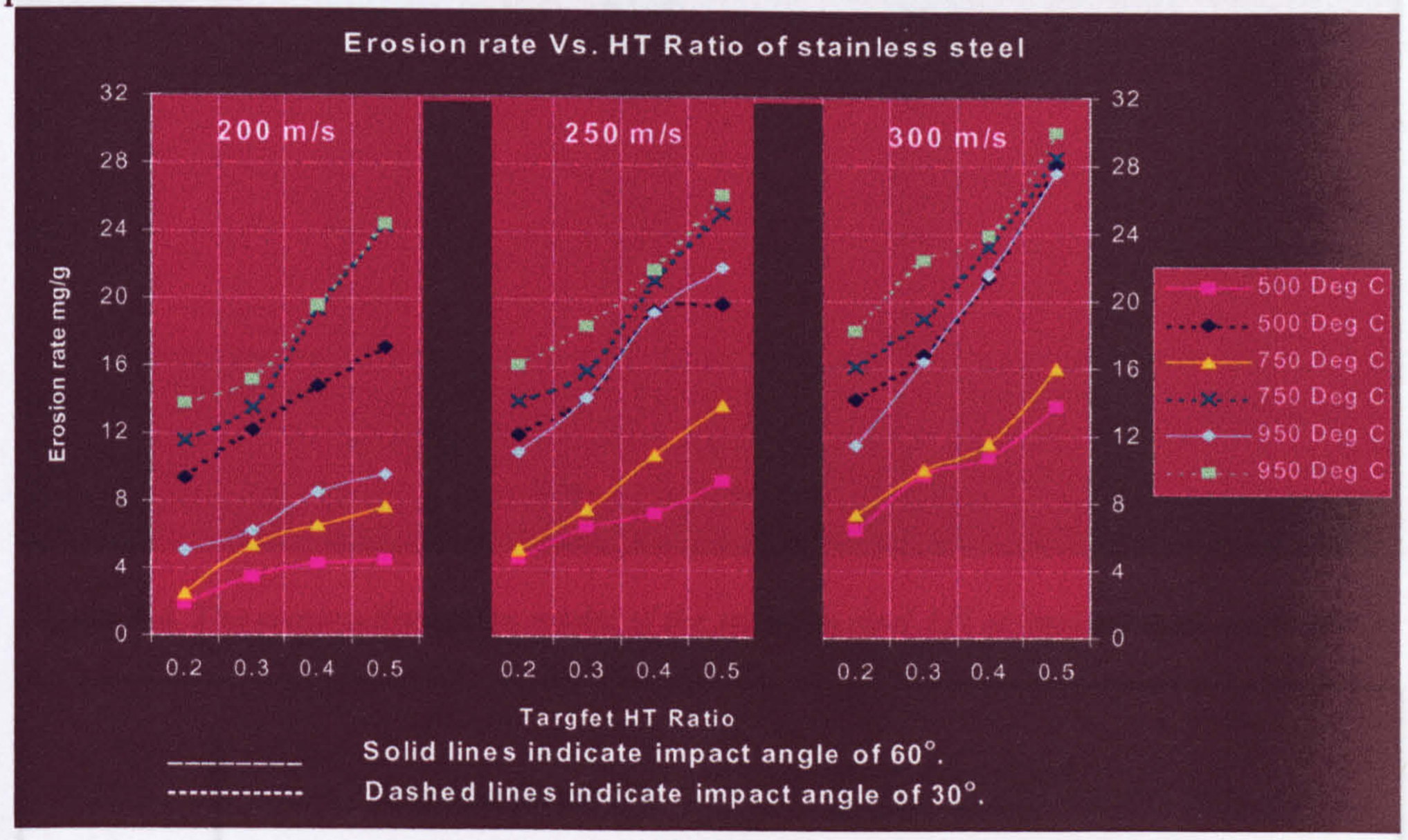


Figure 4-2. The erosion rate verses particle temperature at different target HT ratios and impact velocities.

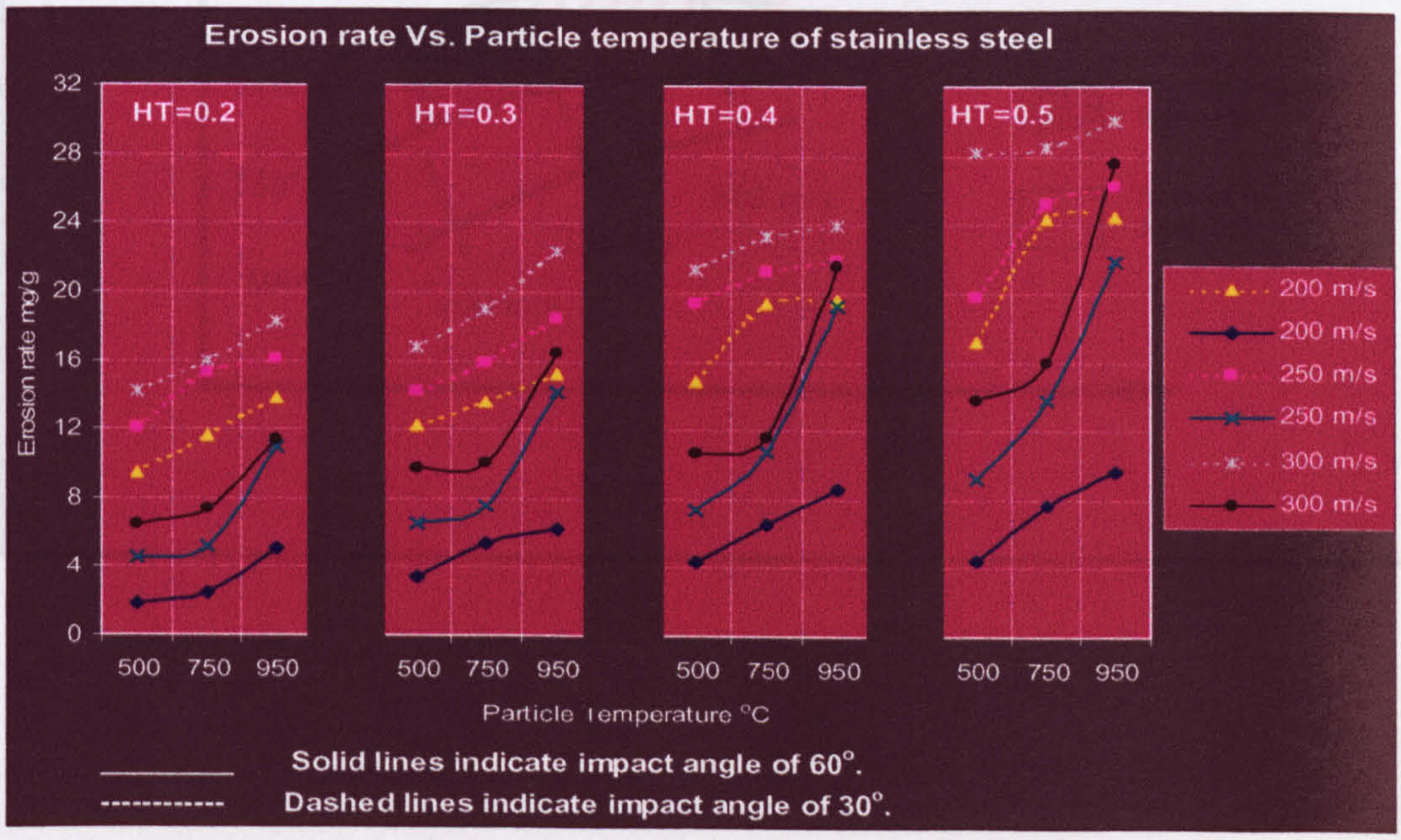


Figure 4-3. The erosion rate verses particle impact velocity at different target HT ratios and particle temperature.

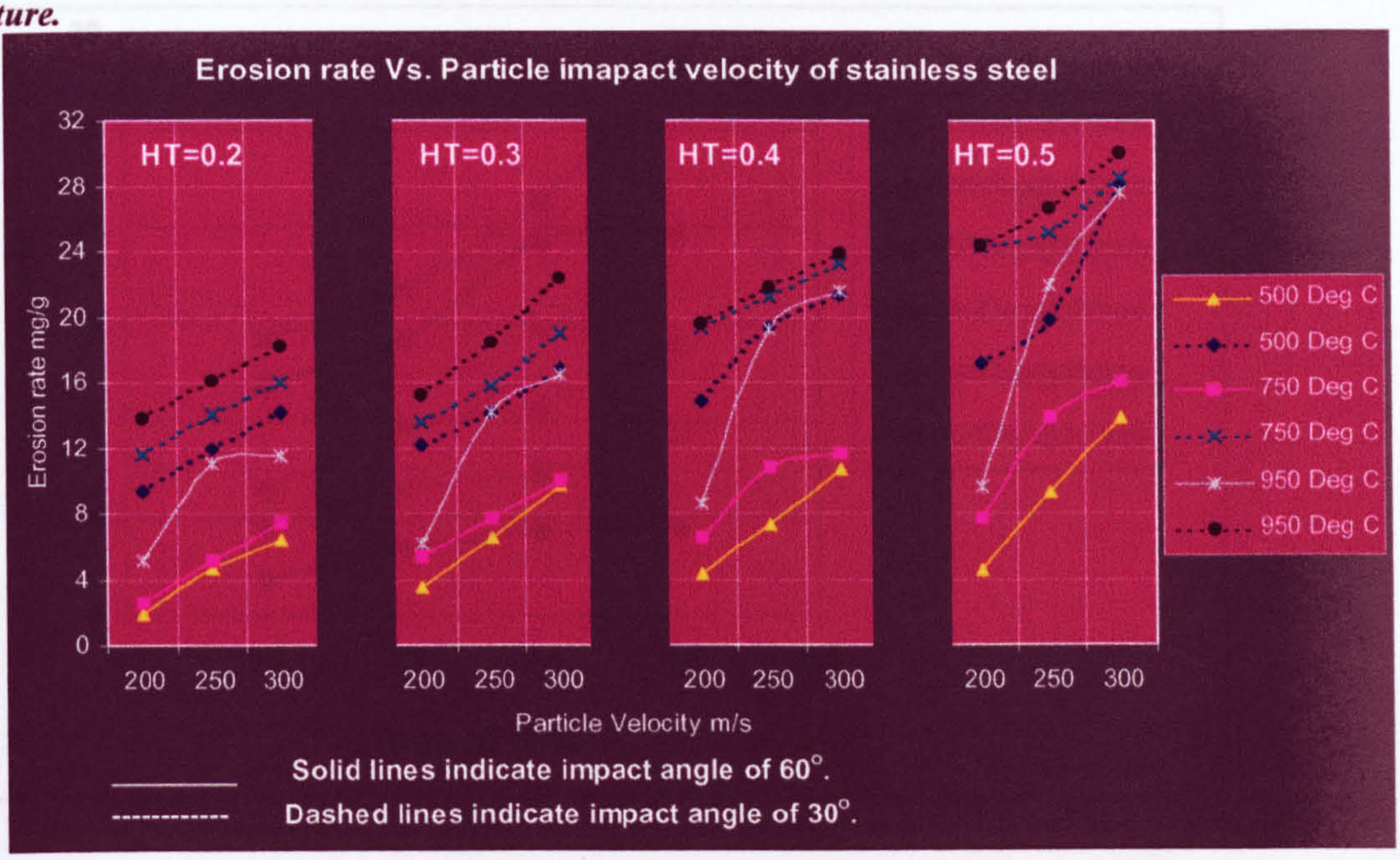


Figure 4-4. The erosion/deposition model of the stainless steel 321 at impingement angle of 30°.

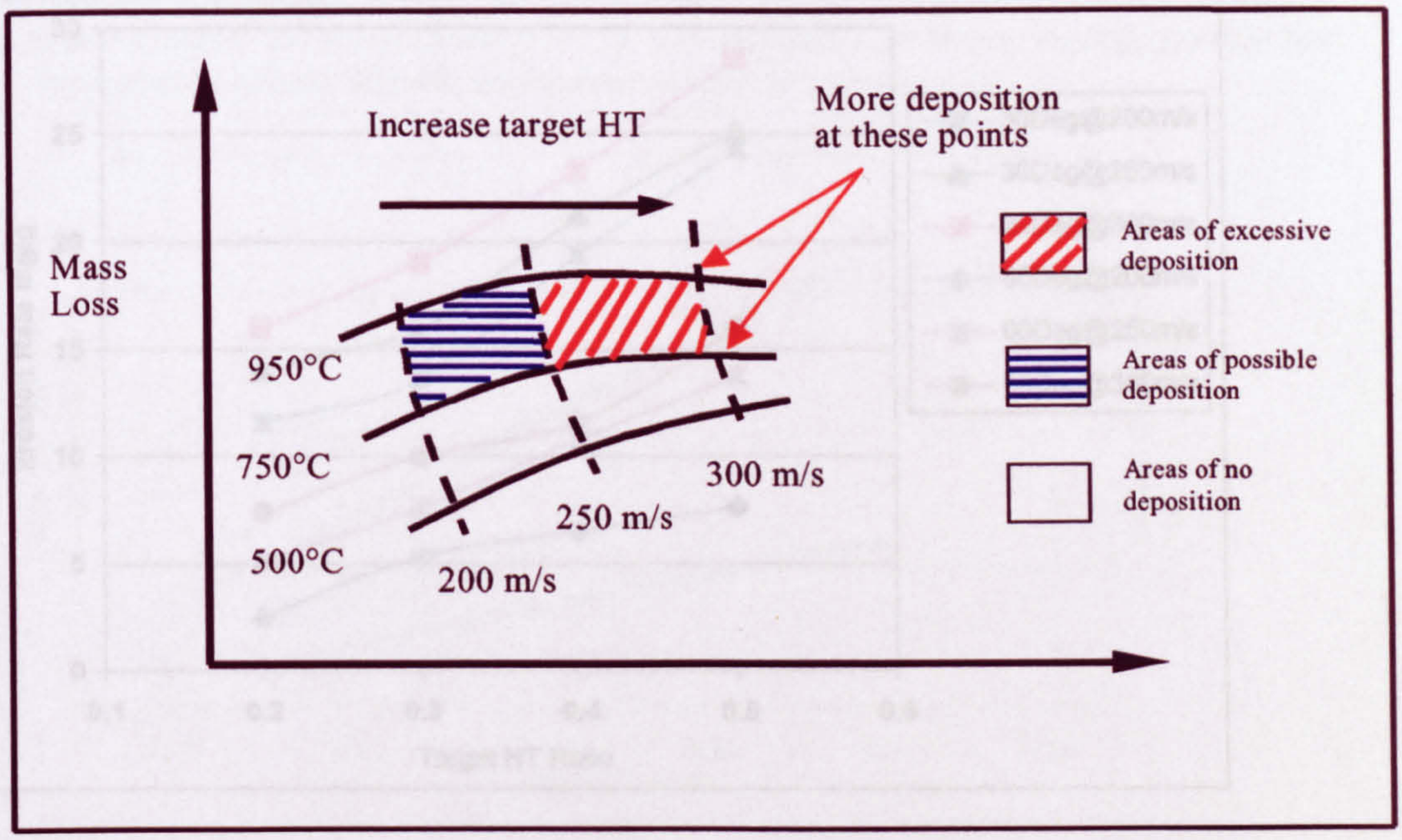


Figure 4-5. Erosion rate versus target temperature at particle temperature of 500℃.

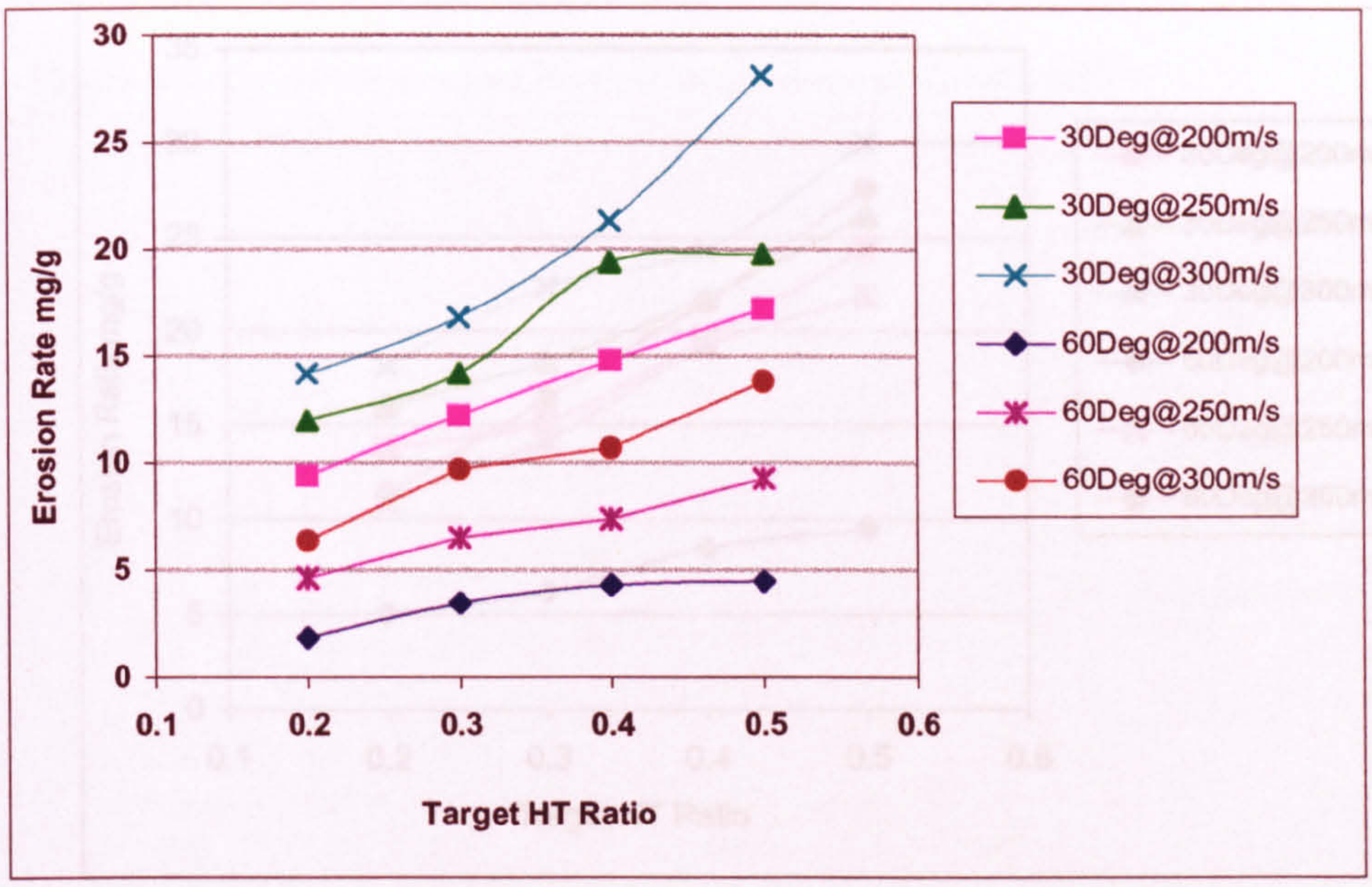


Figure 4-6. Erosion rate versus target temperature at particle temperature of 750℃.

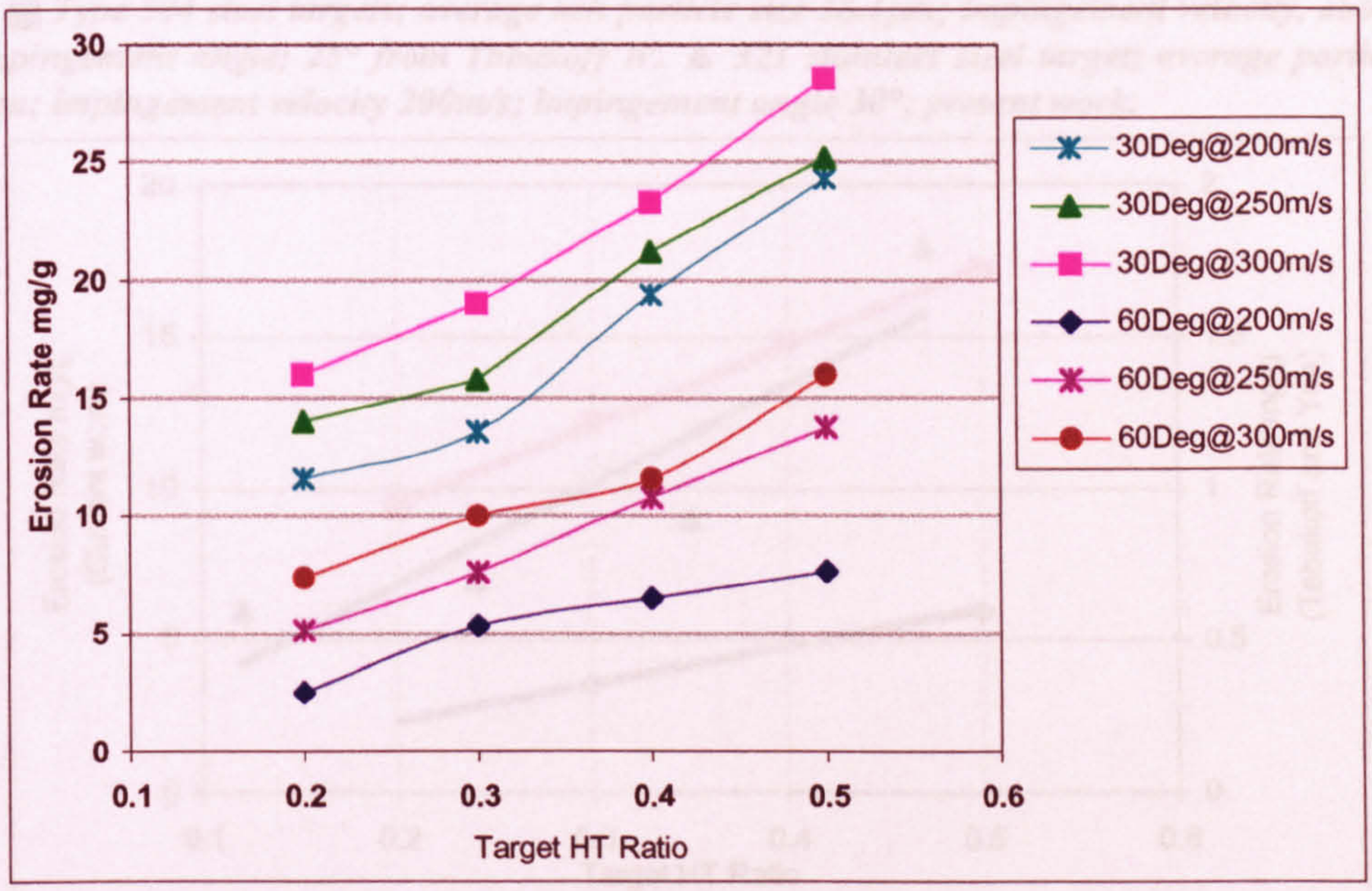


Figure 4-7. Erosion rate versus target temperature at particle temperature of 950℃.

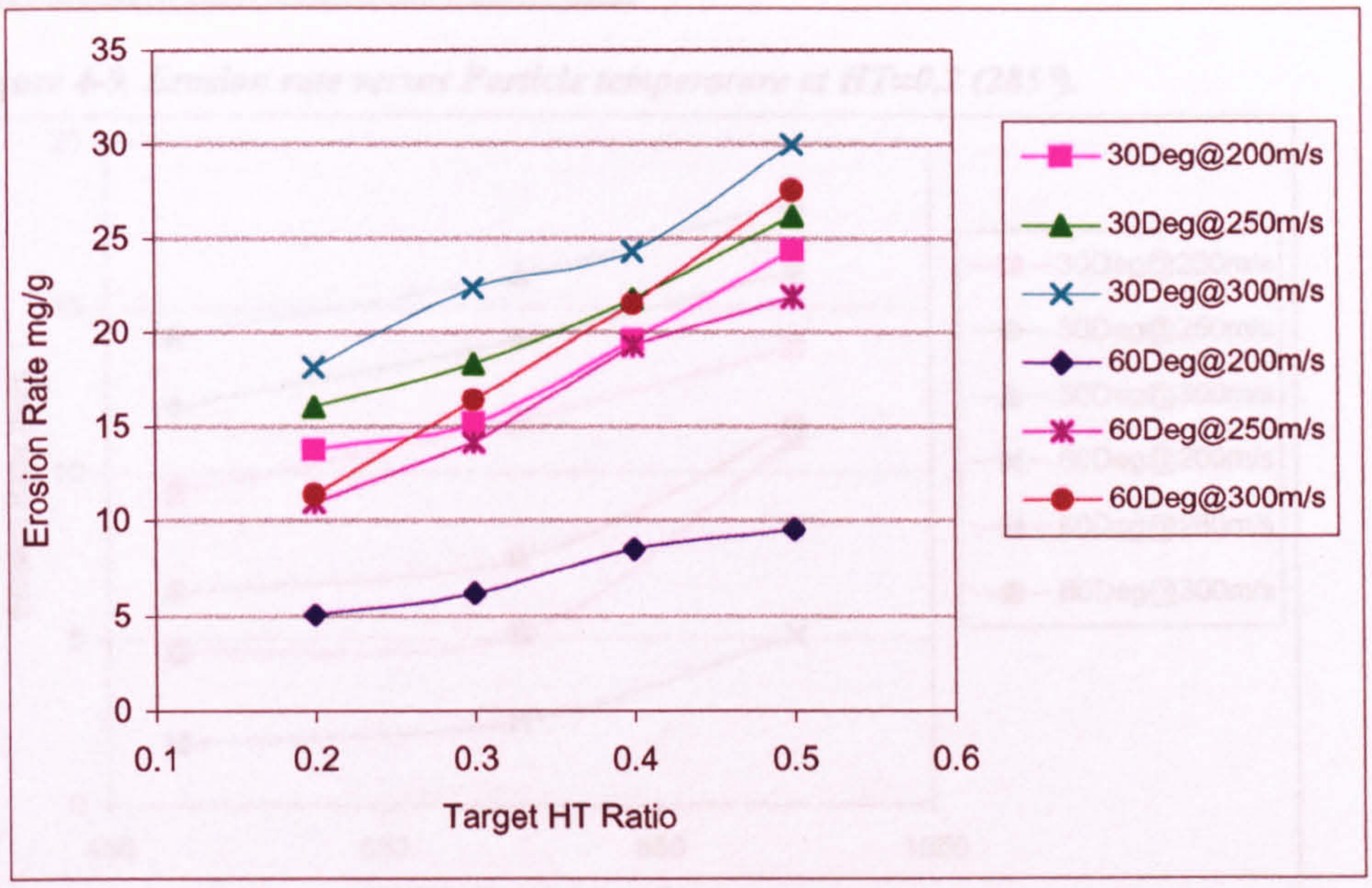
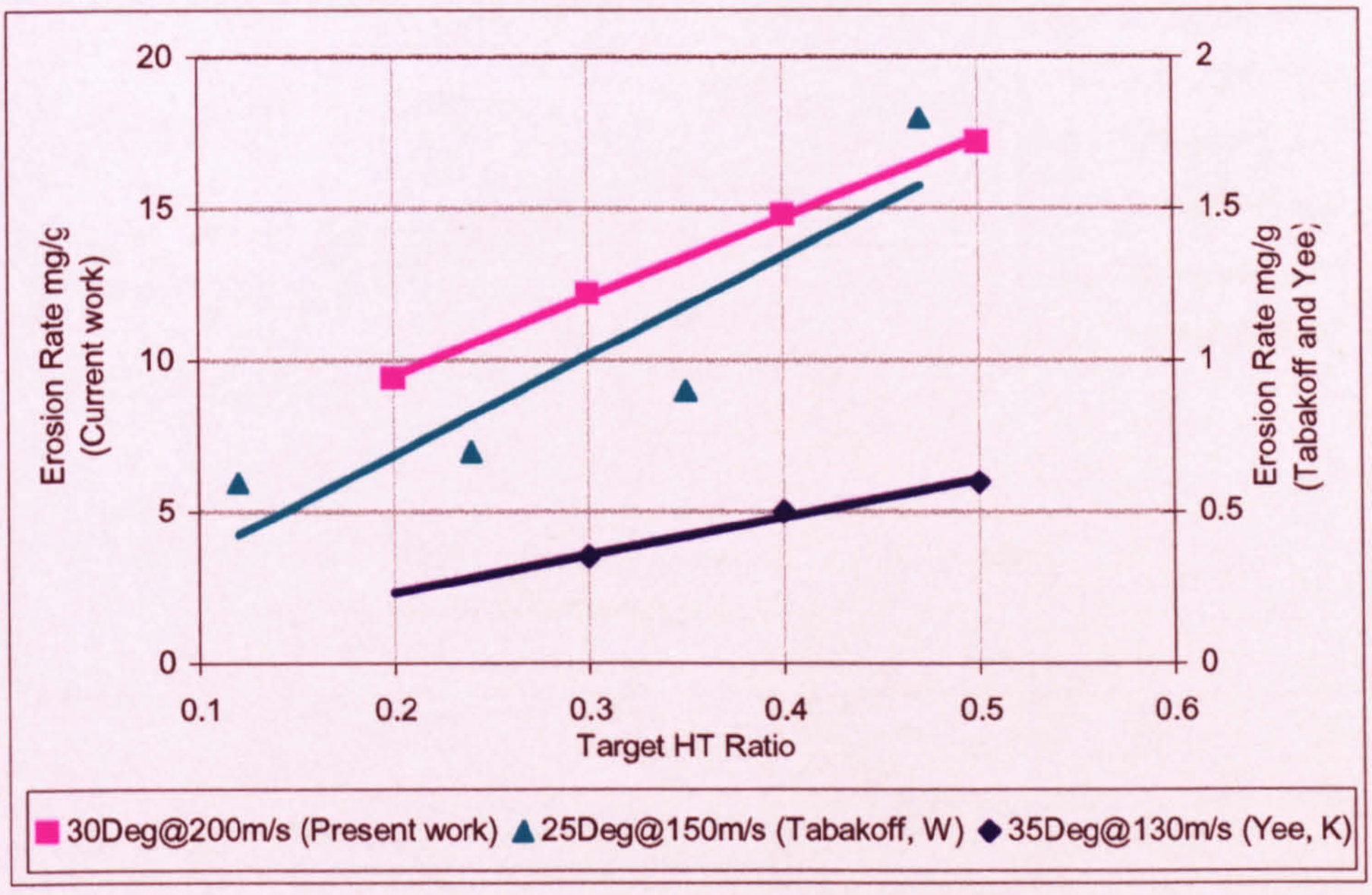


Figure 4-8. Erosion rate versus target HT ratio at particle temperature of 500℃. ◆ BG 303 steel targets, ash particle size 42-66 μm; impingement velocity 130m/s; impingement angle 35°, from Yee K. ■ Type 304 steel targets; average ash particle size 38.4μm; impingement velocity, about, 150 m/s; impingement angle; 25° from Tabakoff W. ▲ 321 stainless steel target; average particle size 20-30μm; impingement velocity 200m/s; impingement angle 30°; present work.



Effect of Particle Temperature

Figure 4-9. Erosion rate versus Particle temperature at HT=0.2 (285 ℃).

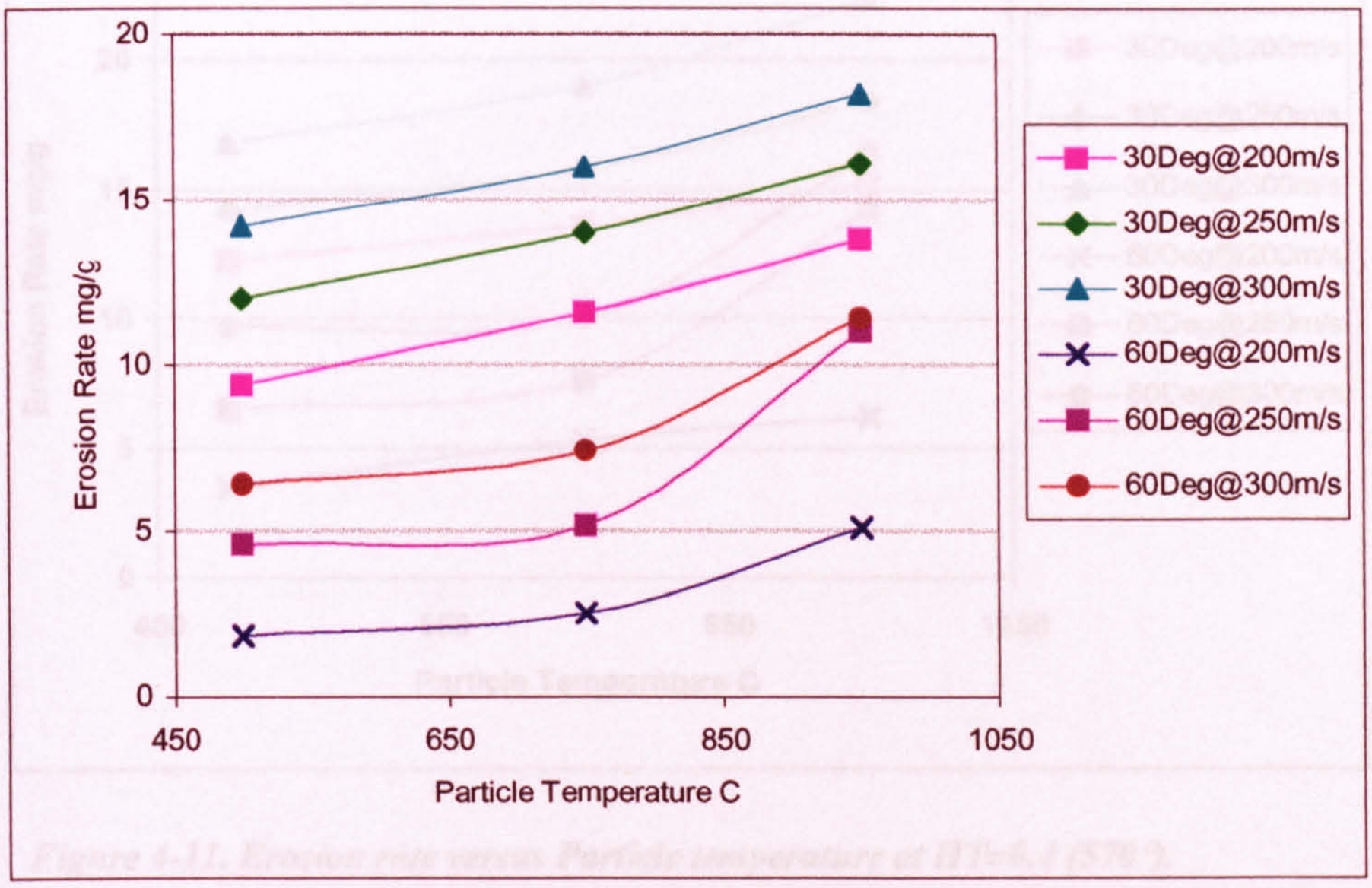


Figure 4-10. Erosion rate versus Particle temperature at HT=0.3 (415 ℃).

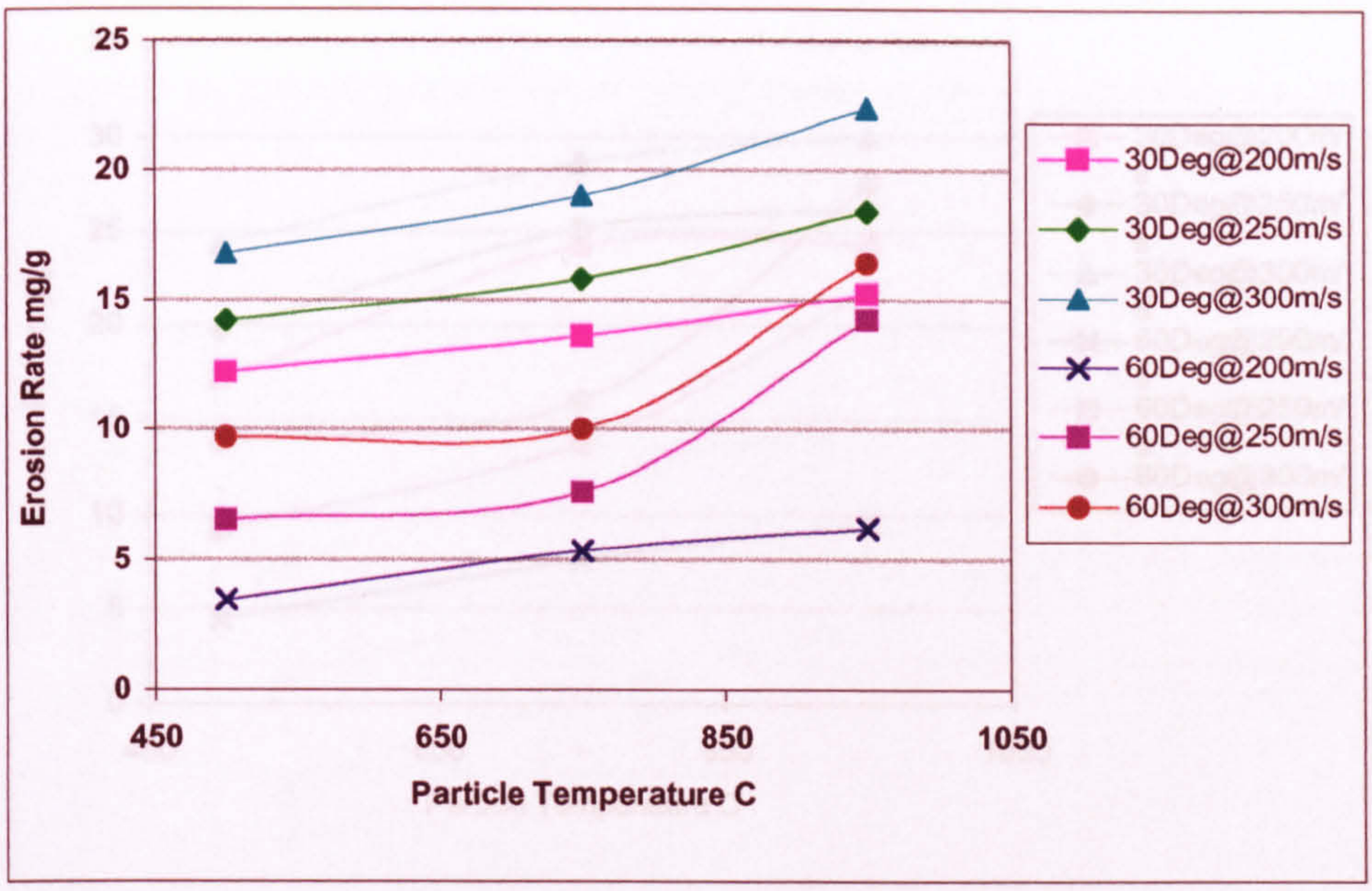


Figure 4-11. Erosion rate versus Particle temperature at HT=0.4 (570 ℃).

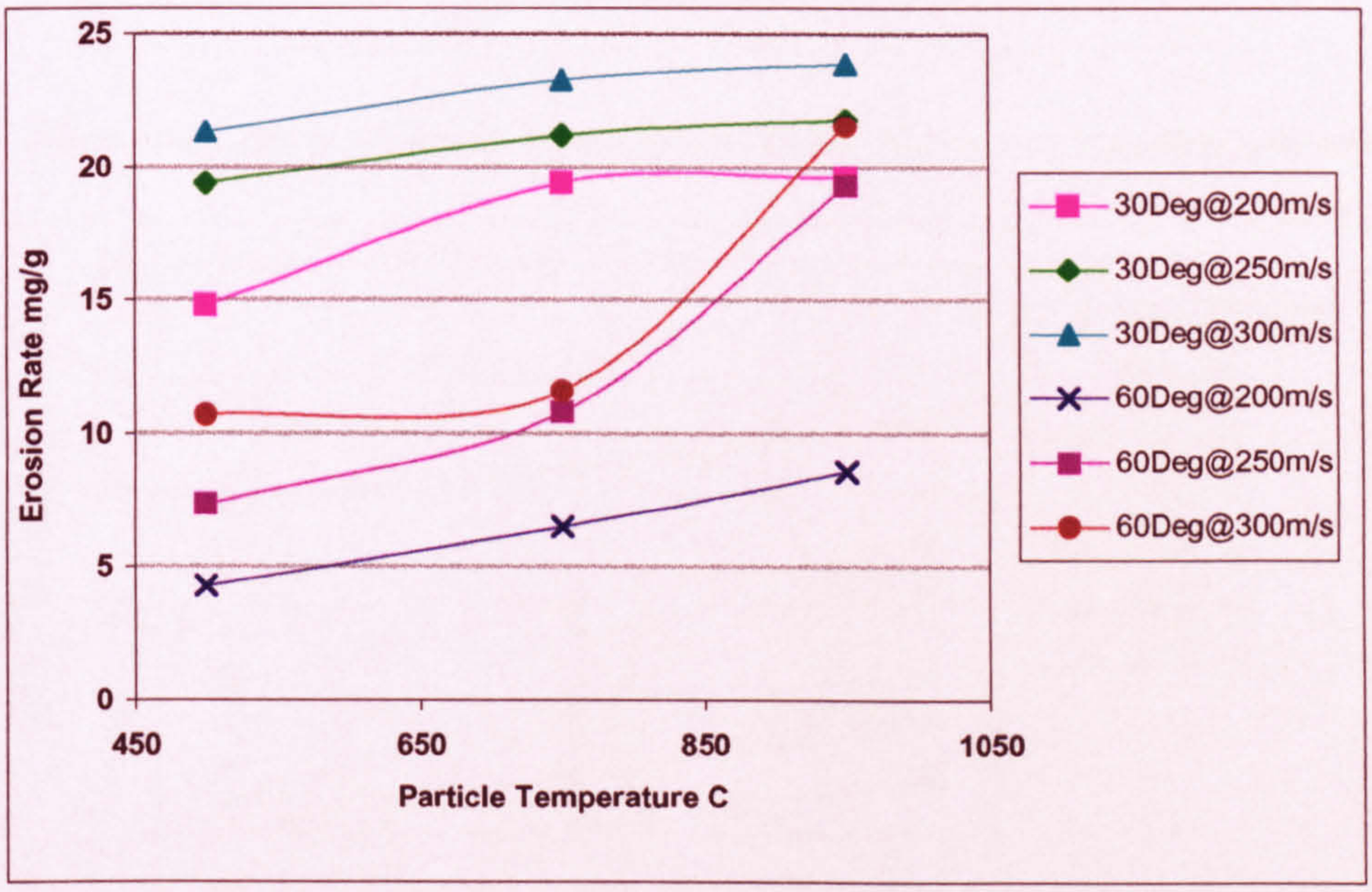
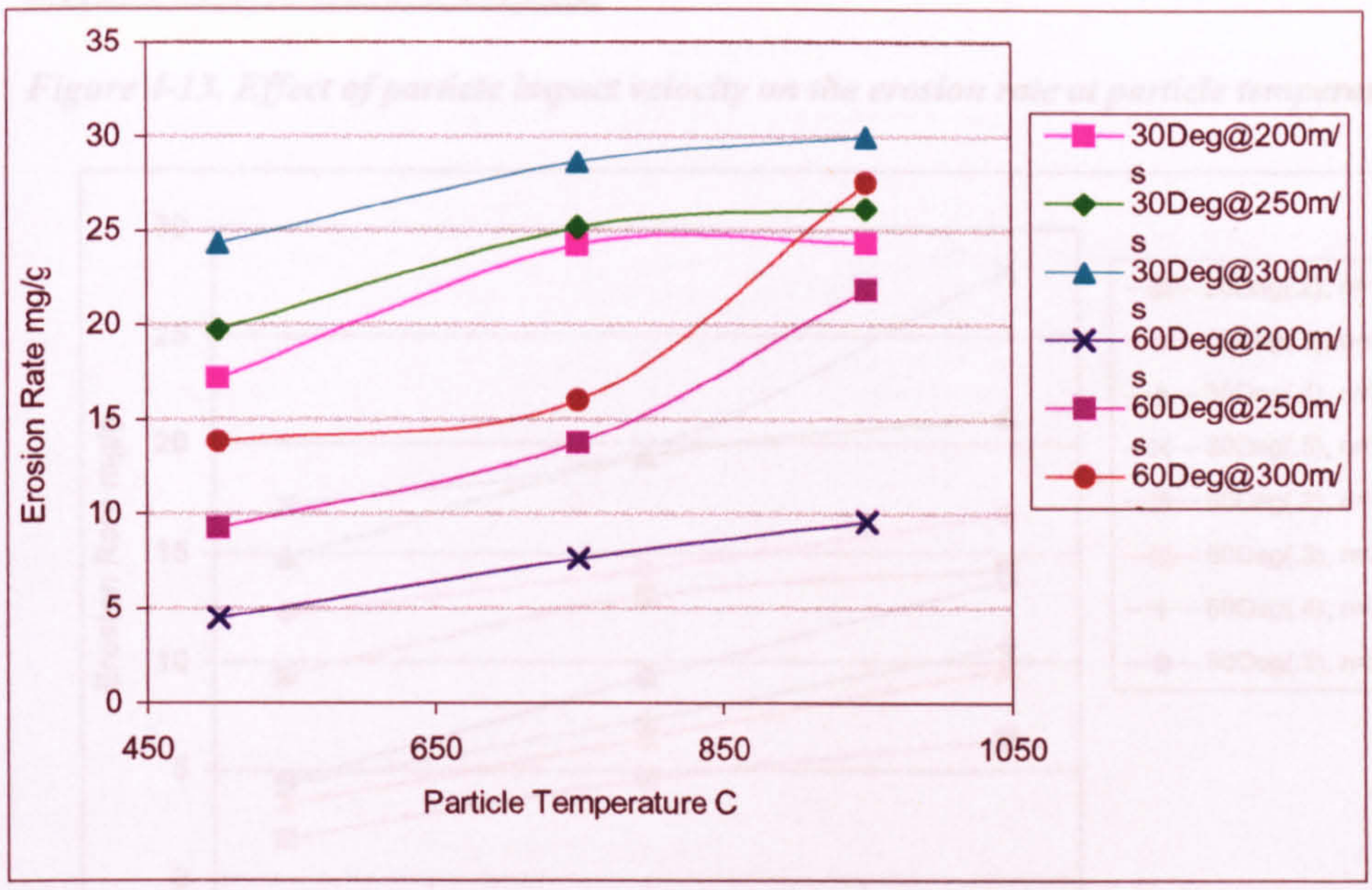


Figure 4-12. Erosion rate versus Particle temperature at HT=0.5 (715 ℃).



Effect of Particle Velocity

Figure 4-13. Effect of particle impact velocity on the erosion rate at particle temperature of 500℃.

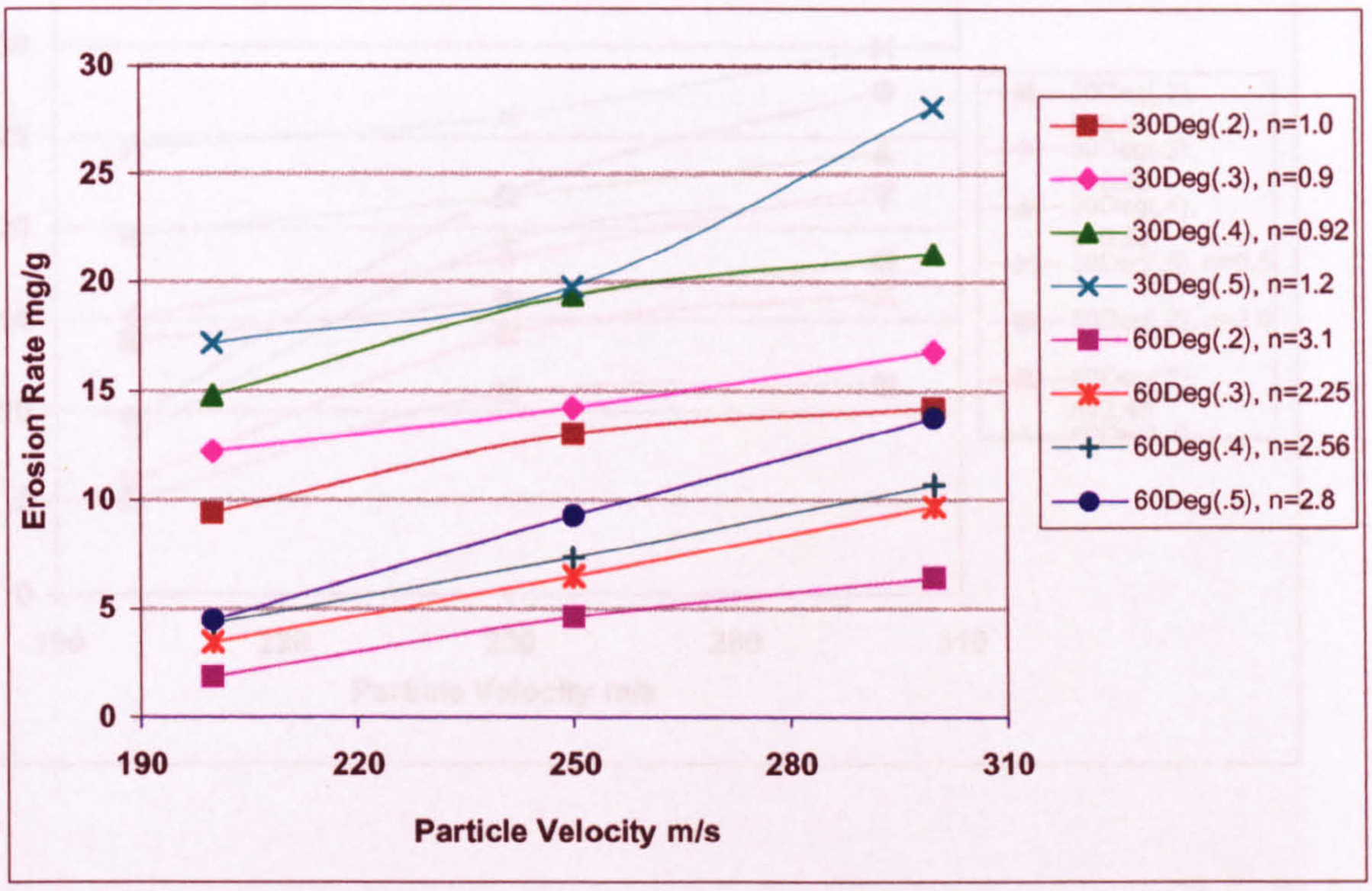


Figure 4-14. Effect of particle impact velocity on the erosion rate at particle temperature of 750℃.

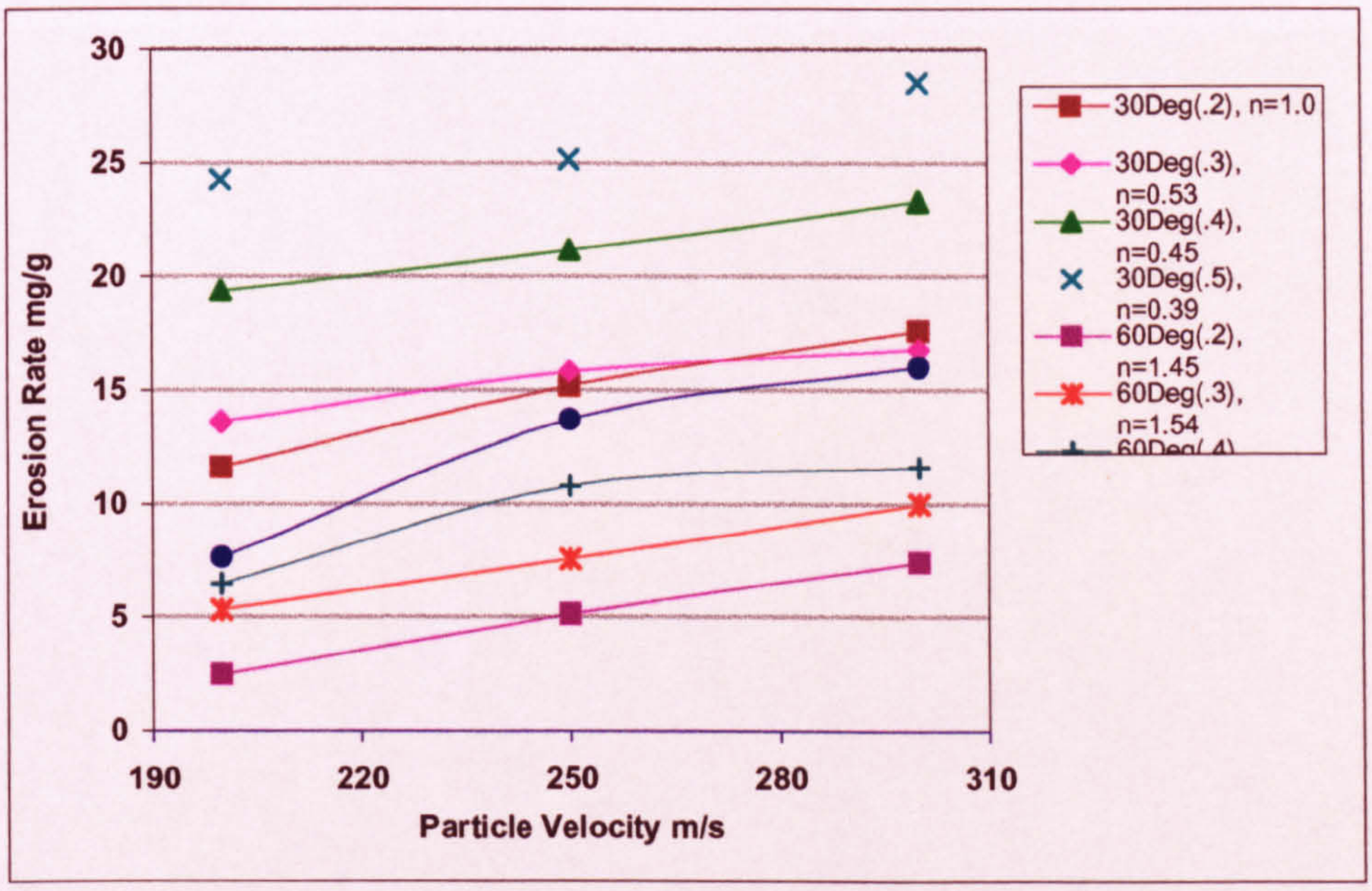
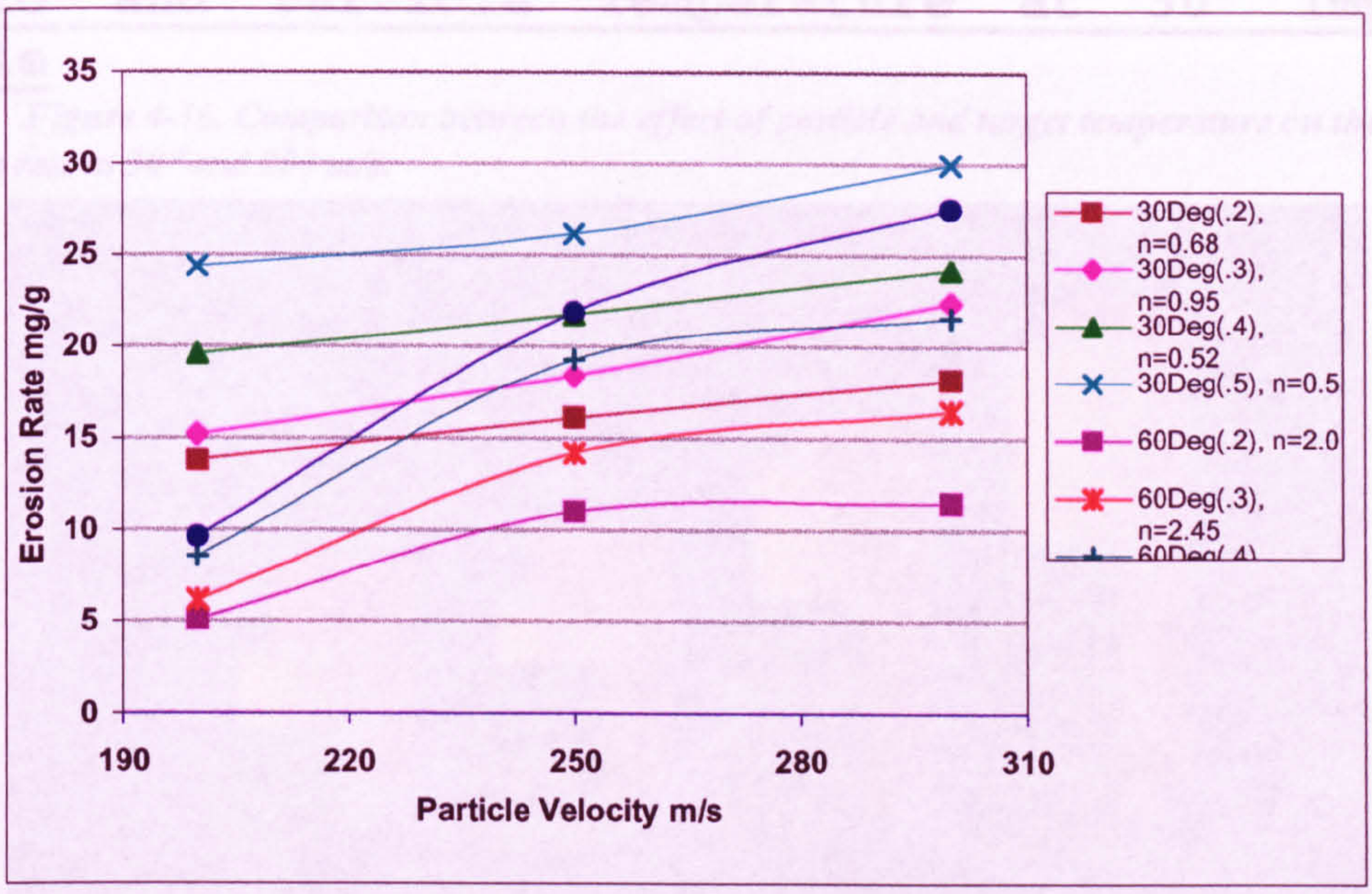


Figure 4-15. Effect of particle impact velocity on the erosion rate at particle temperature of 950℃.



Comparison between the Effect of Target HT Ratio and Particle Temperature at 30° Impact Angle

Figure 4-16. Comparison between the effect of particle and target temperature on the erosion rate at 30° and 200 m/s.

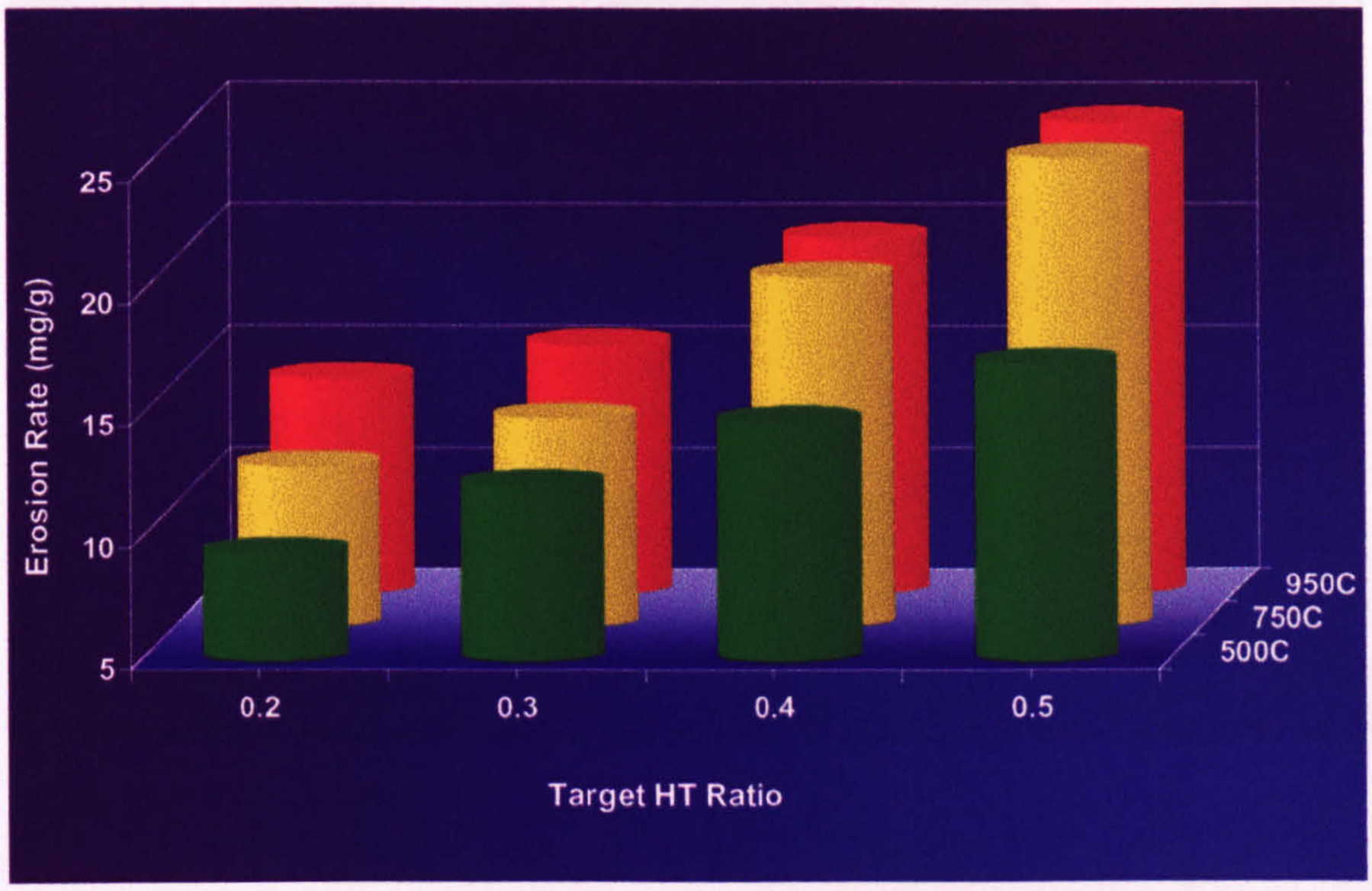


Figure 4-17. Comparison between the effect of particle and target temperature on the erosion rate at 30° and 250 m/s.

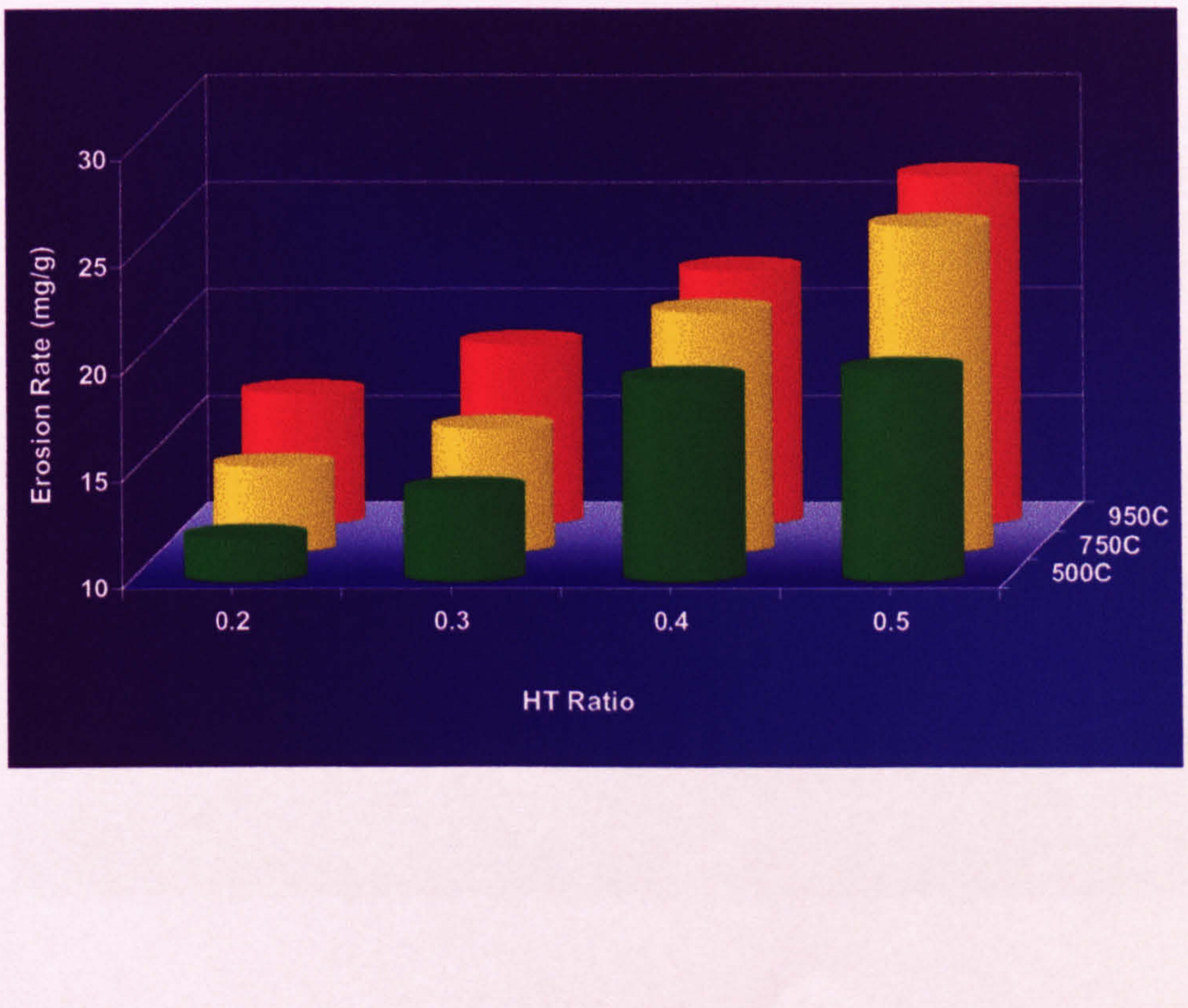
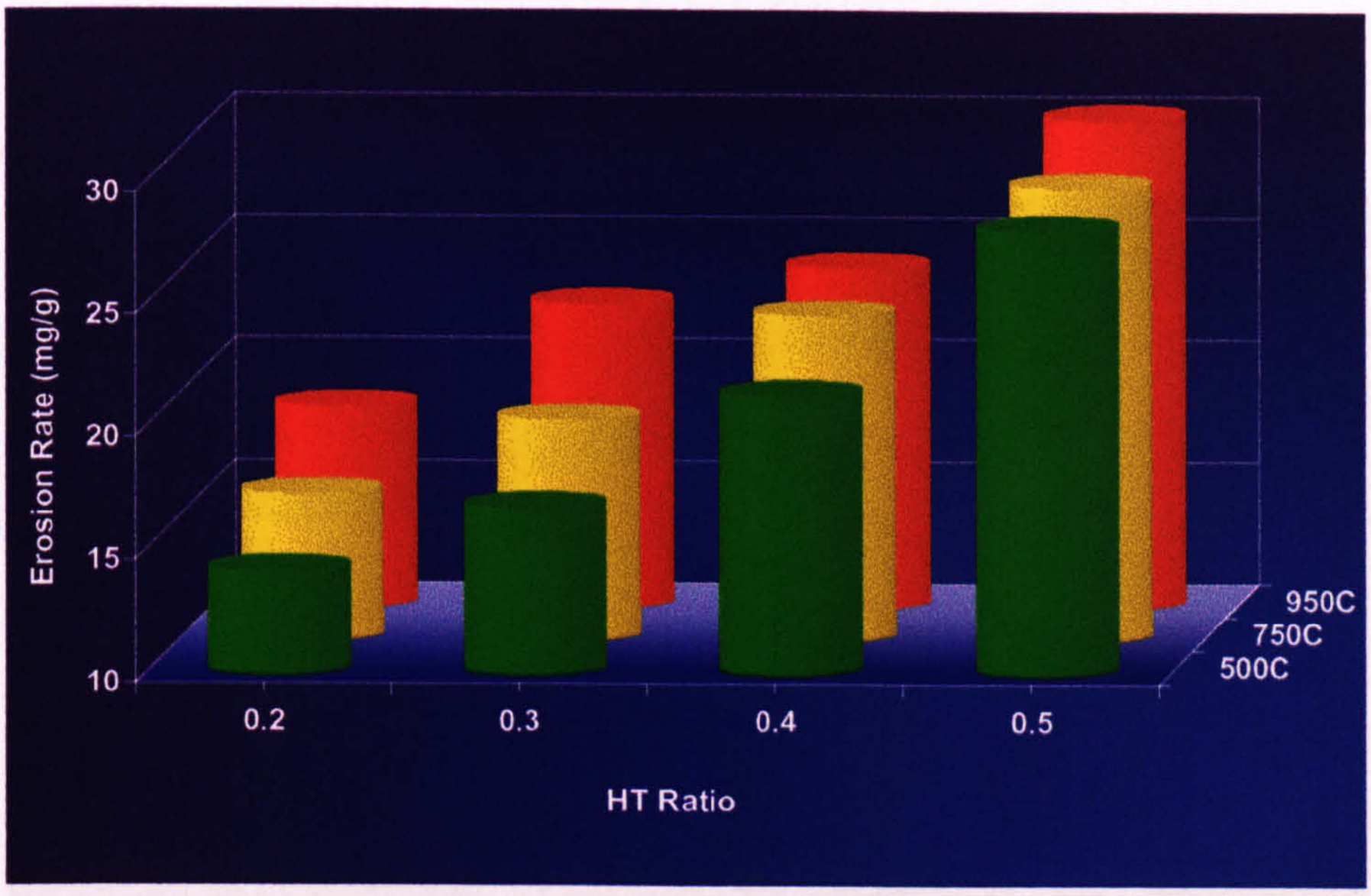


Figure 4-18. Comparison between the effect of particle and target temperature on the erosion rate at 30° and 300 m/s.



Comparison between the Effect of Target HT Ratio and Particle Temperature at 60° Impact Angle

Figure 4-19. Comparison between the effect of particle and target temperature on the erosion rate at 60° and 200 m/s.

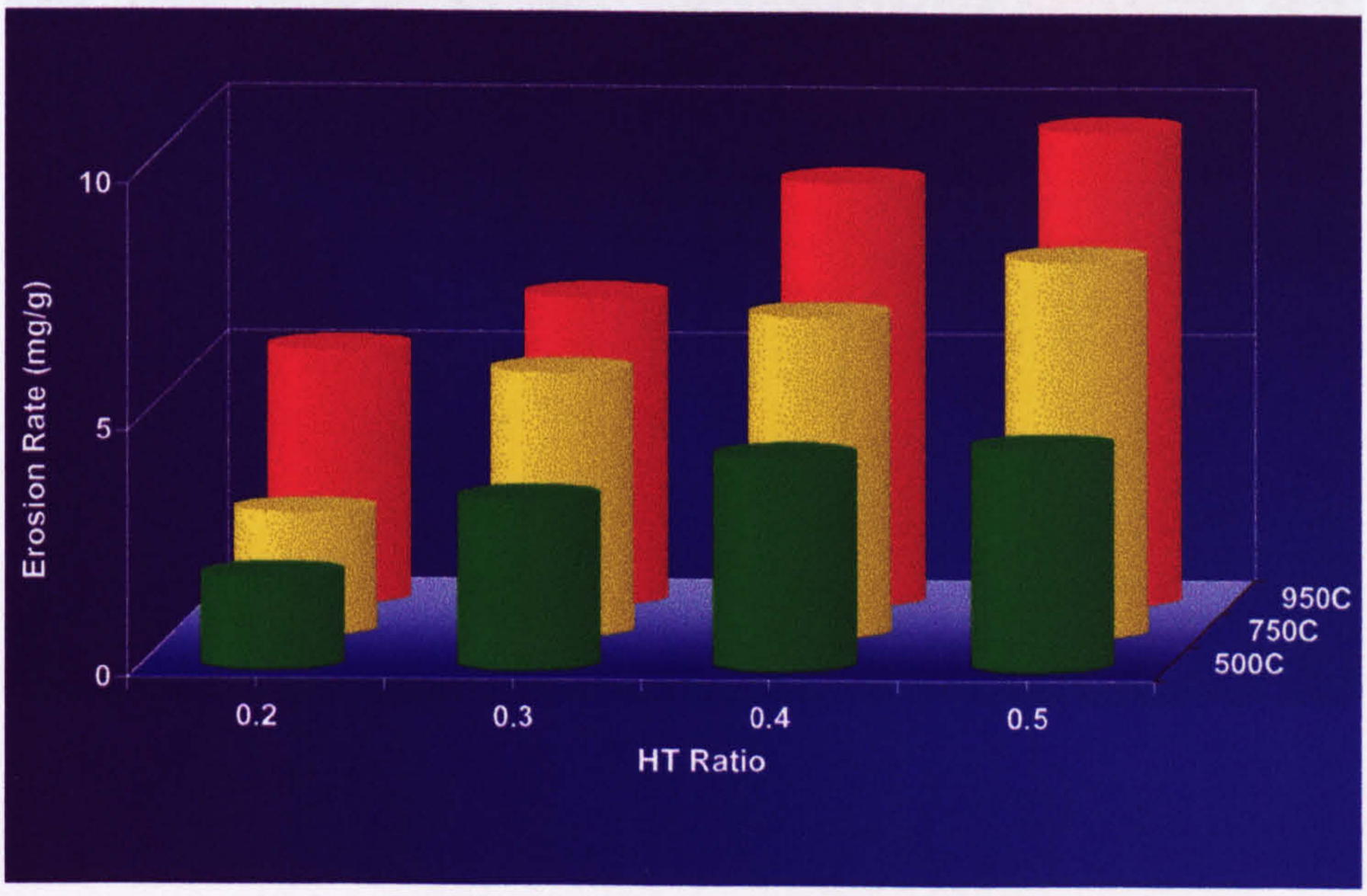


Figure 4-20. Comparison between the effect of particle and target temperature on the erosion rate at 60° and 250 m/s.

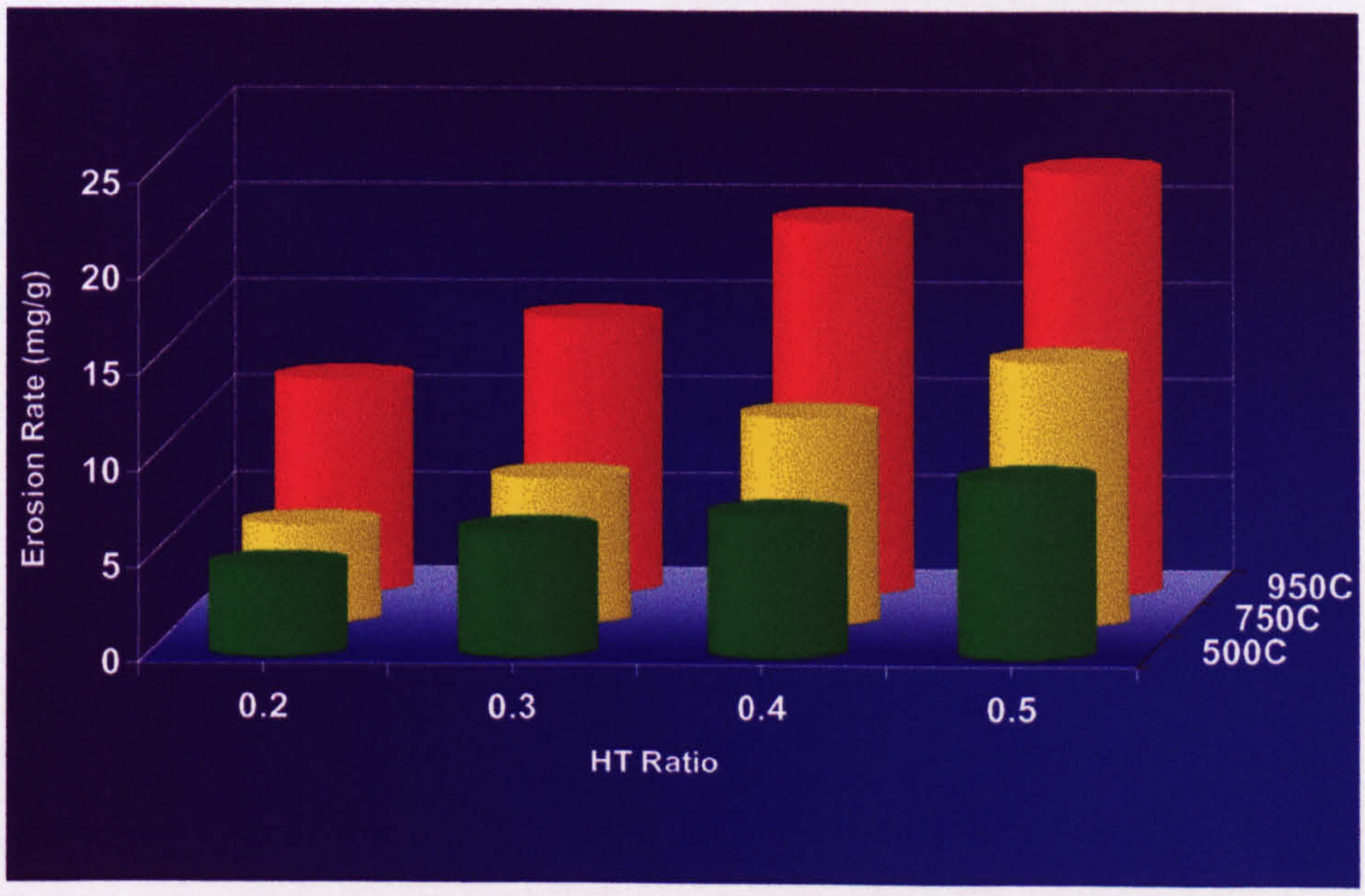
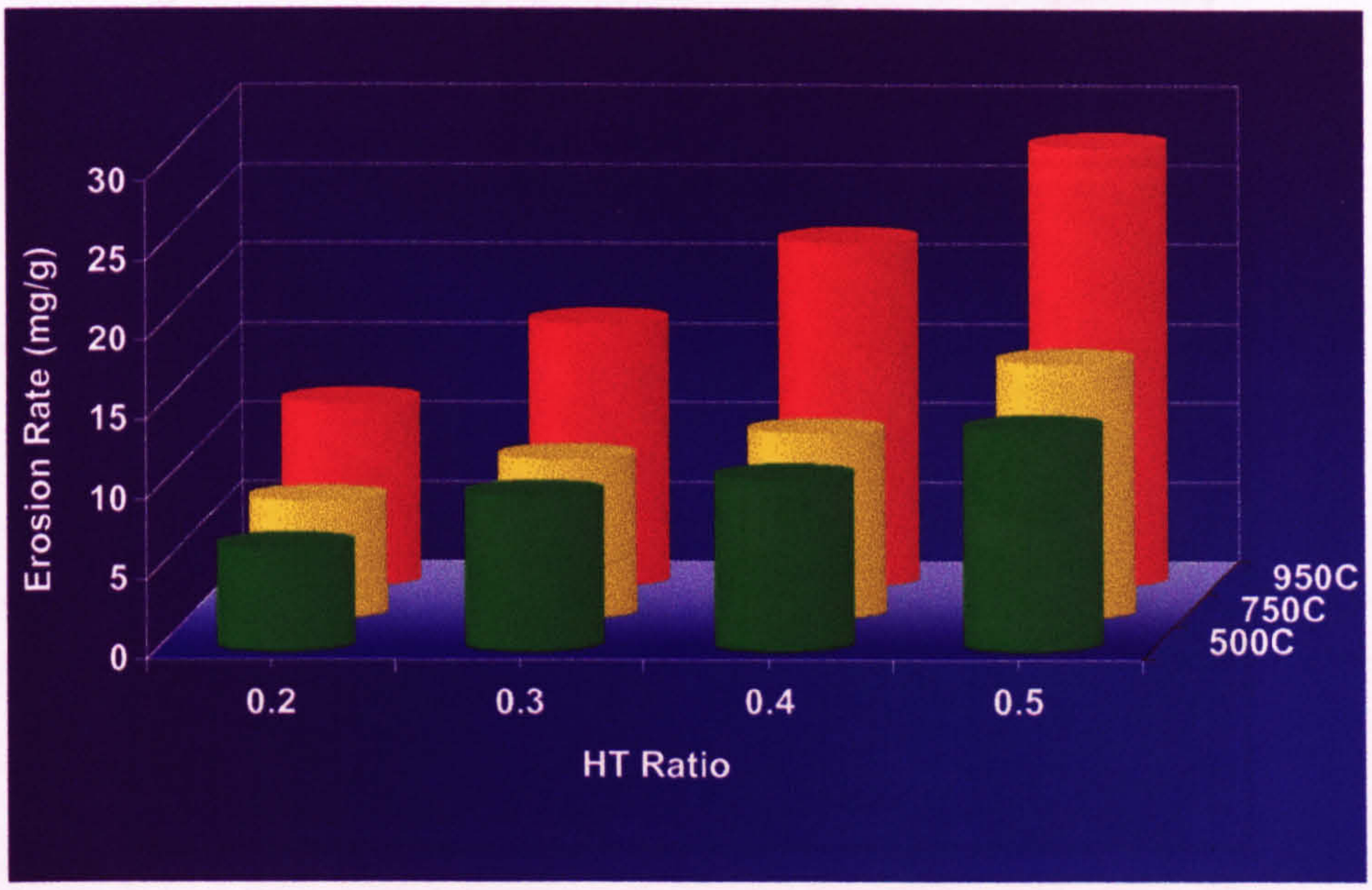


Figure 4-21. Comparison between the effect of particle and target temperature on the erosion rate at 60° and 250 m/s.



Surface Examination Results For Stainless Steel 321 at 30° Impact Angle.

Scanning Electron Microscope (SEM) Results (Impact velocity of 200 m/s.)

Figure 4-22. Beach wave erosion pattern.

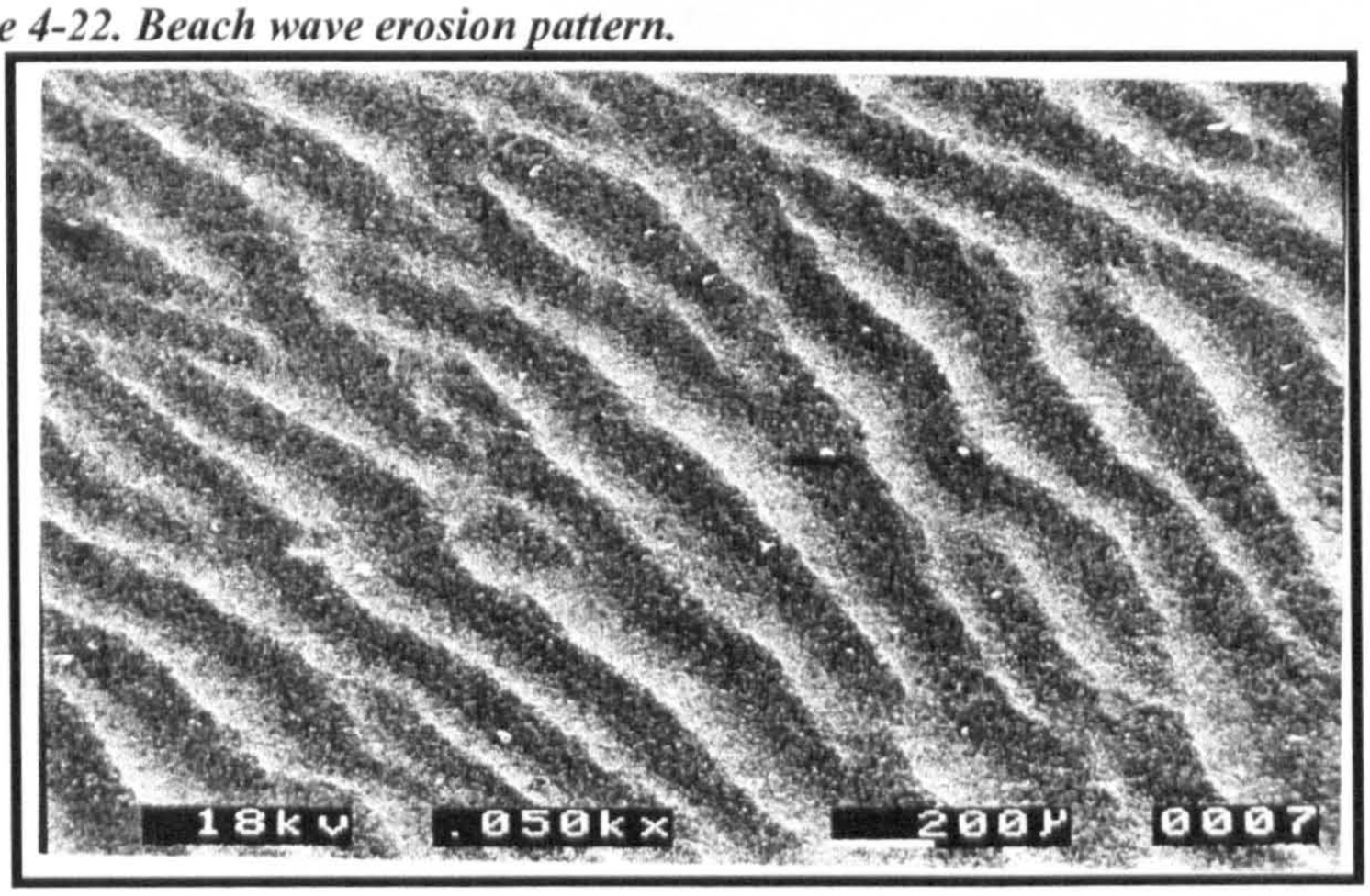


Figure 4-23. Ploughing cut caused by particle of about 30µm size.



Figure 4-24. Type I cut caused by small particle where the lip is very clear.

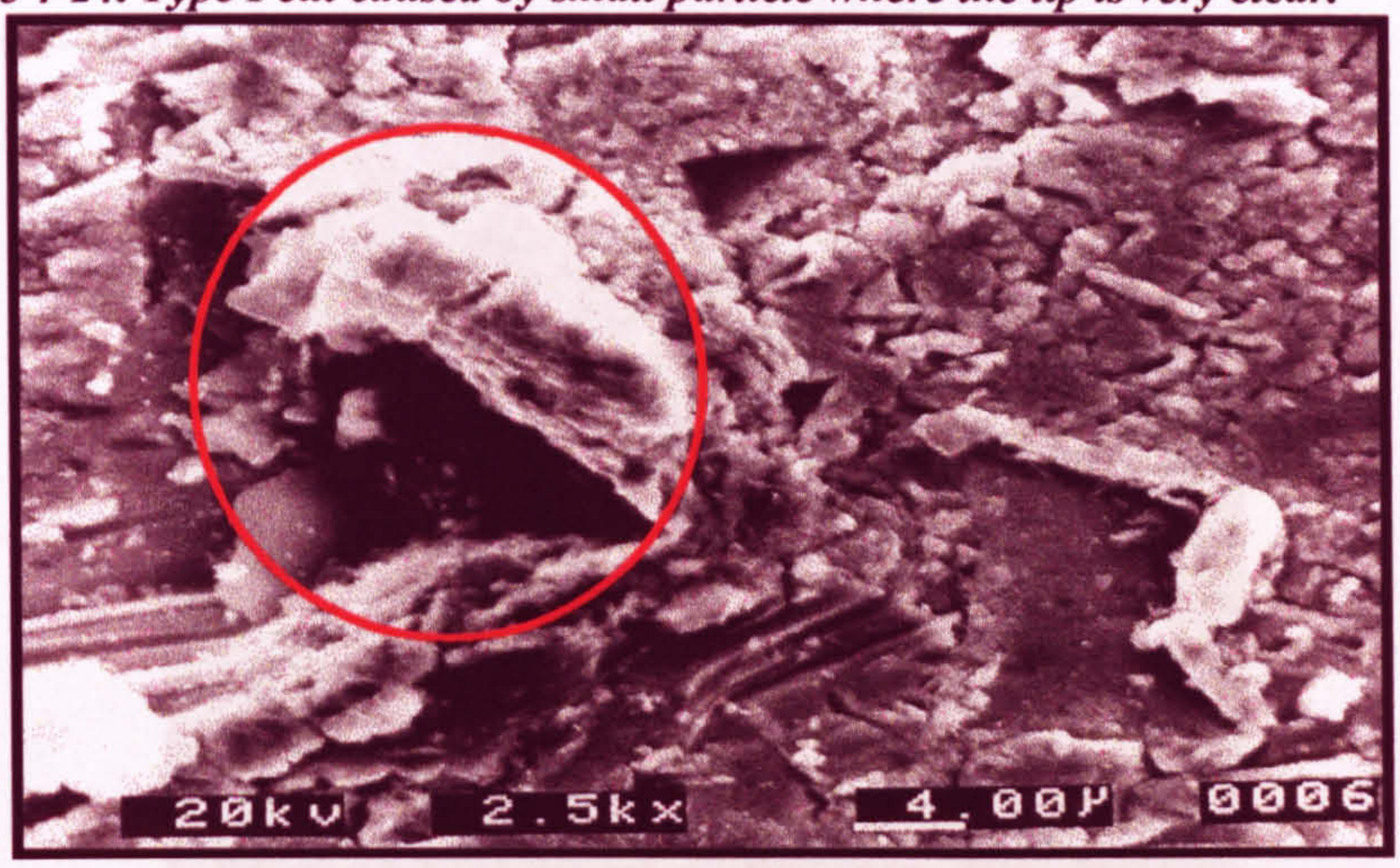
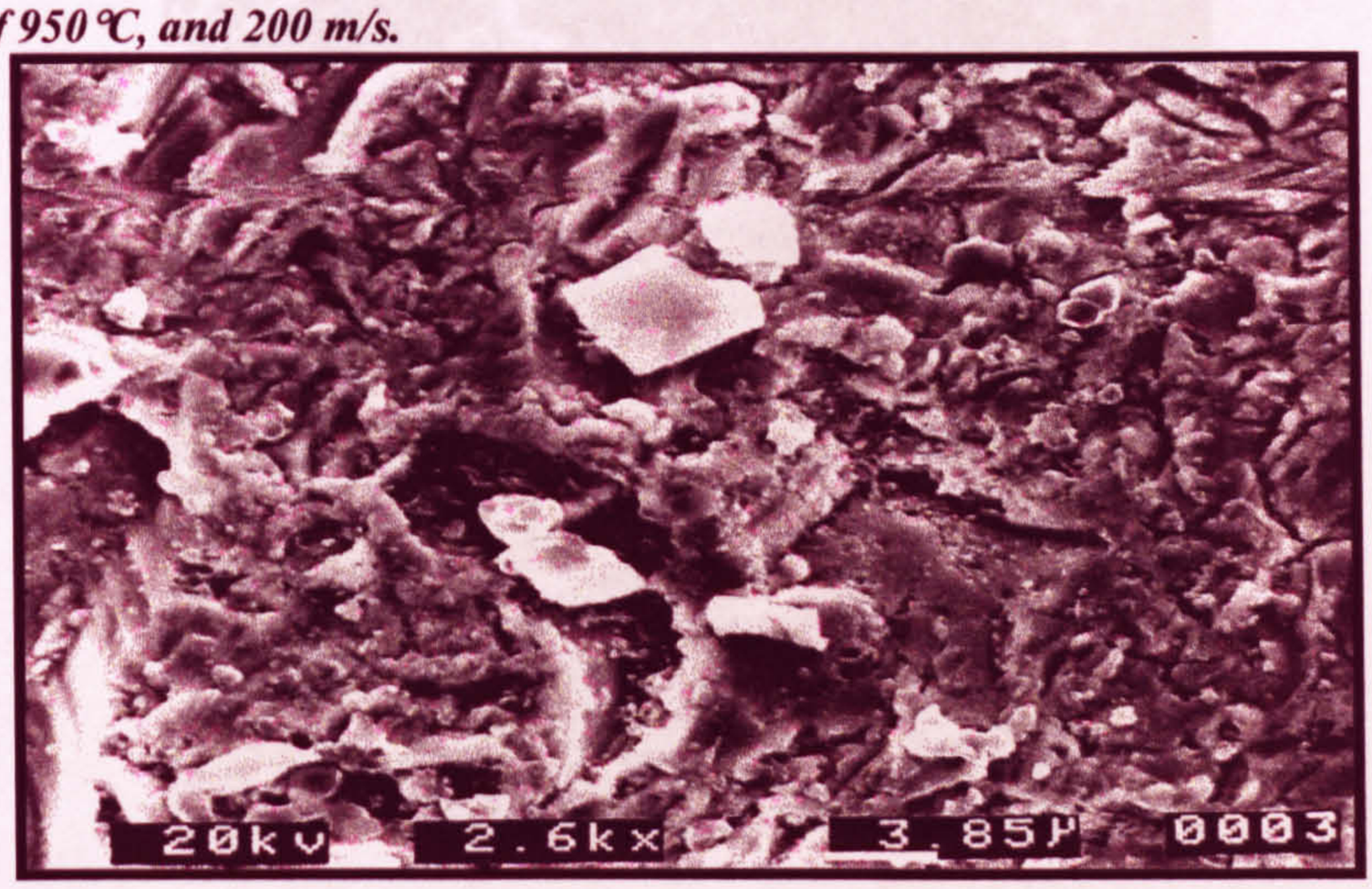


Figure 4-25. Very small particles deposited with no deep cuts at HT=0.5, particle temperature of 950℃, and 200 m/s.



Scanning Electron Microscope (SEM) Results (Impact velocity of 250 and 300 m/s.)

Figure 4-26. Ploughing cut at 250m/s impact velocity.

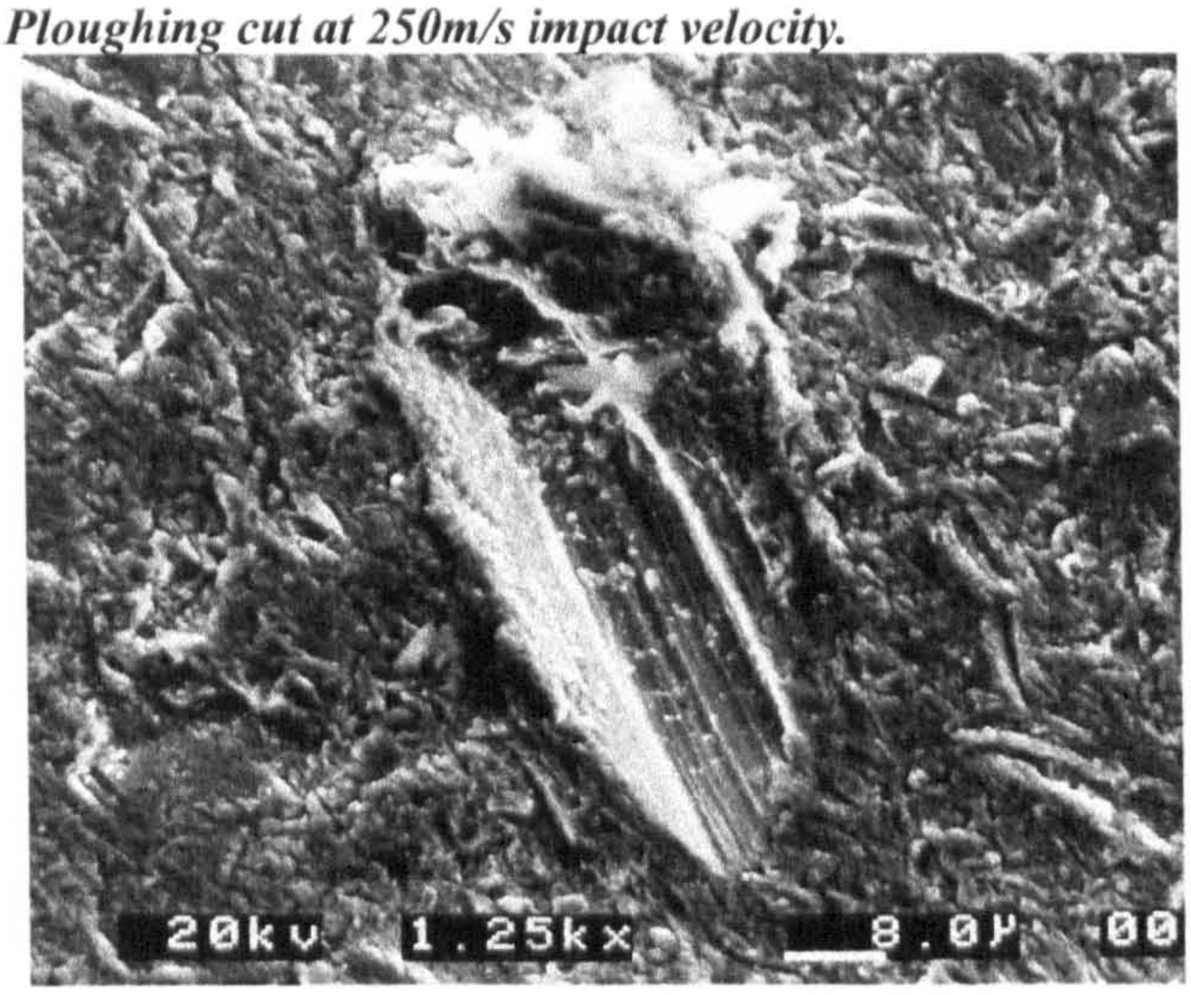


Figure 4-27. Ploughing cut at 250m/s impact velocity.

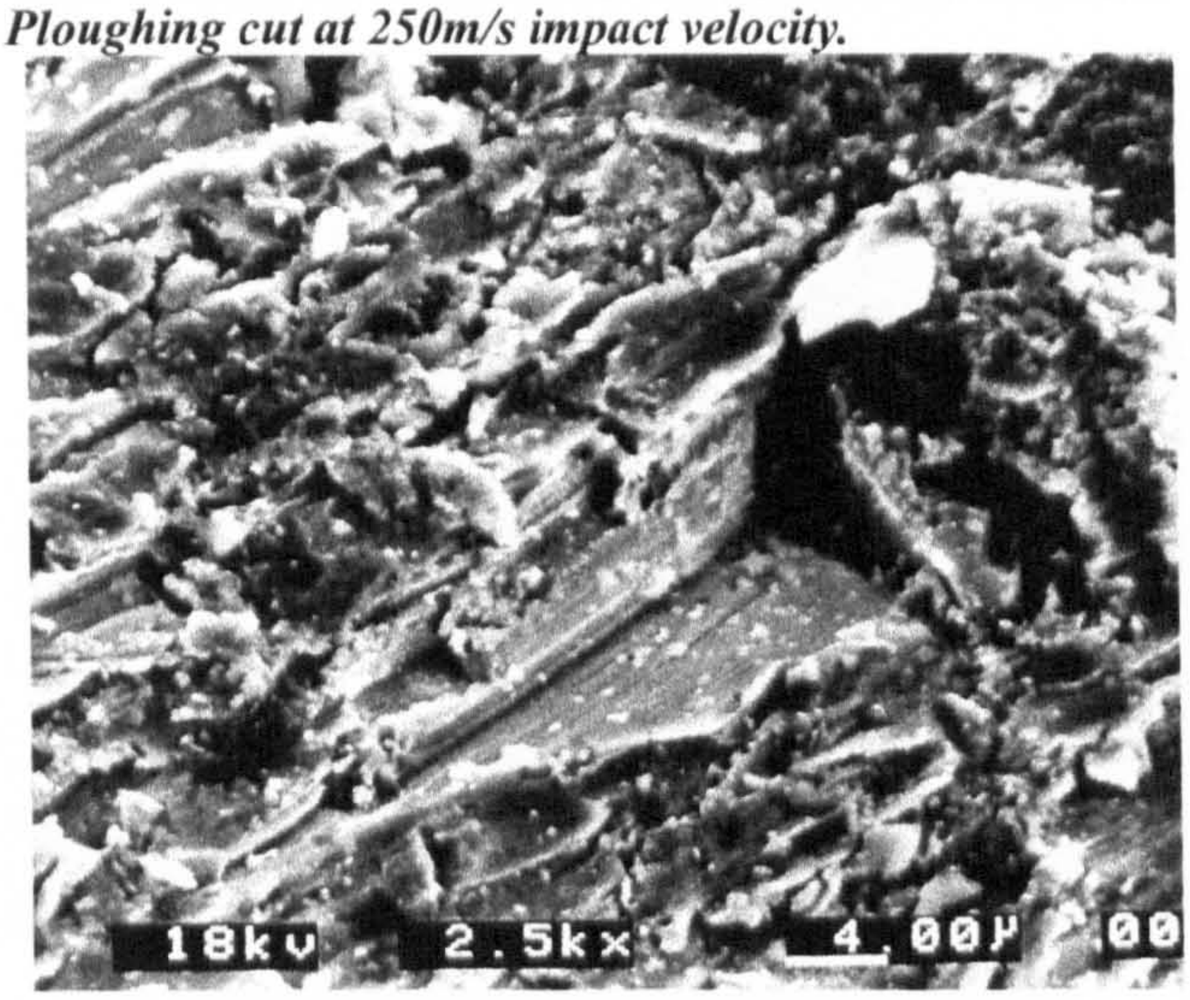


Figure 4-28. Type (I) cut at 250 m/s particle velocity, 0.5HT ratio and 750 ℃ particle temperature

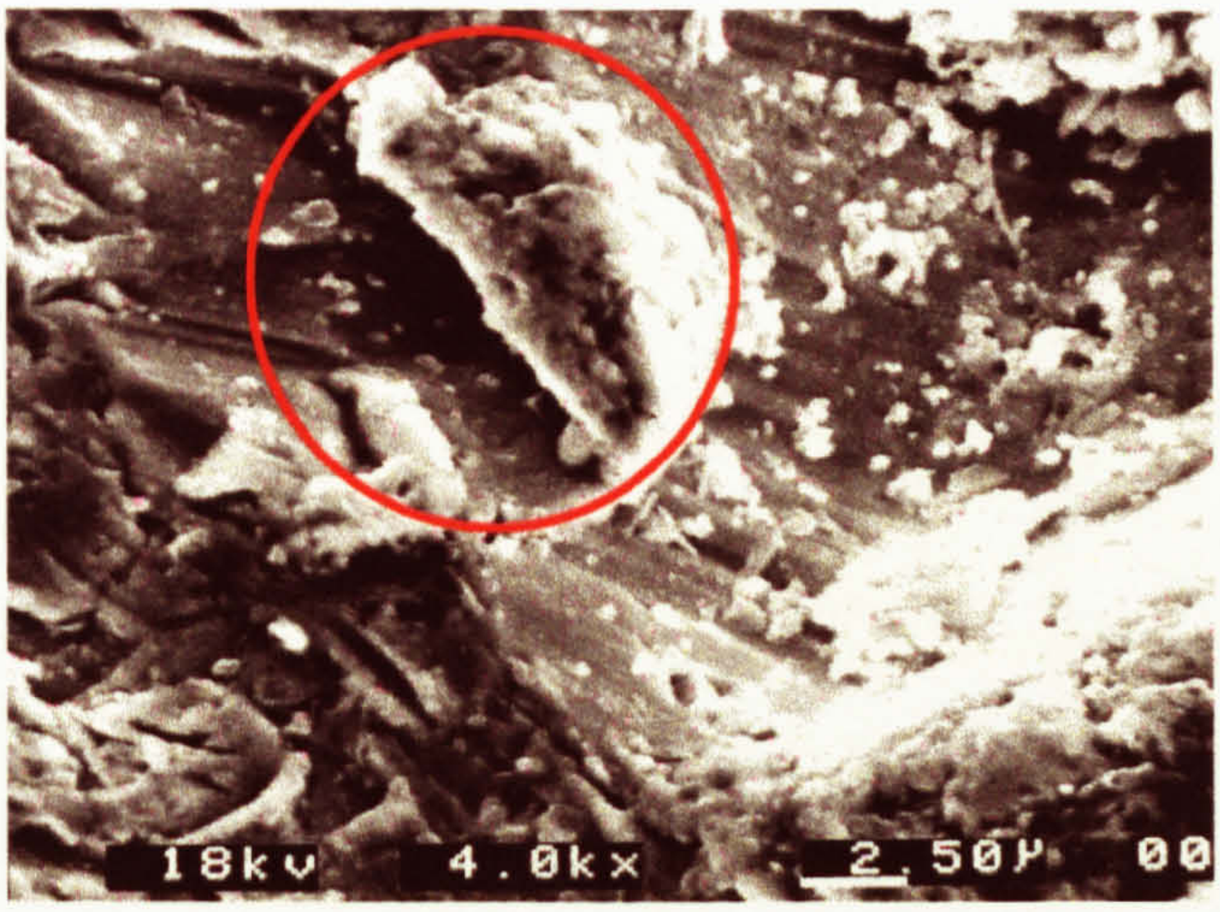


Figure 4-29. Type II cut at 300m/s particle velocity, 0.5 HT ratio and 950 ℃ particle temperature.

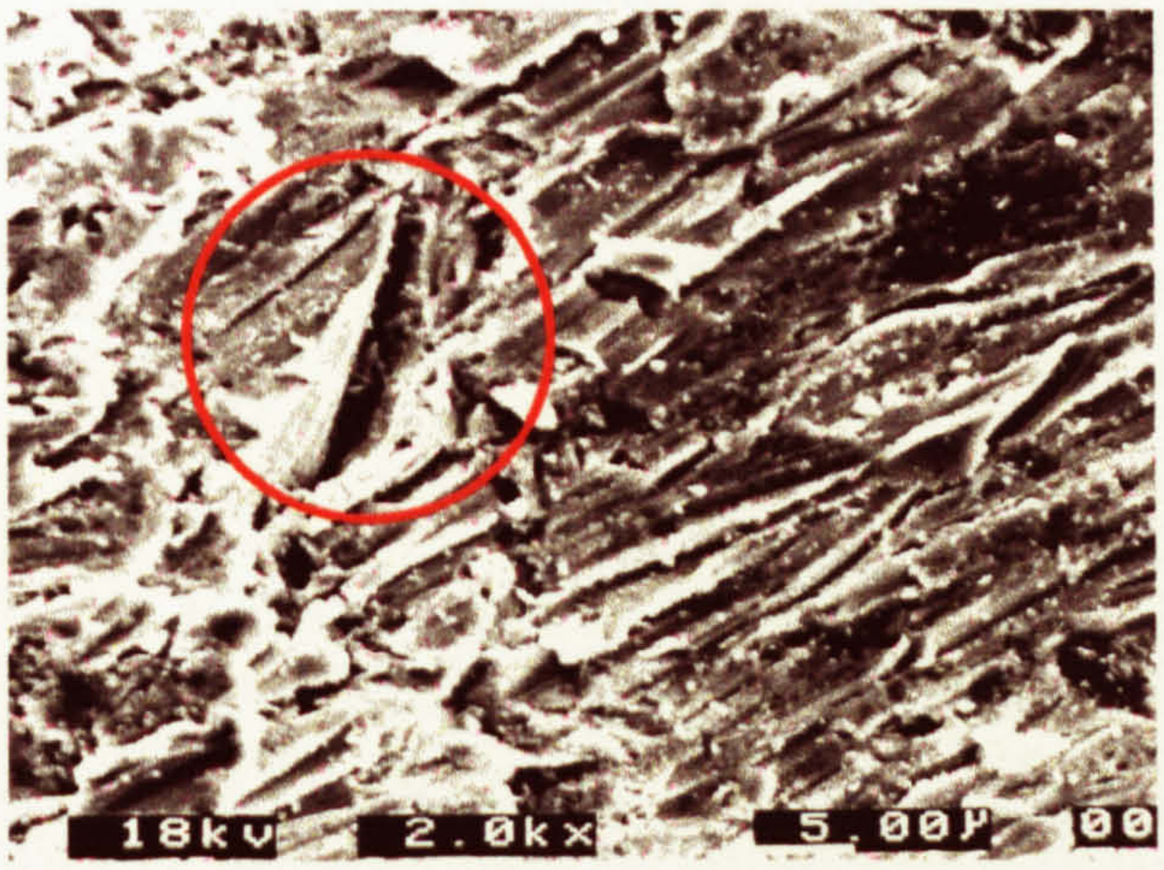


Figure 4-30. Areas of heavy deposited particles at HT ratio of 0.5 and 950 ℃ particle temperature, and 300 m/s particle velocity.

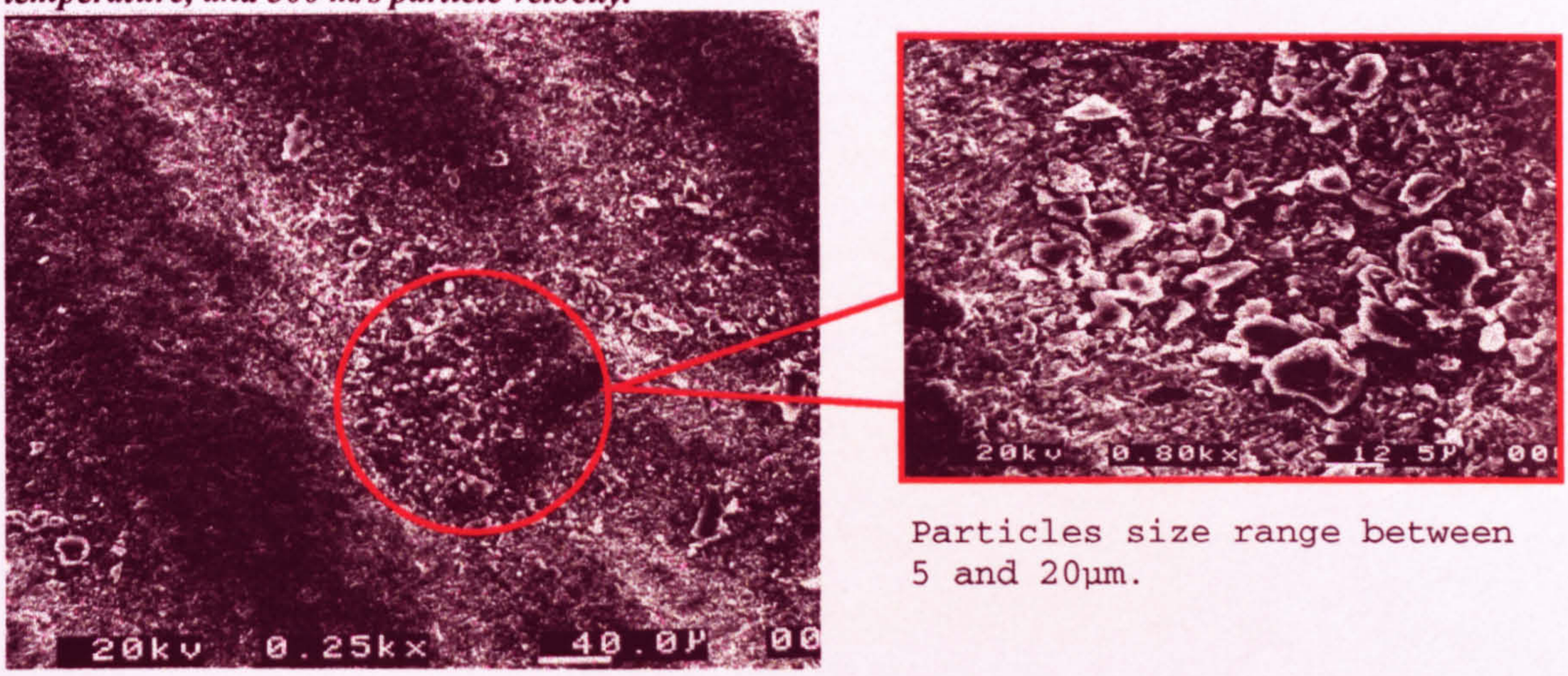


Figure 4-31. Small size particles deposited very deep on stainless steel target surface at HT=0.5, 750 ℃ particle temperature and 300 m/s impact velocity.

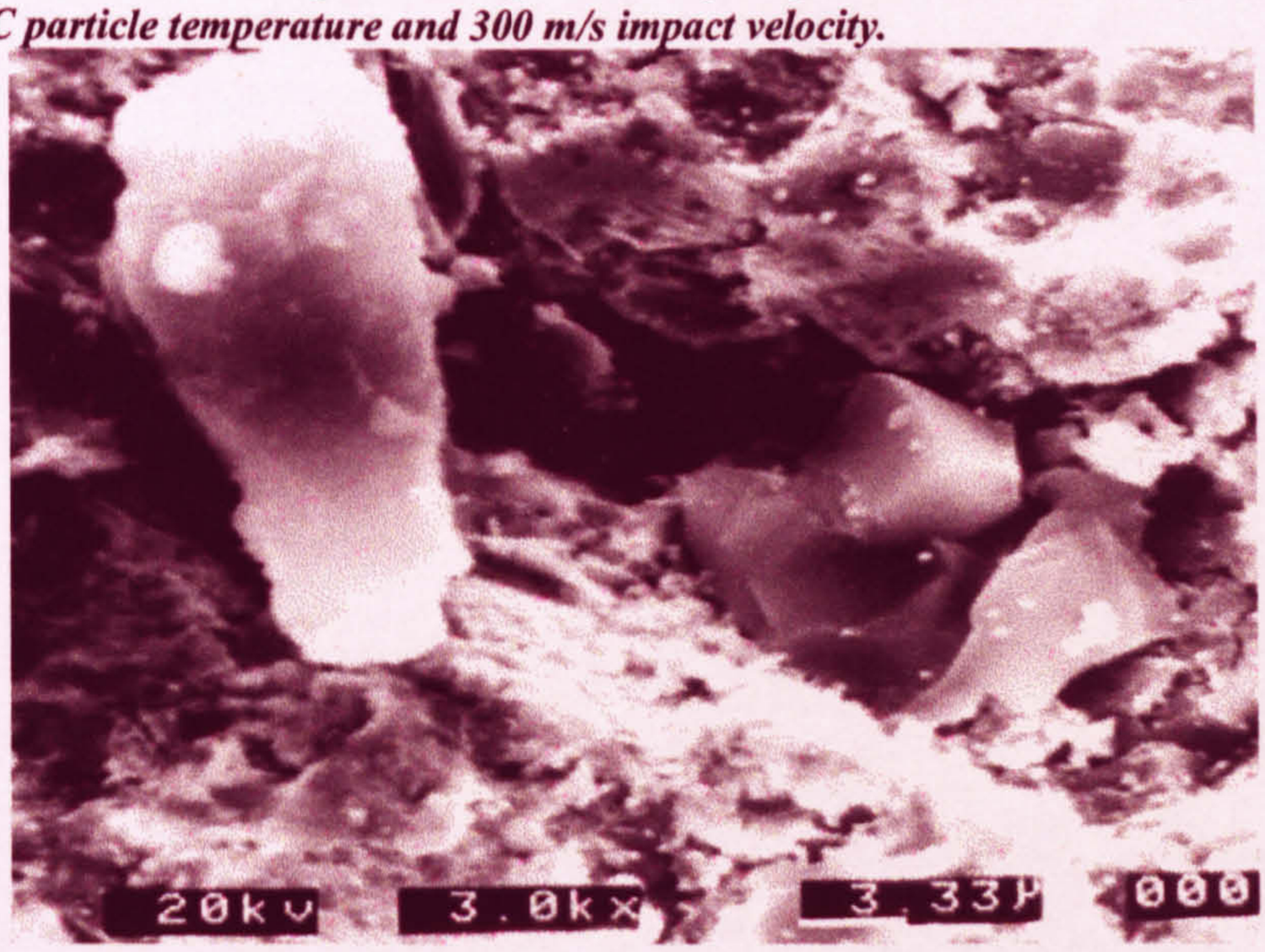
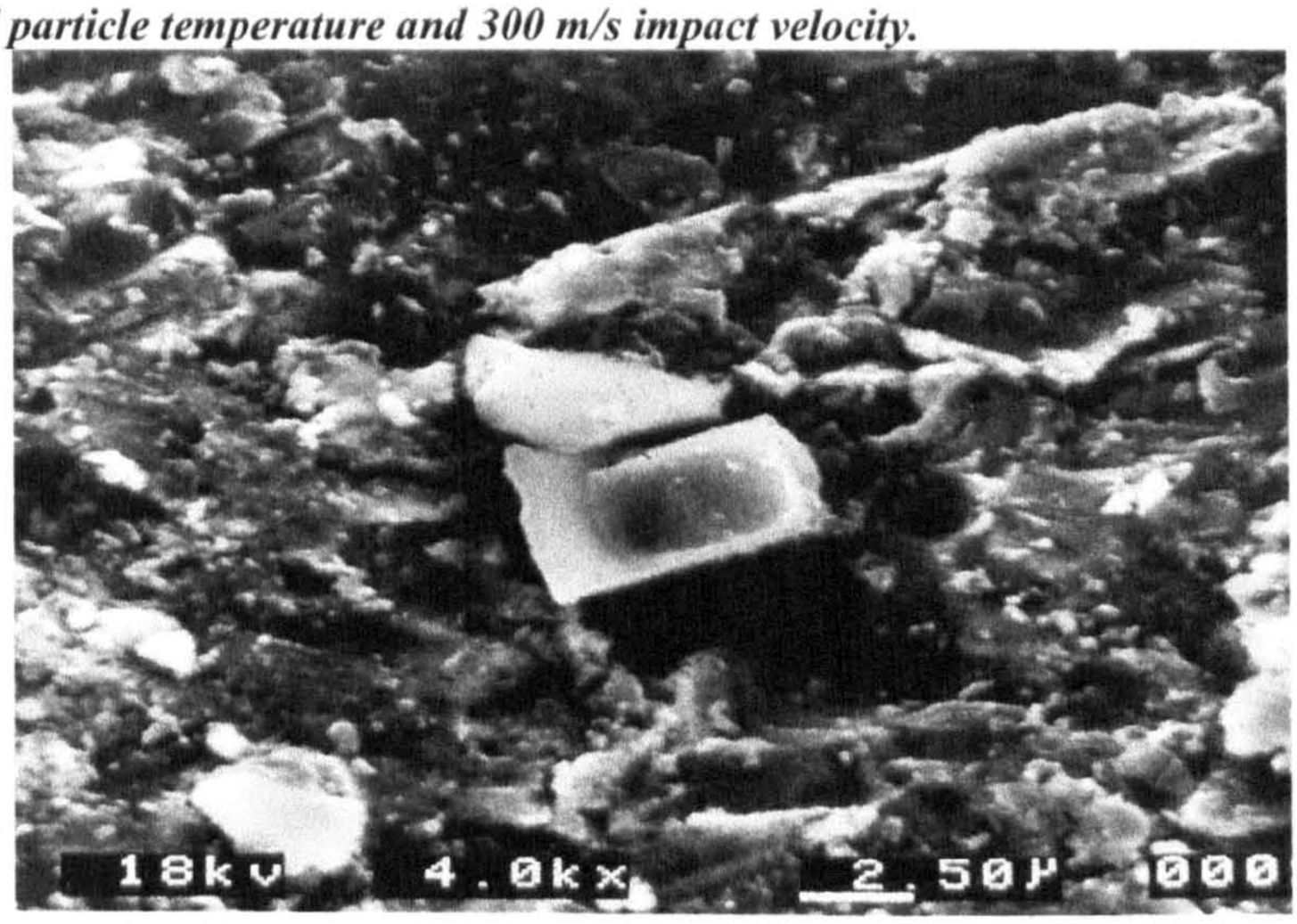


Figure 4-32. Small size particles deposited very deep on stainless steel target surface at HT=0.5, 950℃ particle temperature and 300 m/s impact velocity.



Surface Examination Results For Stainless Steel 321 at 60° Impact Angle.

Scanning Electron Microscope (SEM) Results (Impact velocity; 200, 250 and 300 m/s).

Figure 4-33. Typical cut pattern at 60° angle of impact.

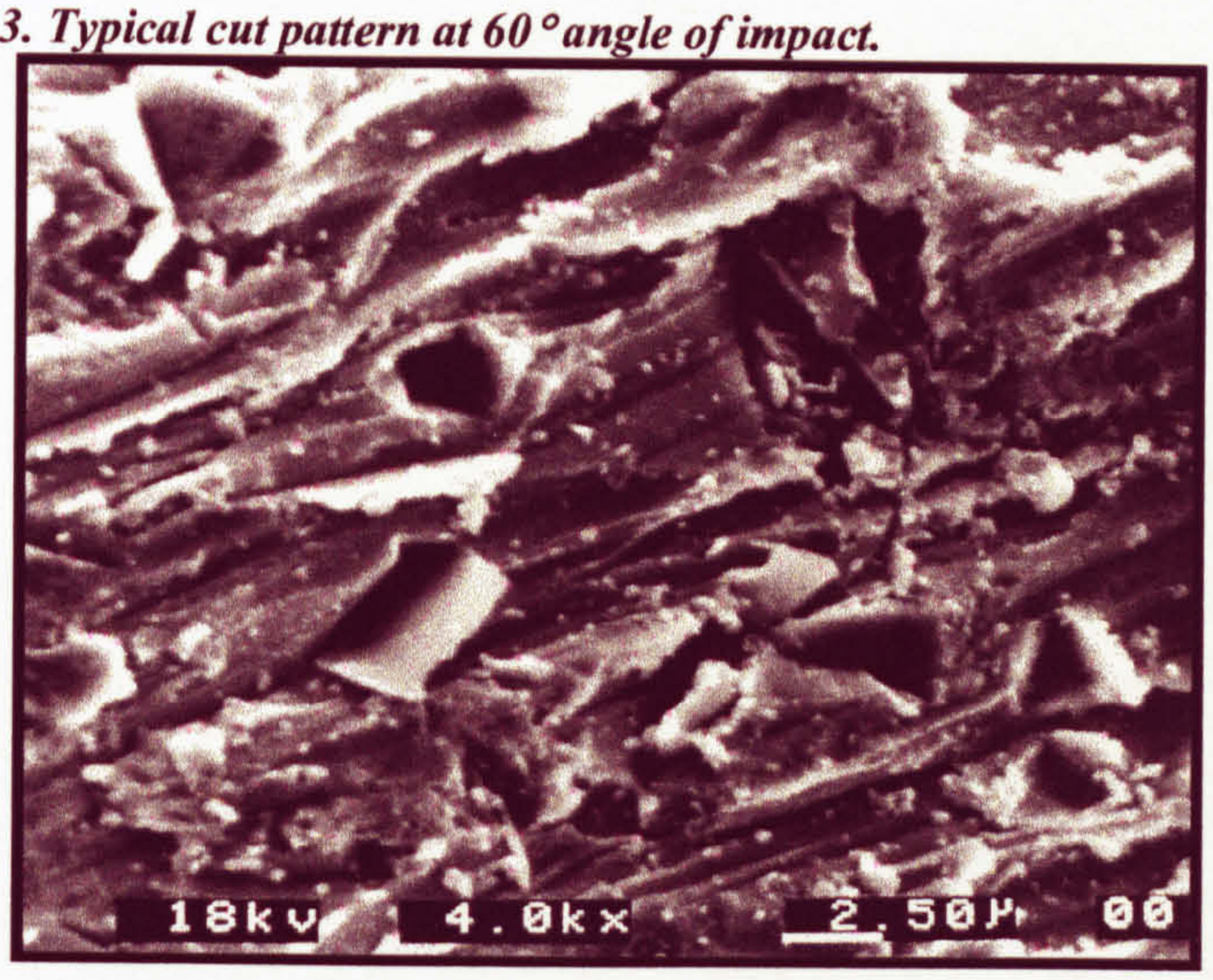


Figure 4-34. Some deposited particles at 200 m/s particle velocity, HT=0.5 and 950 ℃ particle temperature.

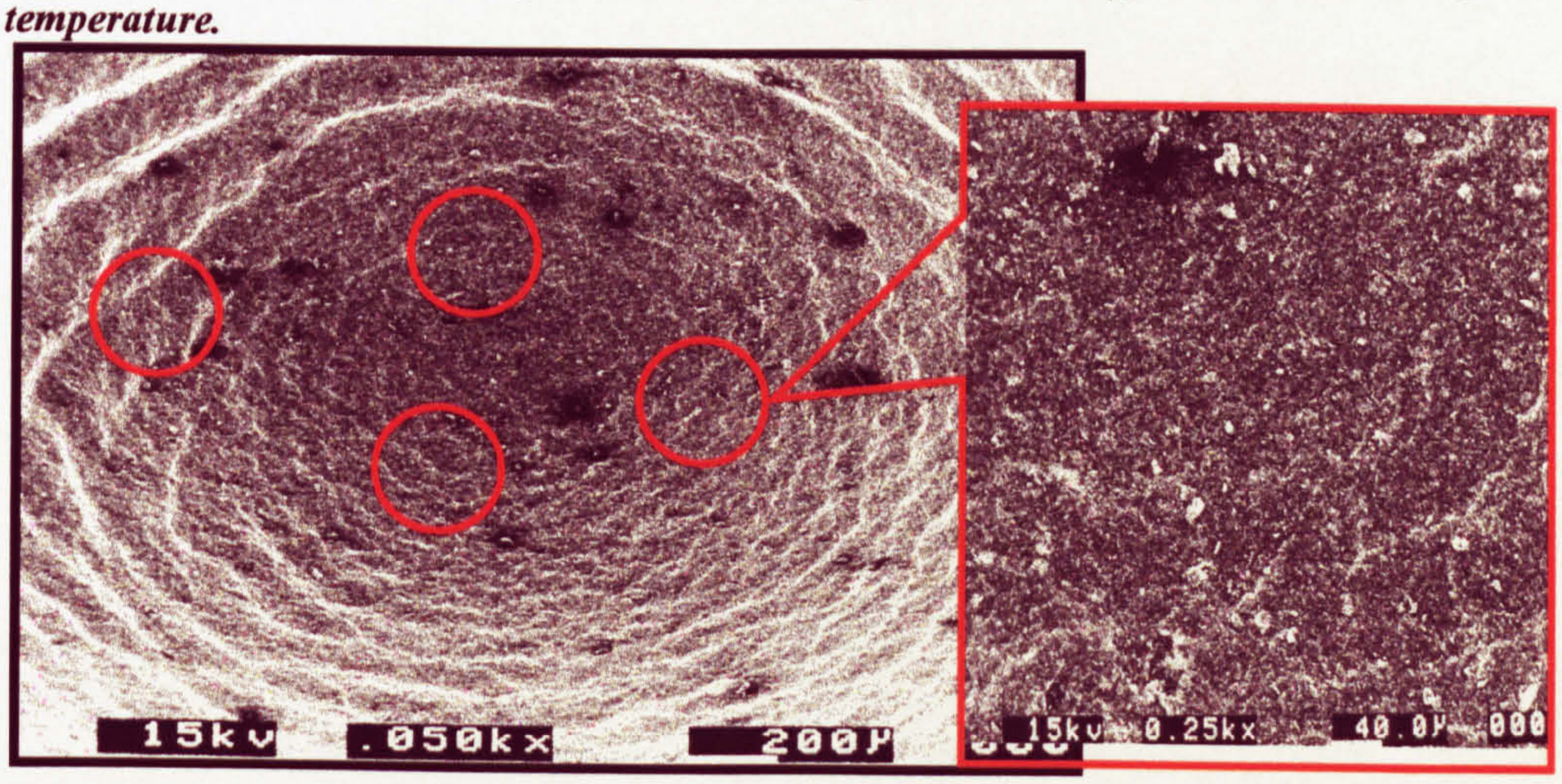
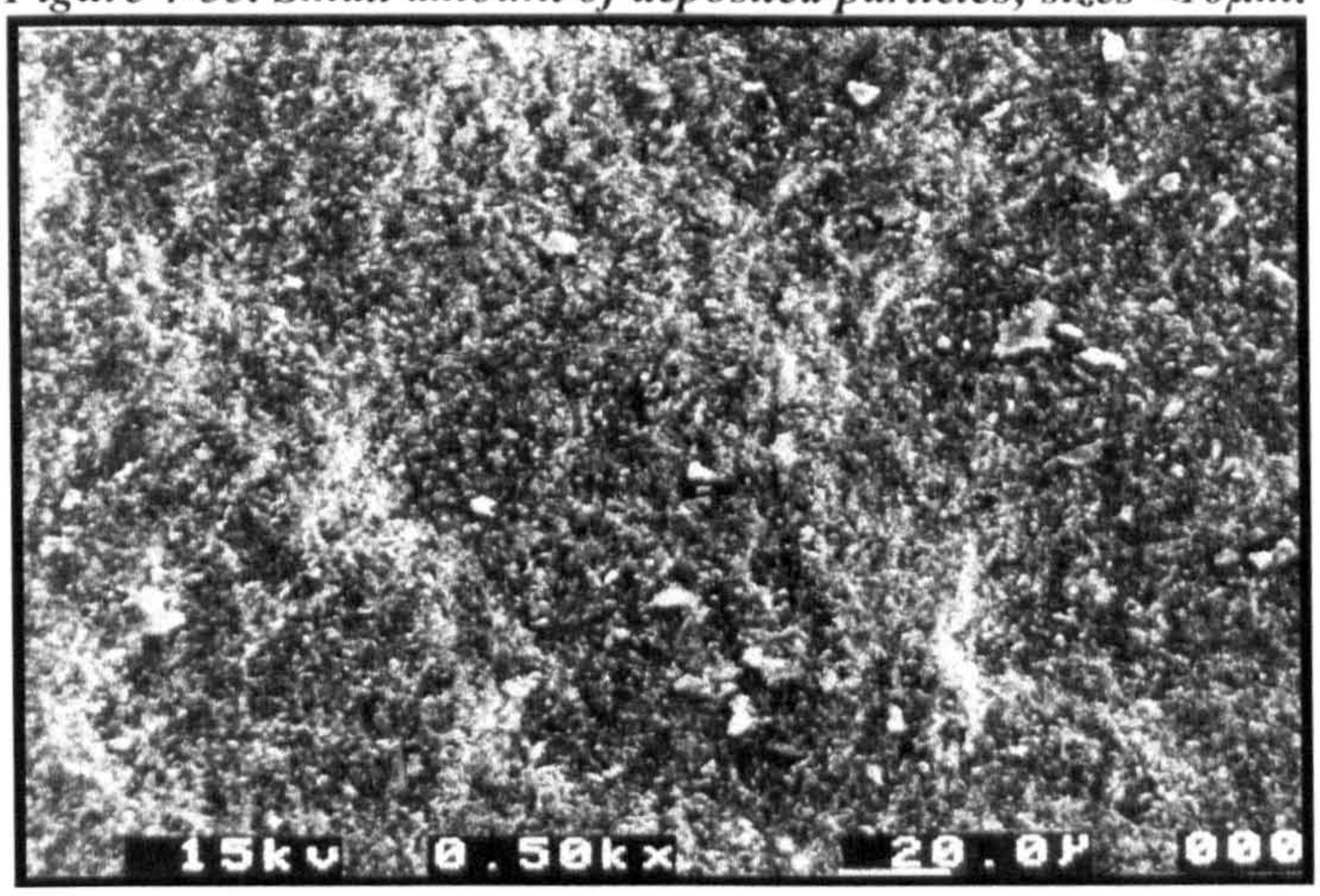


Figure 4-35. Small amount of deposited particles; sizes <10μm.



Blank
In
Original

List of Figures for Nimonic 75

Figure 4-36. The erosion rate verses target HT ratio for Nimonic 75 at different particle temperatures and impact velocities.

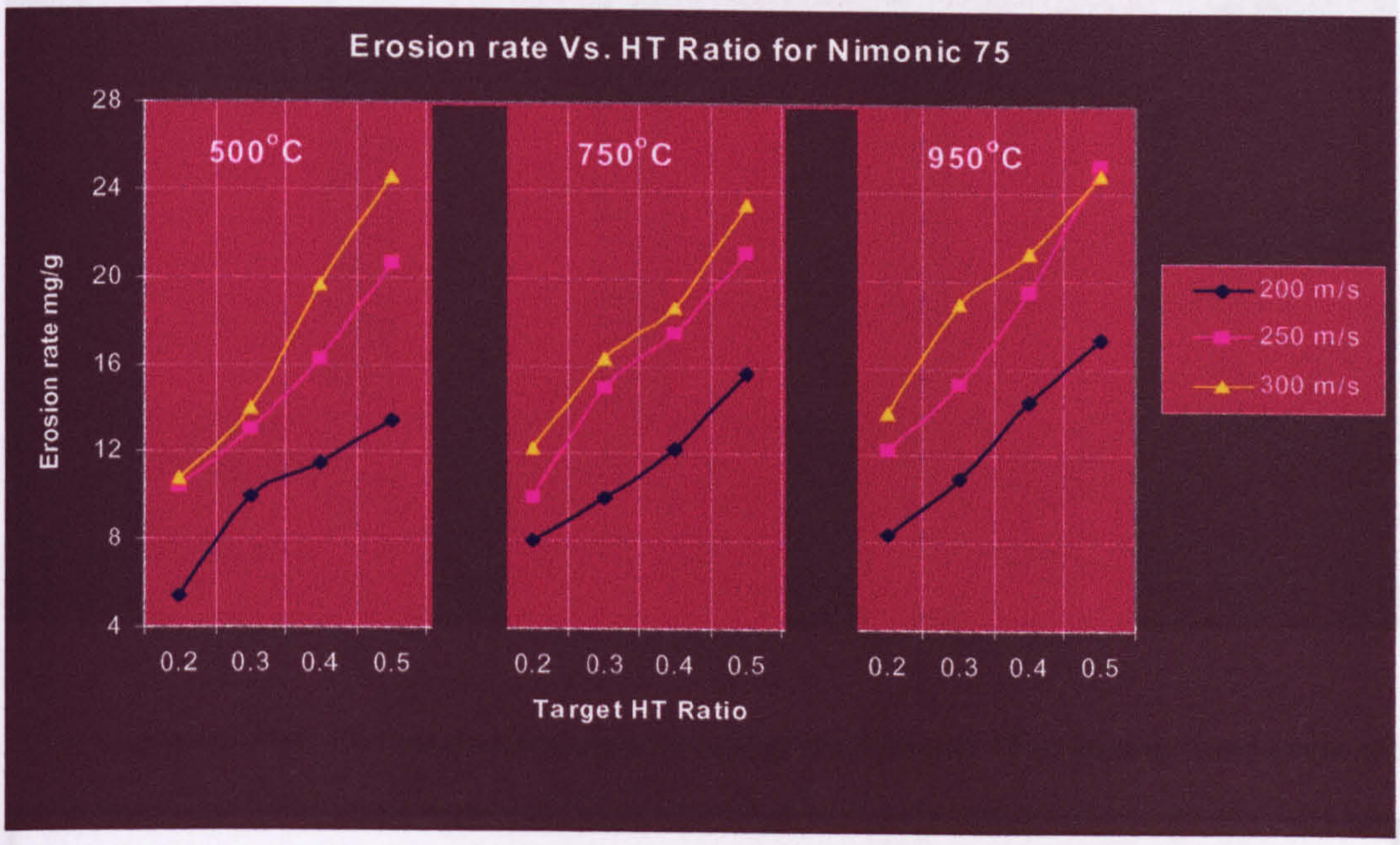


Figure 4-37. The erosion rate verses particle temperature for Nimonic 75 at different particle temperatures and impact velocities.

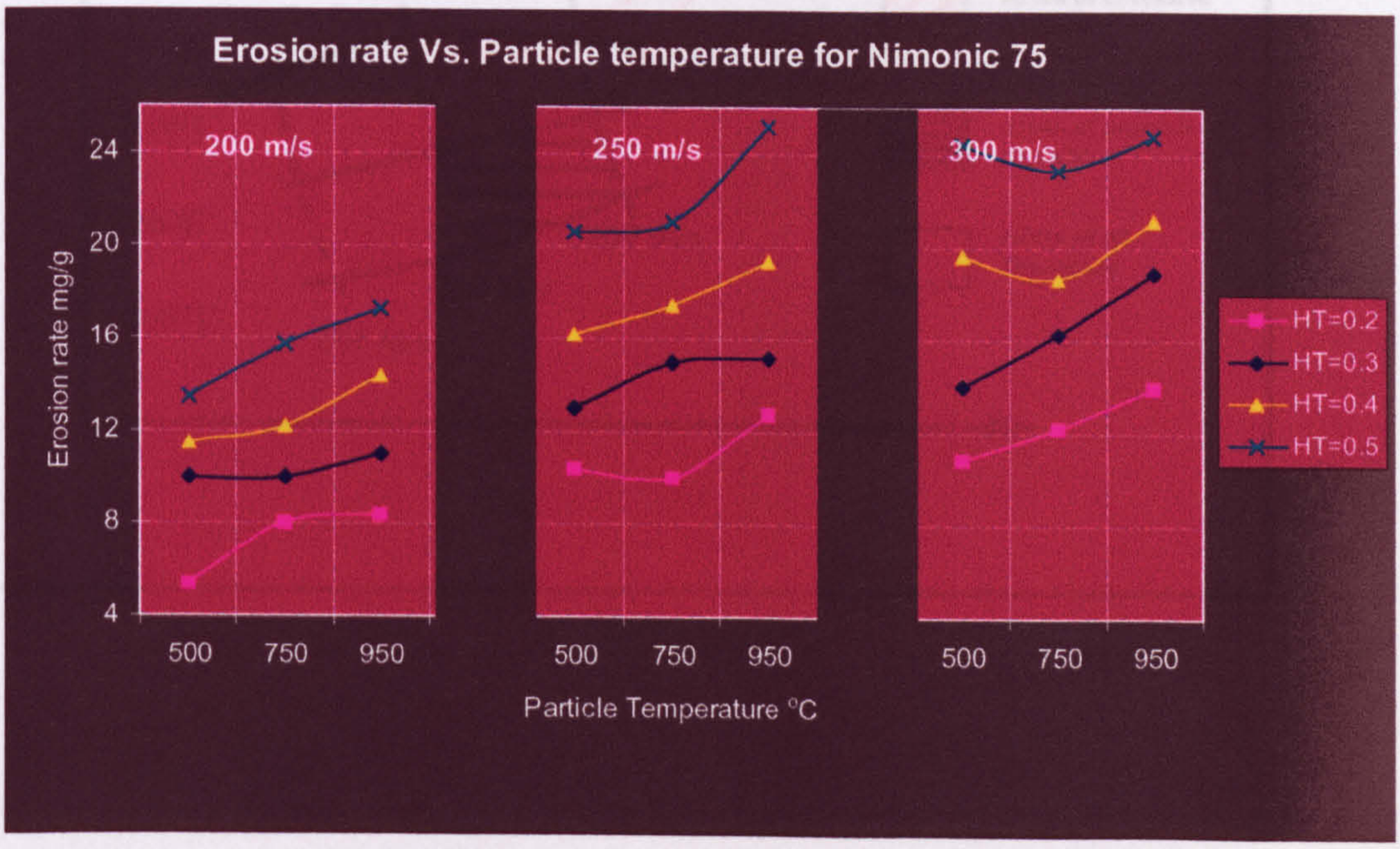


Figure 4-38. The erosion rate verses particle velocity for Nimonic 75 at different particle temperatures and impact velocities.

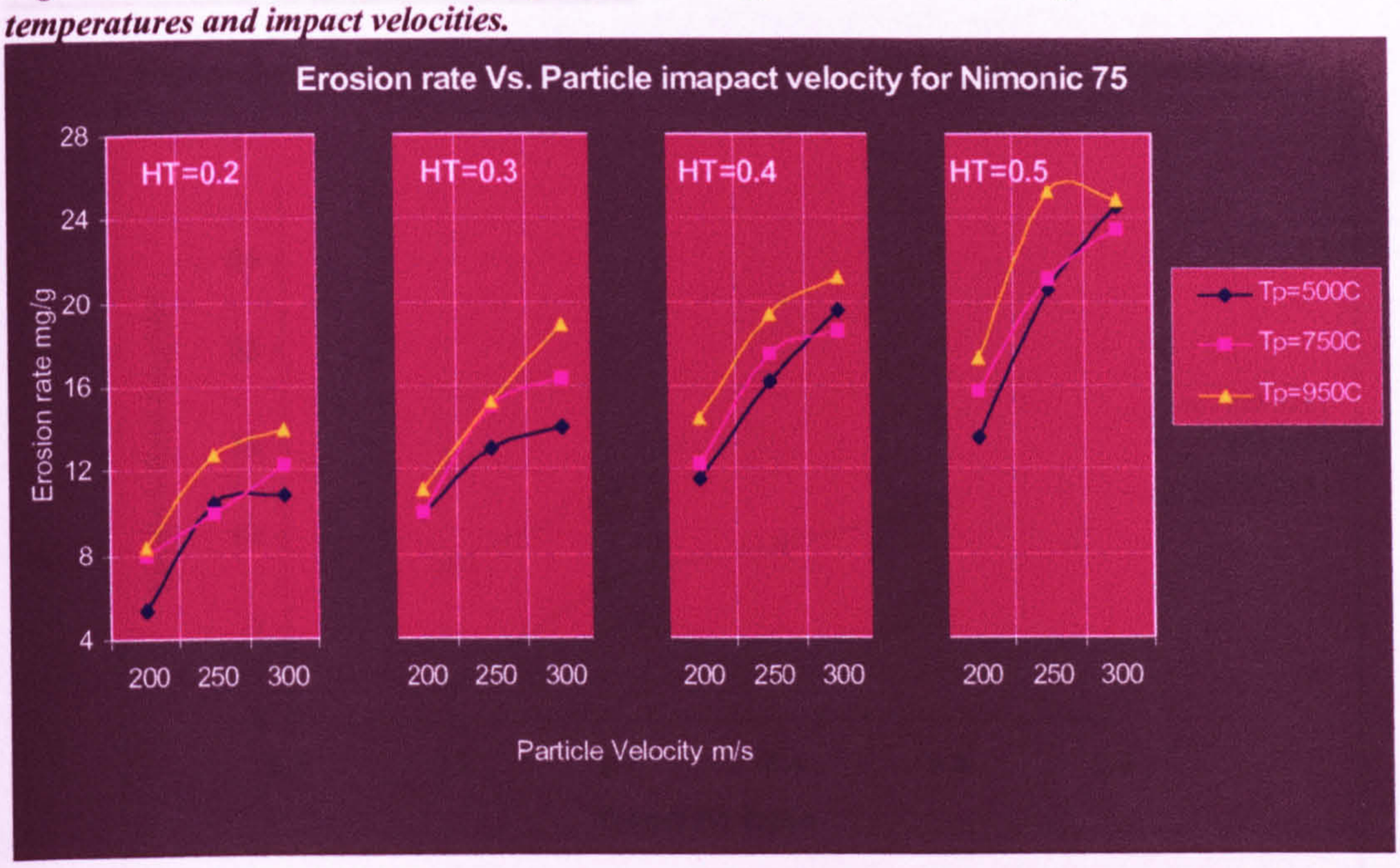
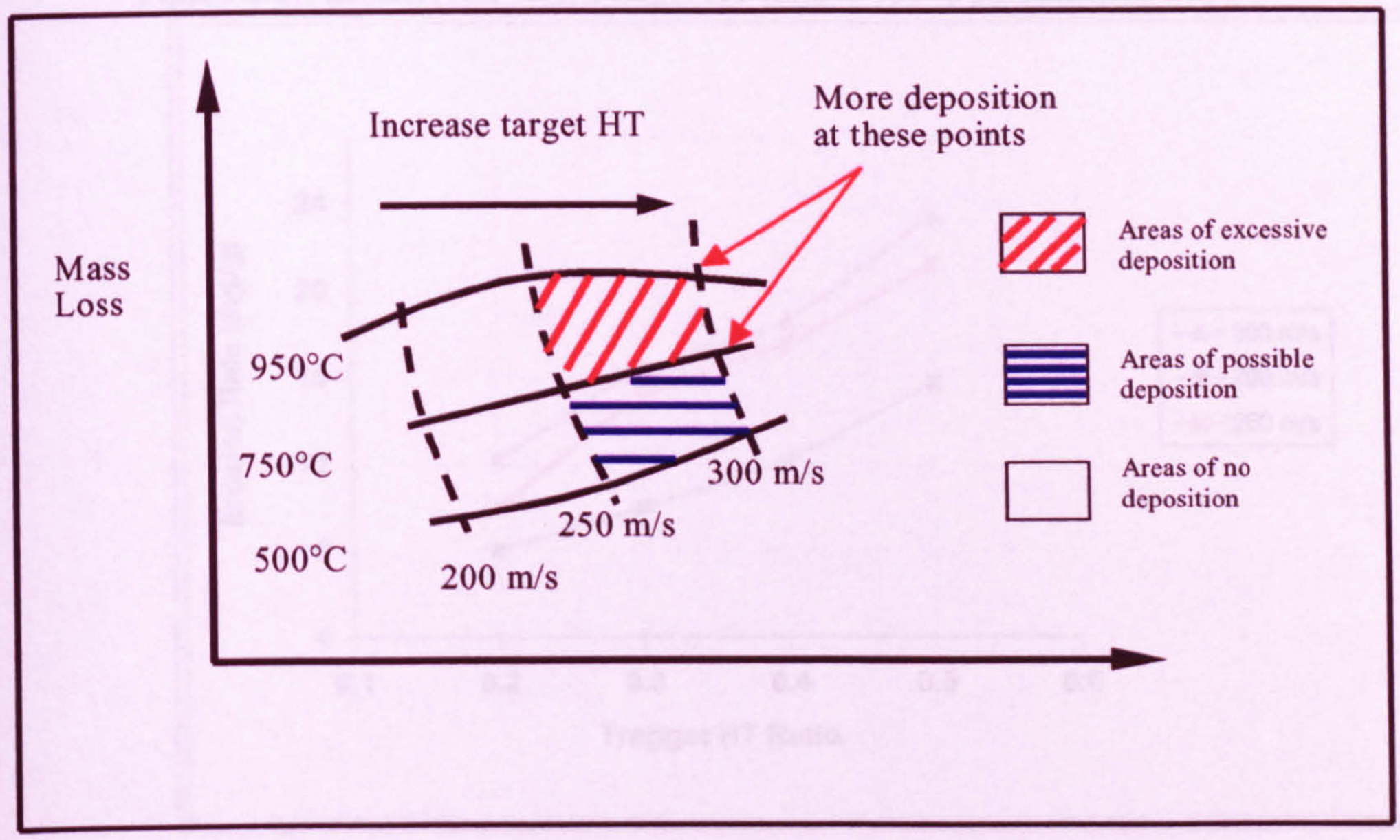


Figure 4-39. The erosion/deposition model of the Nimonic 75 at impingement angle of 30°.



Effect of Target HT ratio

Figure 4-40. Erosion rate versus target HT ratio at 500 ℃ particle temperature.

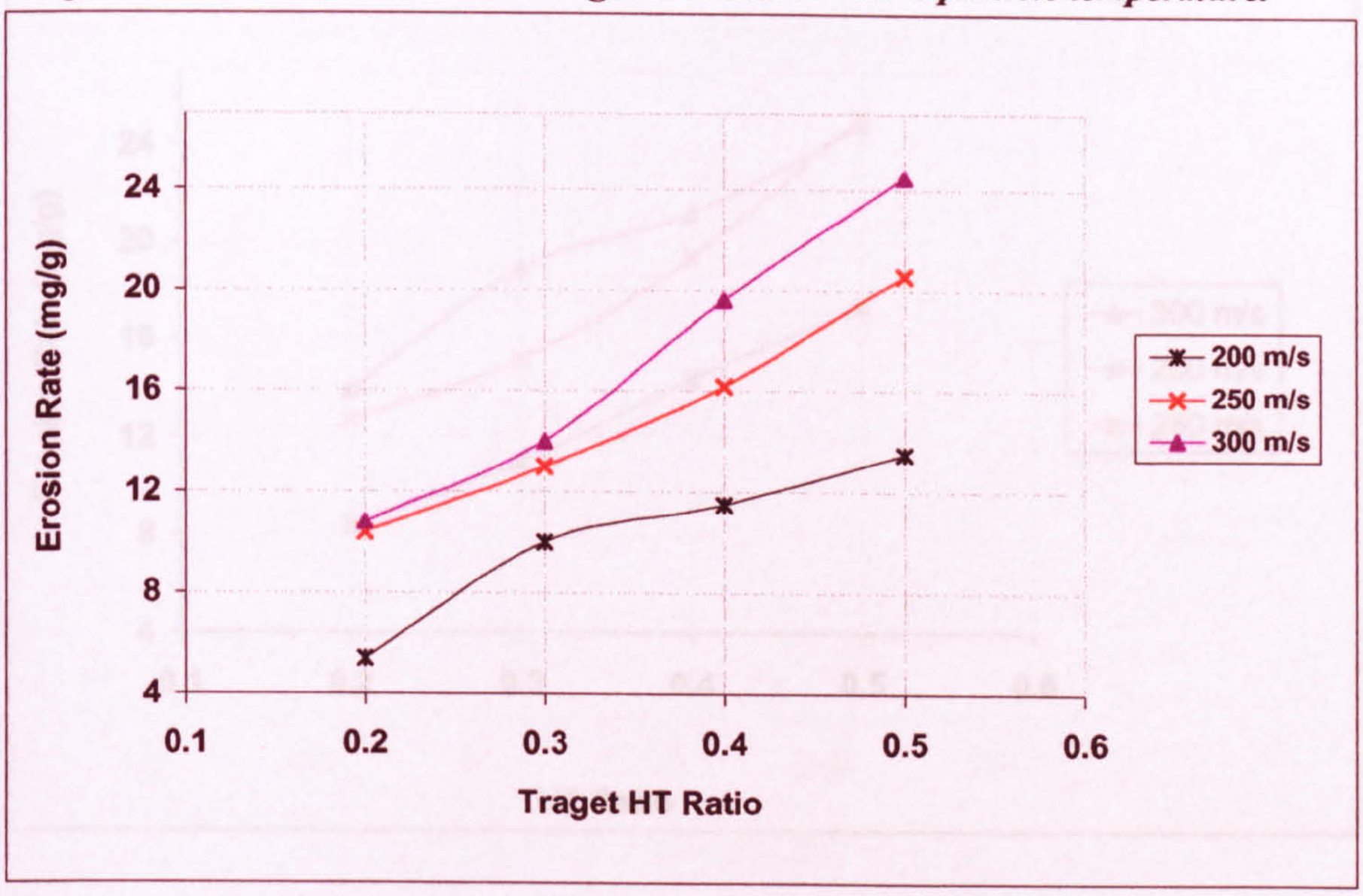


Figure 4-41. Erosion rate versus target HT ratio at 750 ℃ particle temperature.

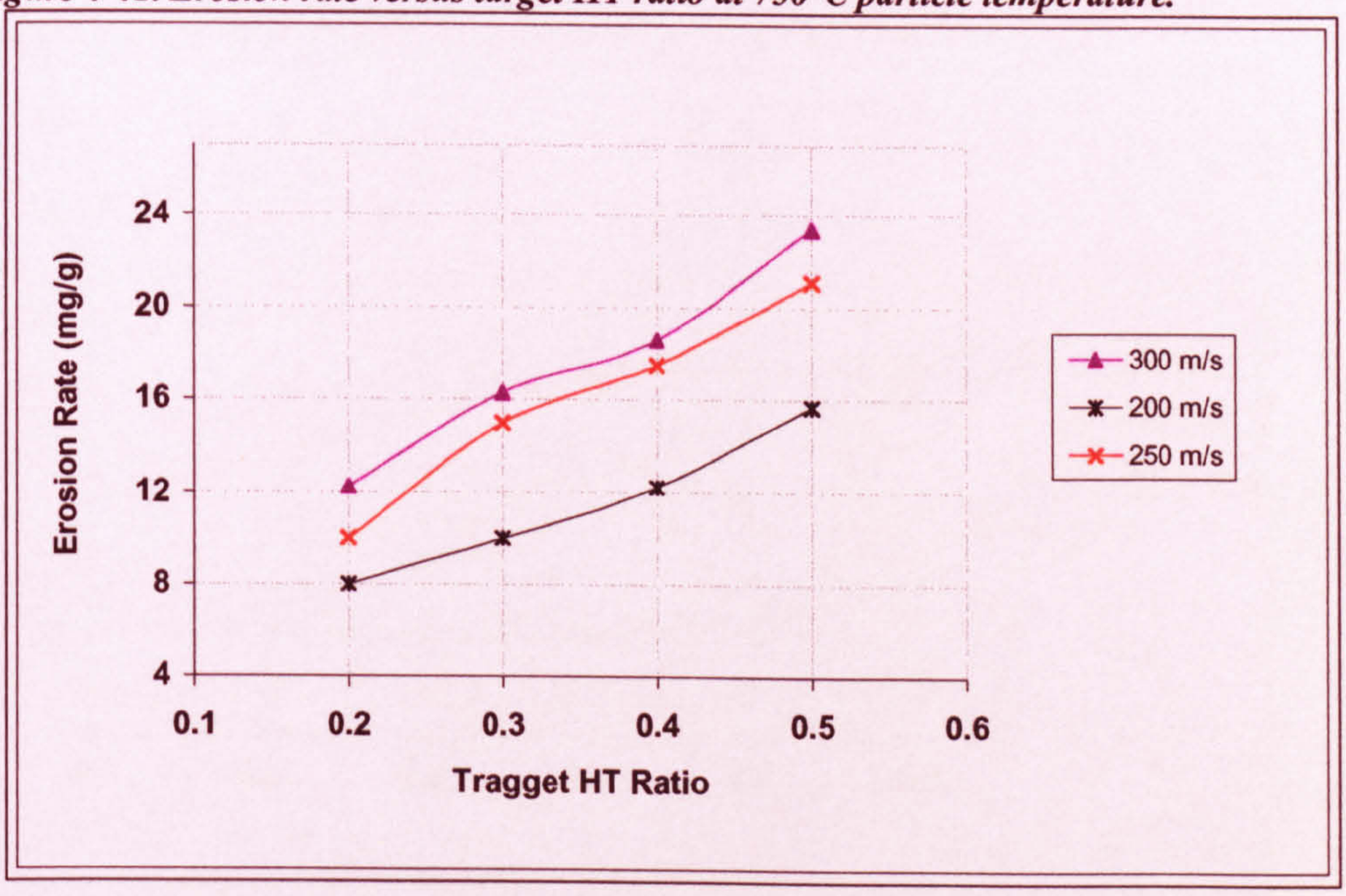
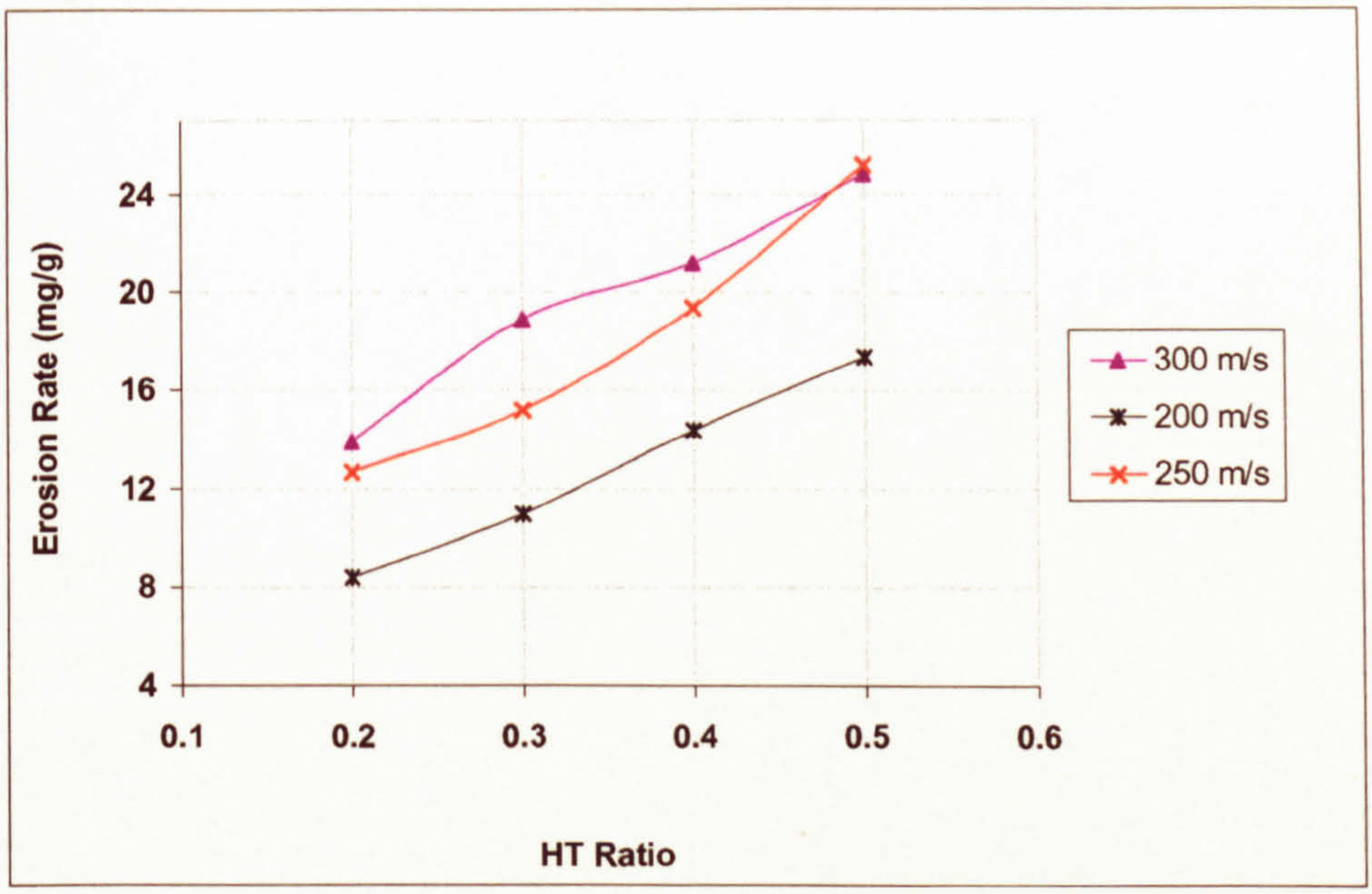


Figure 4-42. Erosion rate versus target HT ratio at 950 ℃ particle temperature.



- ***Effect of Particle Temperature***

Figure 4-43. Erosion rate versus particle temperature at HT=0.2 (275 ℃).

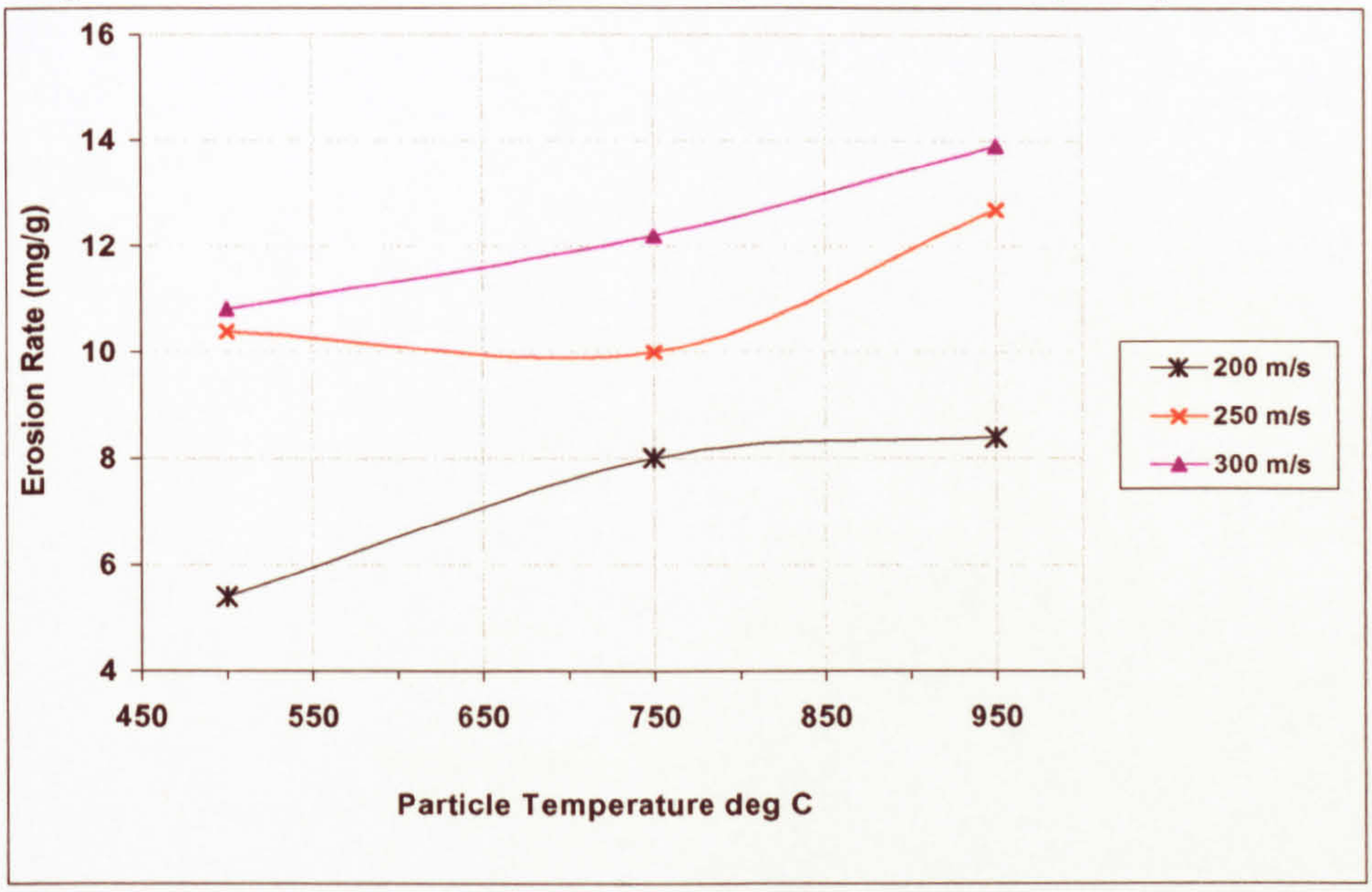


Figure 4-44. Erosion rate versus particle temperature at HT=0.3 (415 ℃).

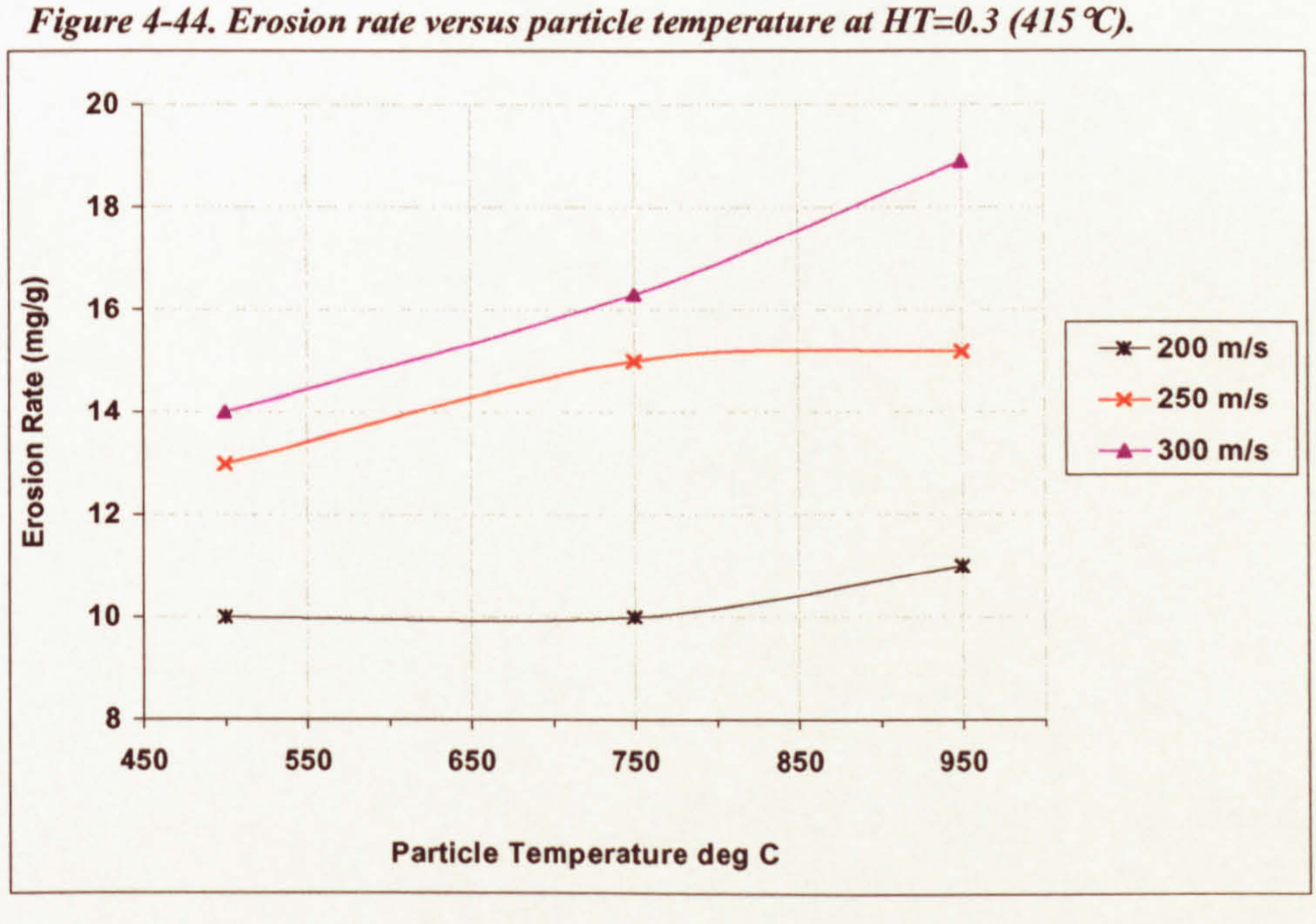


Figure 4-45. Erosion rate versus particle temperature at HT=0.4 (550 ℃).

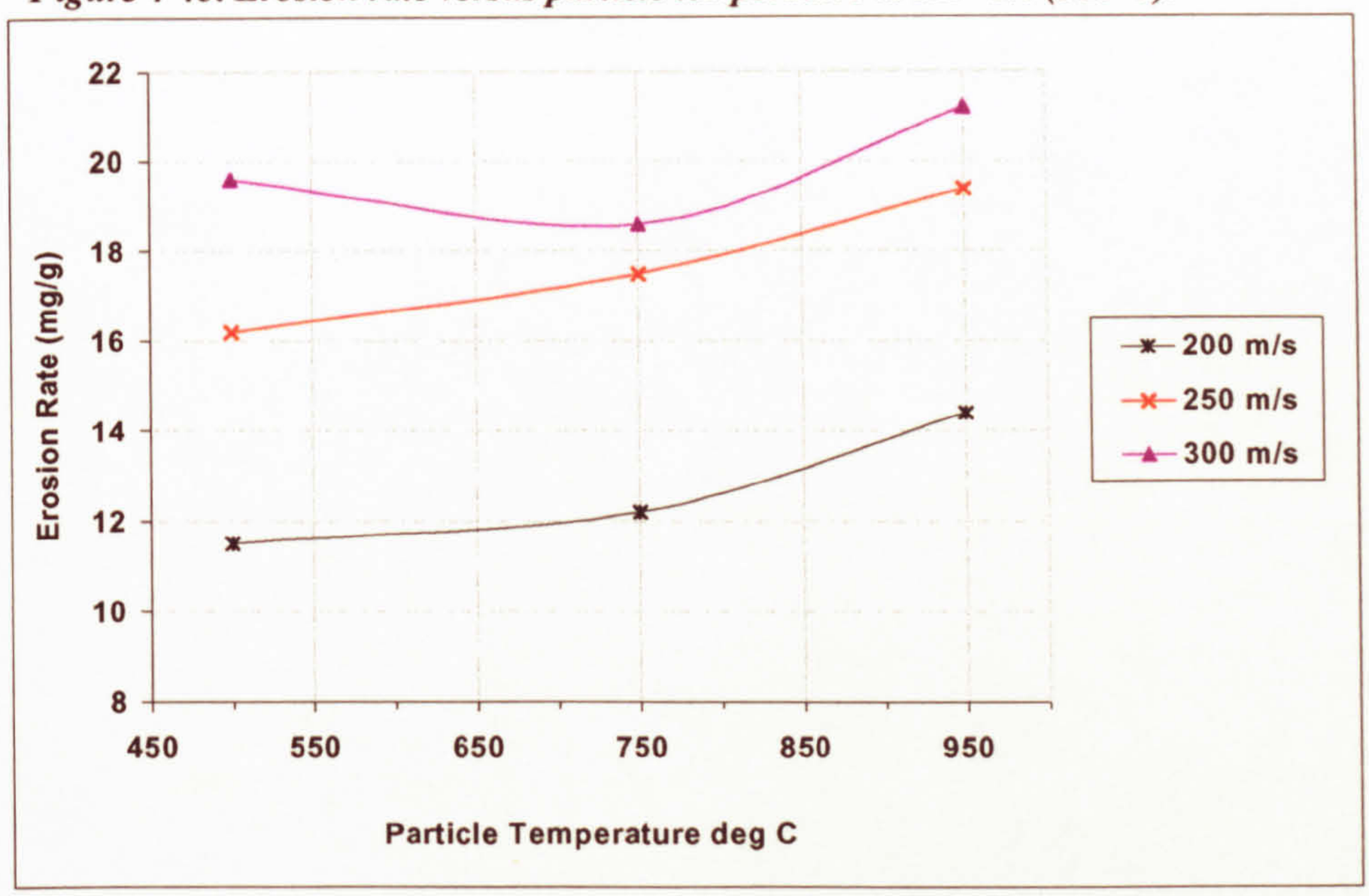
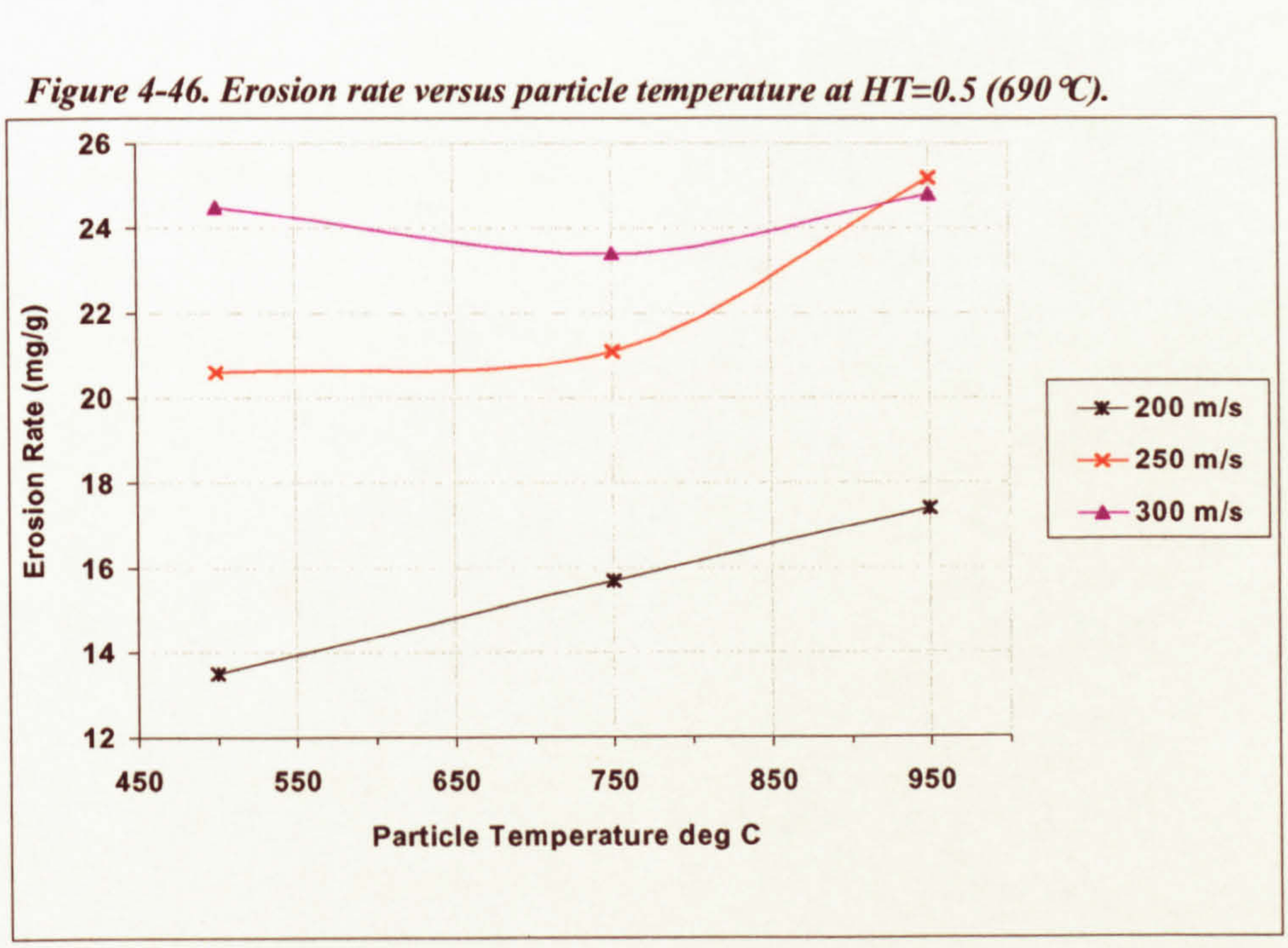


Figure 4-46. Erosion rate versus particle temperature at HT=0.5 (690 ℃).



- **Effect of Particle Velocity**

Figure 4-47. Erosion rate versus particle impact velocity at HT=0.2 (275 ℃).

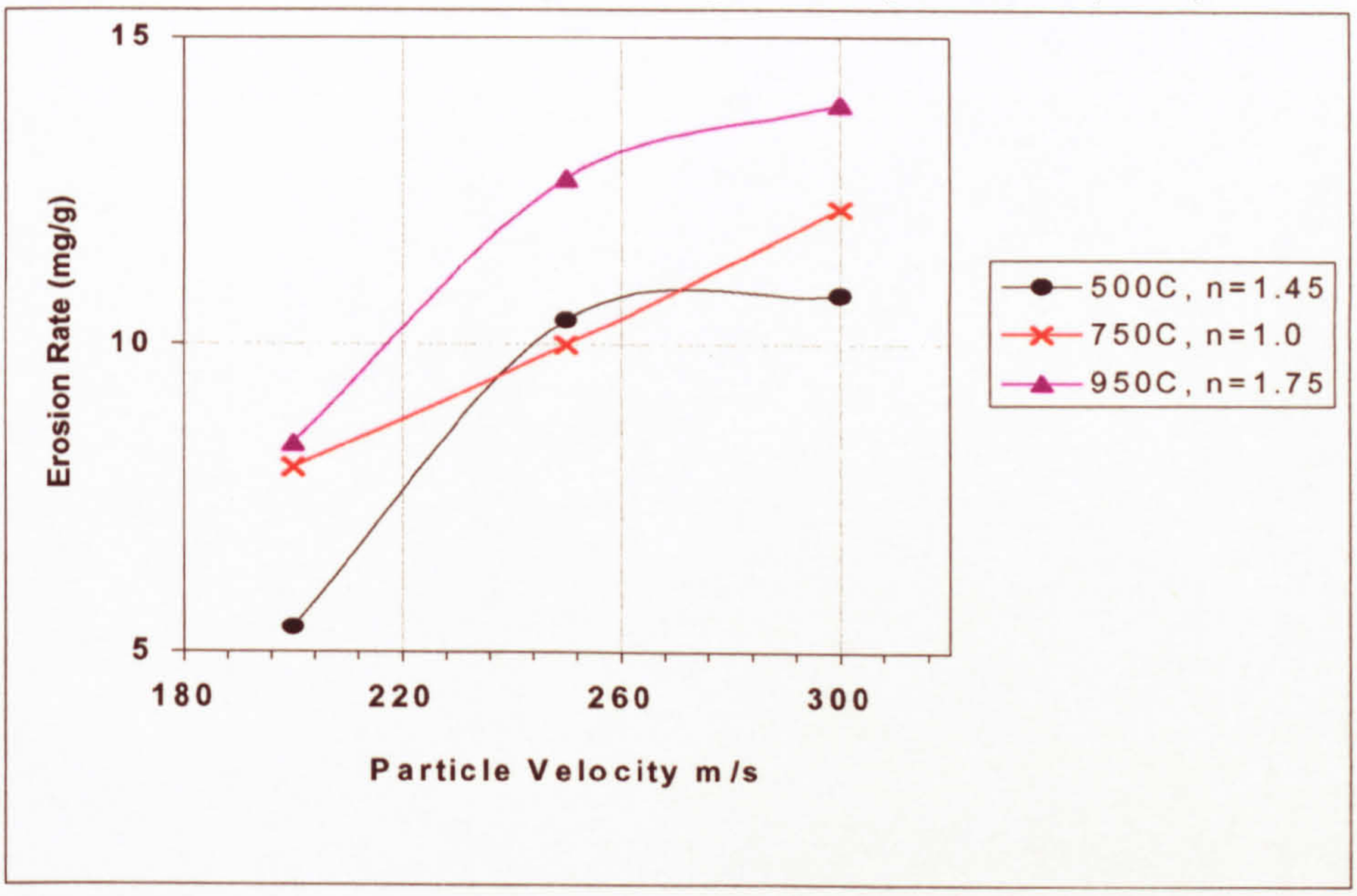


Figure 4-48. Erosion rate versus particle impact velocity at HT=0.3 (415 ℃).

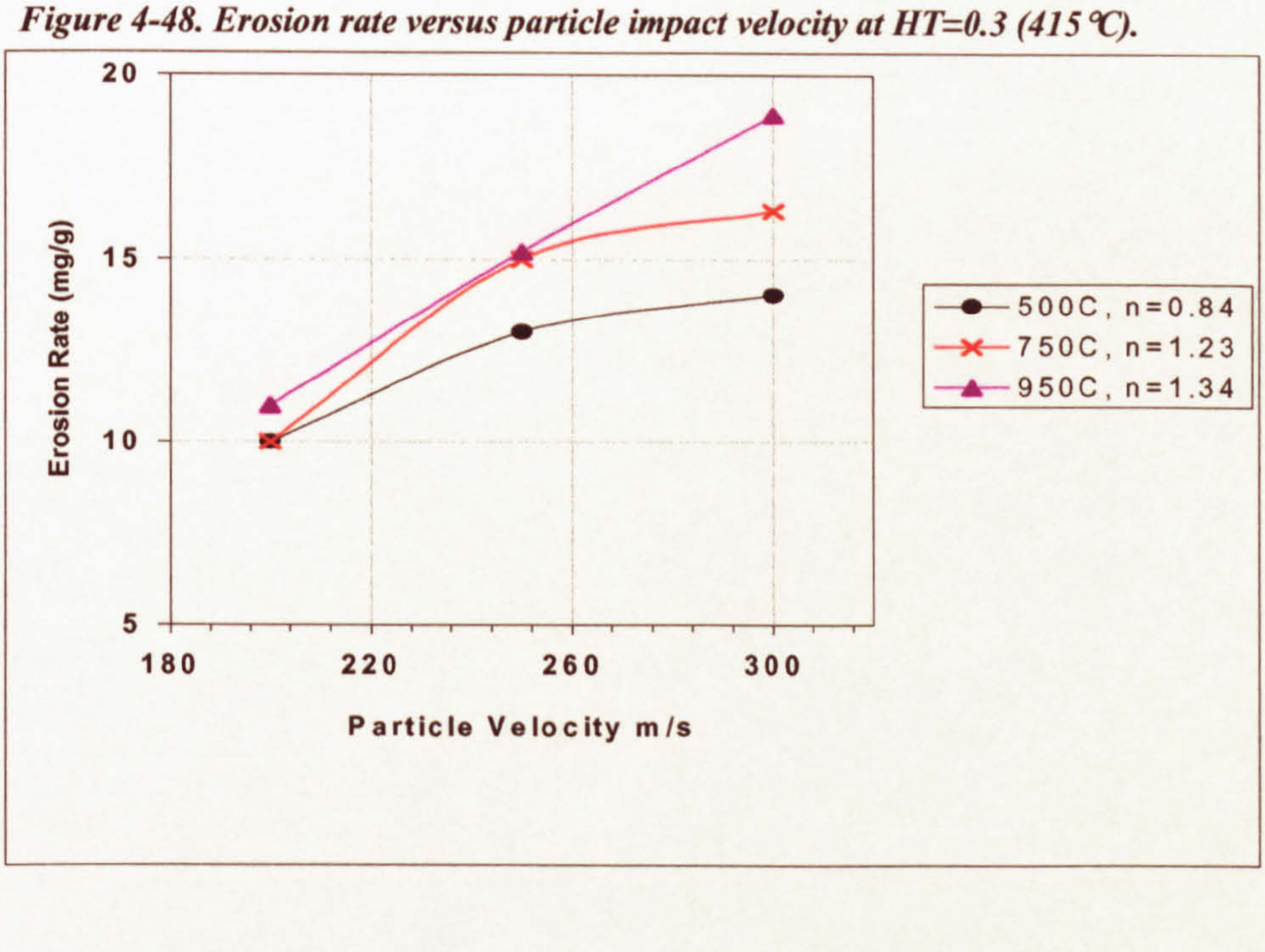


Figure 4-49. Erosion rate versus particle impact velocity at HT=0.4 (550 ℃).

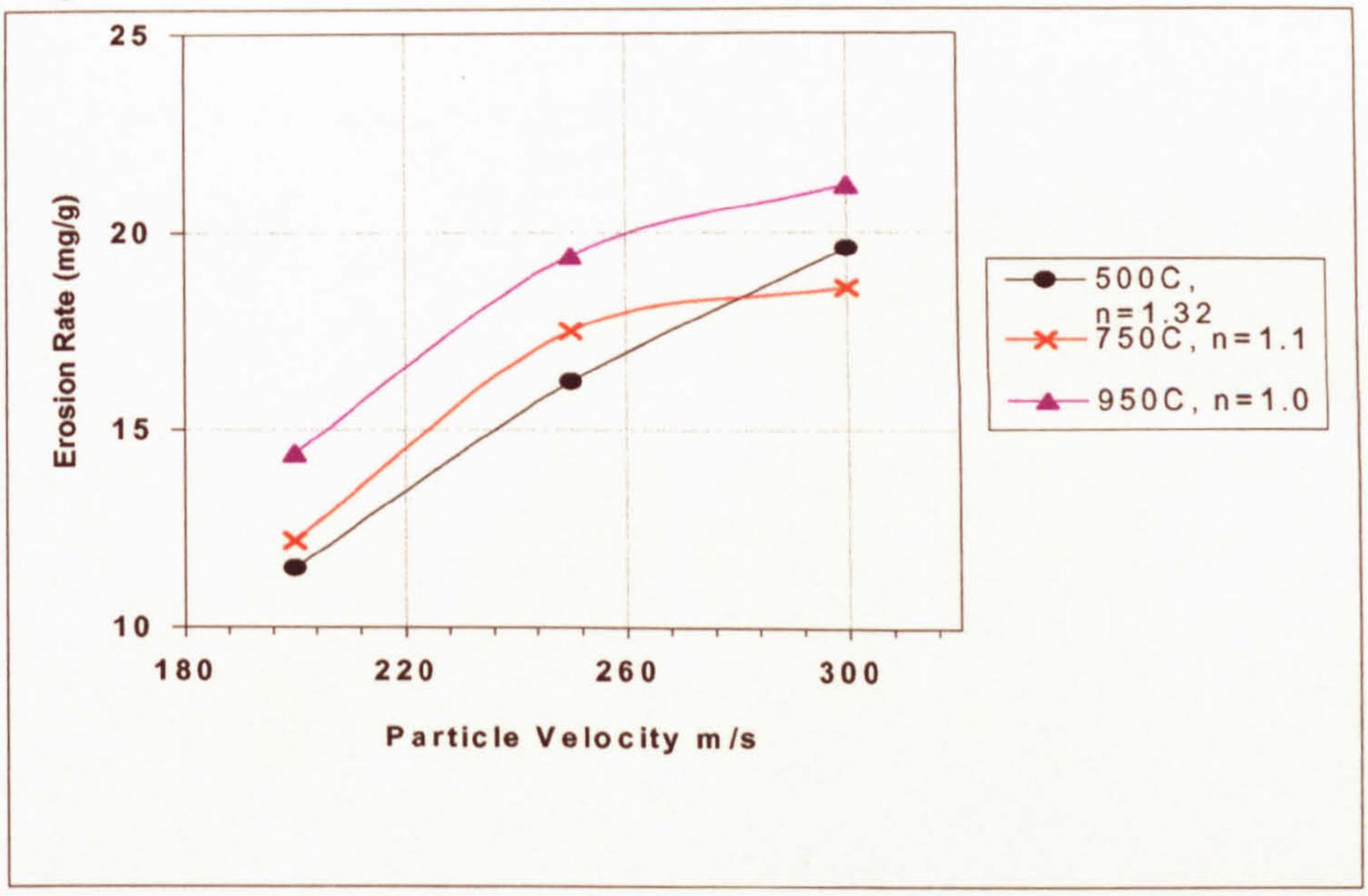
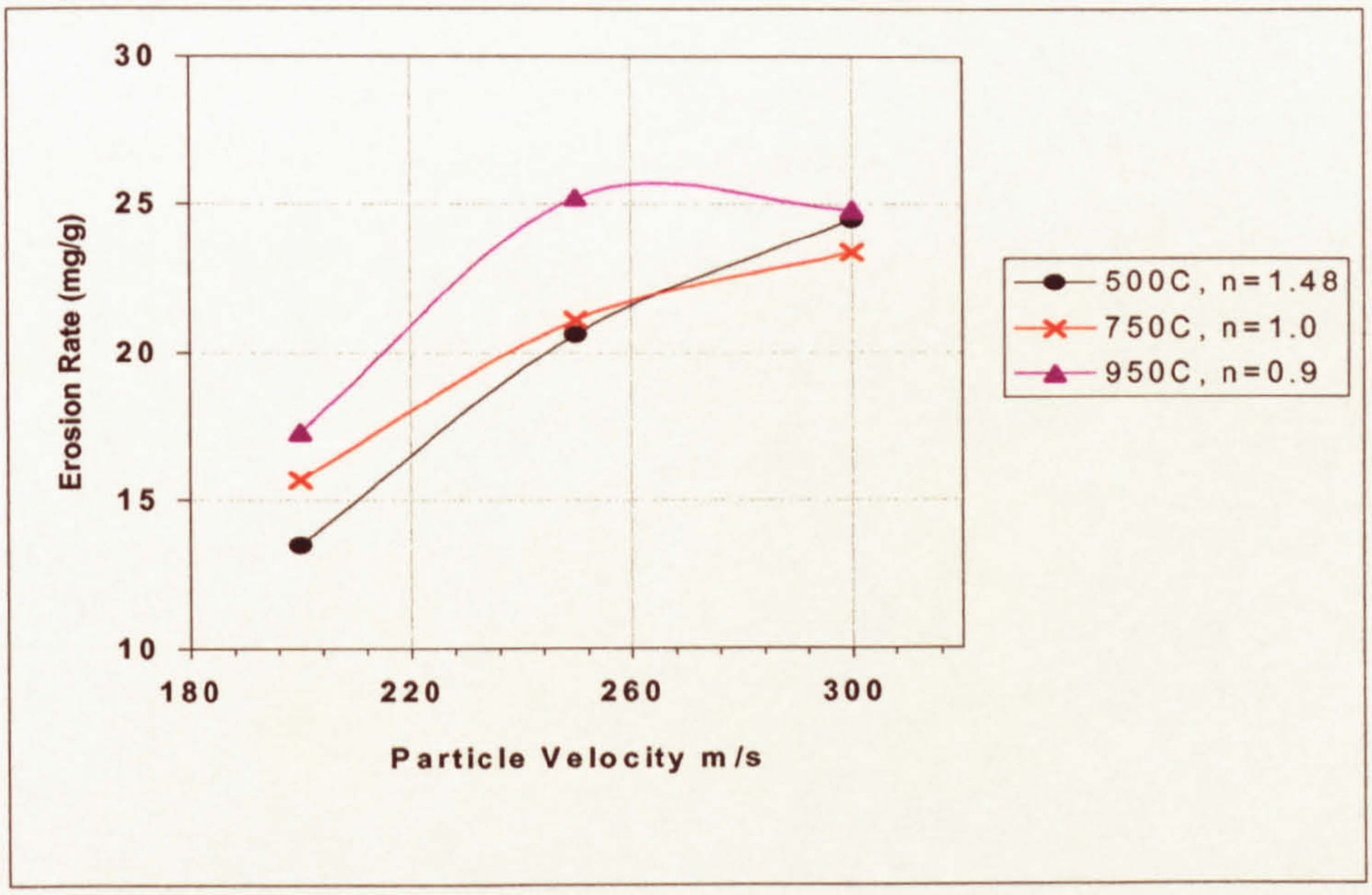


Figure 4-50. Erosion rate versus particle impact velocity at HT=0.5 (690 ℃).



Comparison between the Effect of Target HT ratio and Particle Temperature.

Figure 4-51. Erosion rate versus target HT ratio and particle temperature at 200 m/s particle velocity.

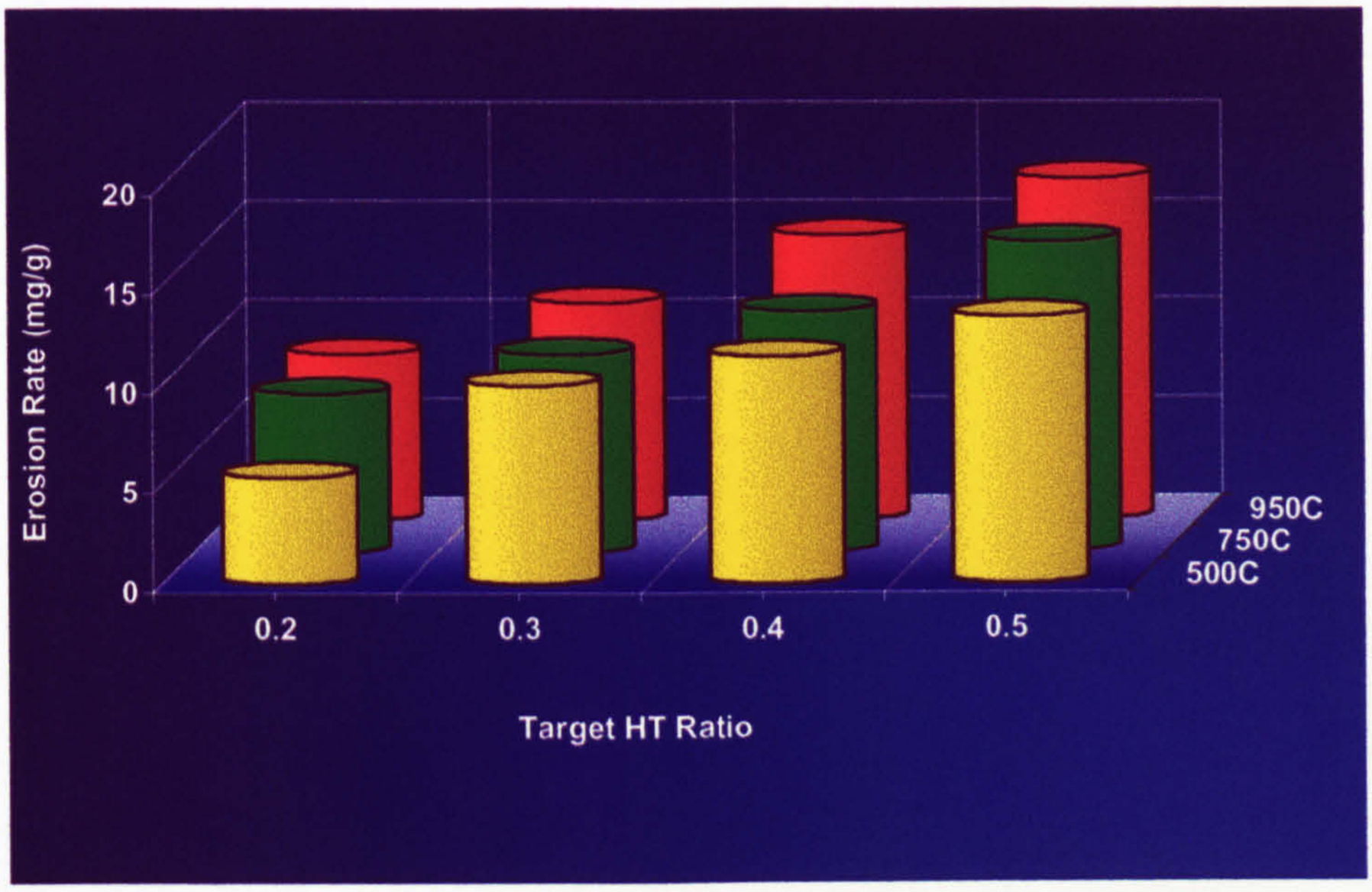


Figure 4-52. Erosion rate versus target HT ratio and particle temperature at 250 m/s particle velocity.

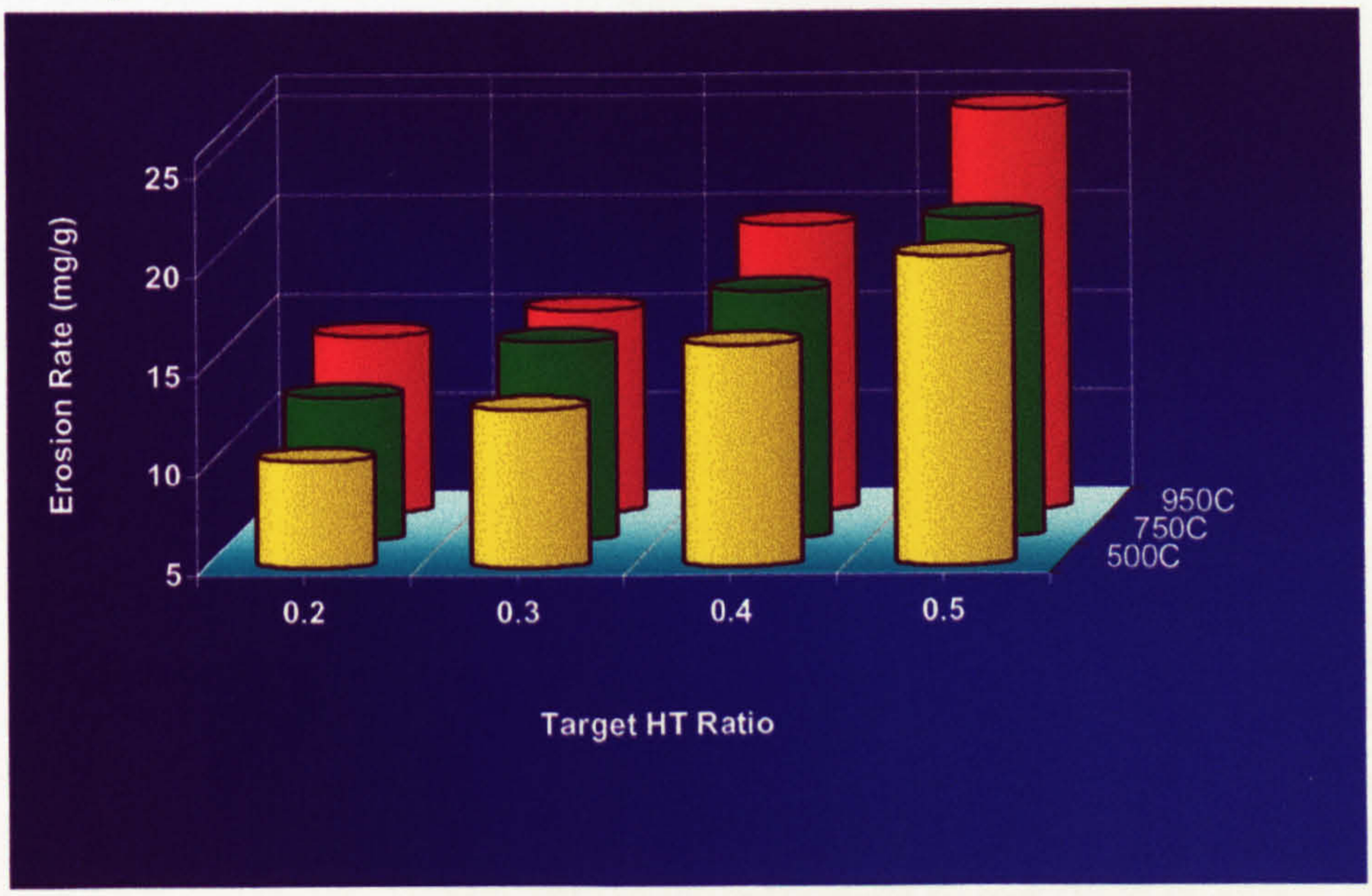
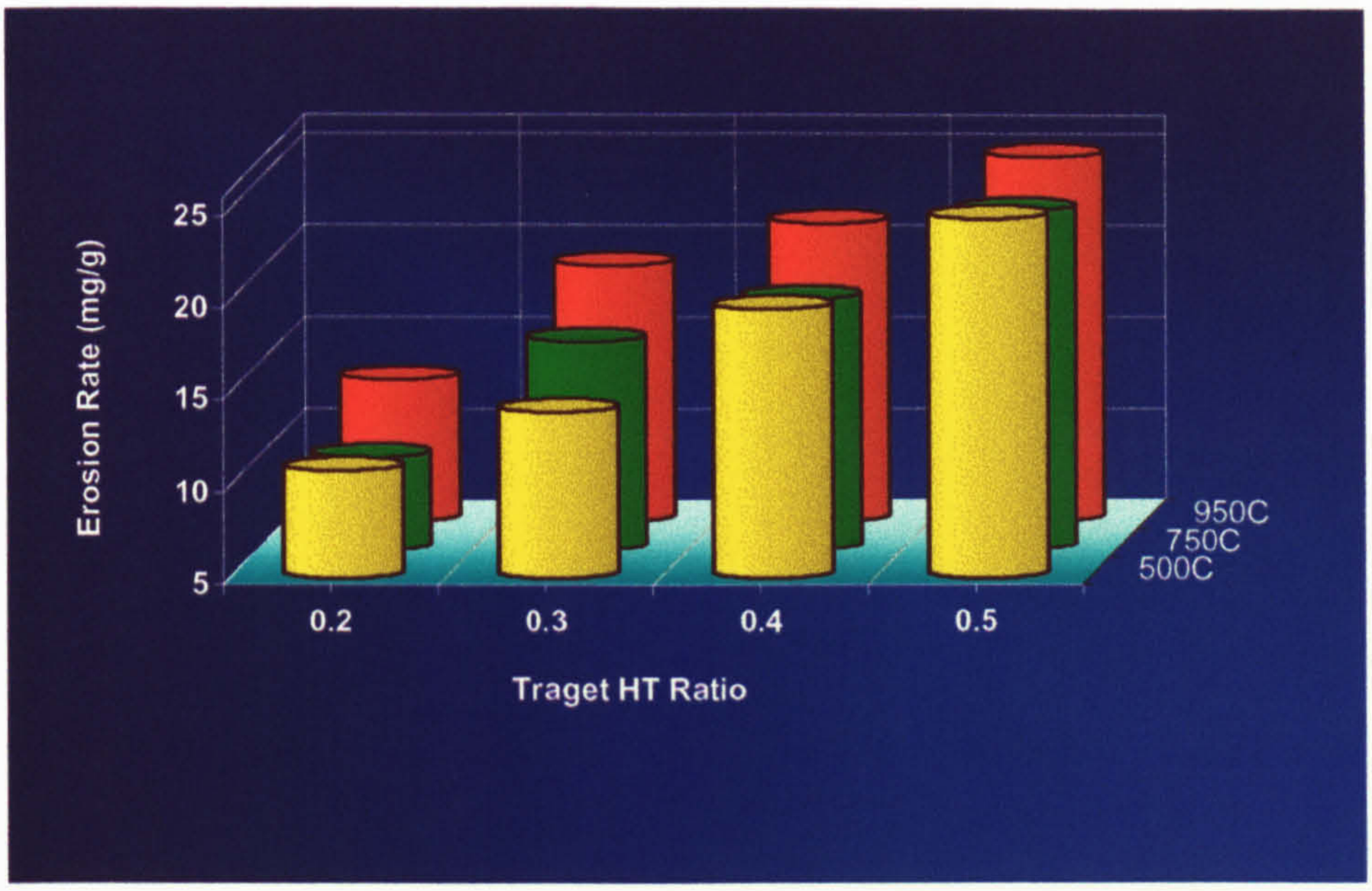


Figure 4-53. Erosion rate versus target HT ratio and particle temperature at 300 m/s particle velocity.



Surface Examination Results For Nimonic 75 at 30° Impact Angle.

- *Scanning Electron Microscope (SEM) Results (Impact velocity of 200 and 250 m/s.)*

Figure 4-54. Beach wave erosion pattern at Nimonic 75 surface, HT=0.4, particle velocity; 200 m/s and 750 ℃ particle temperature.

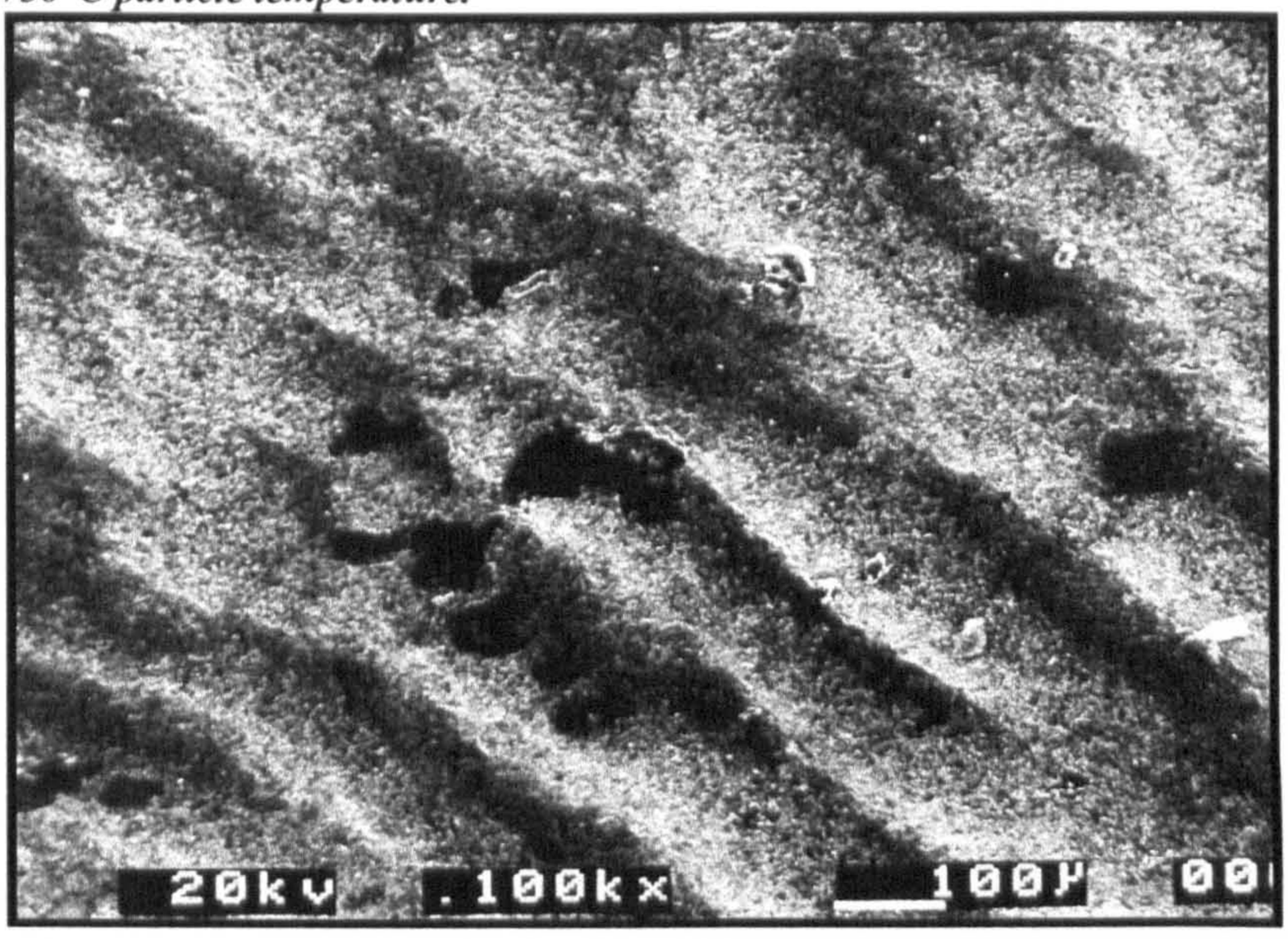


Figure 4-55. Type I cut at 250m/s particle velocity, HT=0.5 ratio and 950 ℃ particle temperature.

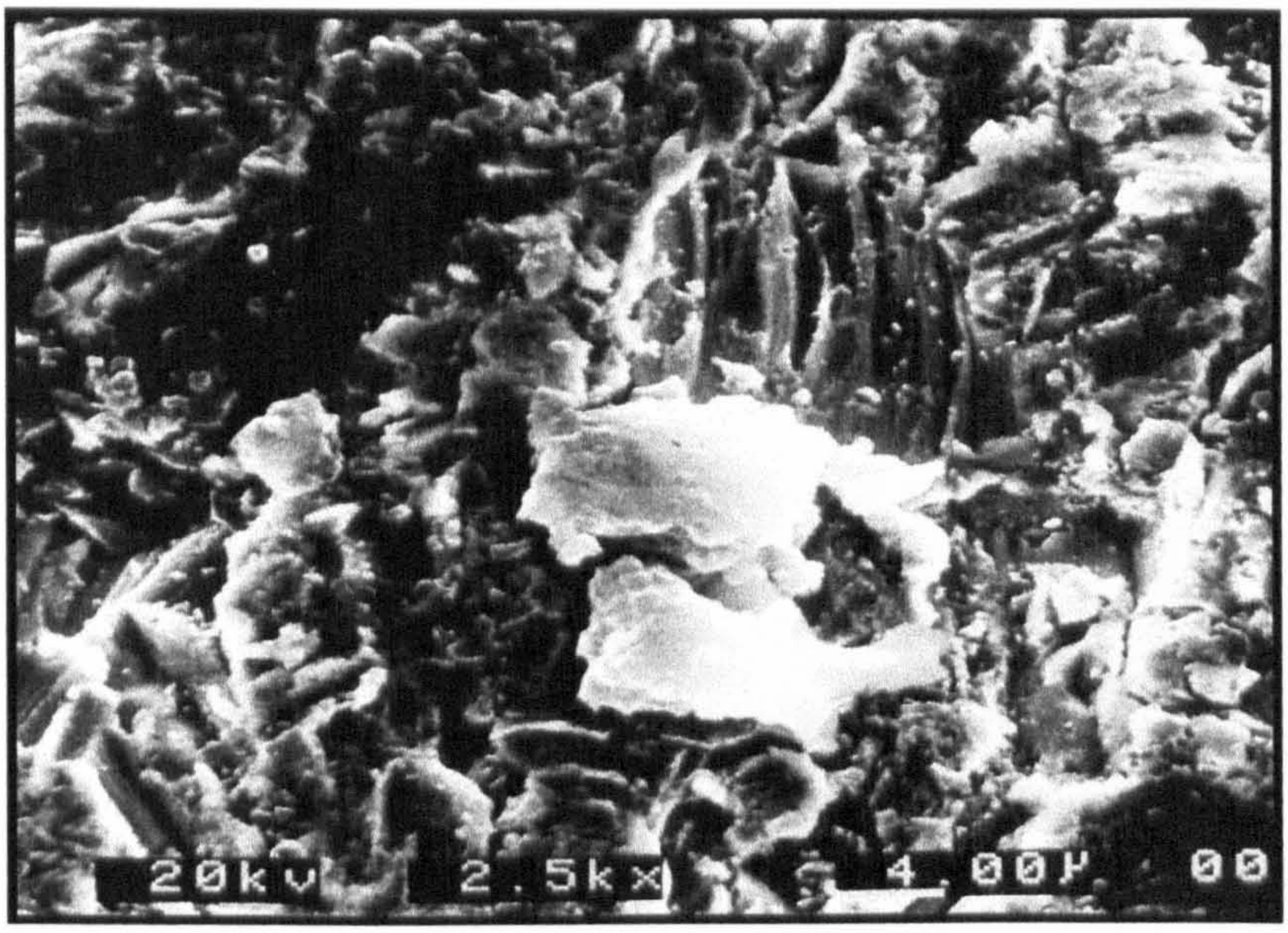
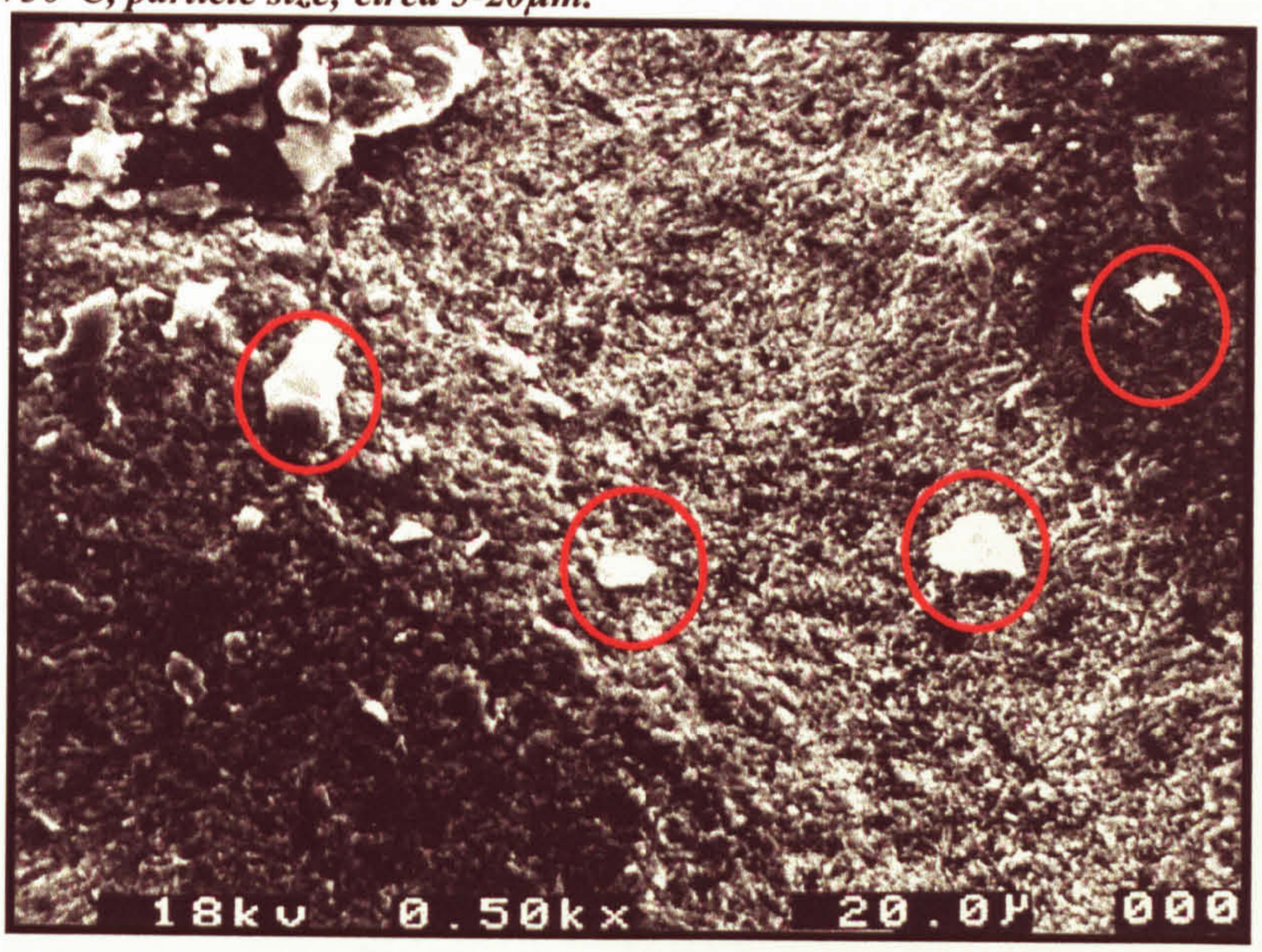


Figure 4-56. Particle deposited on the Nimonic target at 250m/s velocity, HT= 0.4, Particle temperature=750℃, particle size; circa 5-20μm.



- *Scanning Electron Microscope (SEM) Results (Impact velocity of 300 m/s.)*

Figure 4-57. Areas of heavy multi-sizes particle deposited at velocity of 300 m/s, HT=0.5 and 950 ℃ particle temperature.

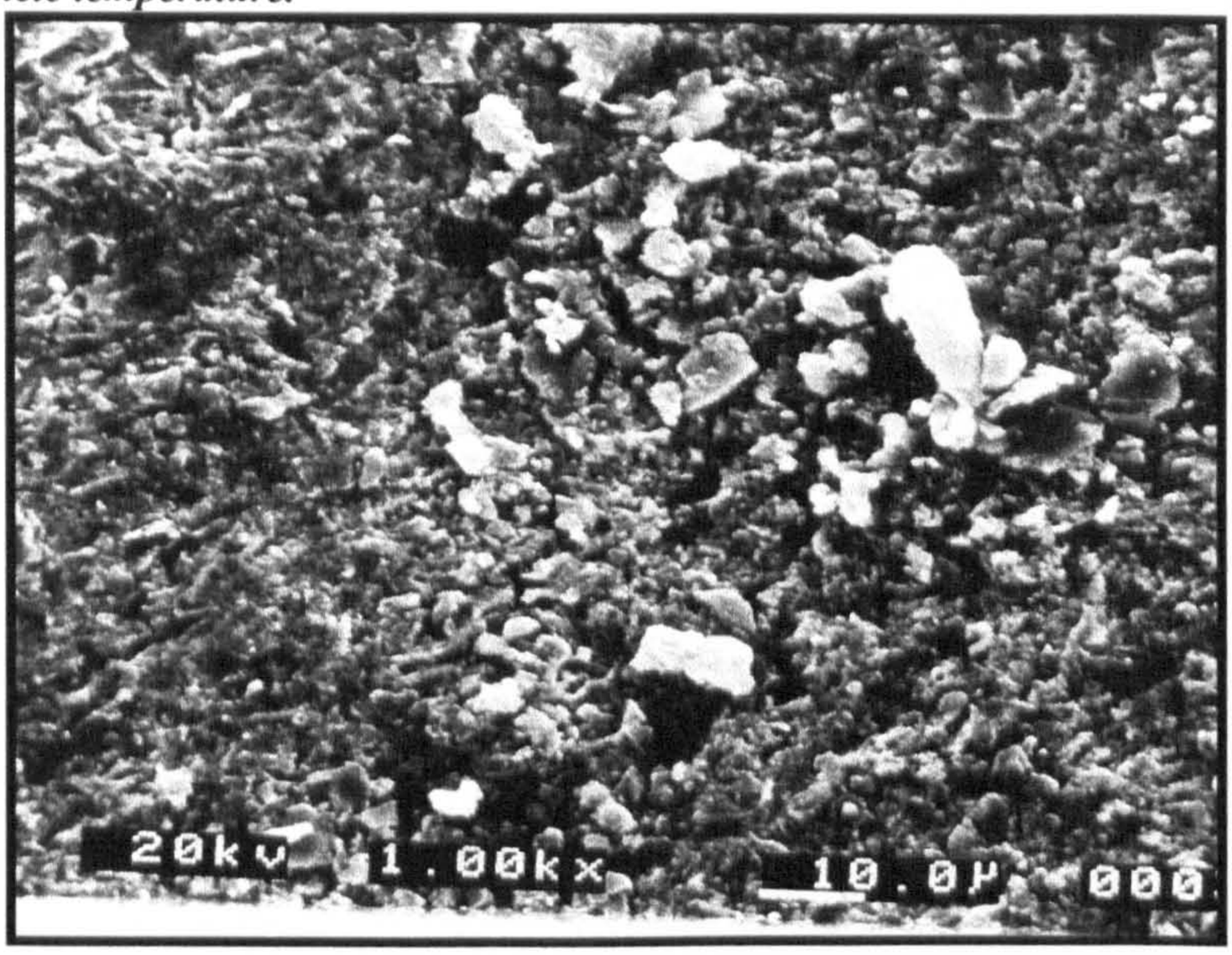


Figure 4-58. An enlargement of figure 5.21 (above).

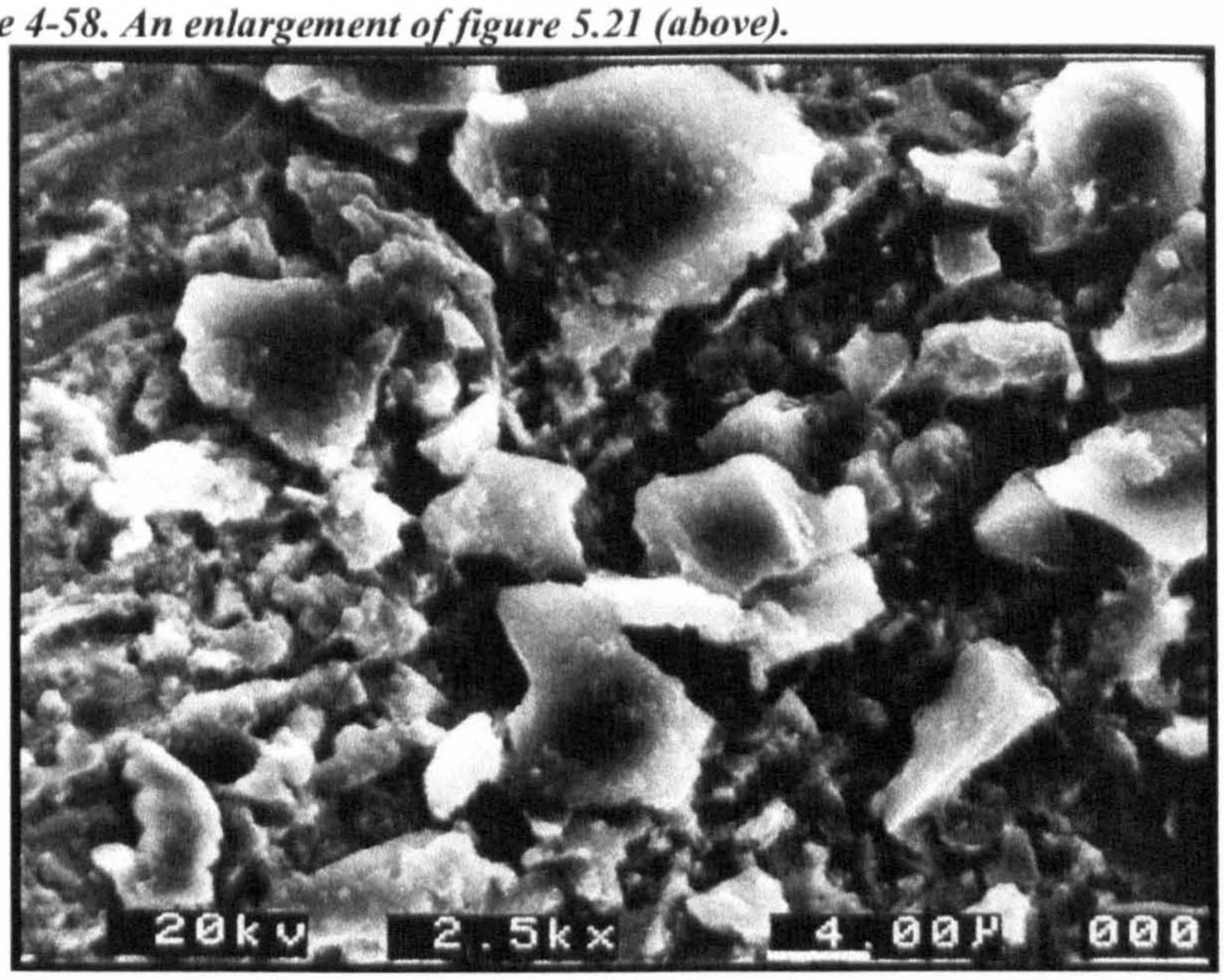
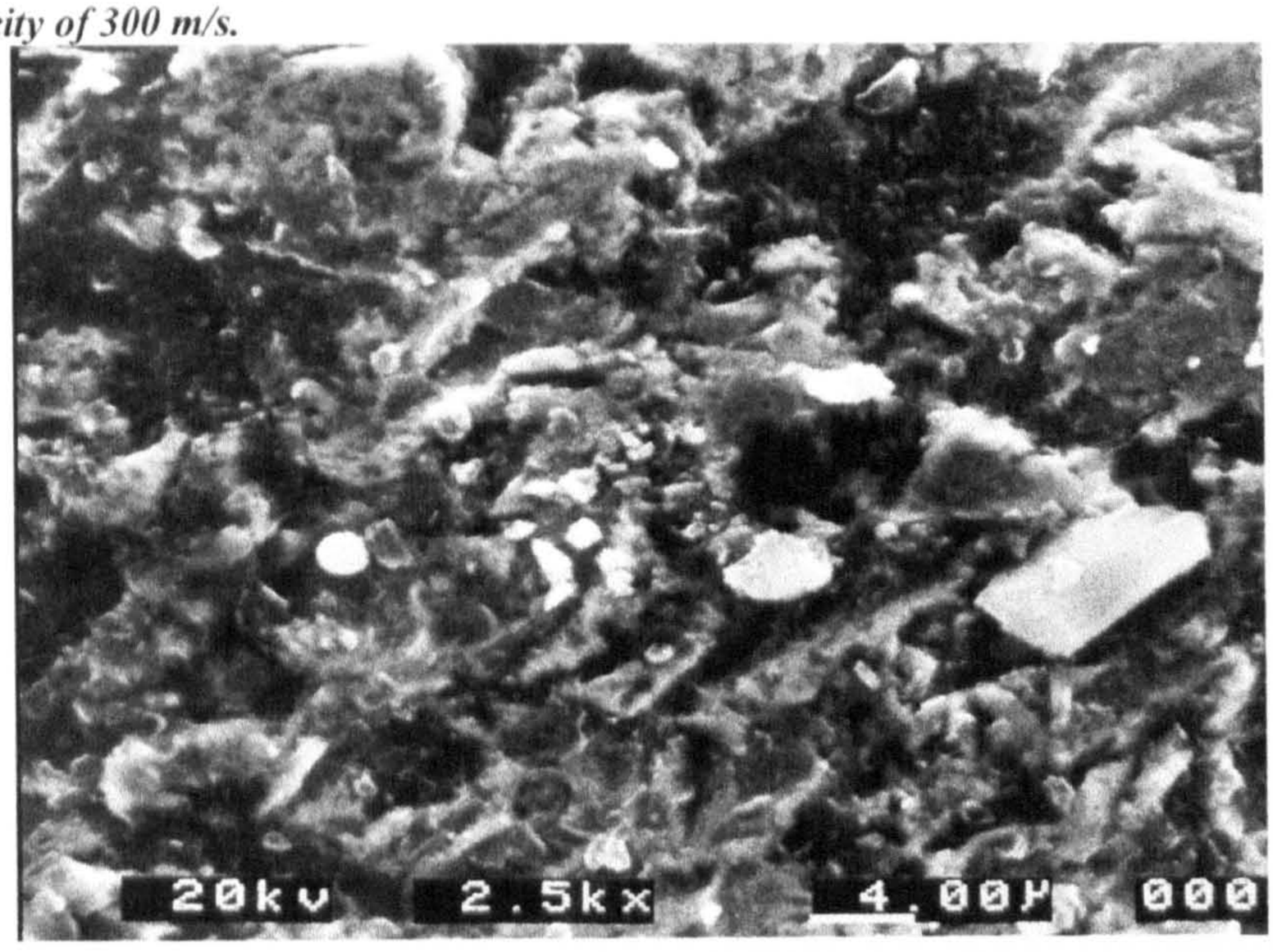


Figure 4-59. Areas of deposited particles at particle temperature= 750 ℃, HT=0.5, and particle velocity of 300 m/s.



List of Figures for the Comparison between the Stainless Steel 321 and Nimonic 75 at 30° Impact Angle

- **Effect of Target HT ratio**

Figure 4-60. The effect of target temperature on the erosion of stainless steel and nimonic at 200 m/s impact velocity.

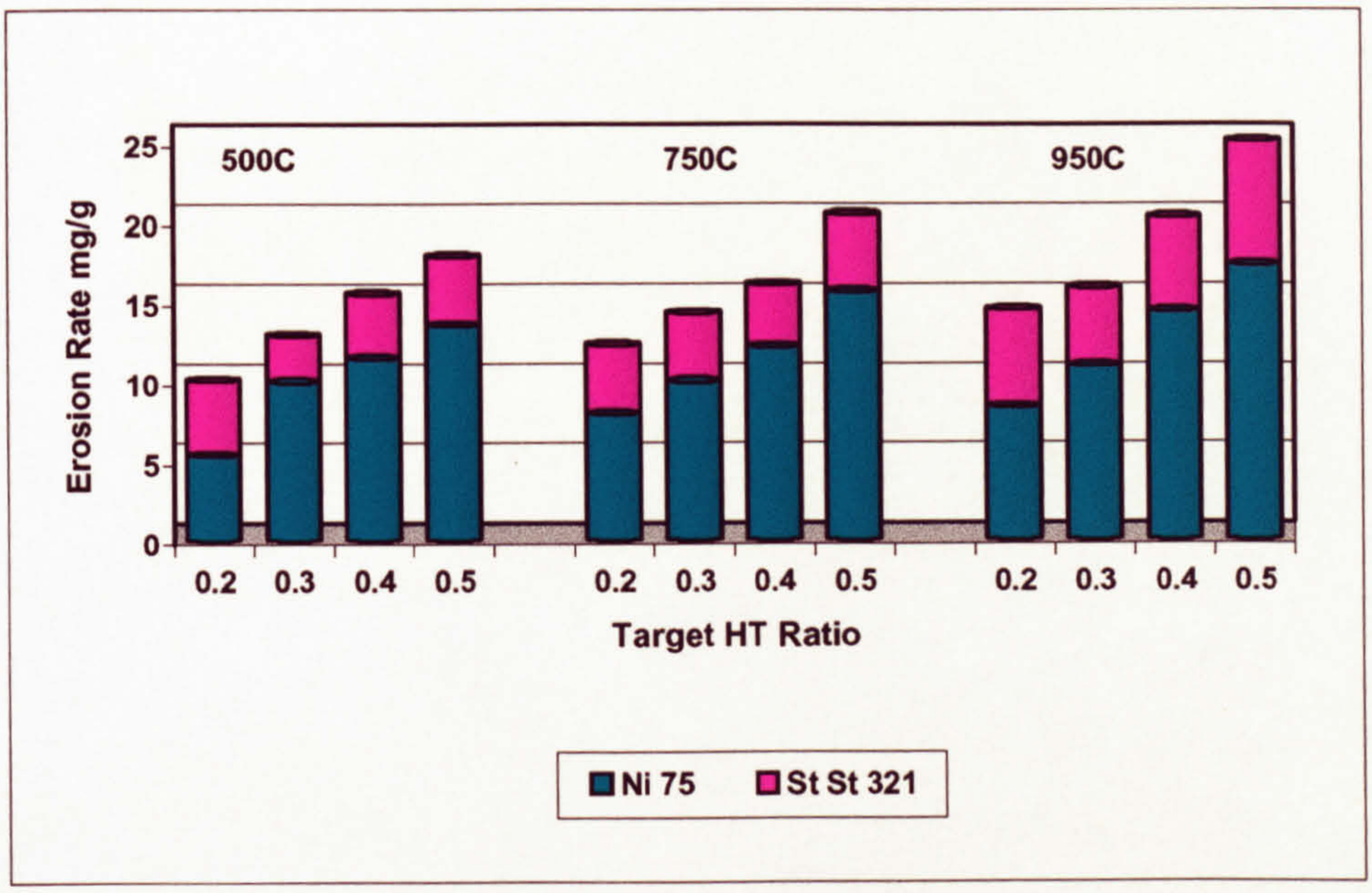


Figure 4-61. The effect of target temperature on the erosion of stainless steel and nimonic at 250 m/s impact velocity.

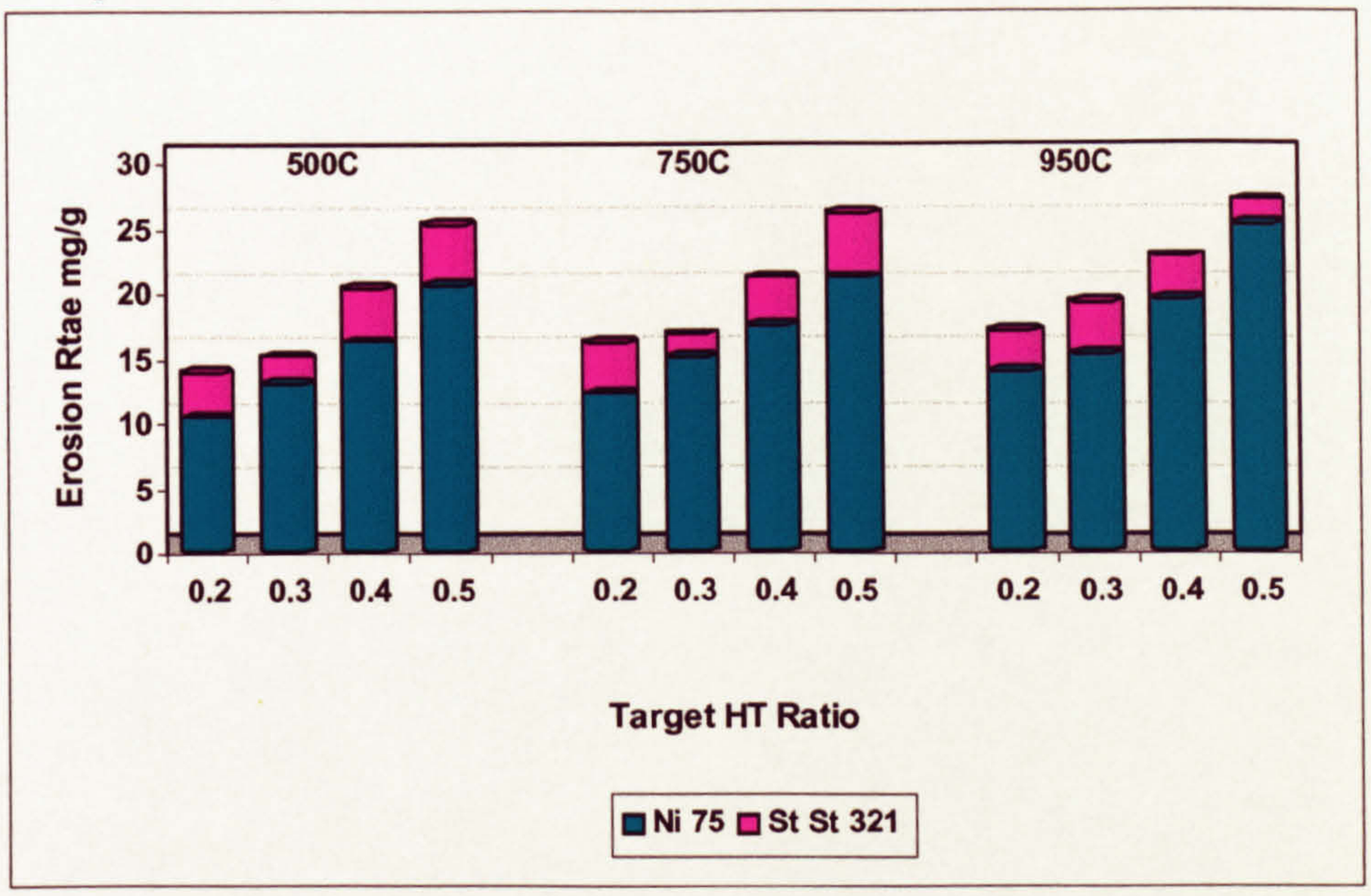
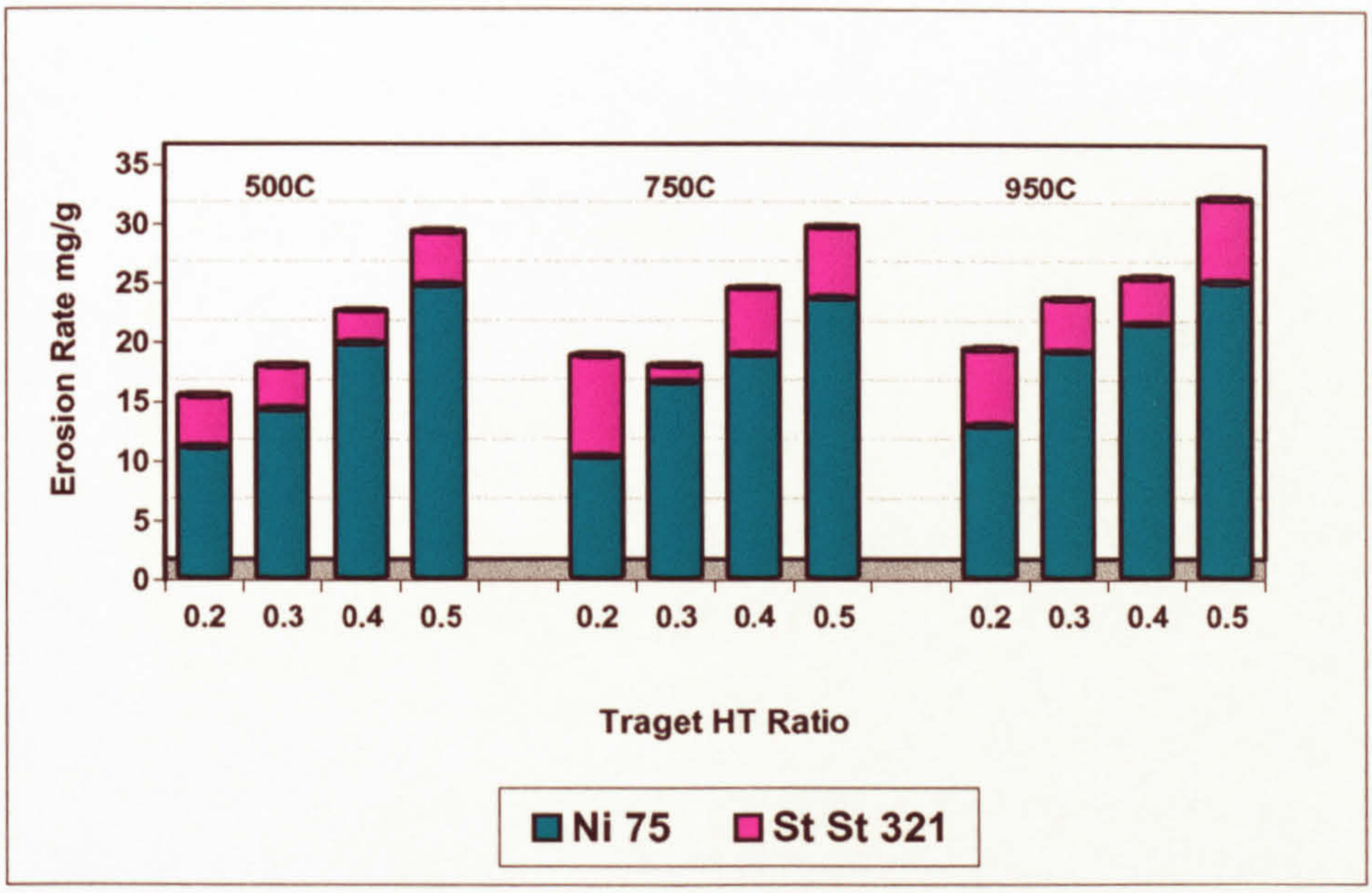


Figure 4-62. The effect of target temperature on the erosion of stainless steel and nimonic at 300 m/s impact velocity.



- **Effect of Particle Temperature**

Figure 4-63. Erosion rate versus particle temperature for stainless steel and nimonic targets at impact velocity of 200 m/s.

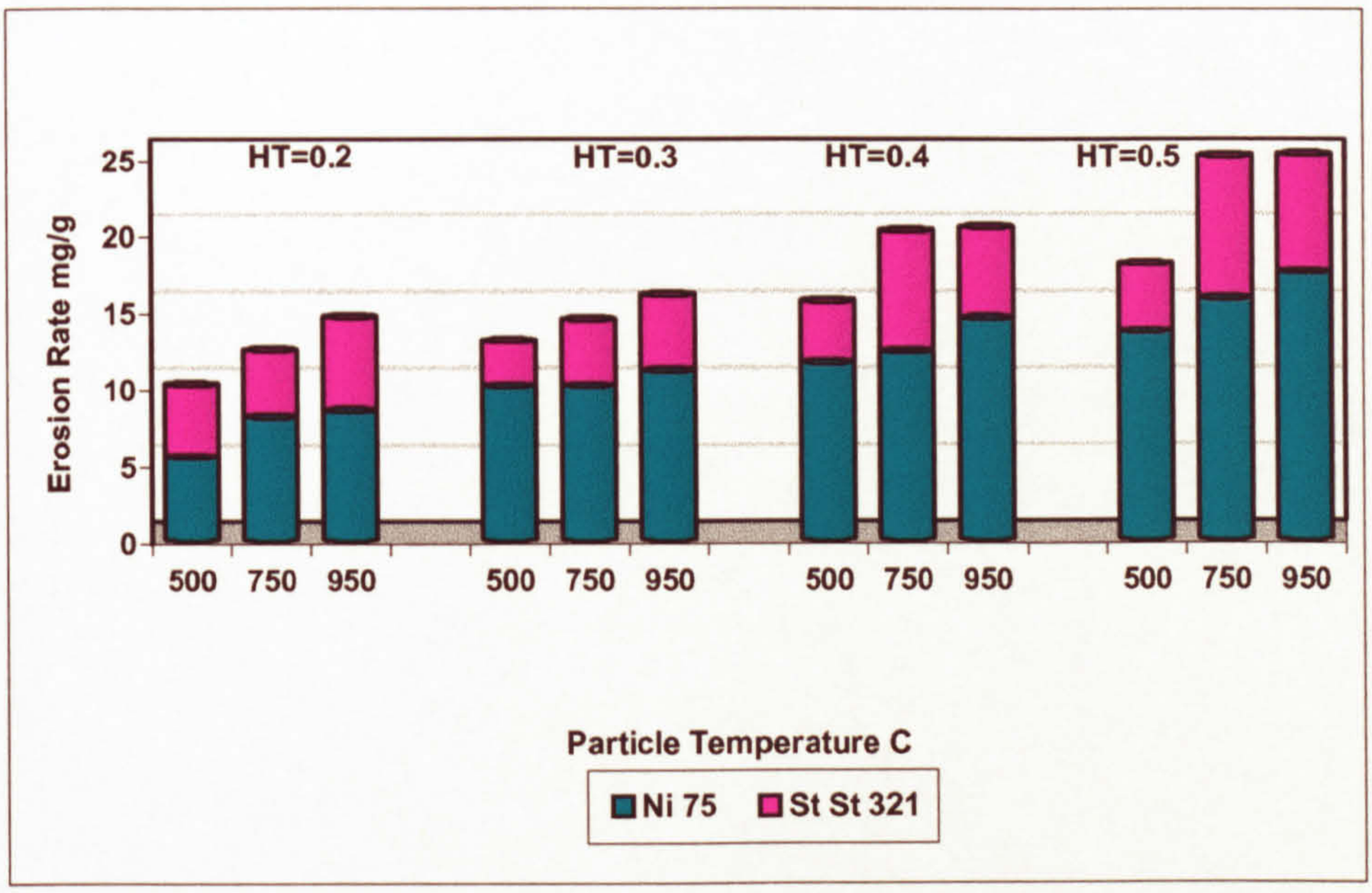


Figure 4-64. Erosion rate versus particle temperature for stainless steel and nimonic targets at impact velocity of 250 m/s.

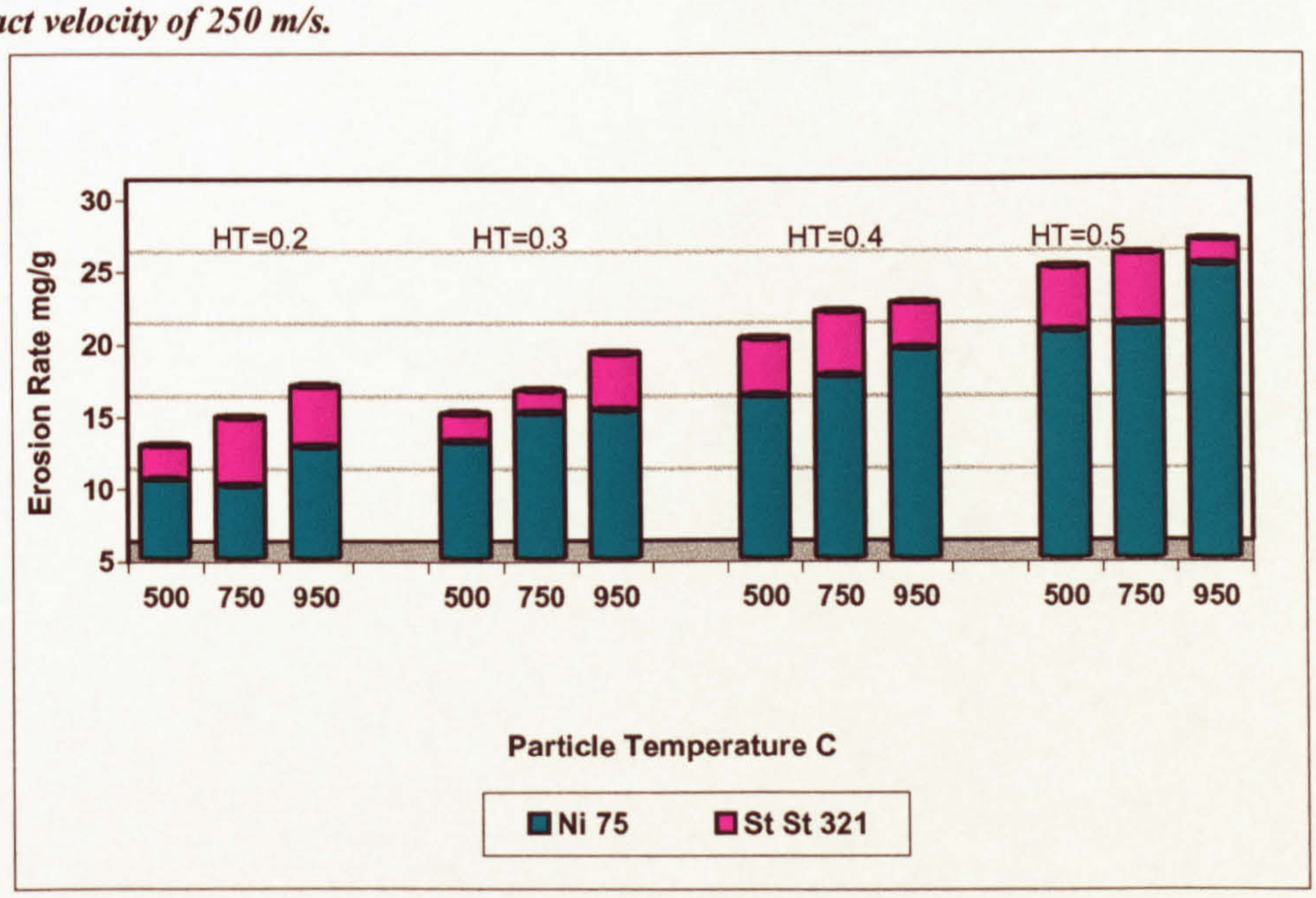
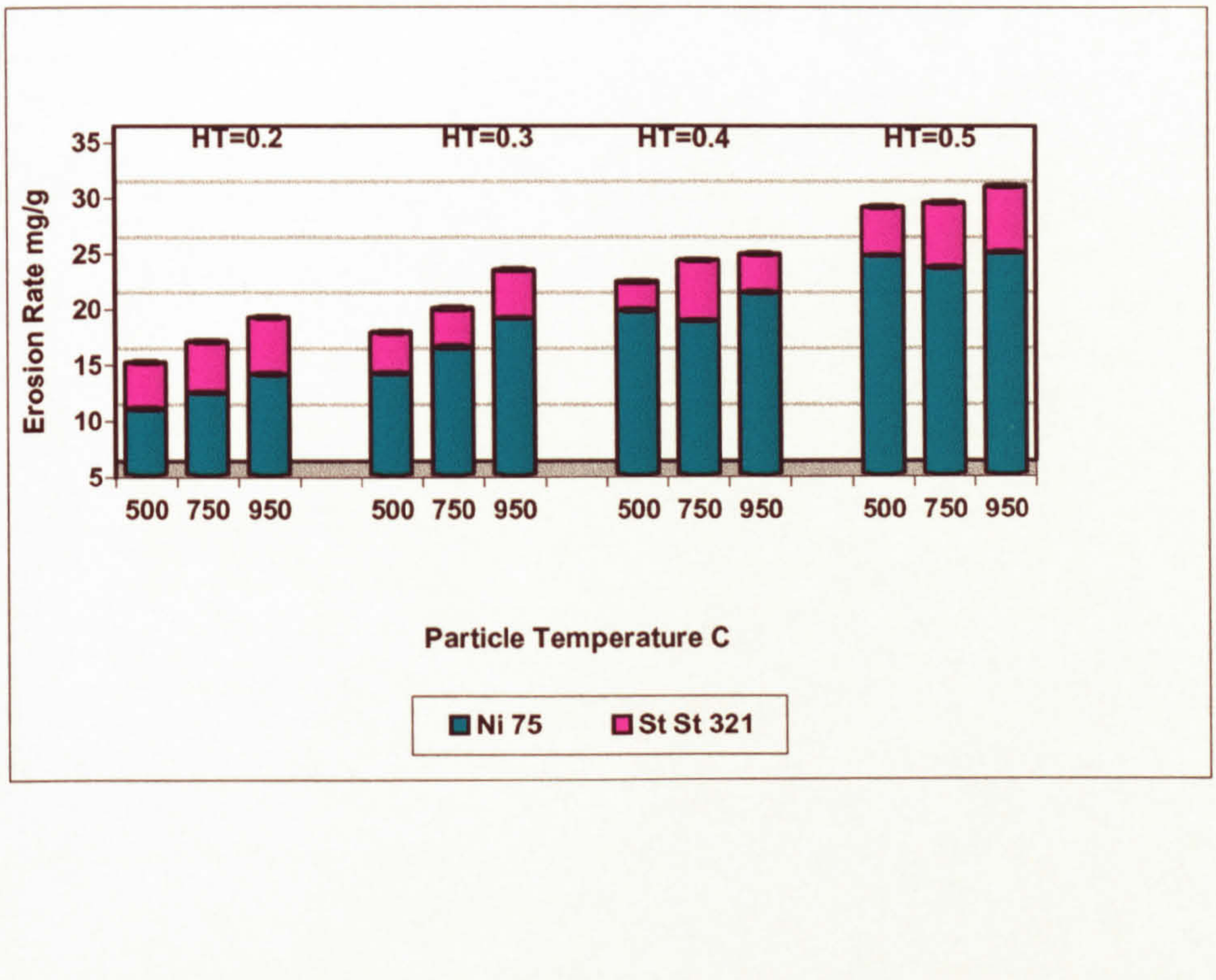


Figure 4-65. Erosion rate versus particle temperature for stainless steel and nimonic targets at impact velocity of 300 m/s.



- **Effect of Particle Impact Velocity**

Figure 4-66. The effect of impact velocity on the erosion of stainless steel and nimonic at 500℃ particle temperature.

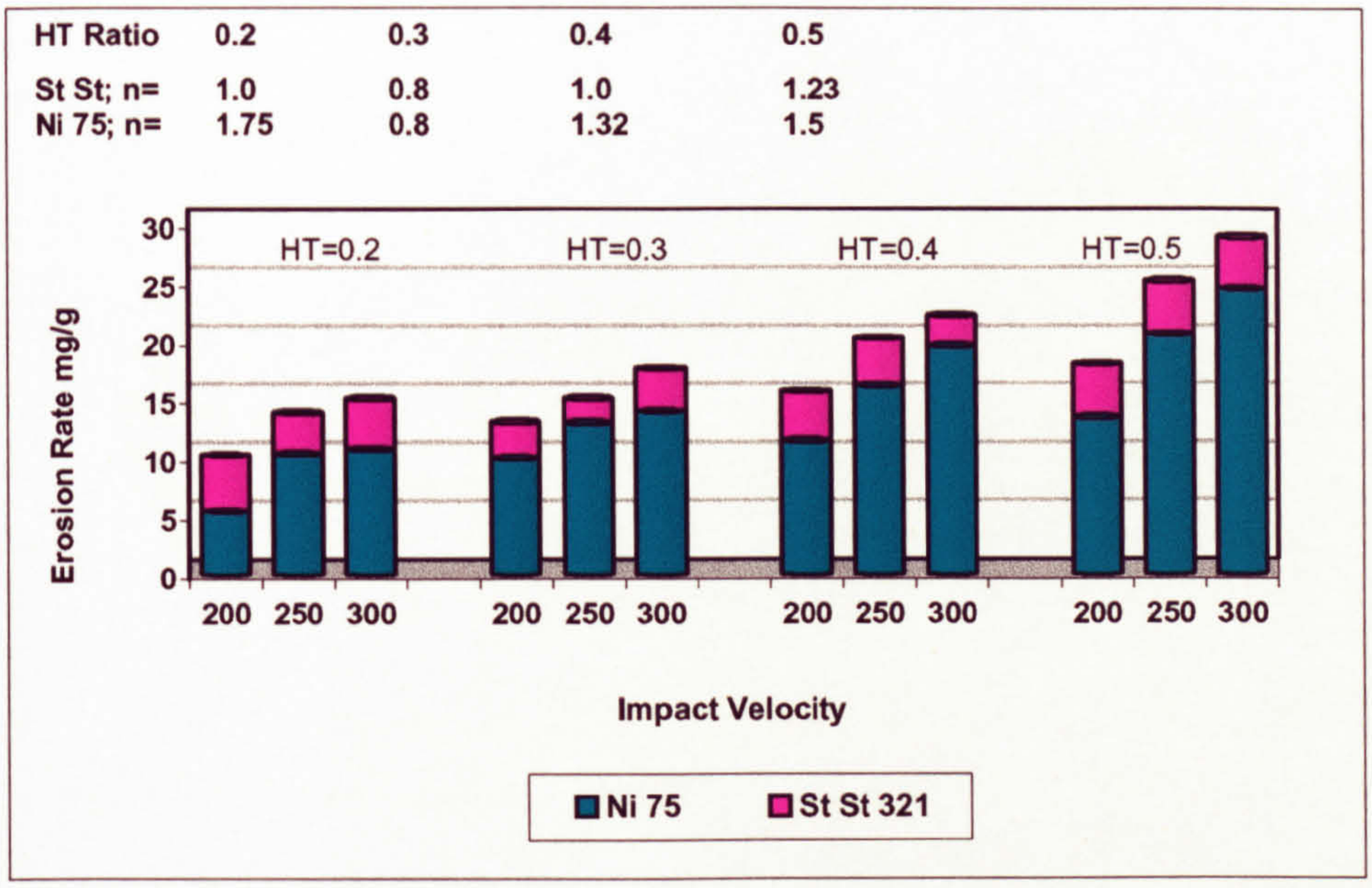


Figure 4-67. The effect of impact velocity on the erosion of stainless steel and nimonic at 750℃ particle temperature.

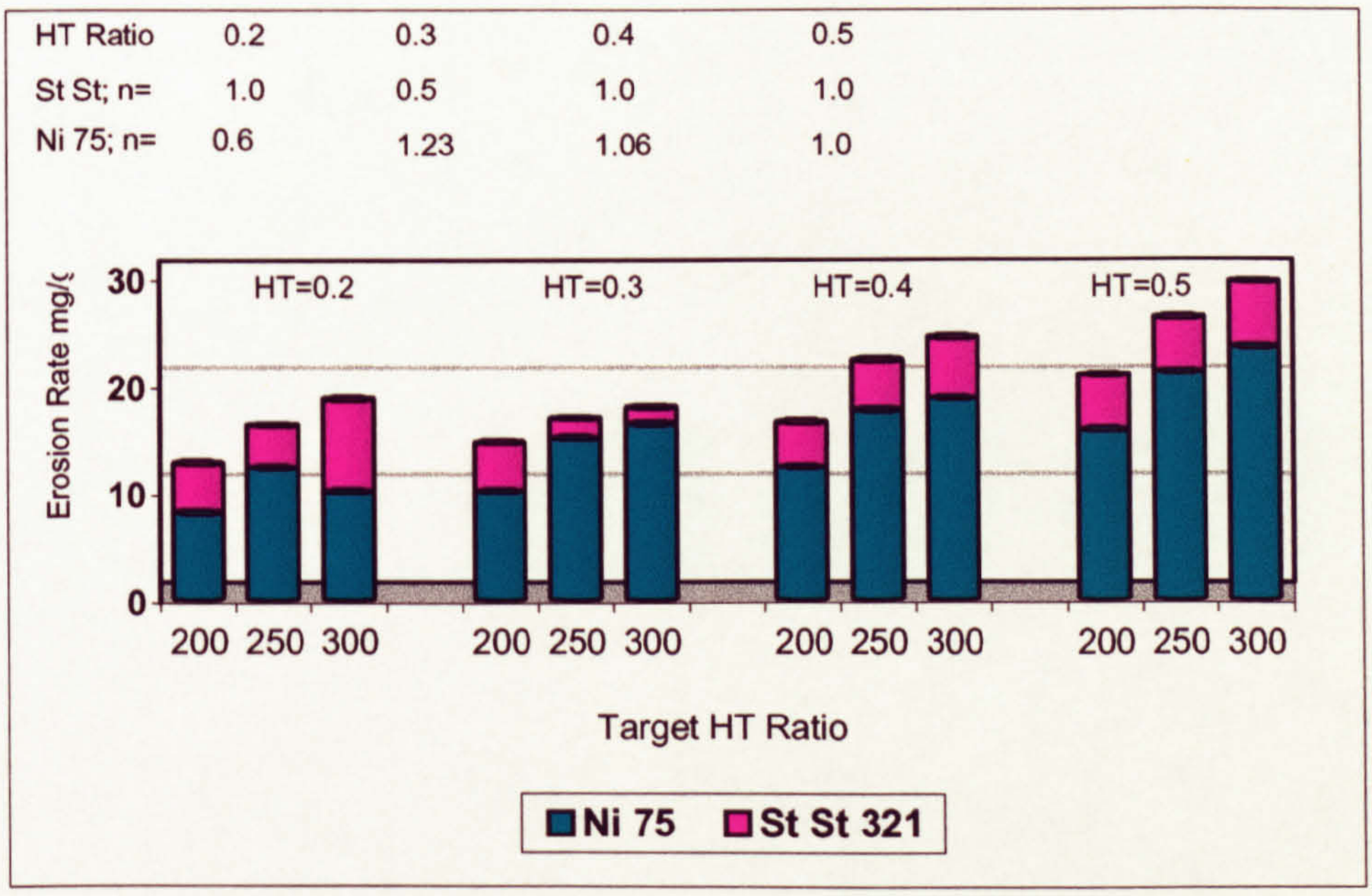
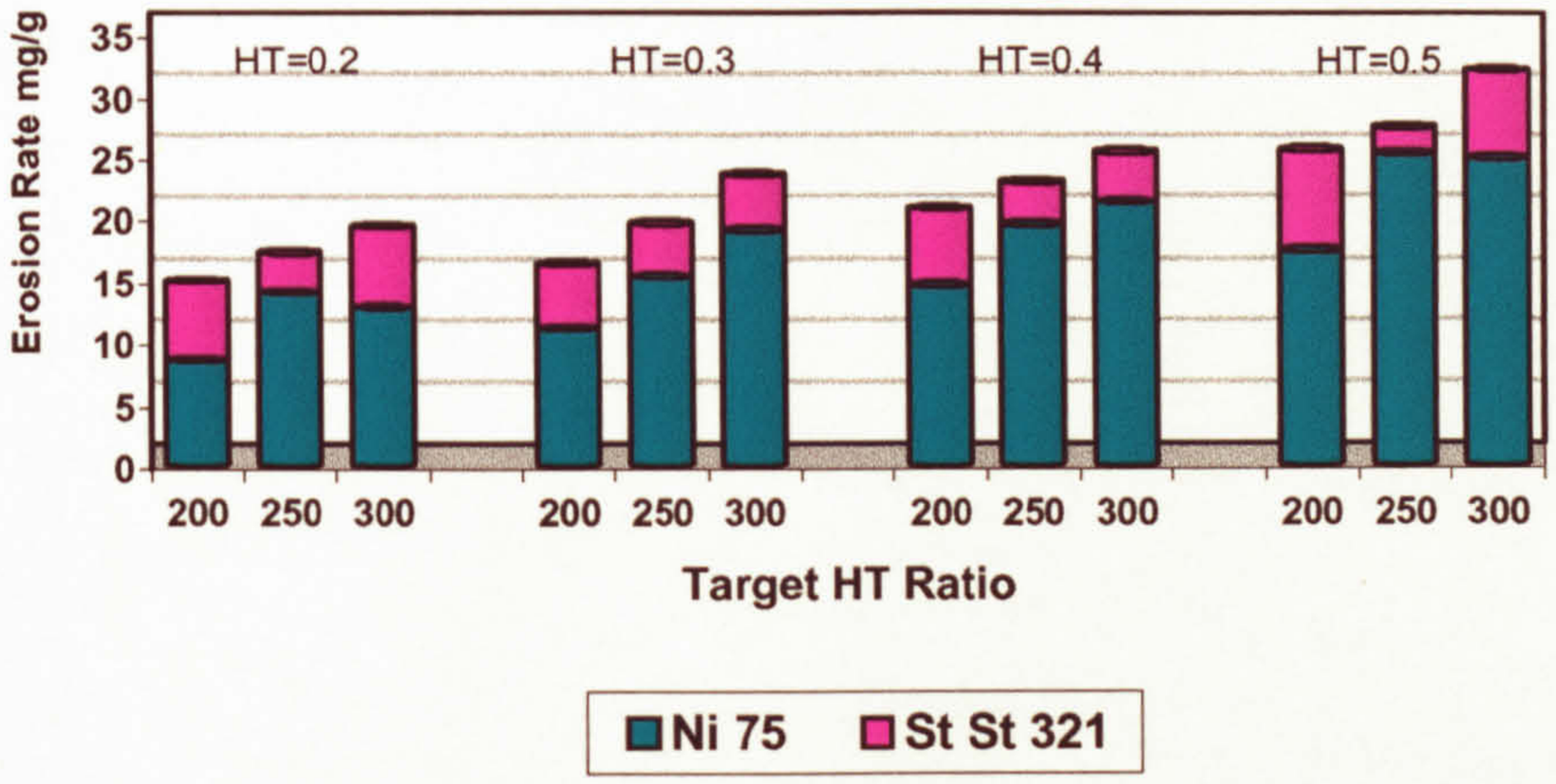


Figure 4-68. The effect of impact velocity on the erosion of stainless steel and nimonic at 950 ℃ particle temperature.

HT Ratio	0.2	0.3	0.4	0.5
St St; n=	0.6	1.0	0.5	0.8
Ni 75; n=	1.1	1.34	1.0	0.92



List of figures for Surface Examination Results For Aluminium at 30° Impact Angle.

Figure 4-69. Effect of Target Temperature (HT) at different particle temperature; impact velocity, 100m/s, impact angle, 30°.

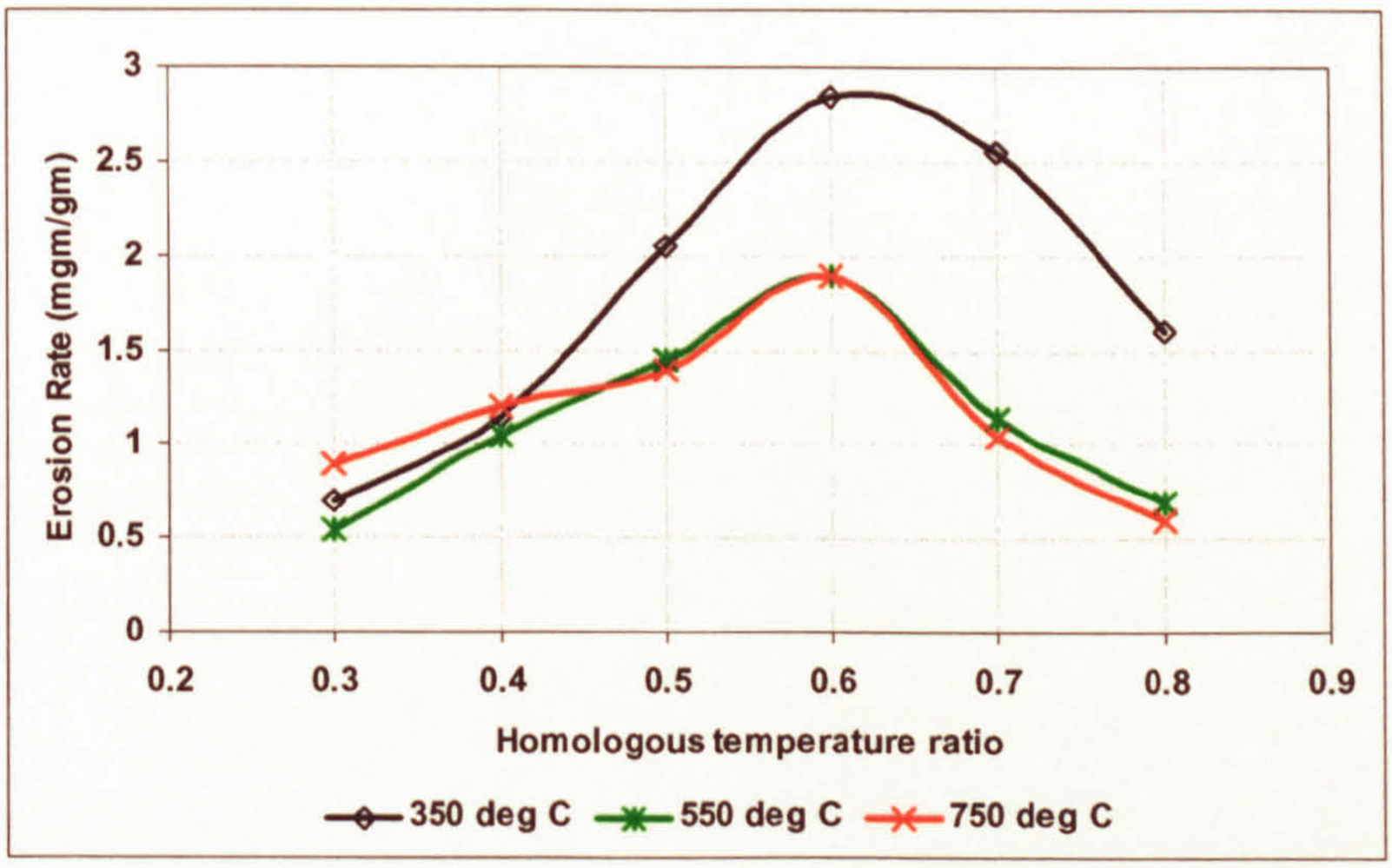


Figure 4-70. Results obtained by Yee for aluminium targets at 35° impact angle, using flyash particles at 135 m/s impact velocity.

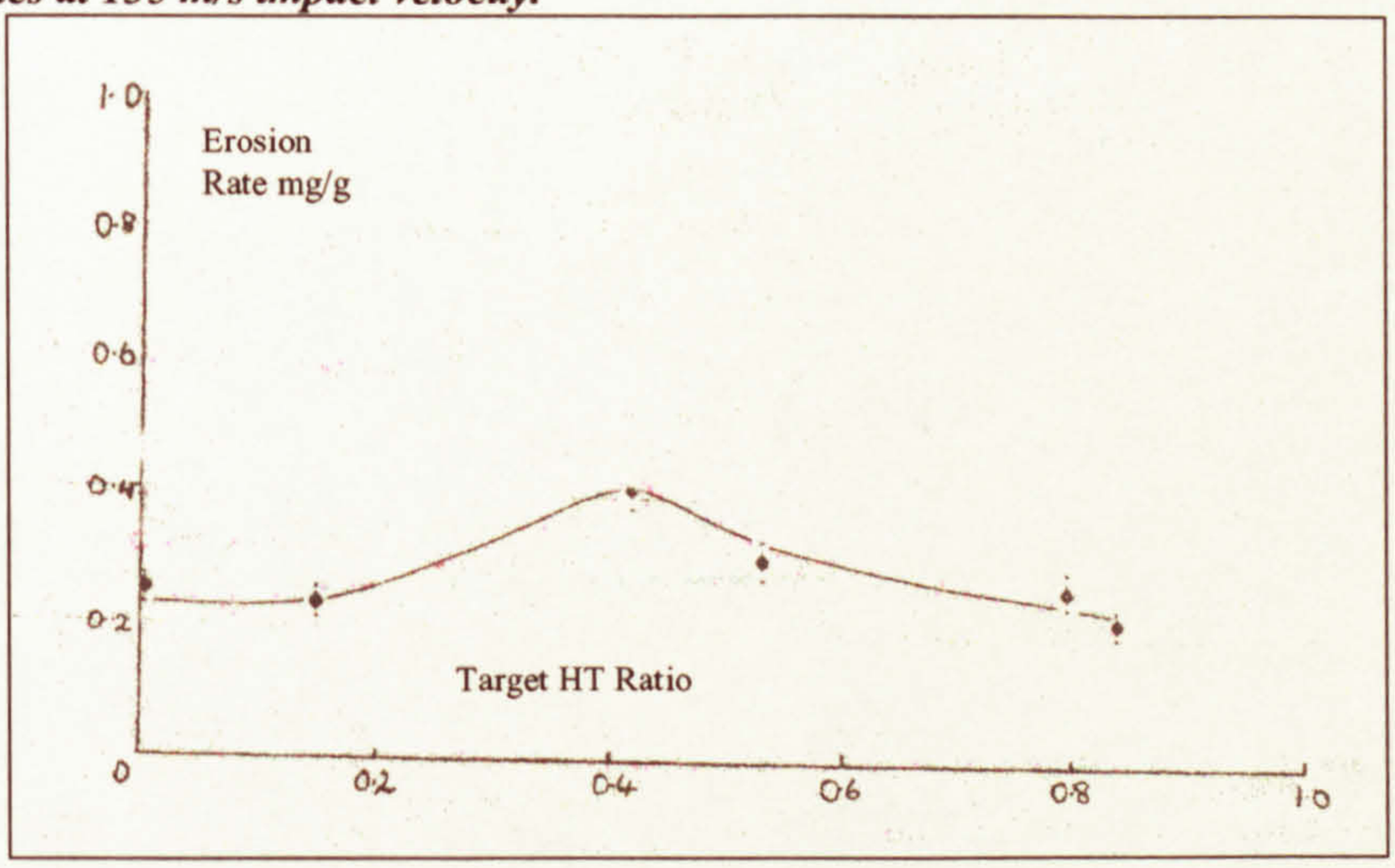
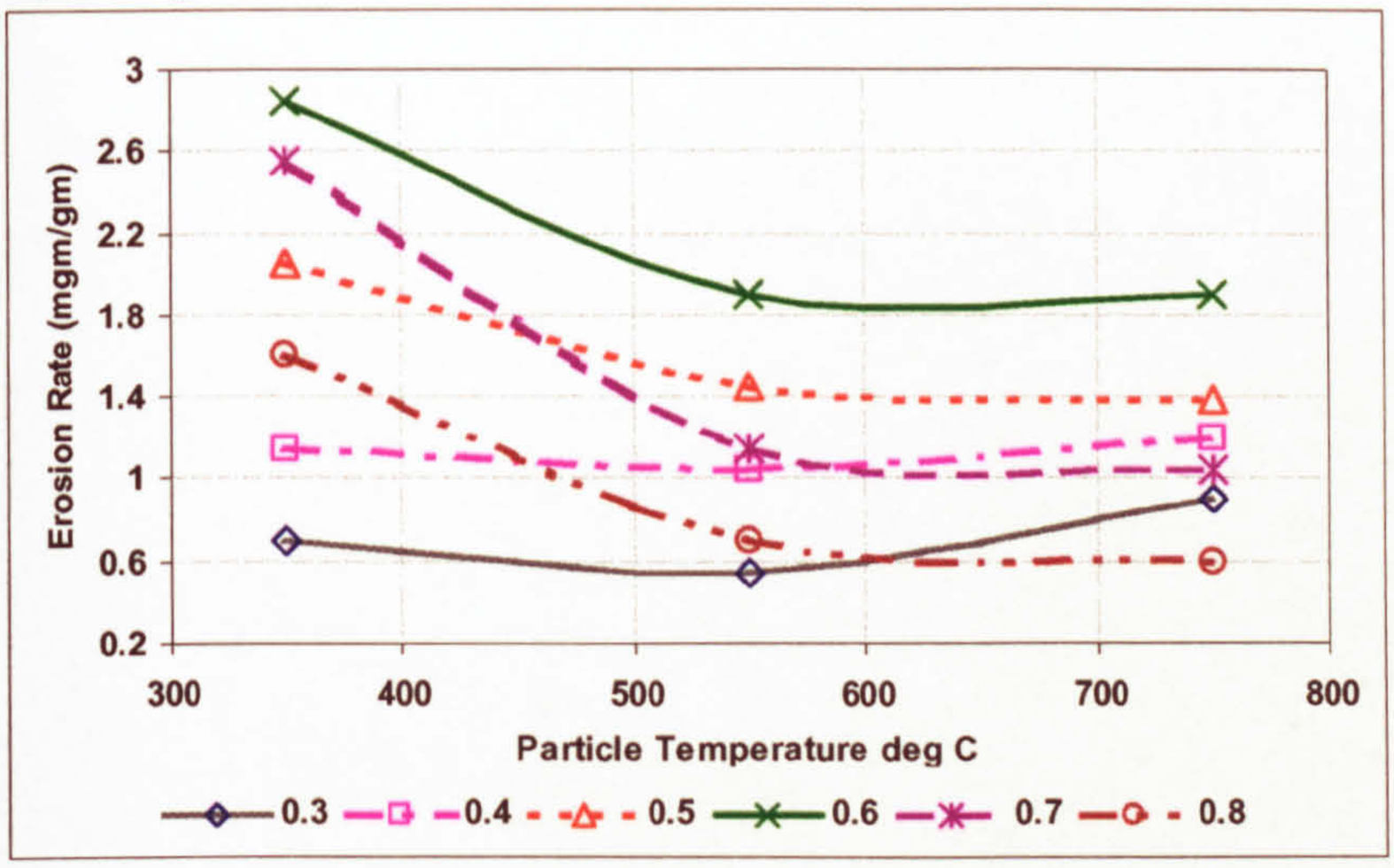


Figure 4-71. Effect of particle Temperature at different HT ratios; impact velocity, 100m/s, impact angle, 30°.



Scanning Electron Microscope (SEM) Results (Impact velocity of 100 m/s.)

Figure 4-72. Erosion pattern (ploughing) for aluminium target at 350 ℃ particle temperature.

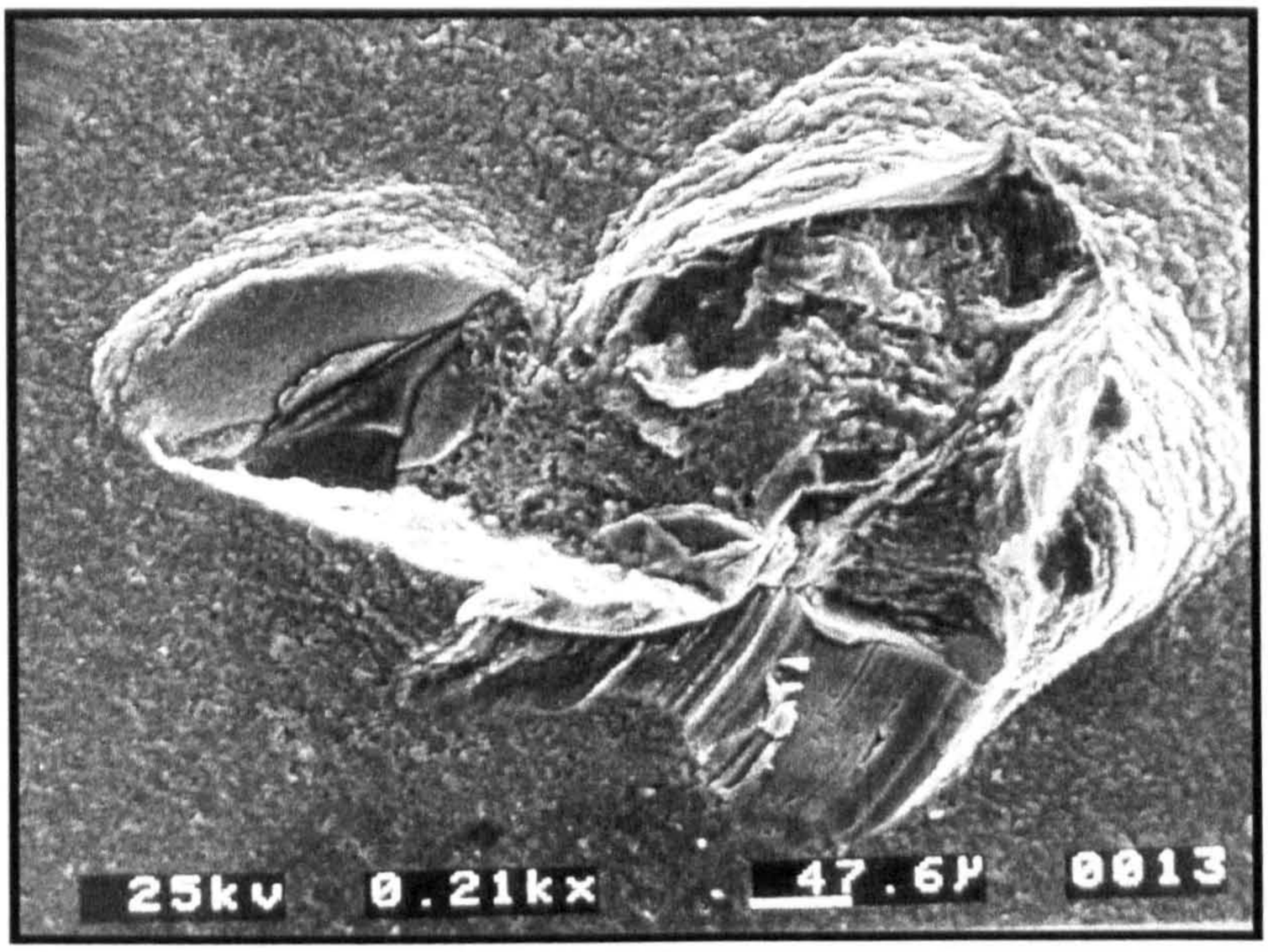


Figure 4-73. Areas of melted material at high HT=0.6 and particle temperature of 550 ℃.

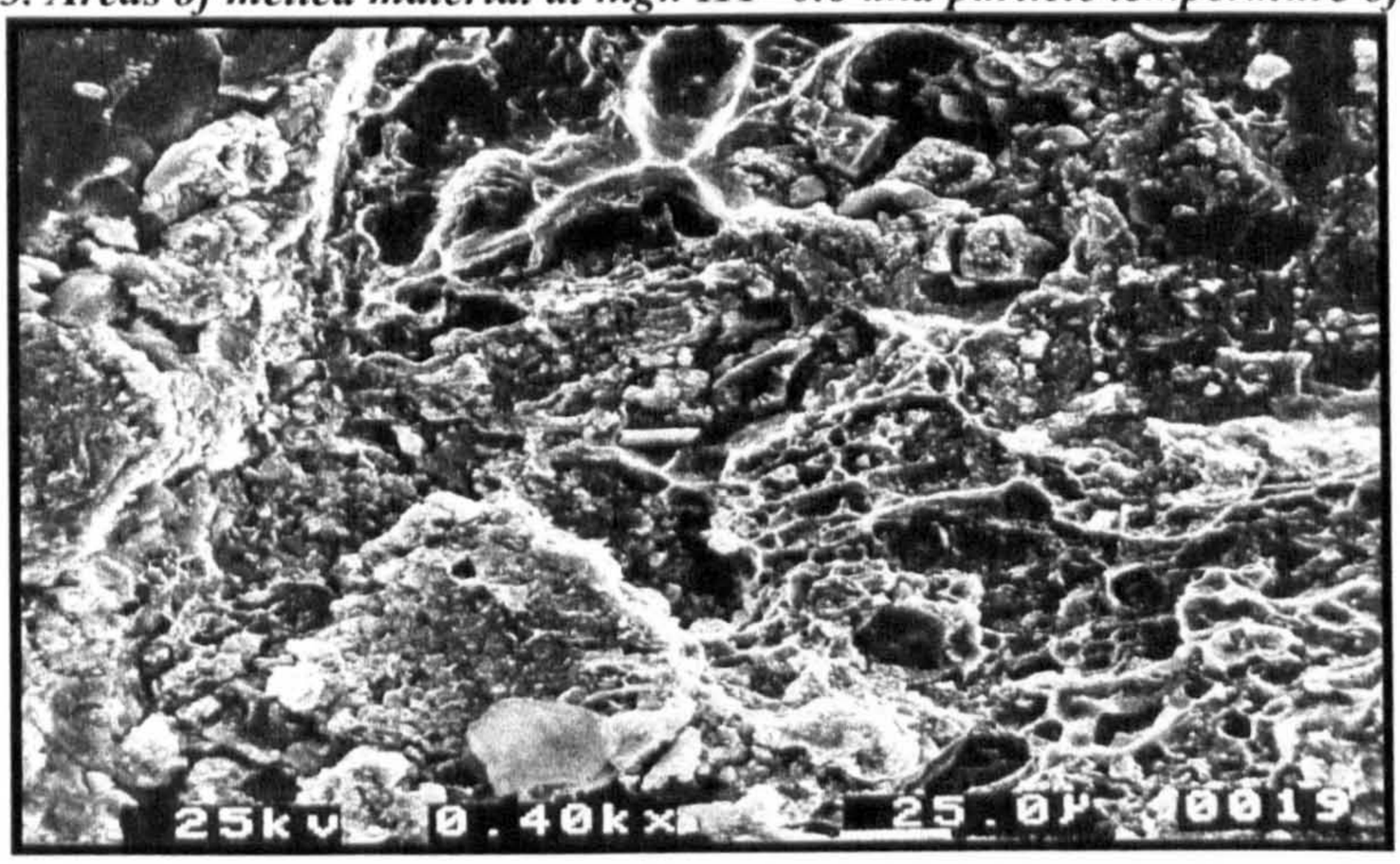


Figure 4-74. Areas of melted material at high HT=0.7 and particle temperature of 750 ℃.

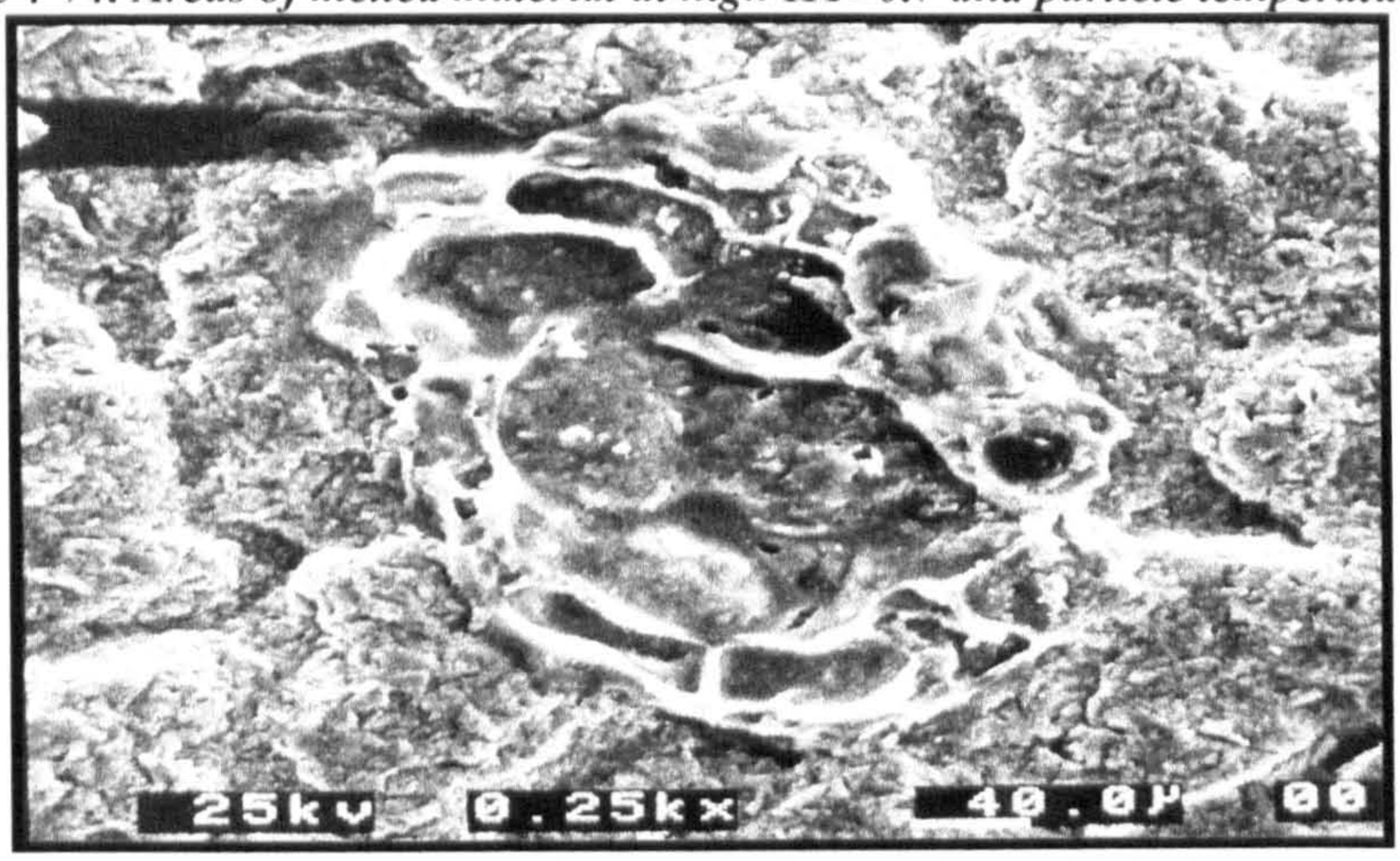


Figure 4-75. Deposition of multi-size particles at 350 ℃-particle temperature, HT=0.7.

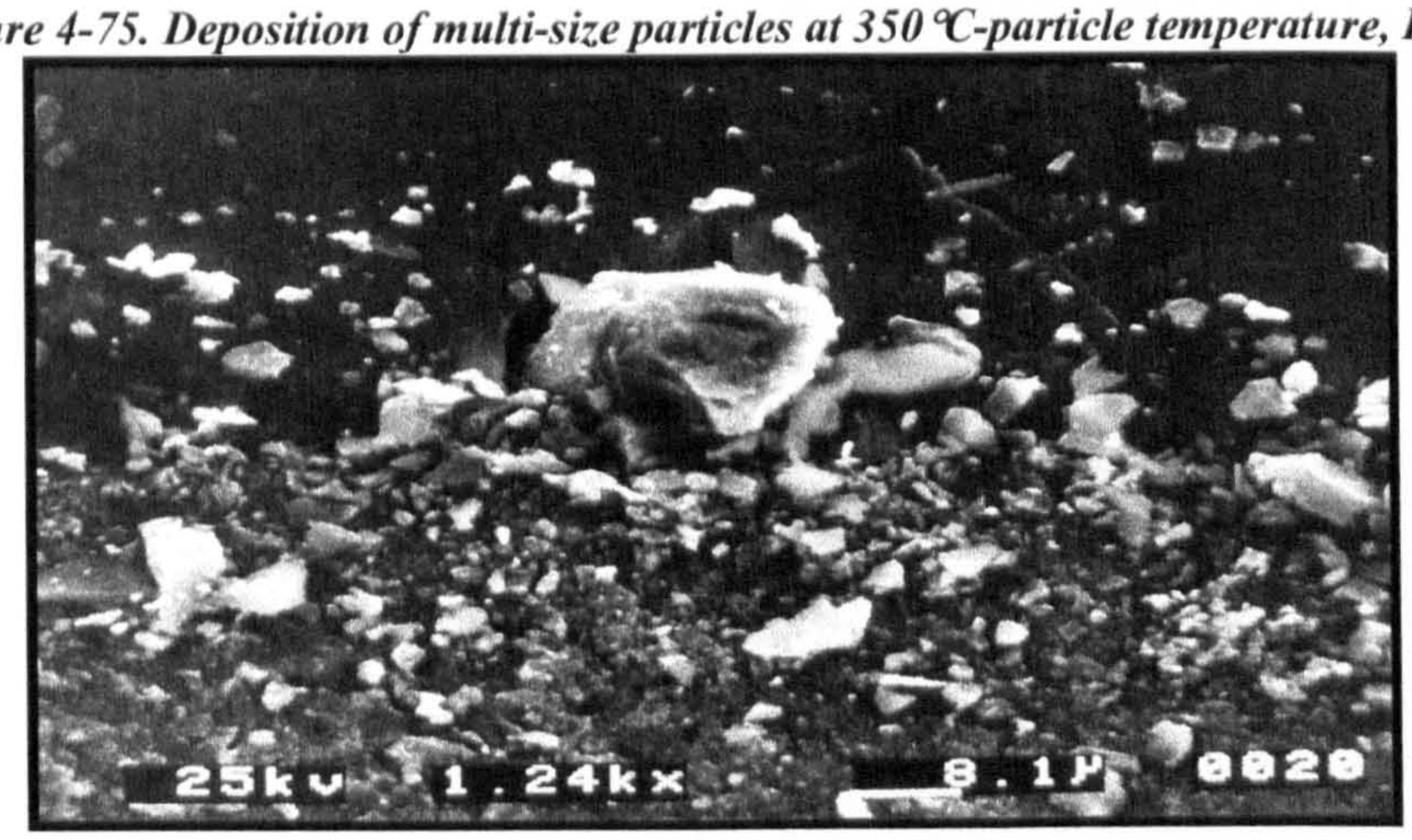
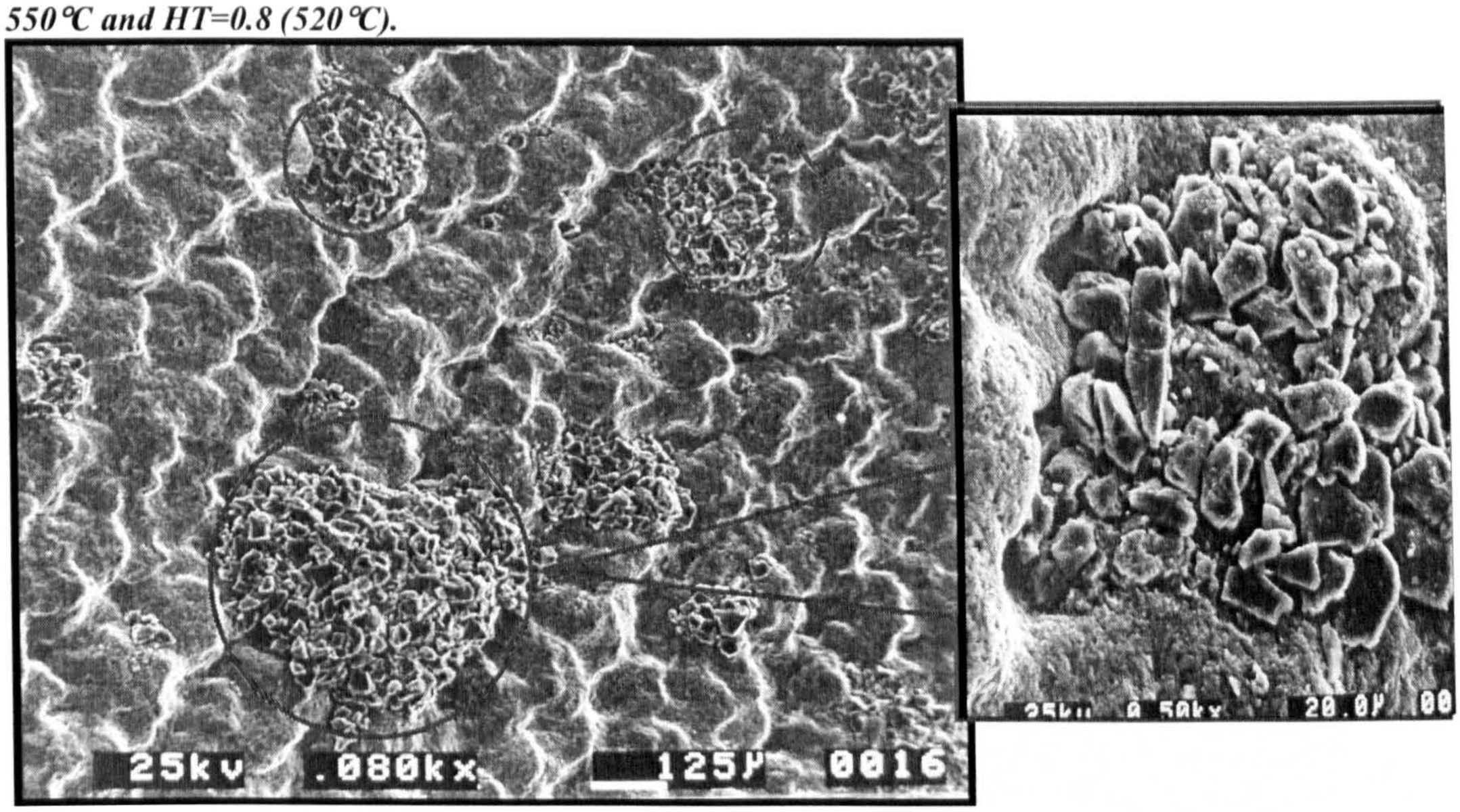


Figure 5-76. Areas of heavy deposition of different particle sizes at particle temperature; 550℃ and HT=0.8 (520℃).



CHAPTER 5

REVIEW, CONCLUSIONS, AND RECOMMENDATIONS FOR FUTURE WORK

6.1 Review

The test facilities used on the current erosion experimental has proven to be very successful, providing enough data for better understanding of the erosion/deposition phenomena under elevated temperature environment.

The erosion test results for stainless steel 321 targets were found to be varied due to the effect of impact angle and velocity and due to the influence of the particle and target temperature. In general, the rate of erosion was found to be increasing with impact velocity and it is higher at lower impact angle of 30°, which is near the impact angle associated with maximum erosion rate. The effect of particle and target temperatures was varied depending on the impact angle and impact velocity, and generally, higher particle and target temperatures will result higher erosion rate at all impact angles and velocities. At threshold target HT ratio (temperature) and particle temperature, impact particles start to form considerable deposits on the target surface. This threshold temperatures was found to be dependent on the impact velocity and incident angle, and found to be at target HT ratio of HT=0.4 (570°C) and particle temperature of 950°C when the impact velocity is in the vicinity of 250 m/s and when the impact angle is at 30°. Furthermore, the size of deposited particles were also found to be different at those conditions. In general, larger

particle were able to form a deposit at higher impact velocities and temperatures than that seen at lower ones and there was only minor particle deposition at lower impact velocities and lower target HT ratios and particle temperature. At 60° impact angle, the erosion rate was found to be very small compared to that at 30°, and hence could be considered as a non-considerable deposition.

On the other hand, the surface damage morphology and material removal mechanisms were found to be different at different impact angles and velocities, where various material removal mechanisms were took place at 30° impact angle, while only pitting erosion dominated at 60°.

The erosion results for the Nimonic 75 targets have shown a variation on the erosion characteristics depending on impact velocity, target HT ratio (temperature) and particle temperature. The general view is that erosion rate increases with HT ratio and particle temperature at different rate depending on the impact velocity, also particle deposition on the Nimonic targets was observed to start at certain target HT ratio and particle temperature depending on the impact velocity. Most of the deposition was found to be at target HT ratio ≥0.4 (≥550°C), 950° particle temperature and when particle velocity is at 300 m/s. for the Nimonic targets, the predominant material removal mechanism was the cutting type (I) at all test conditions.

The compared erosion results of the stainless steel 321 and Nimonic 75 targets at 30° impact angle revealed that the erosion rate of the former is higher than that of the later. On the other hand the deposition on stainless steel surface was occurred over a wider range of particle and targets temperature and found to be more significant than on the Nimonic target surface.

The erosion results of the aluminium targets has shown distinct erosion characteristics depending on particle temperature and target HT ratio (temperature) and generally shown higher erosion rate resulted at lower particle temperature of 350°C compared to that at 550°C and 750°C. The rate of erosion was found to be increased in an accelerated rate with target HT ratio until it reaches the maximum at HT=0.6 (390°C), which then starts to drop to its lowest level. Particle deposition was noticed at all test conditions, and started to be very intense as target HT ratio exceeded 0.6 (390°C) and particle temperature reached 550°C.

6.2 Conclusions

The test facility, which provided a wide range of particle and target temperature as well as impact velocities and angles, has proven to be very successful and could be used in future for other materials and wider test conditions. The experimental results of the erosion/deposition tests of the stainless steel, Nimonic 75 and aluminium targets at high impact velocity and temperatures were proven to be very helpful to establish a better understanding of the phenomena at a gas turbine simulated environment.

For stainless steel targets, at 30° impact angle, particle temperature has had a great influence on the erosion rate at low particle velocity of about 200 m/s, and at low target HT ratio not more than HT of 0.3. The erosion rate was found to be affected to a similar degree as particle temperature increases at different impact velocities and

at low target HT ratio. While target HT ratio has a smaller effect on the rate of erosion as particle temperature and velocity increases. On the other hand particle velocity has the same effect on erosion rate at different target HT ratios (surface temperatures) at all particle temperatures. The erosion rate was less affected by the variation of particle impact velocity at high particle temperature of 950°C than at lower ones of 550°C and 750°C and higher particle velocity leads to smaller change in target weight after impact at high HT ratios and particle temperatures, where deposition starts to form at these conditions. The stainless steel 321 target material reacted in different ways to different particle velocities and temperatures and at different target surface temperatures. The general trend is that more particles deposited on the target surface as particle temperature reaches 950°C and at a velocity higher than 200 m/s, when target HT ratio exceeds 0.4, due to the changes on material properties at high temperatures.

At 60° impact angle, particle temperature has a clear effect on erosion rate of the stainless steel targets. Increasing particle temperature causing an increase in erosion rate, especially at high particle velocities and target HT ratios. On the other hand, target HT ratio has a smaller influence on erosion rate as particle velocity increases and particle temperature decreases, as the erosion rate increases with HT ratio at higher particle temperatures more rapidly when particle velocity reaches 250 m/s. The effect of particle velocity was found to be at the highest level at low particle temperature, which becomes milder at particle temperature of 950°C. At this impact angle of 60, particle deposition rarely existed and it was limited at high target HT ratio of 0.5 and at

particle temperature and velocity of 950°C and 300 m/s respectively.

The stainless steel targets have a different response to the impacting particles, where the material damage at 30° is more severe than that at 60°, as both deposition and erosion occurred at the former, while it is almost limited to erosion at the later.

The erosion tests of the Nimonic targets at 30°C impact angle have shown that particle temperature to have little effect on erosion rate at high target HT ratios of 0.4 and 0.5 compared to that at lower HT ratios of 0.2 and 0.3 when particle velocity is more than 250 m/s. It was also concluded that the erosion rate is more sensitive to the change in target HT ratio than the change in particle temperature. Also particle impact velocity was found to have higher effect on erosion rate at low target HT ratios of HT=0.2 and HT=0.3 especially at particle temperature of 950°C. It was also concluded that particle deposition starts to build up as particle temperature reaches 950°C and when target HT ratio exceeds 0.4 (550°C).

The Nimonic 75 targets exhibited better erosion characteristics than the stainless steel 321 at all impact velocities, particle temperatures and target HT ratios at the 30° impact angle tests. Particles managed to deposit on the stainless steel surface at lower impact velocities and at lower target HT ratios than the Nimonic.

The erosion rate of the aluminium targets has dropped steeply as particle temperature increases from 350°C to 550°C and was almost unchanged as particle temperature

increased to 750°C. On the other hand, the rate of erosion increased very sharply as HT ratio increases from HT=0.3 until it reaches the maximum at HT=0.6. In the same way, erosion rate decreases to approximately its original value as target HT ratio increased further to HT=0.8. Silica particles formed intense deposition on aluminium targets when the HT ratio is greater than 0.6 and particle temperature is higher than 550°C, nevertheless, deposition at lower temperatures was very possible.

PAGE

NUMBERING

AS ORIGINAL

6.3 Recommendations for Future Work

6.3.1 Feasible Improvements to the Test Facilities.

Owing to the limitation of time and resources, some areas of this work would needed to be improved when considering further investigations;

i) Improving the particle feeder in order to provide a steadier particle injection into the acceleration tube.
ii) Particle concentration should be measured at the accelerating tube exit, which will provide another parameter in the study.
iii) Particle temperature could not be measured practically during the tests. Adequate method for measuring particle temperature will help to improve the test conditions.

6.3.2 Expanding the Test Conditions

Test conditions have been limited to a small range of particle and target temperatures and to a single particle size. The future work should be carried out on a wider range of test conditions which may cover the following areas;

i) Wider range of particle type and sizes can provide a database for the effect of particle size and type on the erosion/deposition behaviour under similar test environment.
ii) Carrying out the tests at various angles of impact to provide sufficient information on the effect of angle of impact on erosion/deposition at elevated temperatures similar to those available at ambient impact conditions.

iii) Increasing particle temperature to a point close to the either target softening temperature or to that of the particle itself.

iv) Increasing target temperature further near the melting point (as on the case of aluminium during this test) will give more information on the behaviour of different materials at very high temperatures.

References

1. König, P. Miller, T. Roβmann, A., Damage of high Temperature Components by Dust-laden Air, AGARD Confrence Proceeding 558, *Erosion, Corrosion, and Foriegn Object Damage Effects in Gas Turbines*, Paper No. 25.
2. Raj, R., Deposition Results of a Transpiration Air-Cooled Turbine Vane Cascade in a Contaminated Gas Stream. Journal of Engineering for Gas Turbine and Power, Trans. of ASME, Vol. 105, Oct. 1983, 826-833.
3. Grant, G. and Tabakoff, W. Erosion Prediction in Turbomachinery Resulting from Environmental Solid Particles, J Aircraft, Vol. 12(5), 1975, 471-478.
4. J.E. Goodwin, W. Sage and G.P. Tilly. Study of Erosion by Solid Particles. Proc. Instn. Mechanical Engrs. Vol. 184(15), 1969, 279-292.
5. Tabakoff, W. Lakshminarasimha, A. N. Pasin, M. Simulation of compressor Performance Deterioration Due to Erosion. J. Turbomachinery, 112, 1990, 78-83.
6. Upton, A. W. Axial Flow Compressor and Turbine Blade Fouling: Some Causes, Effect and Cleaning Methods. First Symposium in Gas Turbine Operations and Maintenance, National Research Council of Canada, 1979.
7. Higgins, R. T. and Cale, D. B. Overview of Inlet Protection Systems for Army Aircraft. Proceeding of Rotary Wing Propulsion Specialists Meeting. 13-15 Nov 1990, 78-83.
8. Vittal, B. V. R., Tipton, D. L. and Bennett, W. A. Development of an Advanced Vaneless Inlet Particle Seperator for Helicopter Engines. J. Propulsion, 2(5), 1986, 438-444.
9. Diakunchak, I. S. Performance Deterioration in Industrial Gas Turbines. J. Engineering for Gas Turbine and Power, 114, 1992, 161-168.
10. Rickerby, D. S. and Mathew (Editors). A. Market Perspective and Future Trends. Advanced Surface Coatings: A Handbook of Surface Engineering. Blackie 1991, 343-364.
11. Levy, A. V and Bakker, T. W. Erosion Behaviour of Hard Surface Coatings/Inserts. Proc. Conf. Science of Hard Materials, 23-28 Aug. 1981, Jackson, Wyoming, USA, 499-516.

12. Spriggs, D. R. Solid Particle Erosion Resistant Coating Utilizing Titanium Carbide. United States Patent No. 4704366. 1987.
13. Mroczkowski, S. J. Multilayer Wear Resistant Coatings. European Patent Application No. 0366 289 Al. 1989.
14. Levy, A. V. The erosion-Corrosion Behaviour of protected Coatings. Surface coatings and Technology, 36, 1988, 387-406.
15. Sage, W. and Tilly, G.P. The Significant of Particle Size in Sand Erosion of Small Gas Turbines. JRAeS, Vol. 73, May 1969, 427-728.
16. Field, J. E and Hutchings, I. M. Surface Response to Impact. Material at High Strain Rates (Editor T. Z. Blazynski), Elserier, 1987, 243-293.
17. Raj, R., Deposition Results of a Transpiration Air-Cooled Turbine Vane Cascade in a Contaminated Gas Stream. Journal of Engineering for Gas Turbine and Power, Trans. of ASME, Vol. 105, Oct. 1983, 826-833.
18. Tilly, G.P. Sand Erosion of Gas Turbine Engines. Note for the Turbo Machinery Sub-Committee of the Aeronautical Research Council, ARC 30 948.
19. Yerramareddy, S. and Bahadur, S., Effect of Operational Variables, Microstructure and Mechanical Properties on the erosion of Ti-6Al-4V., Wear, 142, 1991, 253-263.
20. Tilly, G.P. A Two Stage Mechanism of Ductile Erosion. Wear, Vol. 23, 1973, 87-96.
21. Montgomery, J.E. and Clark, J.M. Dust Erosion Parameters for Gas Turbine. Soc Automotive Engr. Summer meeting, Preprint 538A, 1962.
22. Hutching, I.M. Strain Rate Effects in Microparticle Impact. Phys. D: Appl. Phys, 10, 1977, L179-L184.
23. Tan, S.C., Harris, P.K. and Elder, R.L. Particle Trajectories in Gas Turbine Engines, 83rd AGARD PEP Symp. On Erosion, Corrosion and Foreign Object Damage Effects in Gas Turbines, Rotterdam, the Netherlands, 25-28 April 1994.
24. Finnie, I. Erosion of Surface by Solid Particles. Wear, Vol. 3, 1960, 87-103.
25. Finnie, I. Wolak, J. and Routbort, J.L. Erosion of Metals by Solid Particles. J. Materials, Vol. 2, 1967, 682-700.
26. Scattergood, R.o. and Routbort, J.L Velocity and Size dependencies on the Erosion Rate in Silicon. Wear, Vol. 67, 1981, 227-232.
27. Tabakoff, W., Hammed, A. and Racmachandren, J. Study of Metal Erosion in High Temperature Coal Gas

Streams. Trans. Of ASME, J. of Eng. For Power. Vol. 102, Jan 1980.
28. Ives, L.K. and Ruff, A.W. Electron Microscopy Study of Erosion Damage in Copper. ASTM Proc. ASTM Symp. Erosion: Preventing and Useful Applications, Edited By Adler, W.F, ASTM STP 664, 1979, 5-35.
29. Stephenson, D.J., Nicholls, J.R and Hancock, P. The Influent of Scale/Substrate Properties on High Temperature Erosion in Gas Turbines. 6th Int. Conf. On Erosion by Liquid and Solid Impact, Cambridge, 5-8 Sep. 1983, Paper 48.
30. Yee, K. H., Shayler, P. J., and Collings, N., Erosion of Matals by Flyash Particles, Wear, Vol.91, (1983), p. 161-170.
31. Hockey, B.J., Wiederhorn, S.M. and Johnson, H. Erosion of Brittle Materials by Solid Particle Impact. Fracture Mechanisms of Ceramics, Vol. 3, Edited by Bradt, R. Hasselman, D. and Lange, F.m Plenum Press, New York, 1978.
32. Hasen, J. S. Relative Erosion Resistace of Several Materials. Proc. ASTM Symp. Erosion: Prevention and Useful Applications (Edited by W. F. Alder). ASTM STP 664, 1979, 148-162.
33. Ives, L. K. Erosion of 310 Stainless Steel at 975°C in Combustion Gas Atmospheres. J. Eng. Mater., 99, 1977, 126-132.
34. Finnie, I. Levy, A. and McFadden, D. H. Fundamental Mechanisms of the erosive Wear of Ductile Metals by Solid Particles. Proc. ASTM Symp. Erosion: Prevention and Useful Applications (Edited by W. F. Alder). ASTM STP 664, 1979, 37-57.
35. Bitter, J.G. A Study of Erosion Phenomena: Part I, Wear, Vol. 6, 1963, 5-21.
36. Bitter, J.G. A Study of Erosion Phenomena: Part II, Wear, Vol. 6, 1963, 169-190.
37. Levy, A., Mostafa. A, and Hichey, G. The Effect of Test Variables on the Platelet Mechanism of Erosion, Wear, Vol. 70, 1981, 269-281.
38. Cousens, A.K. and Hutchings, I.M. Proc. 6th Int. Conf. On Erosion by Solid and Liquid Impact, Cavendish Laboratory, University of Cambridge, Cambridge, UK, 1983, Paper 41.
39. Sheldon, G.L. and Finnie, I. On the Ductile Behaviour of Normally Brittle Materials During Erosive Coating. J. Eng. Industrial Trans. Vol. 88, 1966, 387-400.
40. Oka, Y. I., Matsumura, M. and Kawabate, T. Relationship Between Surface Hardness and Erosion

Damage Caused by Solid Particle Impact. Wear, 162-164, 1993, 688-695.
41. Tilly, G. P. Erosion Caused by Impact of Solid Particles. Treatise on Materials Science and Technology, Vol. 13, 1970, 447-465.
42. Zhu, W. and Mao, Z. Y. Study of Erosion by Relatively Soft Particles. Proc. Int. Conf. Wear of Materials 1983 (Editor K. C. Ludema), Houston, Texas, 5-9 April ASME 1978, 787-796.
43. Evans, A. G. Impact Damage Mechanisms: Solid Projectiles. Treatise on Material Sci. and Tech. (Edited by C. M. Preece). Academic Press, 1979, 16, 1-67.
44. Ruff, A. W. and Wiederhorn, S. M. Erosion by Solid Particle Impact. Treatise on Material Sci. and Tech. (Edited by C. M. Preece). Academic Press, 1979, 69-129.
45. Shewmon, P. and Sundararajan, G. the Erosion of metals. Ann. Rev. Material Sci., Vol. 13, 1983, 301-318.
46. Salesses, I. Modelling the Erosion of Compressor Materials and Coatings, Master's Thesis, School of Industrial and Manufacturing Sci. Cranfield Institute of Technology, 1993.
47. Hutchings, I. M. and Winters, R. E. and Field, J. E. Solid particles Erosion of Metals: The Removal of Surface by Spherical Projectiles. Proc. R. Soc. London, A., 348, 1976, 379-392.
48. Söderberg, S., Hogmark, S., Engman, U. and Swahn, H. Erosion Classification of Materials Using a Centrifugal Erosion Tester. Tribology Int., Vol. 14 (6), 1981, 333-343.
49. Hutchings, I.M. A Model for the Erosion of Metals by Spherical Particles at Normal Incidence. Wear, Vol. 70, 1981, 269-281.
50. Gupta, A.K and Jackson, T.W., J. The Institute of Energy, 103 Sep 1985.
51. Moore, M.J. and Crane, R.I., 1973, " Deposition and corrosion in gas turbine"
52. [edited by Hart, A.B. and Cutler, A.J.B], Ch. 4., John Wiley and Sons, New York.
53. Vermes, G. 1979, Trans. ASME. J. Engineering Power, 101, 542-548.
54. Morse, T.F., Wang, C.Y and Coplla Jr. J.W. (1985). Trans. ASME, J. Heat Transfer, 107, 155-160.
55. Pratsinis, S.E. and Kim, K.S. (1989), J. Aerosol Sci. 20, 775-785.

56. Richards, G.A. Logar, R.G., Meyer, C.T. and Anderson, R.J. (1992), Trans. ASME., J. Engineering For Gas Turbine And Power. 114, 132-138.
57. Ahluwalia, R.K. Im, K.H. and Wanglarz, R.A. (1989), Trans. ASME. J. Power Engineering For Gas Turbine. 111, 672-678.
58. Dahneke, B. (1971), J.Colloid Interface Sci., 37, 342-353.
59. Wang H.C. (1986), J. Aerosol Sci., 17 (5), 827-837.
60. Wang, H.C., (1988), "Adhesion And Removal", [Edited by, Mihal, K.L], pp211, Plenum Press, New York.
61. Wall, S. John, W. Wang, H.C. and Goren, S.L., (1990), Aerosol Sci. Technl. 12, 926.
62. Rosner, D. E. Tassopoulos, M. and Makowski, D.W. (1992), Proceeding of the Conference: "Inorganic Transformation and Ash Deposition During Combustion" pp. 585-606. ASME Engineering Foundations.
63. Fuchs, N.A., (1964), "The mechanisms of Aerosol", Pengamen, New York.
64. Frindlander, S.K. (1977), "Smoke, Dust and Haze-Fundamentals of Aerosol Behaviour", Wiley, New York.
65. Rosner, D.E. (1986), Butterworth-Heinemann, Stoneham. MA. "Transport Processes in Chemically Reacting Flow System".
66. Israel, R. and Rosner, D.E., (1983), Aerosol Sci. Technol. 2, 45-51.
67. Smith, M. C. G., A Theoretical note upon the Mechanism of Deposition in Turbine Blade Fouling, N.G.T.E: M145, Feb. 1952.
68. Down, M. G. and Williams, M. J. Out of Area Experiences With the RB199 in Tornado. AGARD Confrence Proceeding 558, *Erosion, Corrosion, and Foriegn Object Damage Effects in Gas Turbines*, Paper No. 1.
69. Talbot, L., Cheng, R.K., Schefer, R.W and Willis, D.K. (1980), J. Fluid Mech., 101, pp. 737.
70. Montassier, N. Boulaud, D. and Renoux, A. (1991), J. Aerosol Sci., 22, 677-687.
71. Goren, S.L., (1977), J. Colloid Interface Sci., 61, 77-85.
72. Walker, K.L., Homsy, G.M. and Geyling, F.T. (1979), J. Colloid Interface Sci., 69, 138-147.
73. Anderson, R. J., Romanowsky, C. J. and France, J. (1984), DOE/METC-85/2007.
74. Kim, J., Dunn, M.G., Baran, A.J. Wade, D.P. and Tremba (1993). J. Engineering For Gas Turbine and Power, 115, 641-651.

75. Kim, J.Y and Kim, S.S. (1991), J. Aerosol Sci., 22, 201-214.
76. Bellman, R. and Levy, A. Erosion Mechanism in Ductile Metals. Wear, 70, 1981, 1-27.
77. Follansbee, P. S., Sinclair, G. B. and Williams, J. C. Modelling of Low Velocity Particulate Erosion in Ductile Materials by Spherical Particles., 74, 1981-1982, 107-122.
78. Emiliani, M. and Brown, R. Erosion of Ti-6Al-4V by spherical Silica Particles at 90° Impact Angle. Proc. 6th
79. Halling, J. The Tribology of Surface Coatings, Particularly Ceramics. Proc. Inst. Mech. Engrs., 100(C1), 1986, 31-40.
80. Burnett, P. J. and Rickerby, D. S. The Erosion Behaviour of TiN Coatings. Wear, 166, 1993, 7-16.
81. Ninham, A. J. and Hutchings, I. M. A Computer Model for Particle Velocity Calculation in Erosion Testing. Proc. 6th Int. Conf. On Erosion by Solid and Liquid Impact, Cavendish Lab. Unervisity of Cambridge, 5-8 Sepr 1983, paper 50.
82. Tabakoff and Wakeman. The Test Facilitt for Material Erosion at High Temperature. Proc. ASTM Symp. Erosion: Prevention and Usfull Applications (Edited by W. F. Alder). ASTM STP 664, 1979.
83. Rickerby, D. S. Development of Advanced Erosion Resistant Coatingd for Gas Turbine Compressor Applications. Final Technical Report. Brite Program BE-3339. 1994.
84. Olsson, M., Hedenqvist, P., Stridth, B. and Söderberg, S. Solid Particle Erosion of Hard Chemically Vapour Deposited Coatings. Surf. Coat. Tech., 37, 1989, 321-337.
85. Liebard, M. and Levy, A. V. the Effect of Erodent Particle Characteristics on the Erosion of Metals. Proc. Int. Conf. Wear of Metals (editor K. C. Ludema), Orlando, Florida, 7-11 April, ASME, Vol. 1, 123-127.

APPENDIX 1

1.1 Laser two-spot Anemometer (L2F)

The (L2F or time-of-flight) laser two-spot anemometer is a non-intensive instrument for measuring flow velocity, figure 1-1. It relies on a particle passing through two focused beams, figure 1-2. This is achieved using an optical arrangement such as that shown in figure 1-3. These two beams form a 'light gate' in that particle passing through both beams produces two successive pulses of scattered light. The time elapsed between these pulses, together with the beam separation, are used to determine the velocity of the particle.

The main advantages of the two-spot arrangement anemometer that it provides a shorter probe length, allowing measurement to be taken closer to solid surfaces. The higher light intensity in the probe volume produces larger optical pulses and easier detection, especially when operating in a backscatter arrangement. A disadvantage is that measurements are only made for particles travelling in the plane of the two beams, and necessarily a search has to be performed to find the mean direction of the flow.

The principle of operation of the anemometer is that as a particle passes through the two beams, producing a double light pulse, the scatter light from each is received by a photo-multiplier tube (PMT) (one tube for one beam). These pulses are then passed either to a digital correlator, or multichannel analyser, both techniques building up a histogram of the transit times of the particles passing through both beams, figure 1-4. In

addition the histogram will contain a certain amount of noise that is generated by particles that pass through one beam only and by the flare from the solid surfaces. This histogram contains information about the velocity distribution of the flow.

A computer program called L2F was used to extract the information from the produced histograms. The programme outputs the values of velocities, flow angle, turbulence, and also includes an option to store raw data, should more detailed analysis be required off-line. The program has been described to be very efficient in calculating the outputs since the computations are carried out on-line as this ensures that sufficient data has been taken at each measurement point.

Figure 1-1. L2F system components.

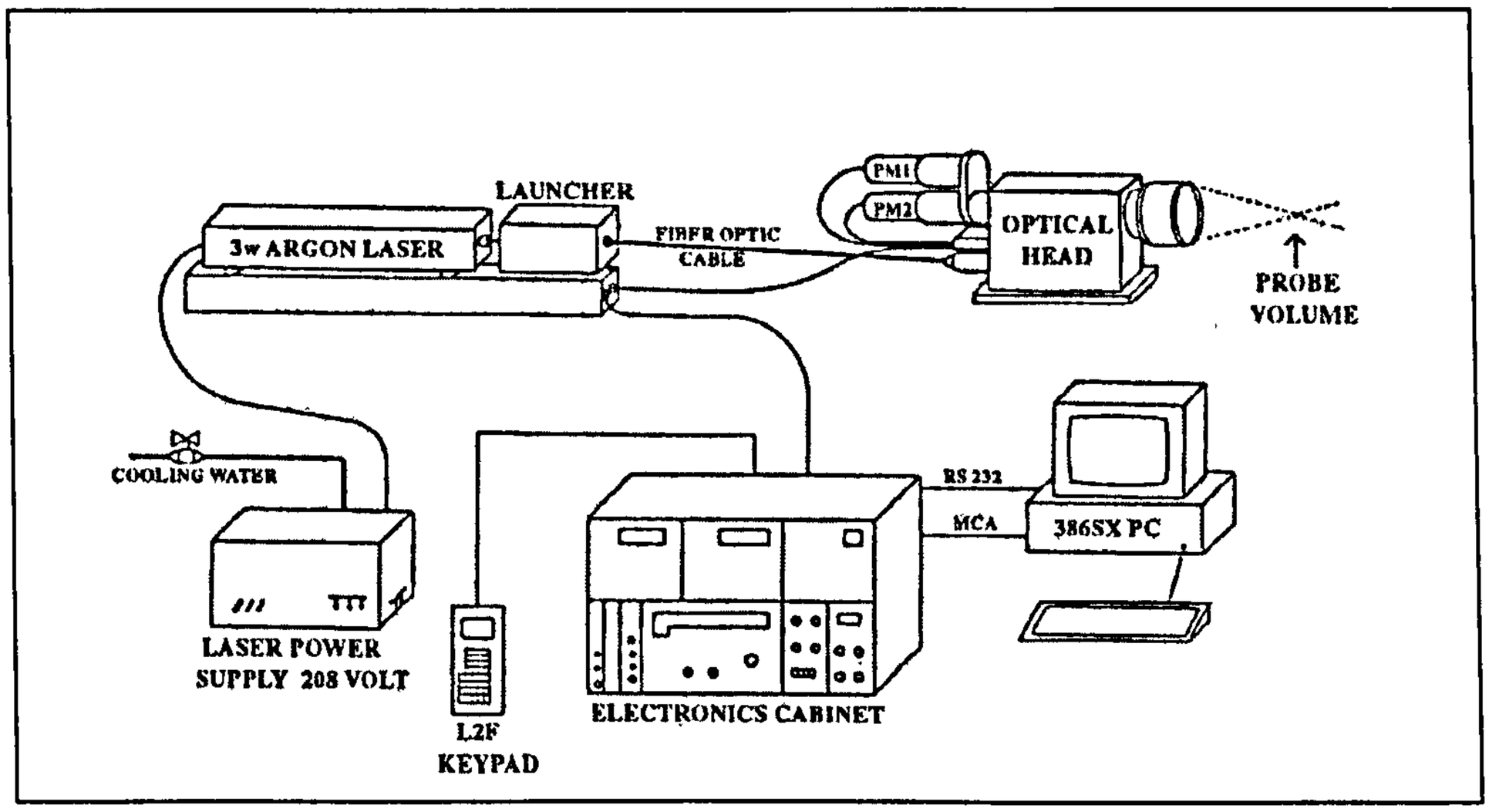


Figure 1-2. Highly focused parallel light beams generated.

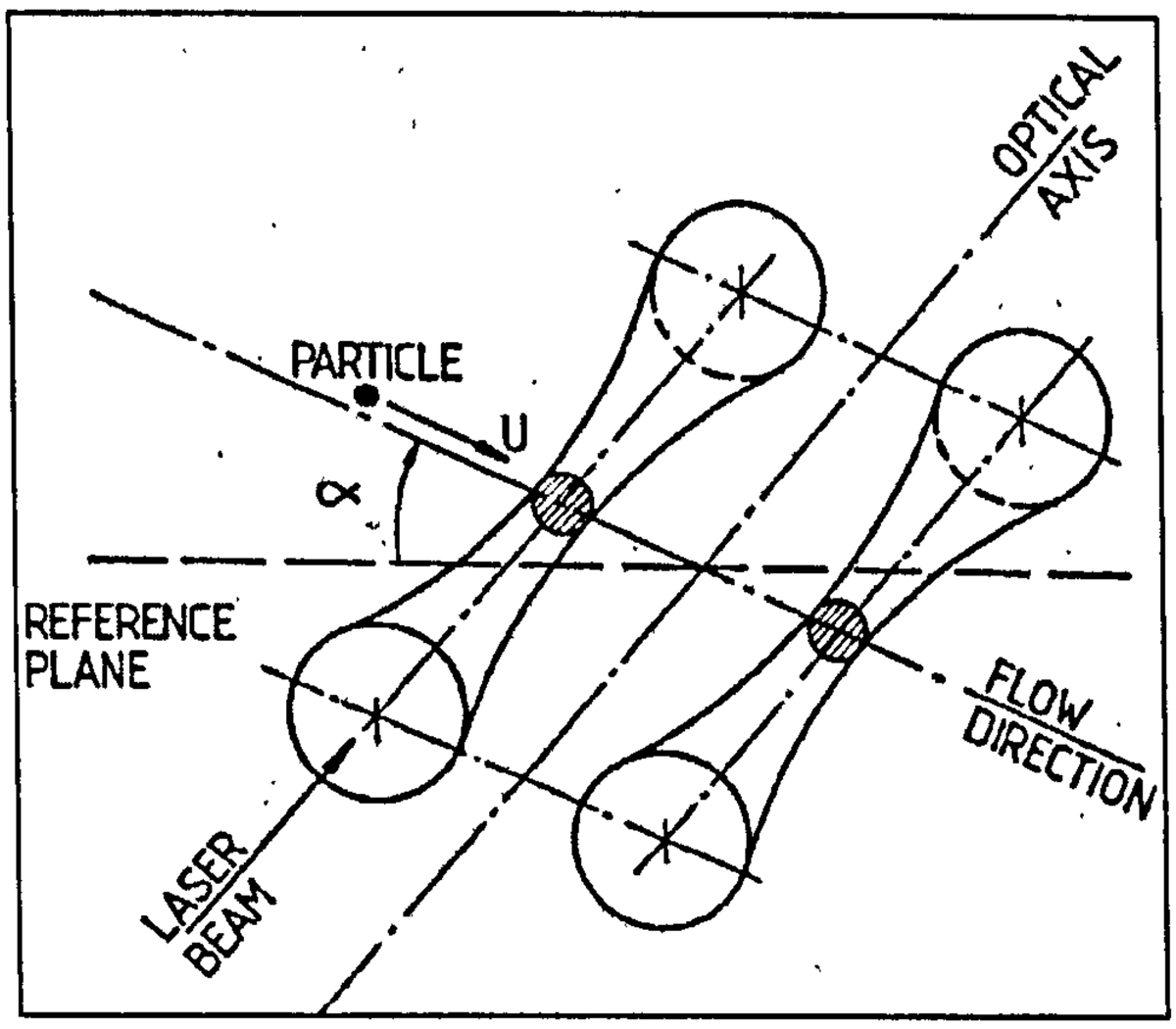


Figure 1-3. Optical arrangements that generate the highly focused beams.

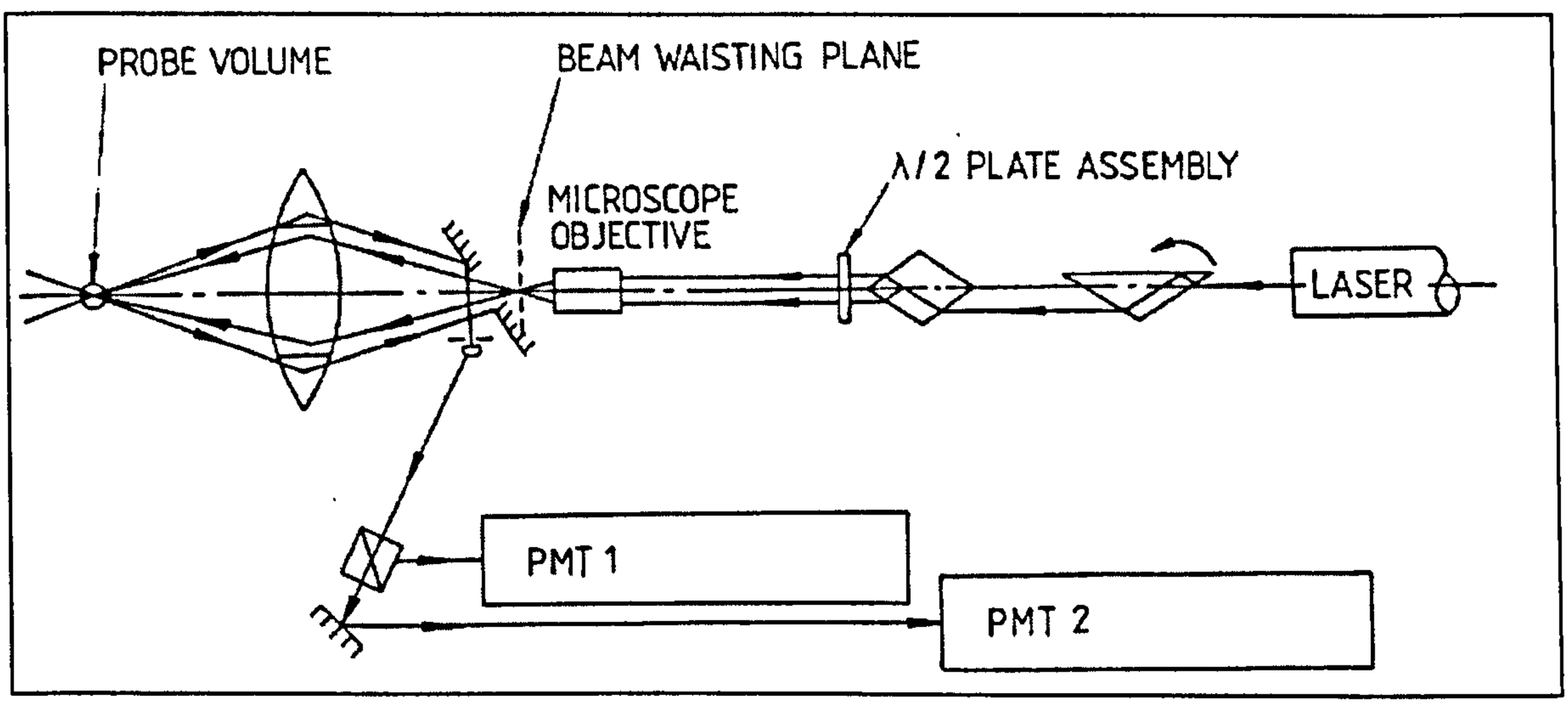
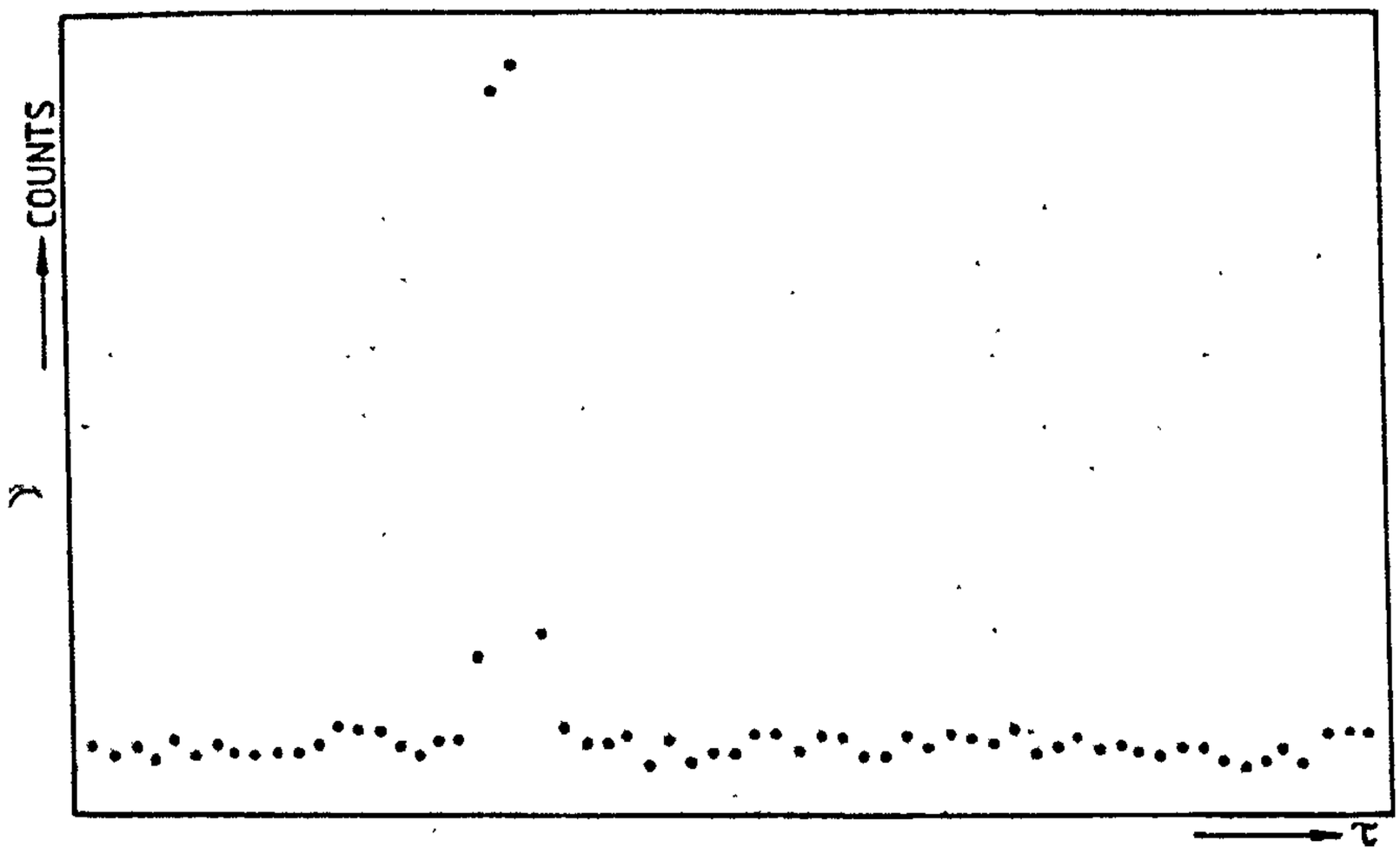


Figure 1-4 . Histogram of the transit times of the particles passing through both beams.



APPENDIX 2

2.1 CFD Simulation results of particle and gas temperature and velocity

The FLUENT CFD package has been used to simulate the test conditions. The simulation has been carried out to determine both particle and gas temperature and velocity at different test conditions. The outputs show that particle temperature is very close to that of gas temperature at low and high particle velocities. Never the less, at low gas velocity, particles are more capable to catch more of gas temperature. On the other hand, particle velocity is very close to gas velocity at the outlet at different velocities and temperatures. Velocity distribution at the tube exit shows that the highest particle and gas velocity covers more than half of the tube diameter.

The presentation of CFD results will be limited only to two inlet velocity settings and tree tube wall temperatures. Two gas inlet velocities chosen are 40 and 140 m/s, which correspond to 0.703kg/hr and 2.46 kg/hr flow rates respectively.

The tube geometry was very simple with 4m long and 0.004m inner diameter. The computations were carried out on a two-dimensional H-type structured grid. A computational grid, which gave 20,000 cells geometry as shown in figure 2-1, was found to be sufficient to yield a solution. The number of faces increases as we move towards the tube exit and become very intensive at the end of the tube. The tube wall temperature was set as a 3^{rd} degree polynomial function based on the experimental readings of

the tube wall temperature at different runs. One of the functions is shown on figure 2-2, which shows the variation of the wall temperature as a function of distance. The blue line shows the wall temperature distribution, while the white lines show the solution conversion of the gas temperature.

Figure 2-1. The computation grid.

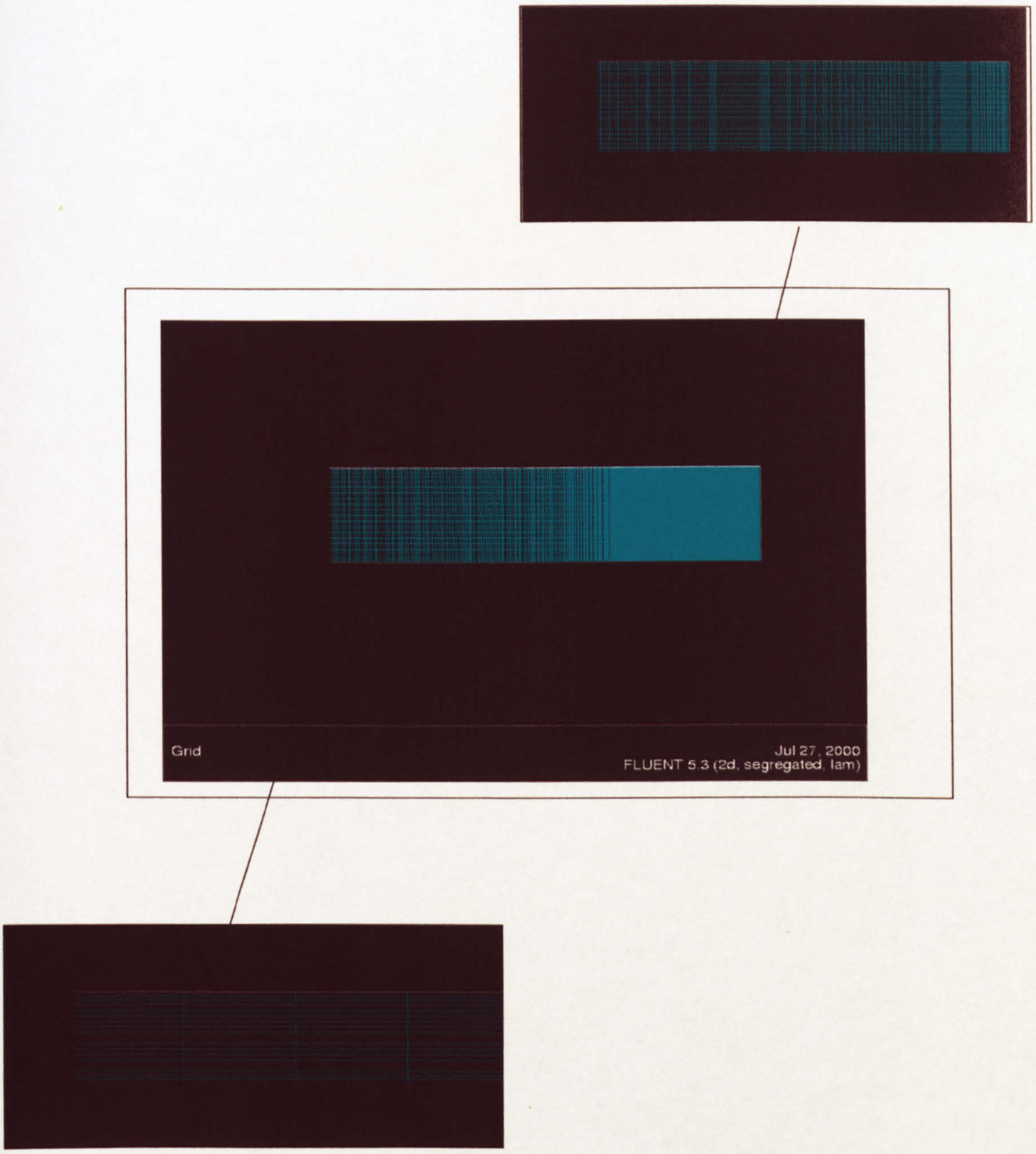
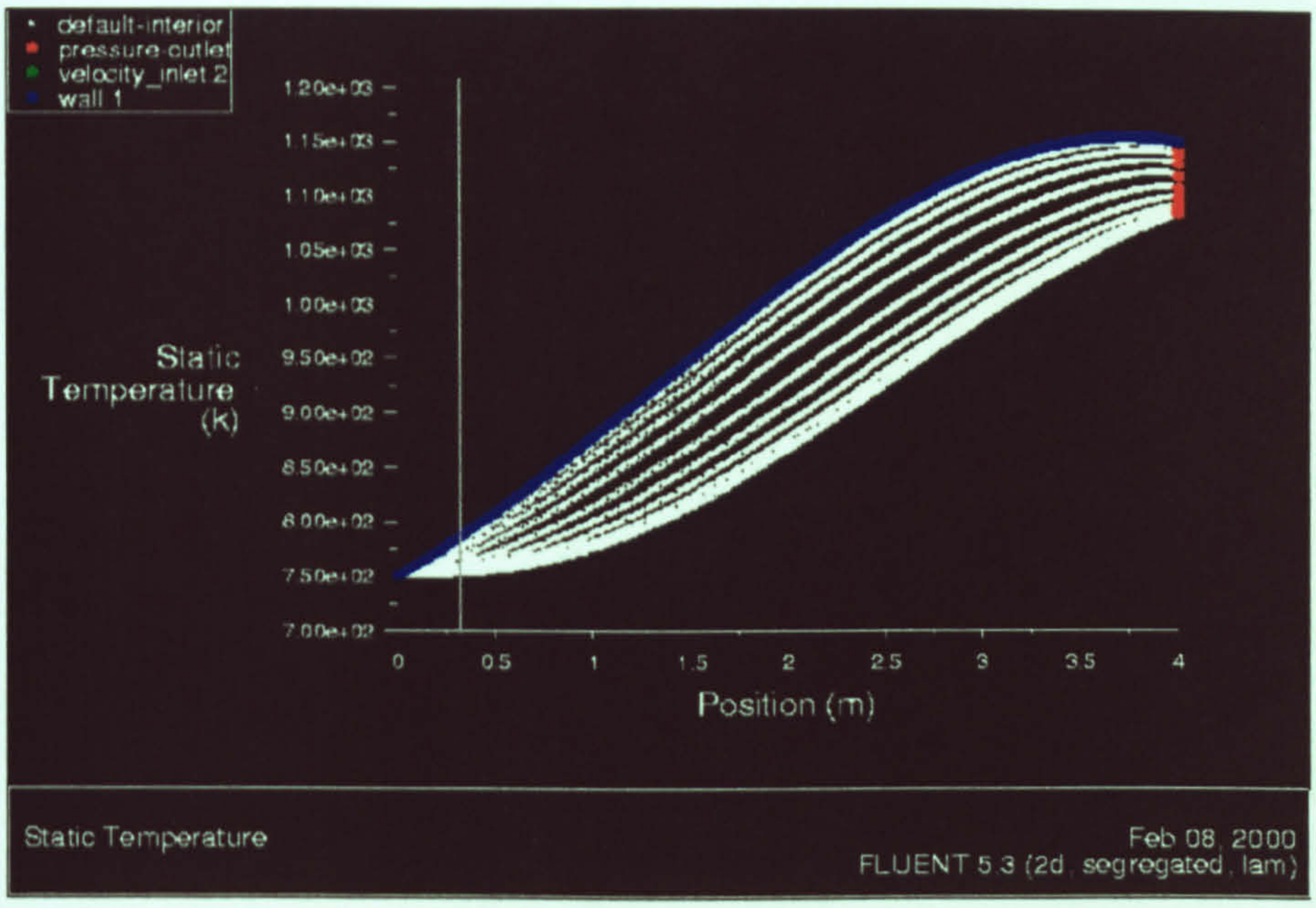


Figure 2-2. Wall temperature polynomial function and conversion criteria.



The particle size during the CFD computational calculation was chosen to be of 50μm-diameter, which forms the maximum possible size found on the particle size distribution during the experimental tests. The particle was considered have zero inlet velocity, which is the case of the experimental conditions. The inlet particle temperature was set with accordance of the experimental setting of ambient temperature of 300K.

2.1.1 CFD Results for 550°C Gas Temperature.

1. Inlet Velocity of 40 m/s (0.703kg/hr)

Figure 2-3. Static temperature distribution.

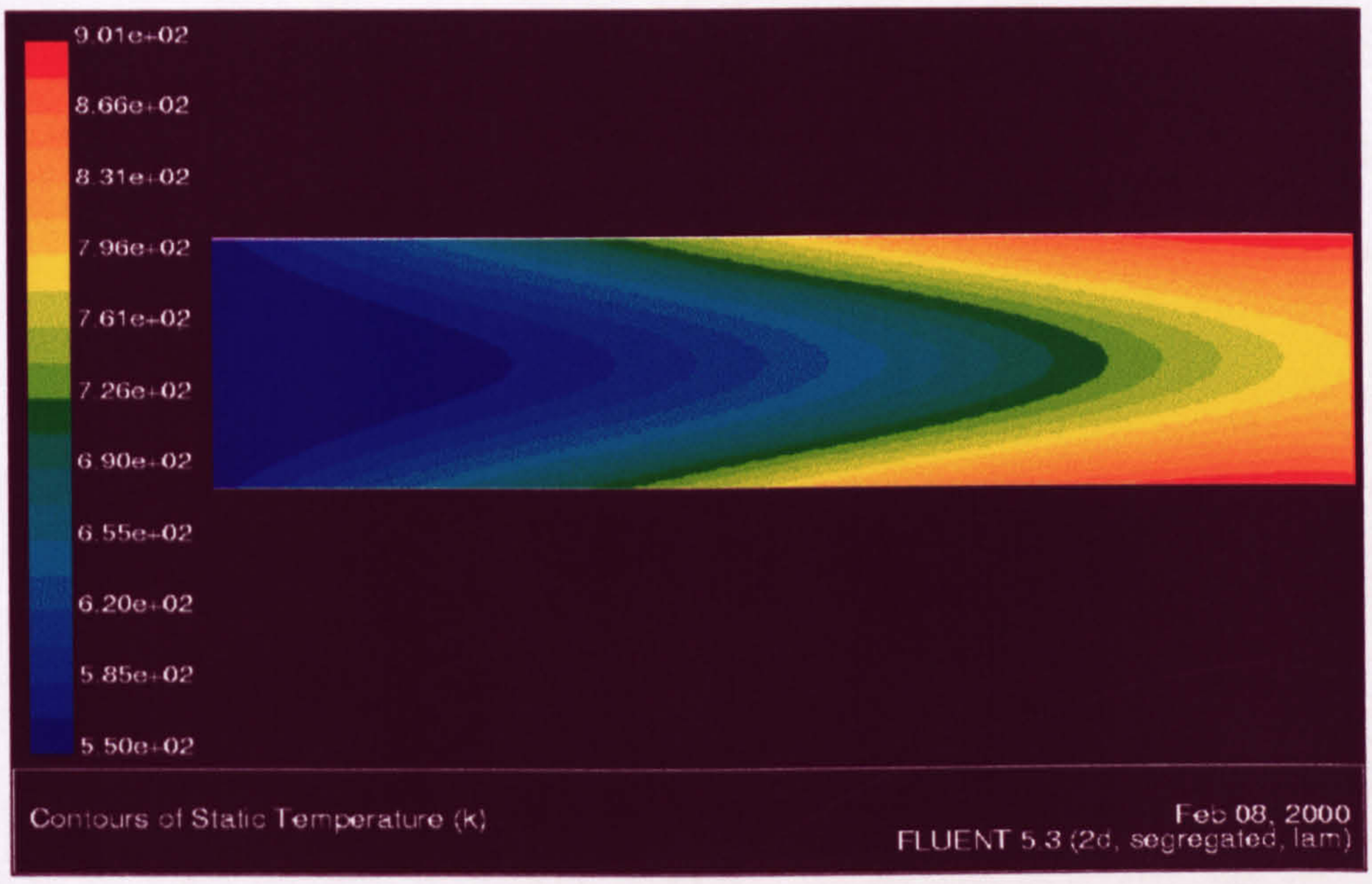


Figure 2-4. Particle temperature distribution.

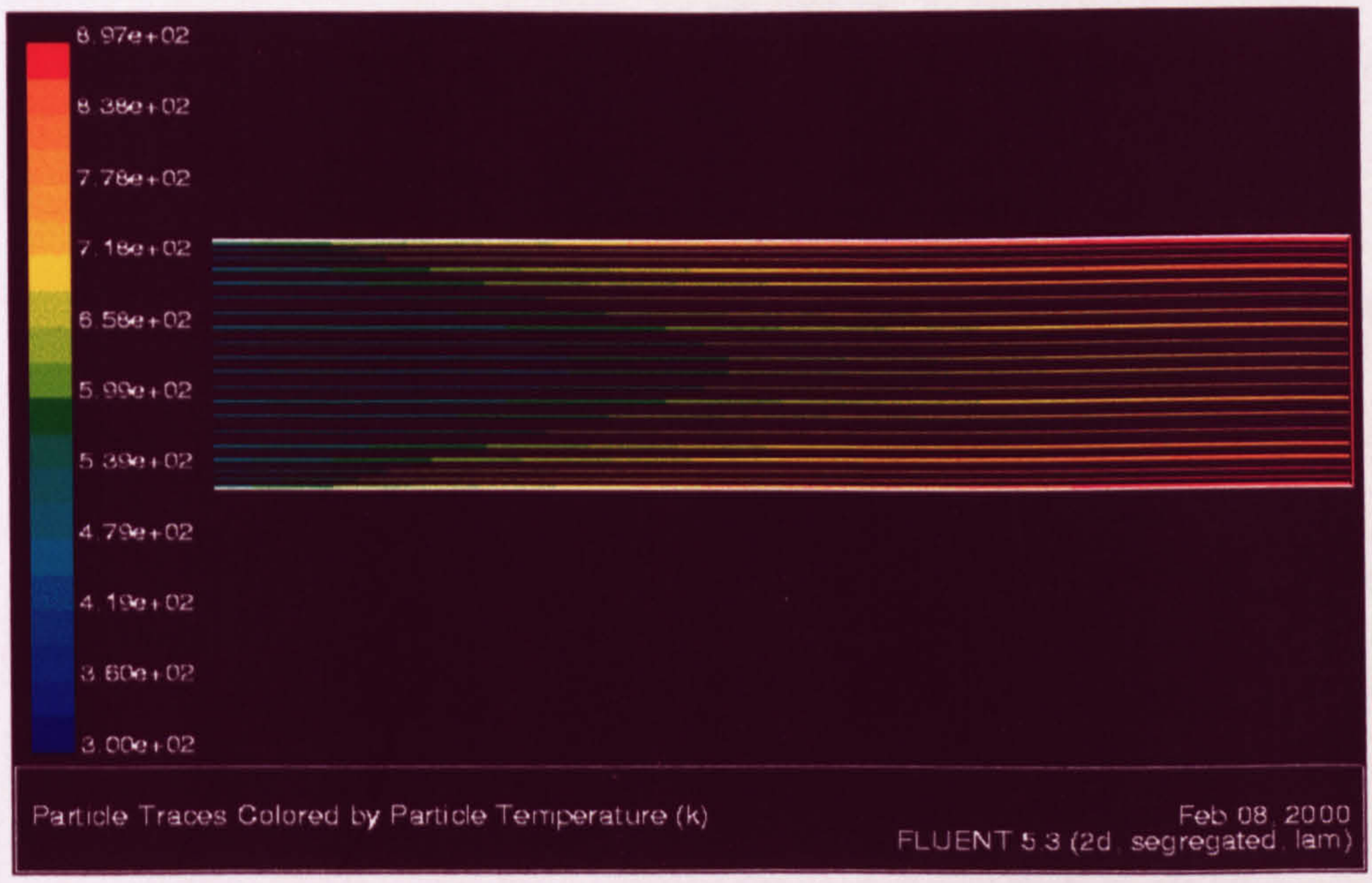


Figure 2-5. Flow velocity distribution.

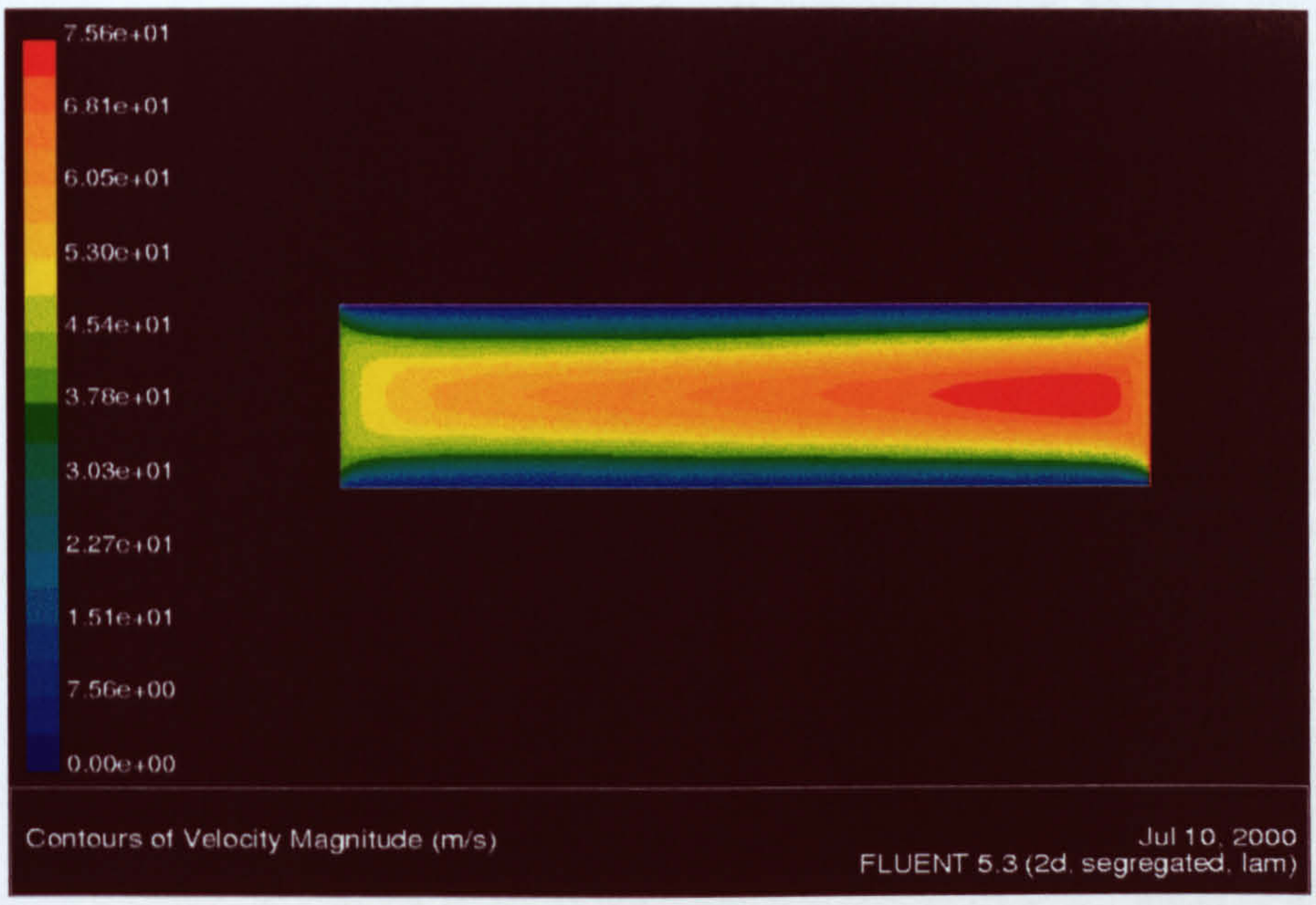
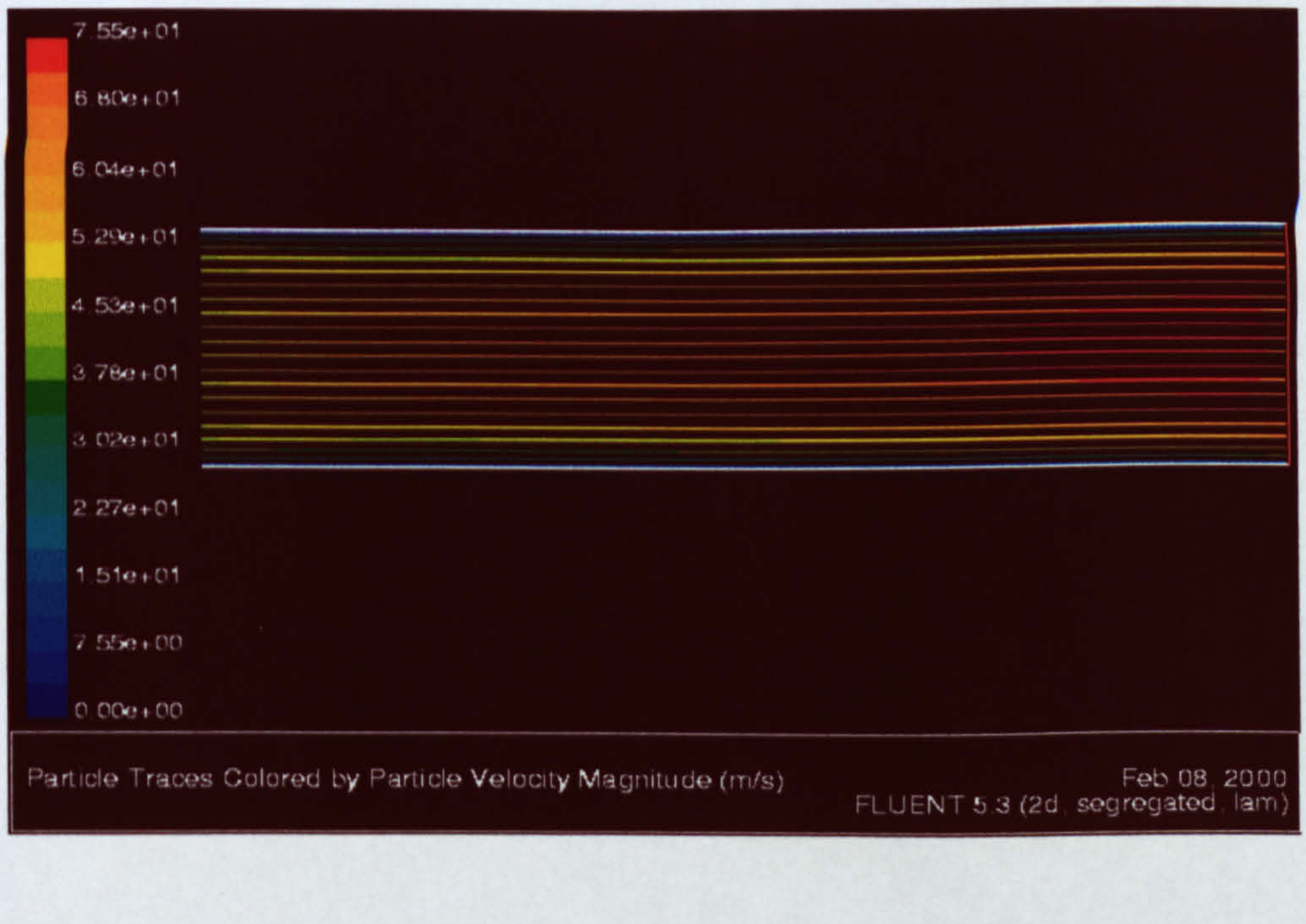


Figure 2-6. Particle velocity distribution.



2. Inlet Velocity of 140 m/s (2.46kg/hr)

Figure 2-7. Static temperature distribution.

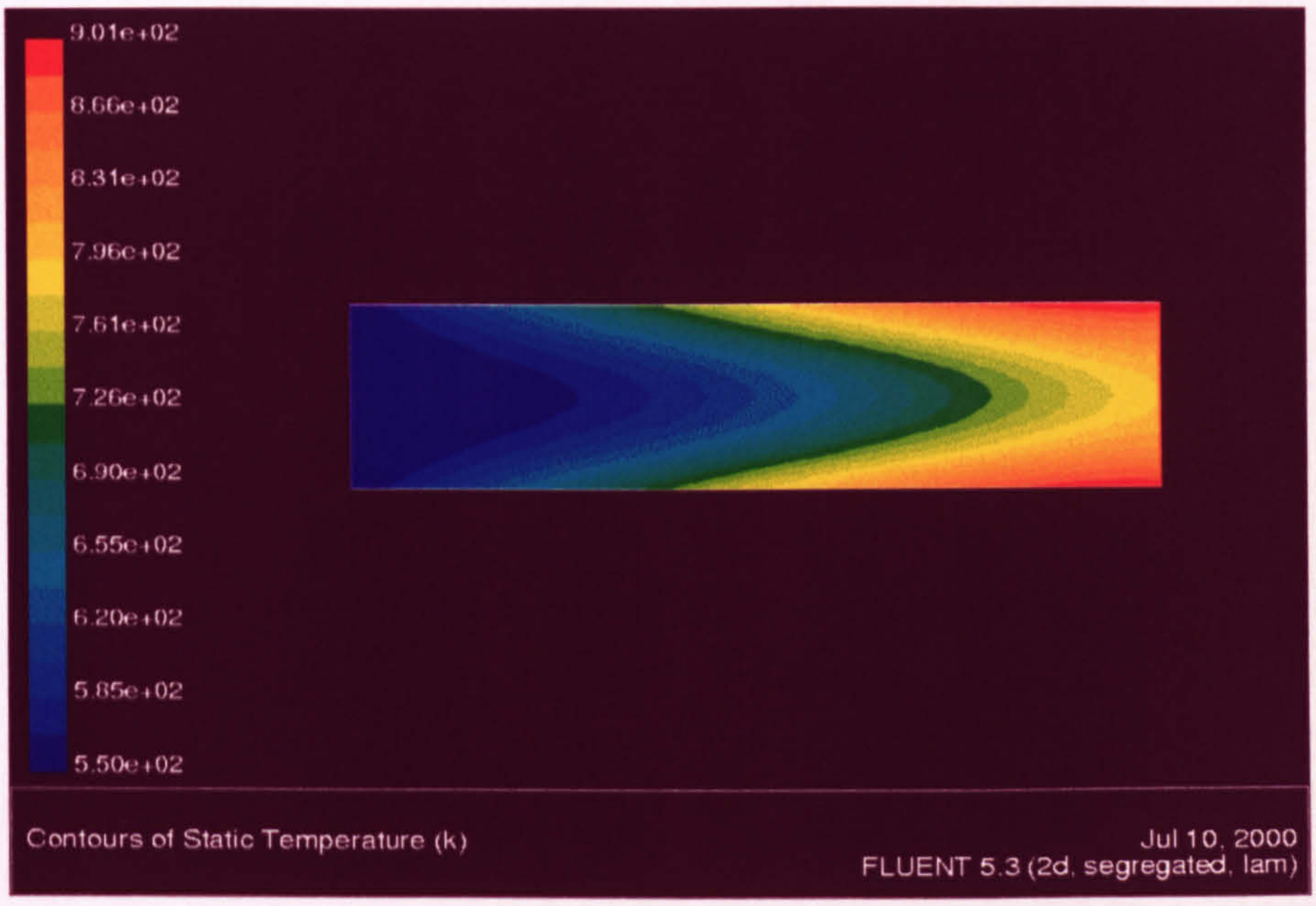


Figure 2-8. Particle temperature distribution.

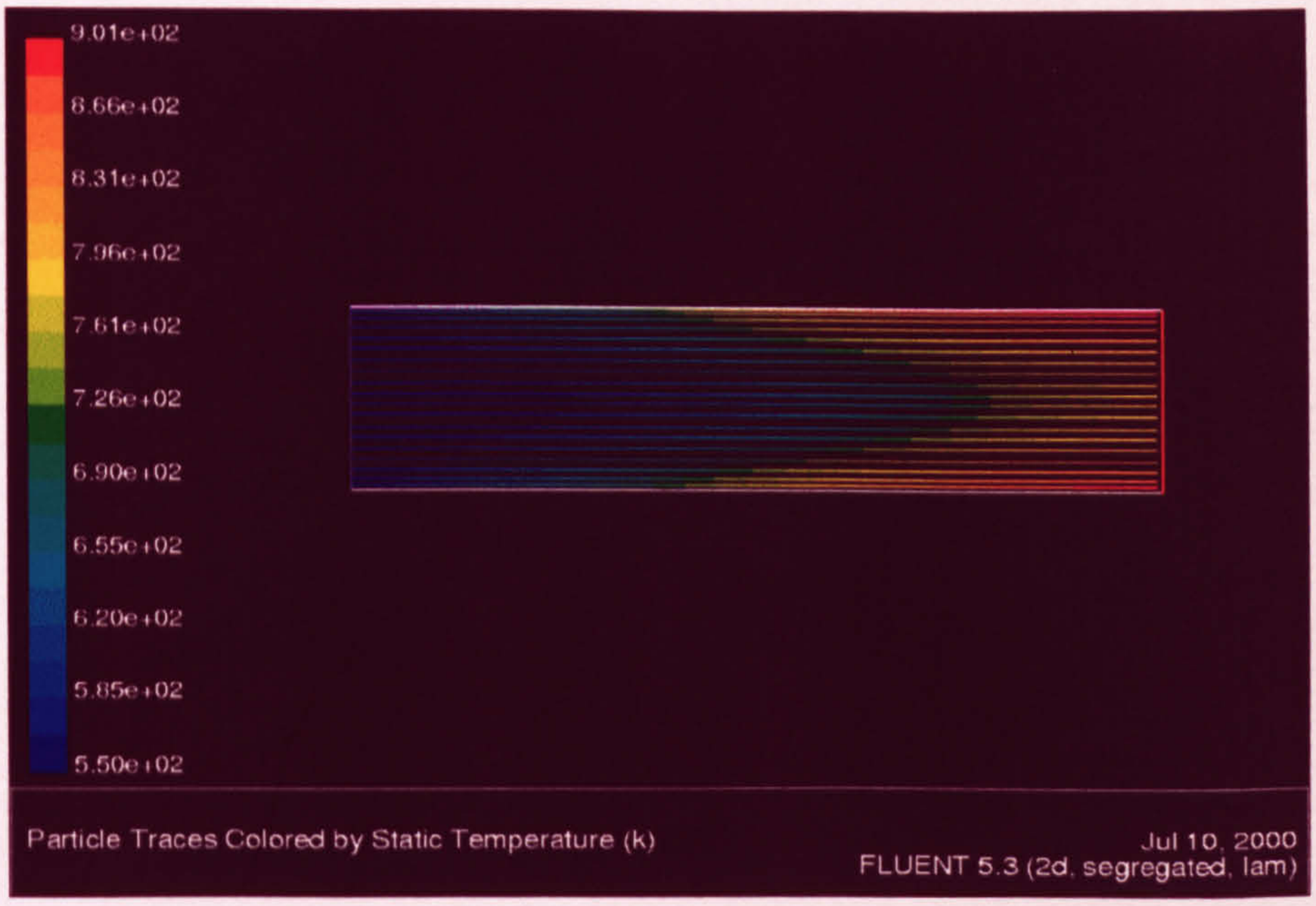


Figure 2-9. Flow velocity distribution.

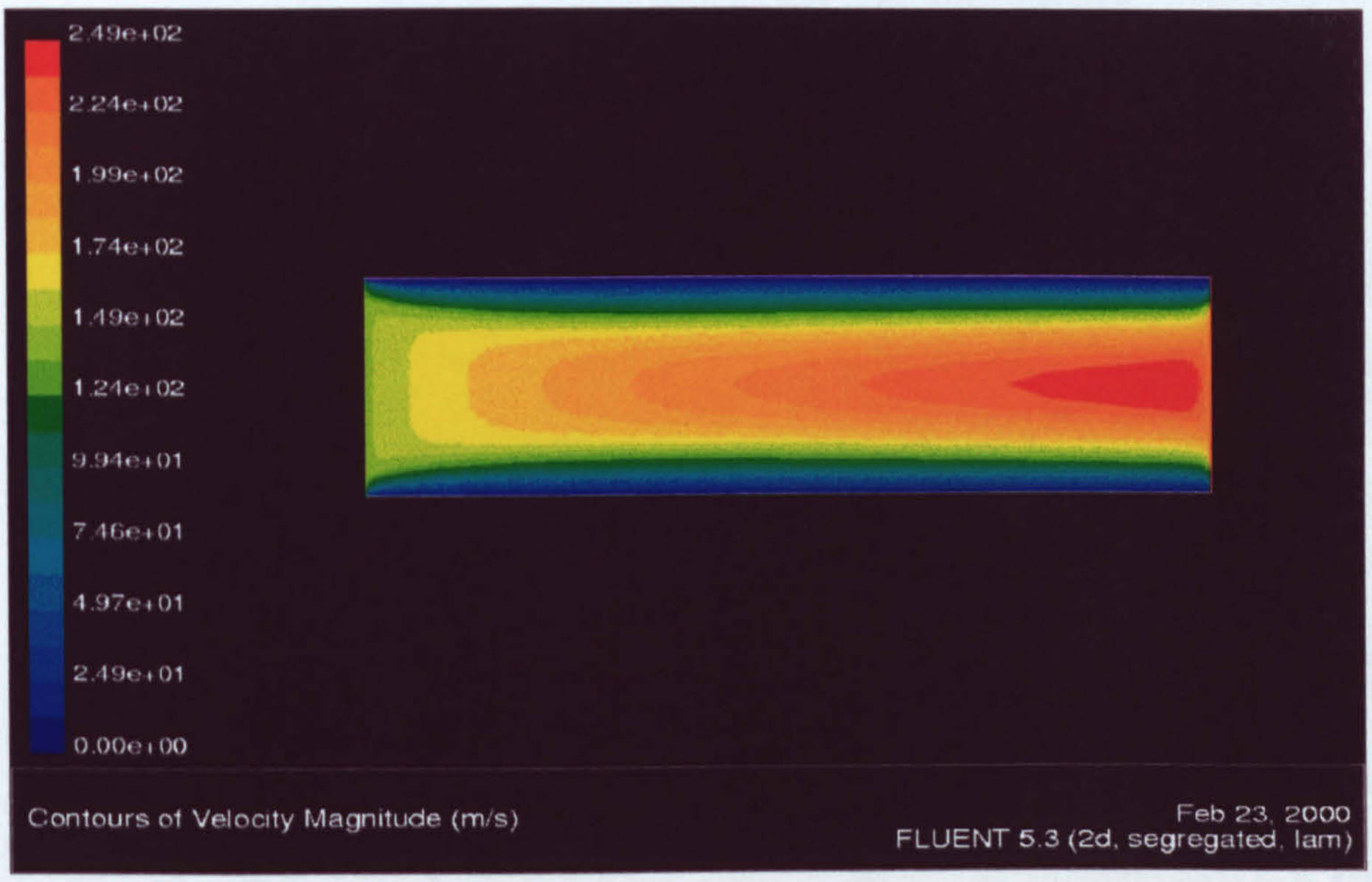
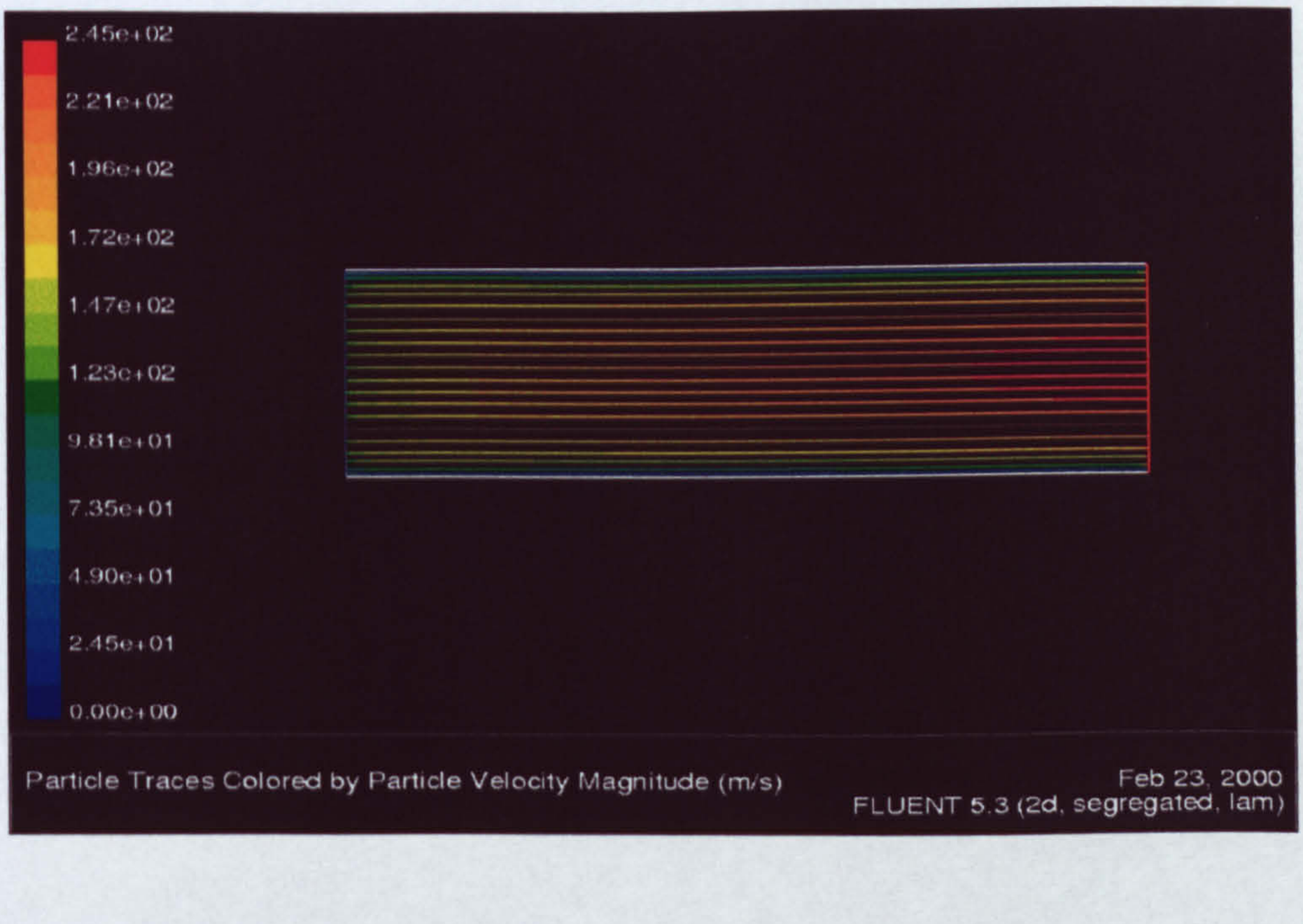


Figure 2-10. Particle velocity distribution.



2.1.2 CFD Results for 750°C Gas Temperature

1. Inlet Velocity of 40 m/s (0.703kg/hr)

Figure 2-11. Static temperature distribution.

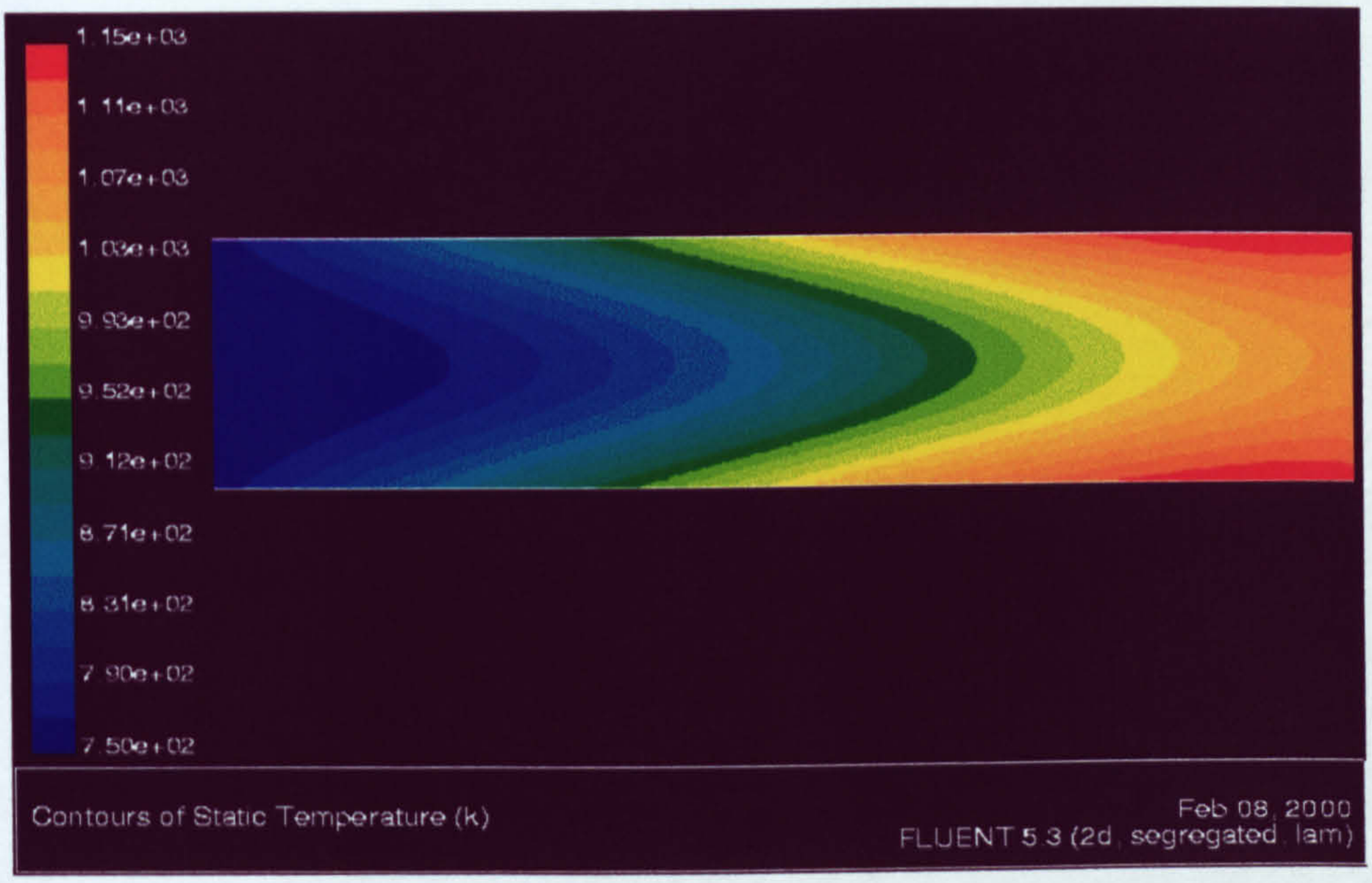


Figure 2-12. Particle temperature distribution.

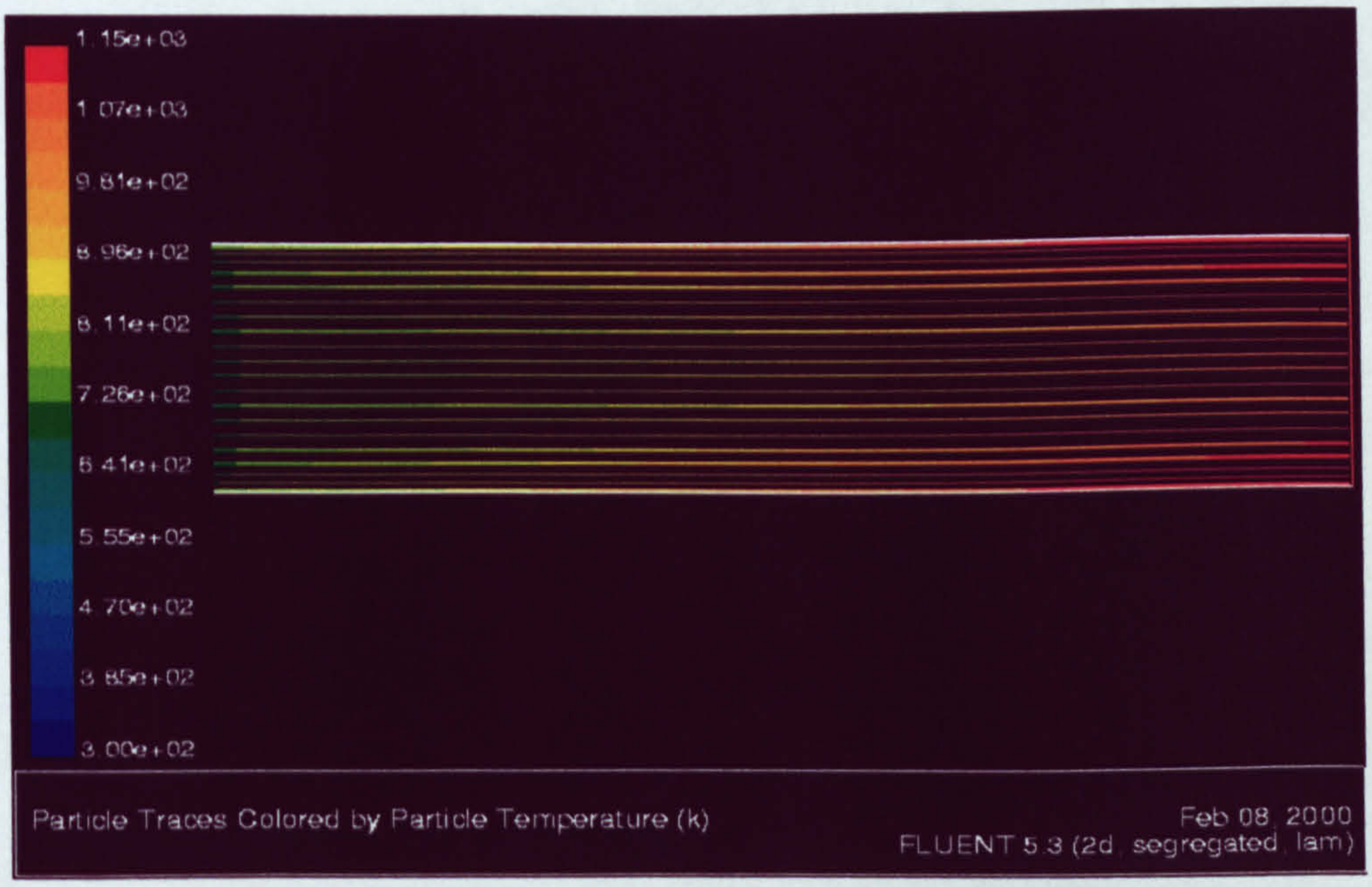


Figure 2-13. Flow velocity distribution.

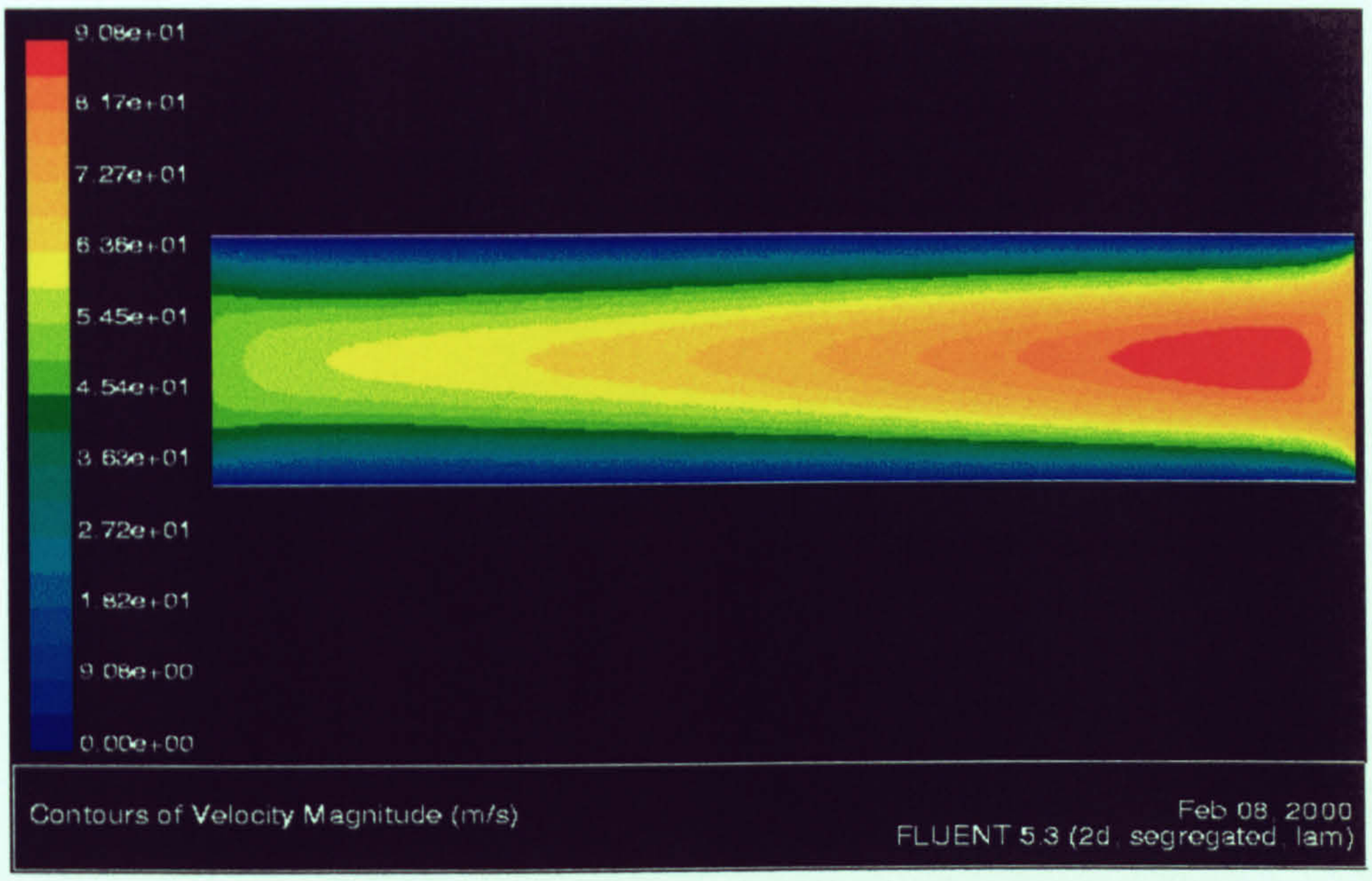
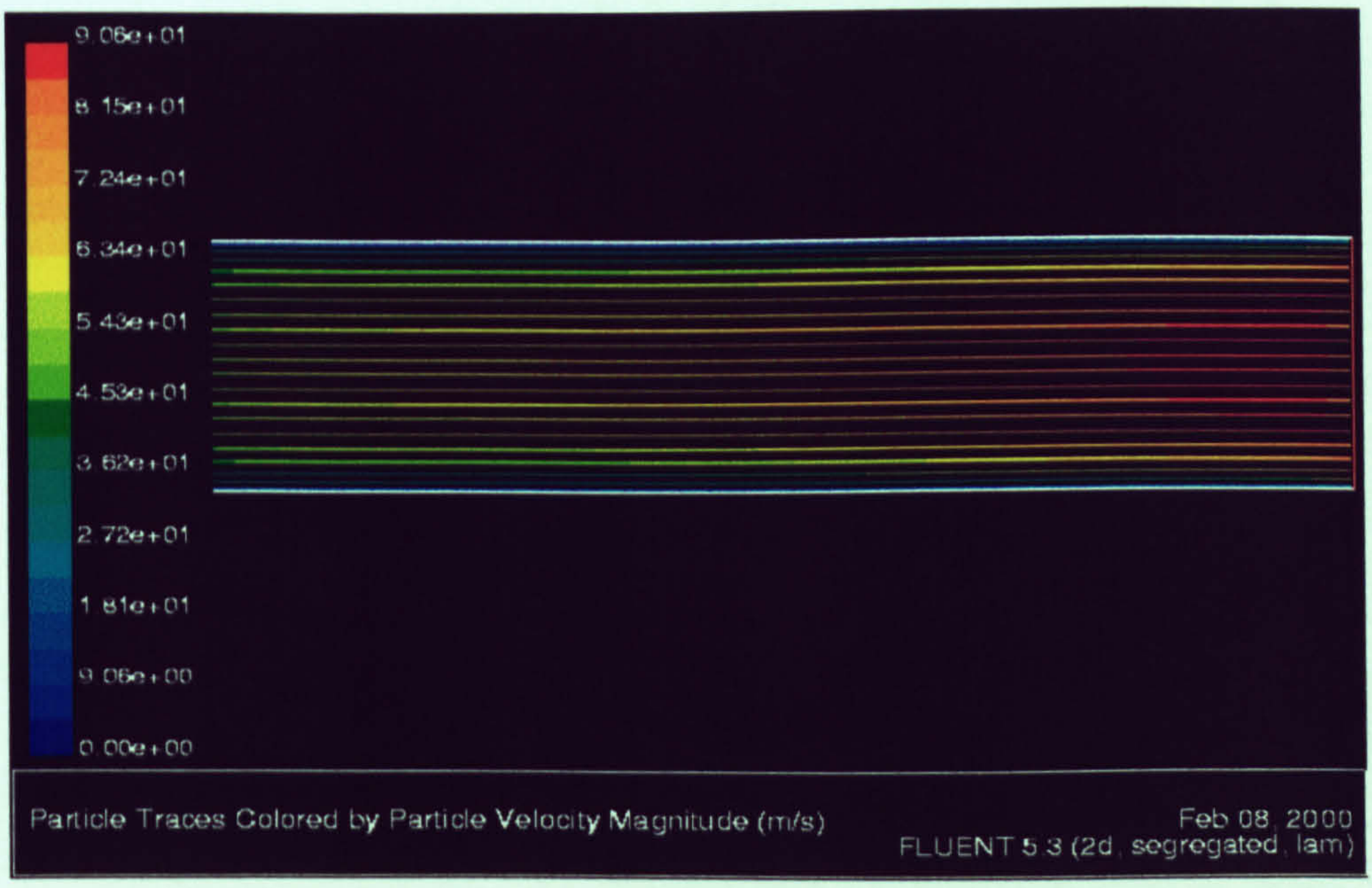


Figure 2-14. Particle velocity distribution.



2. Inlet Velocity of 140 m/s (2.46kg/hr)

Figure 2-15. Static temperature distribution.

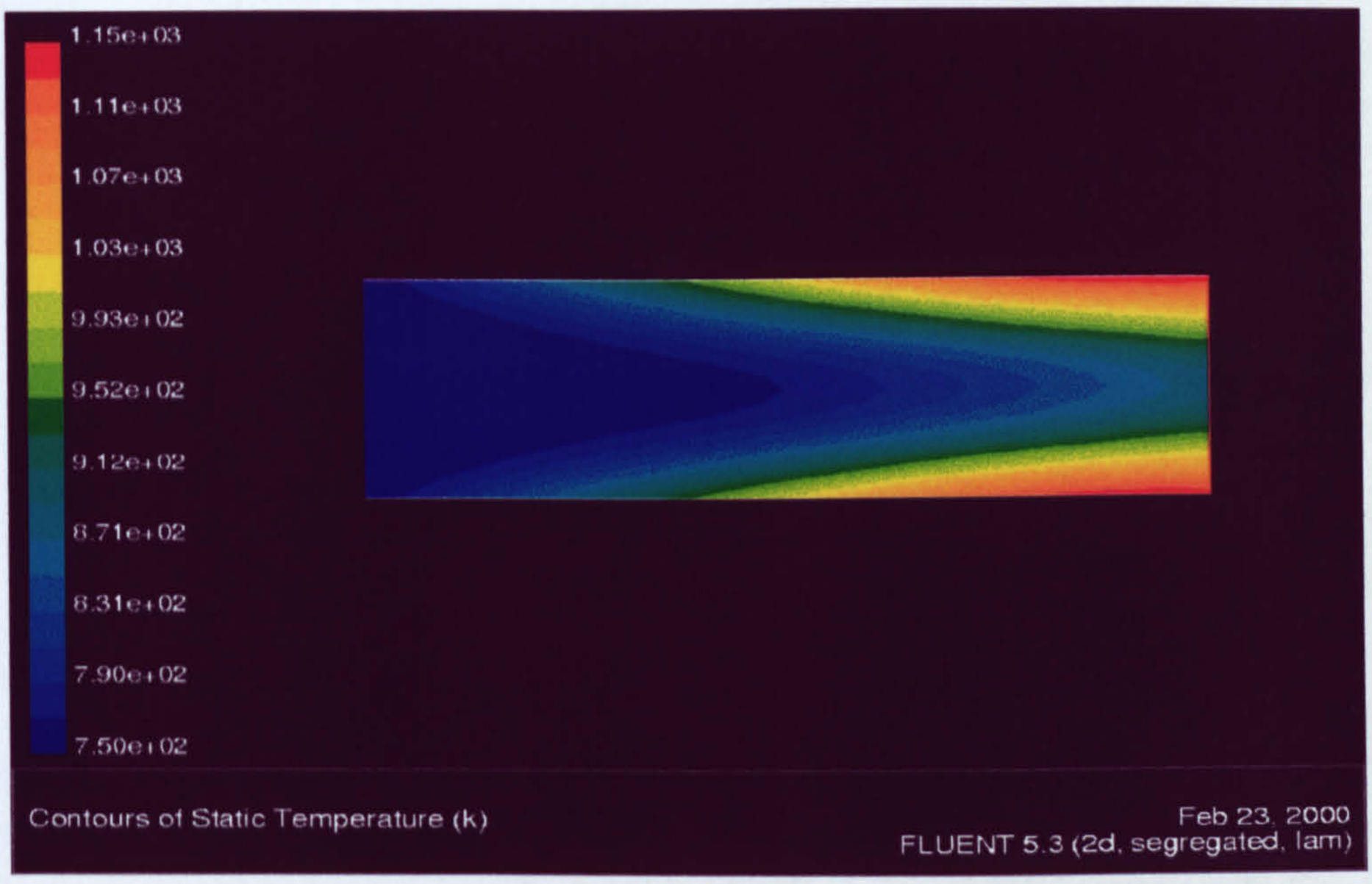


Figure 2-16. Particle temperature distribution.

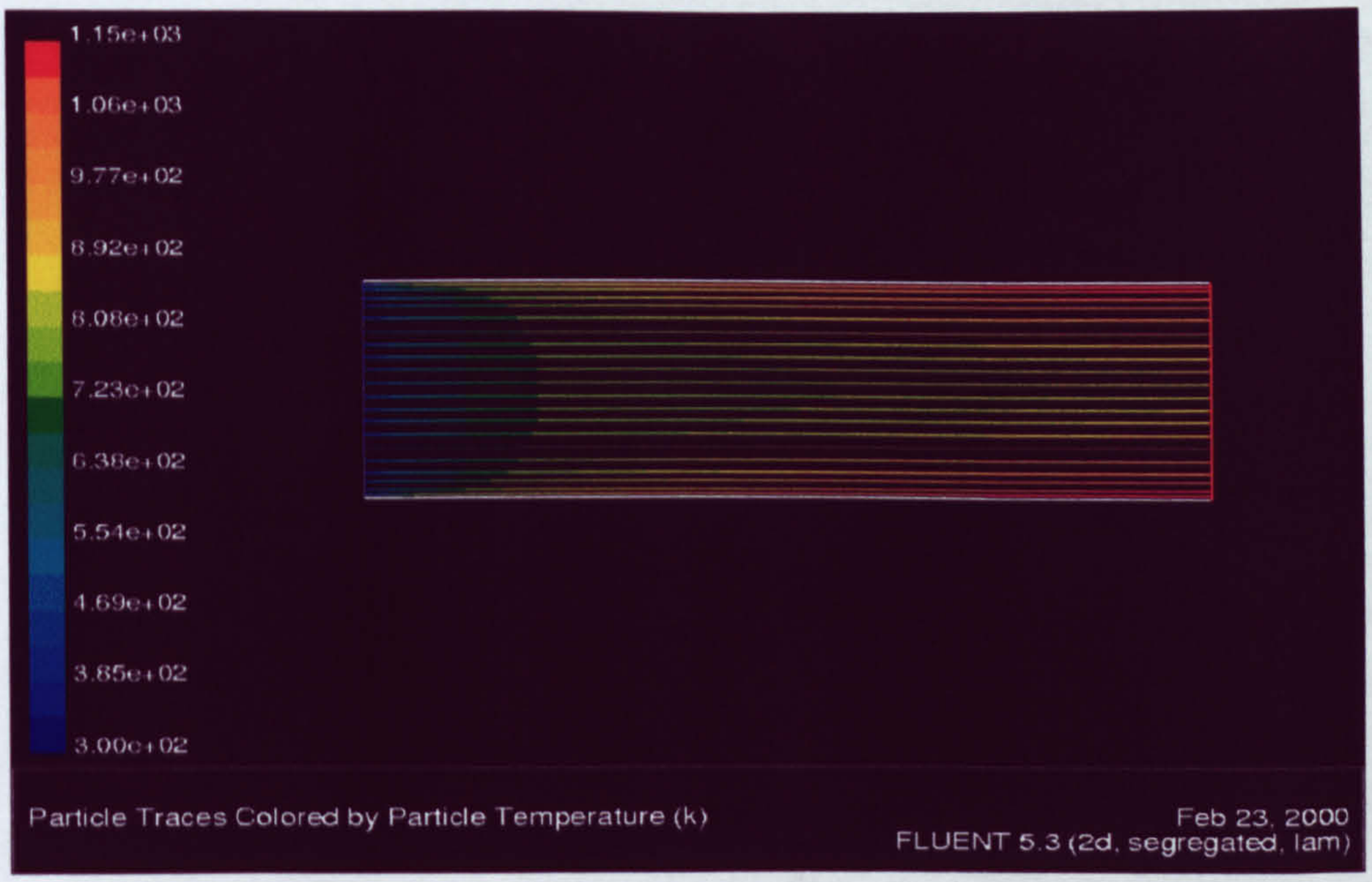


Figure 2-17. Flow velocity distribution.

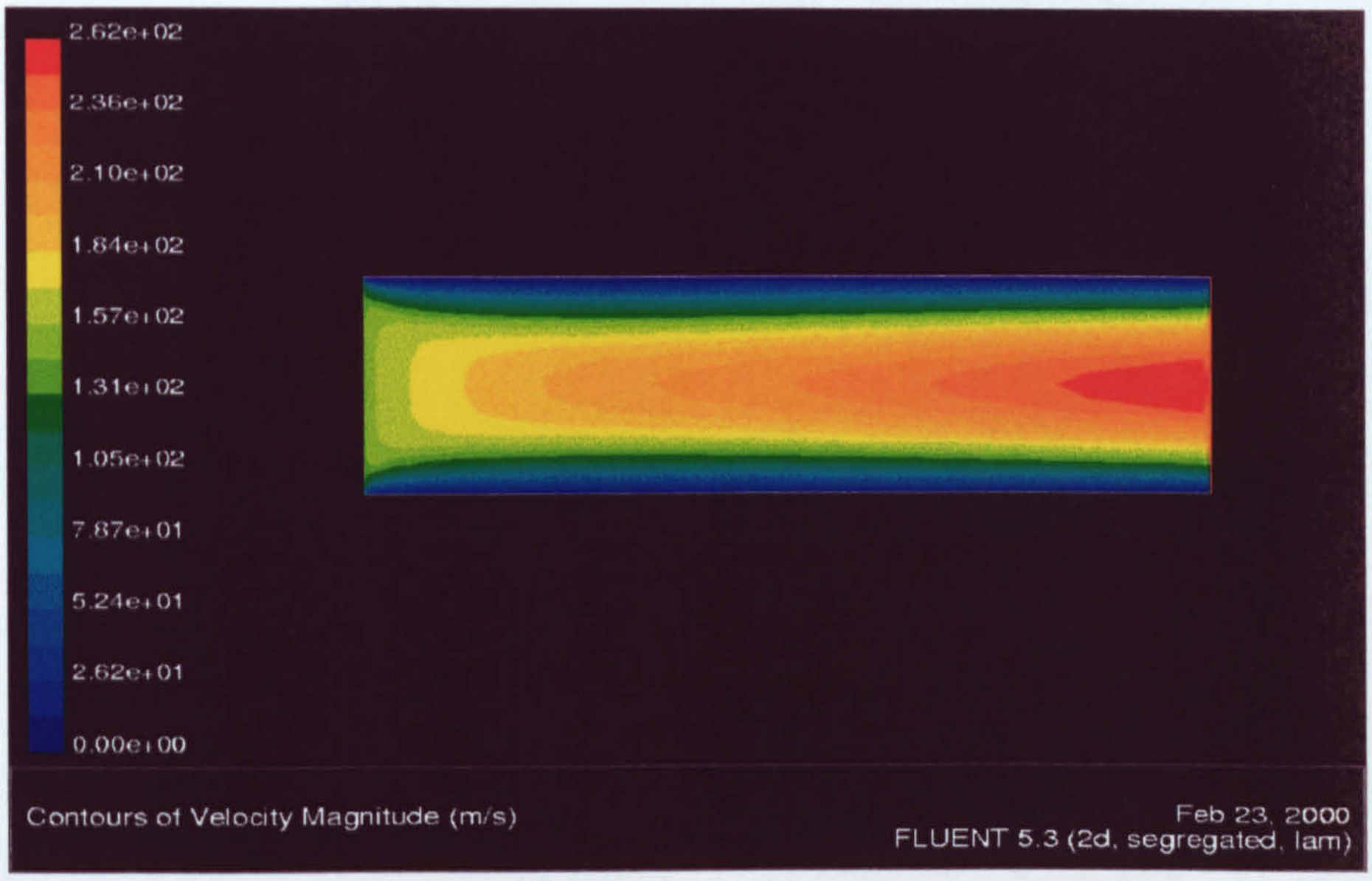
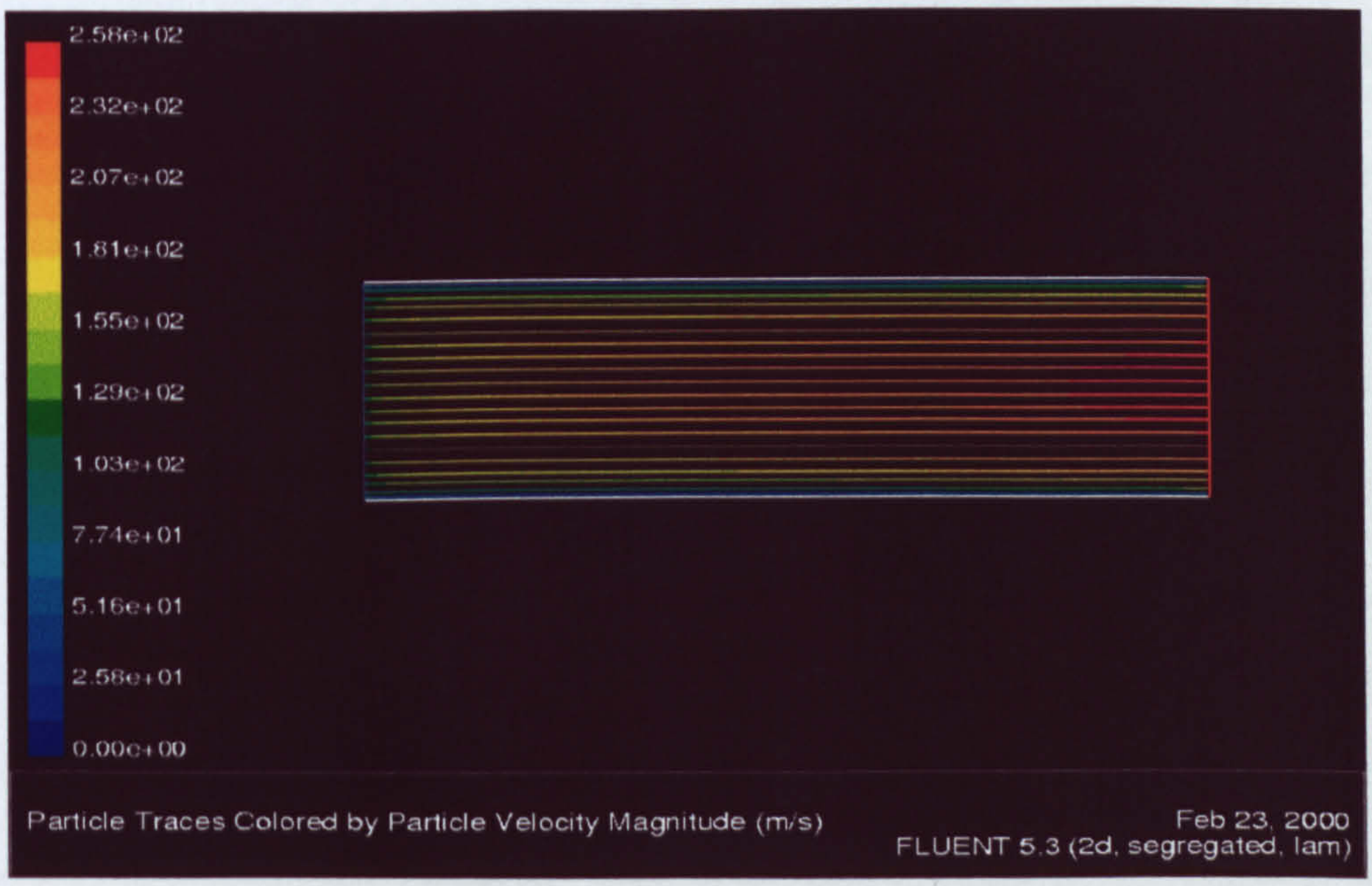


Figure 2-18. Particle velocity distribution.



2.1.3 CFD Results for 950°C Gas Temperature.

1. Inlet Velocity of 40 m/s (0.703kg/hr)

Figure 2-19. Static temperature distribution.

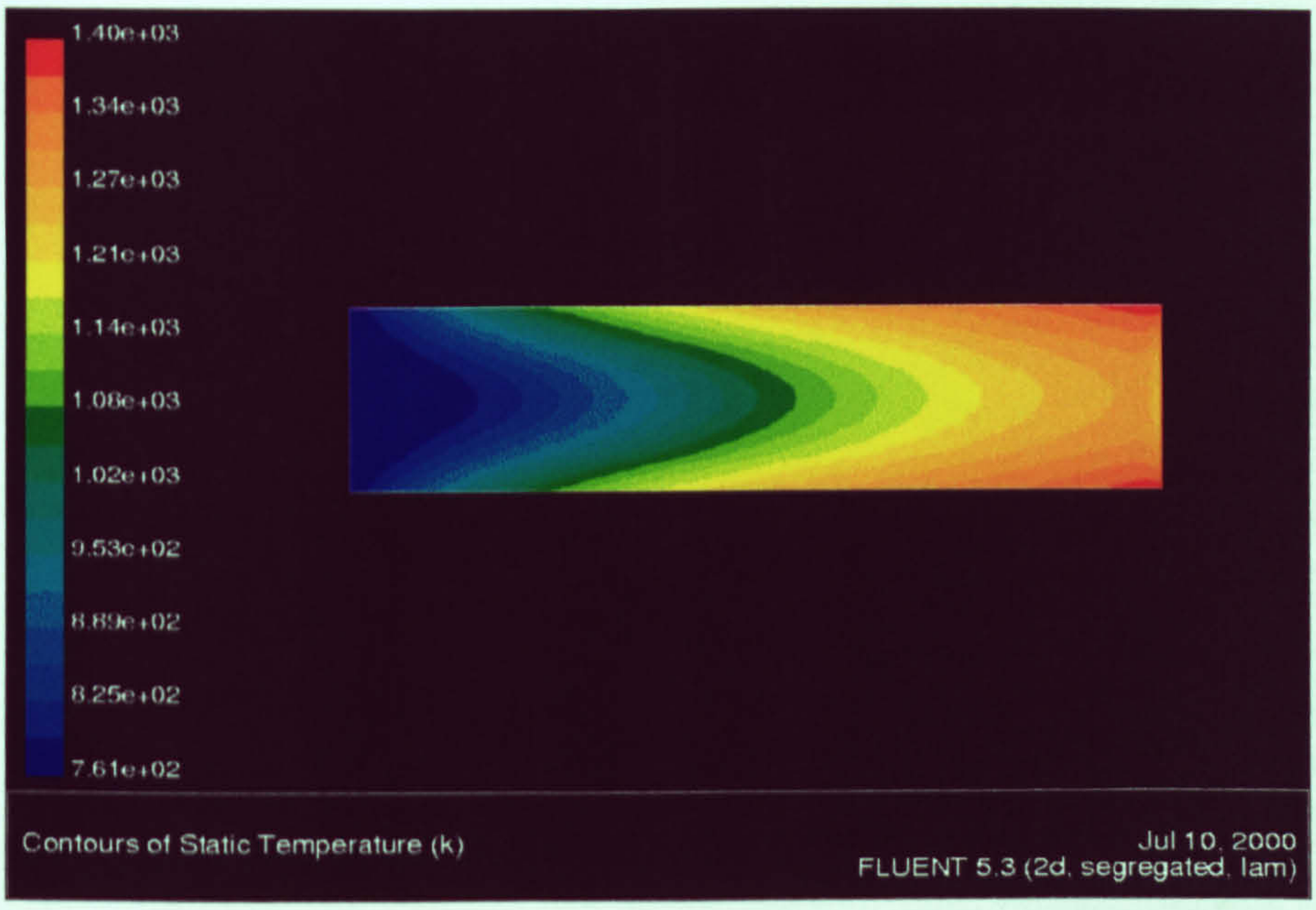


Figure 2-20. Particle temperature distribution.

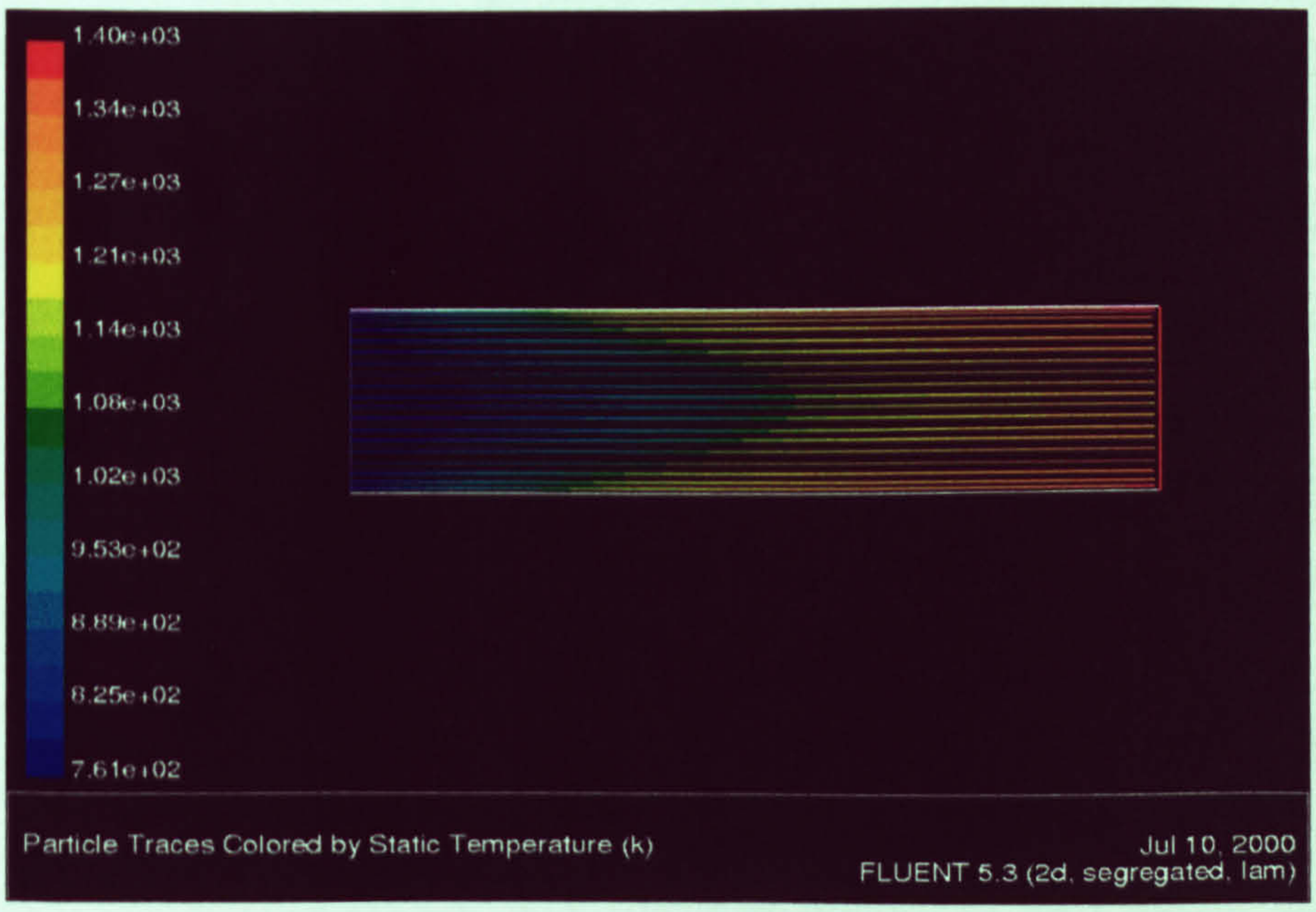


Figure 2-21. Flow velocity distribution

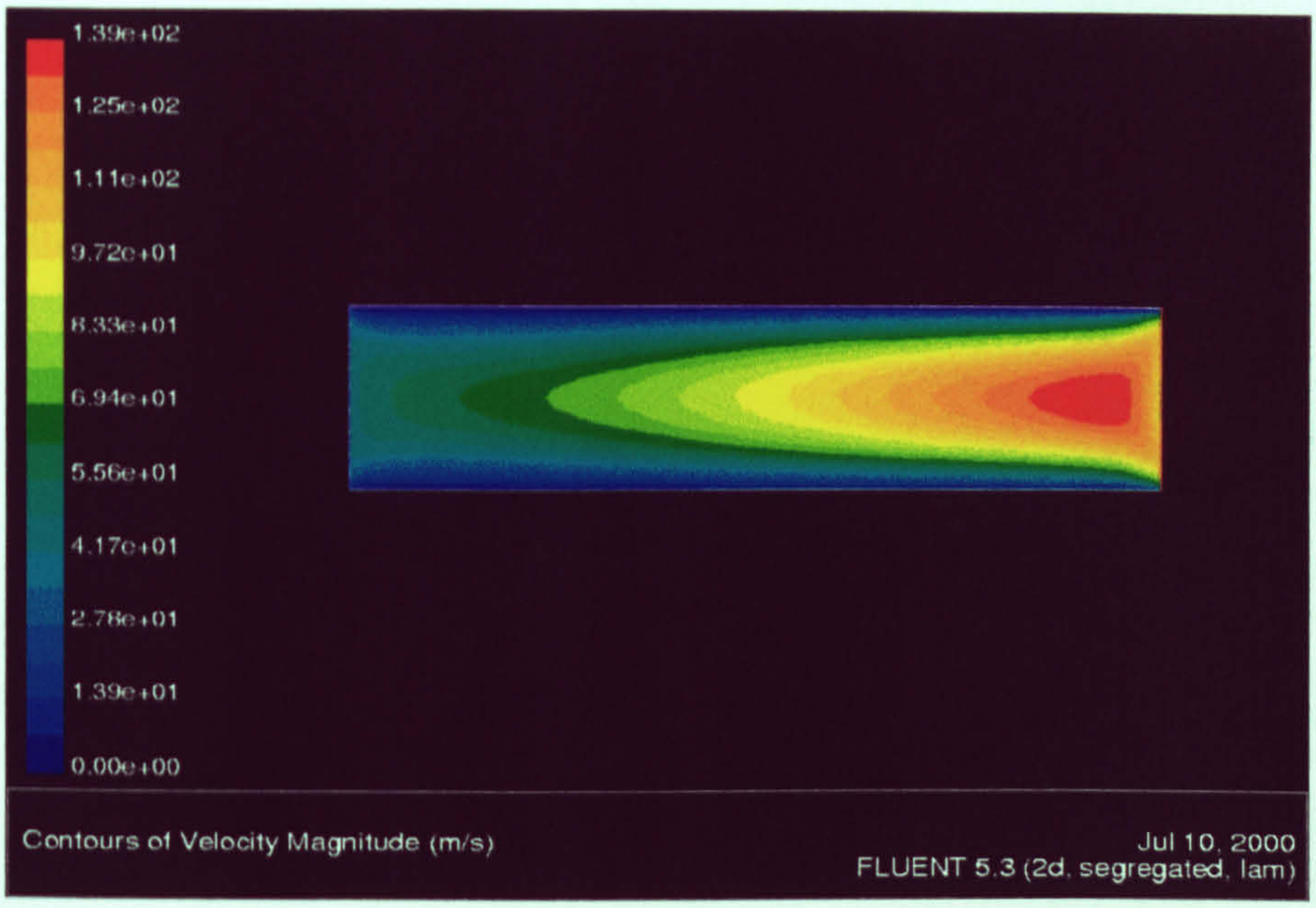
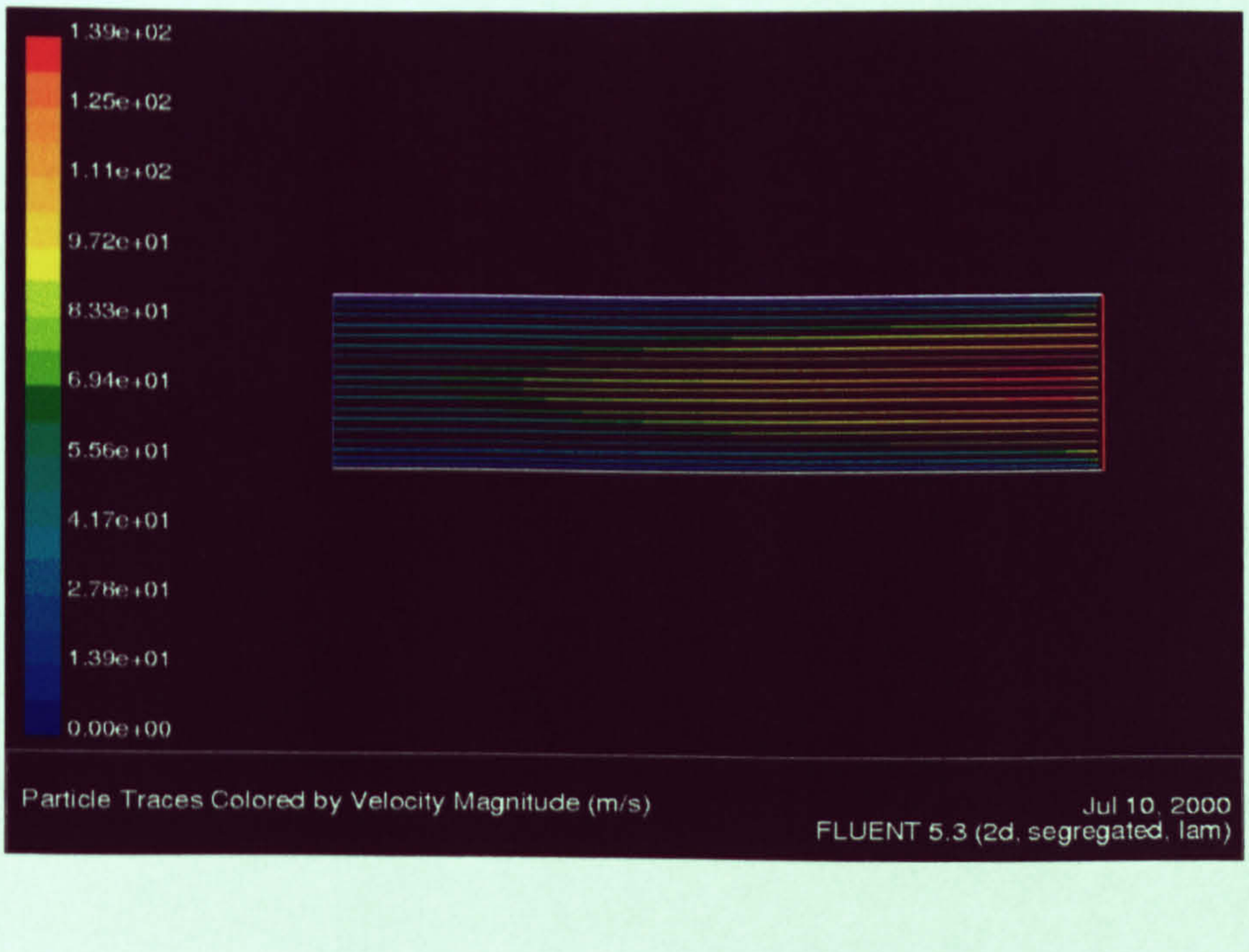


Figure 2-22. Particle velocity distribution.



2. Inlet Velocity of 140 m/s (2.46kg/hr)

Figure 2-23. Static temperature distribution.

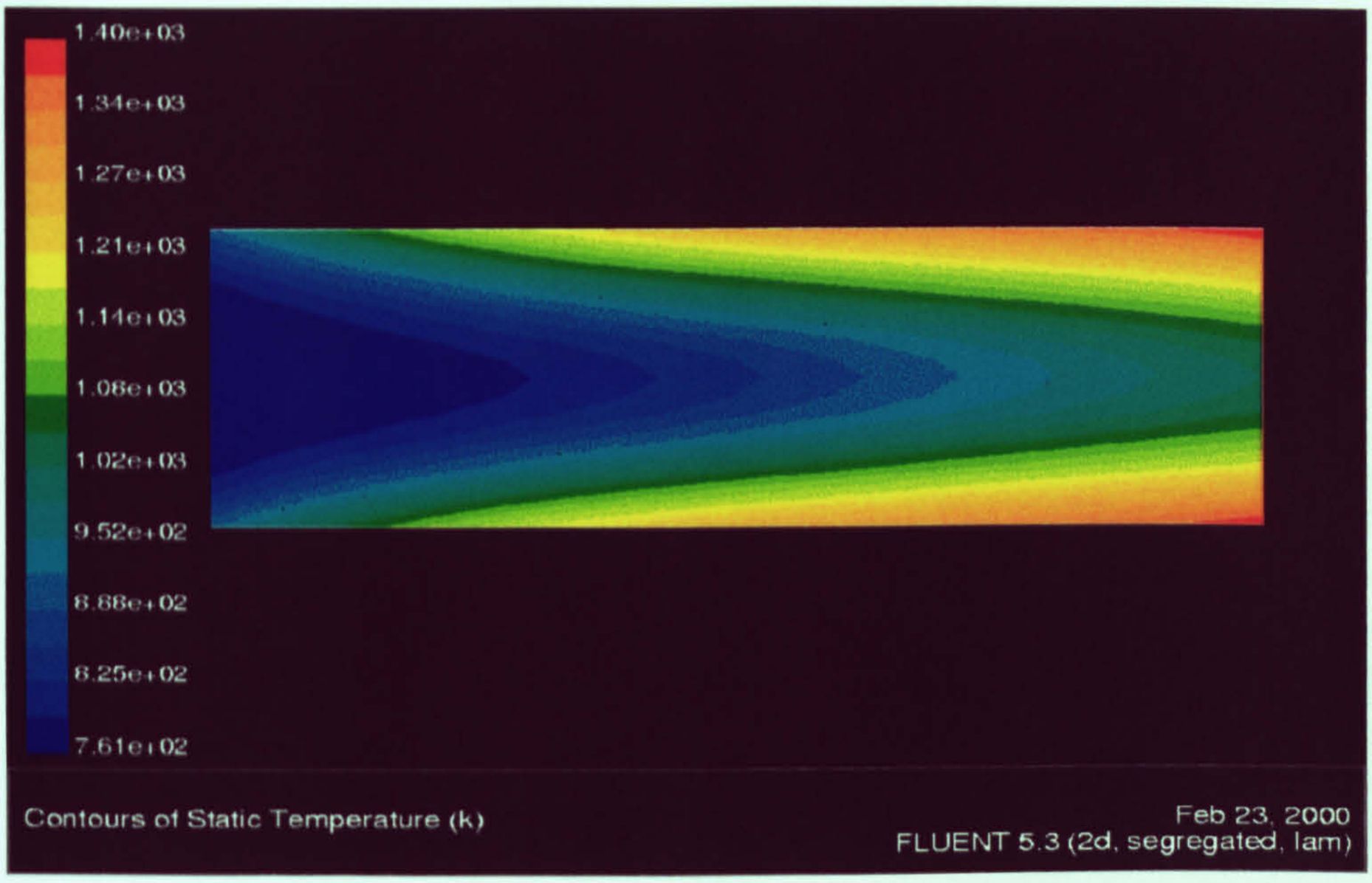


Figure 2-24. Particle temperature distribution.

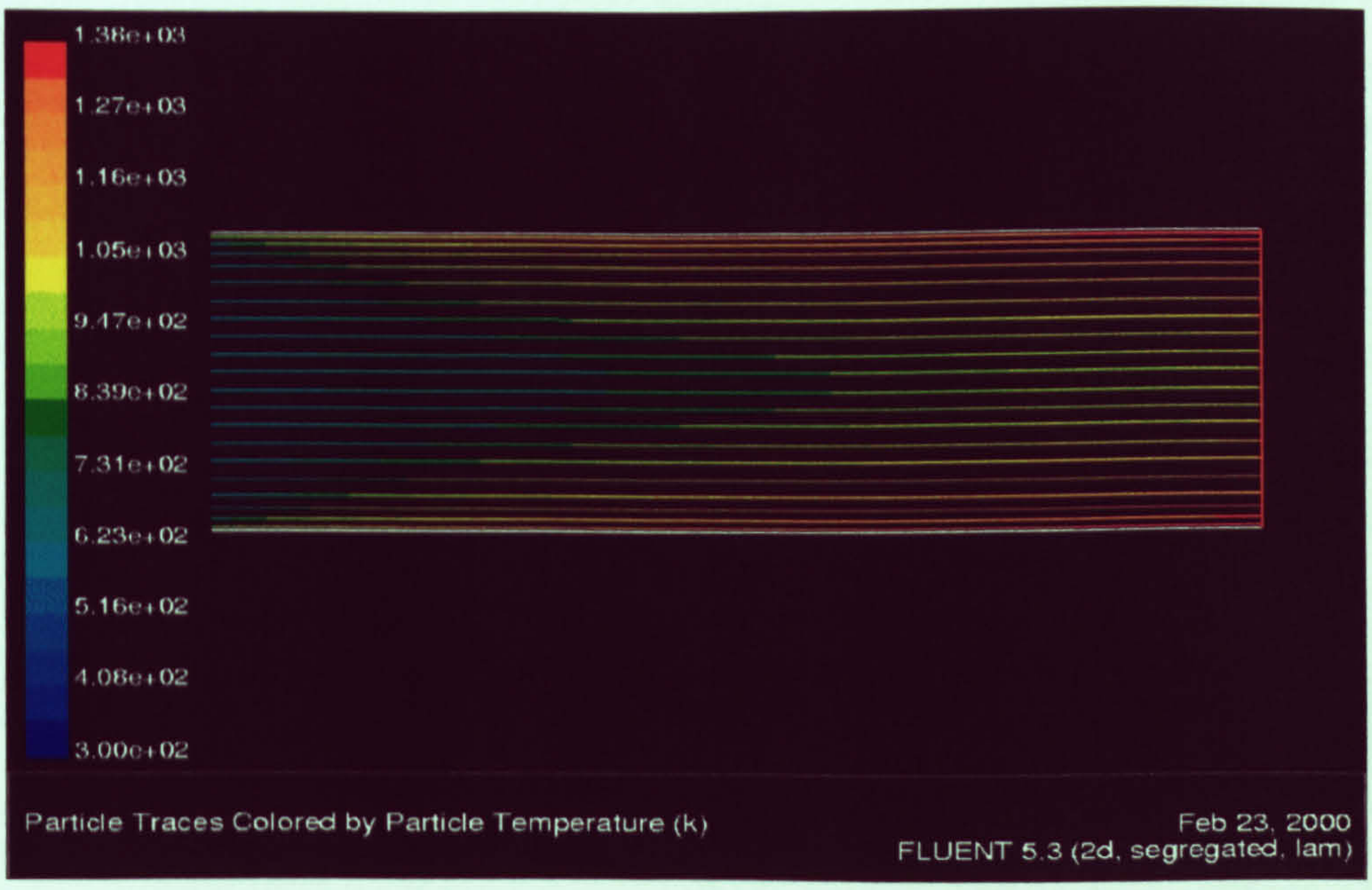


Figure 2-25. Velocity distribution.

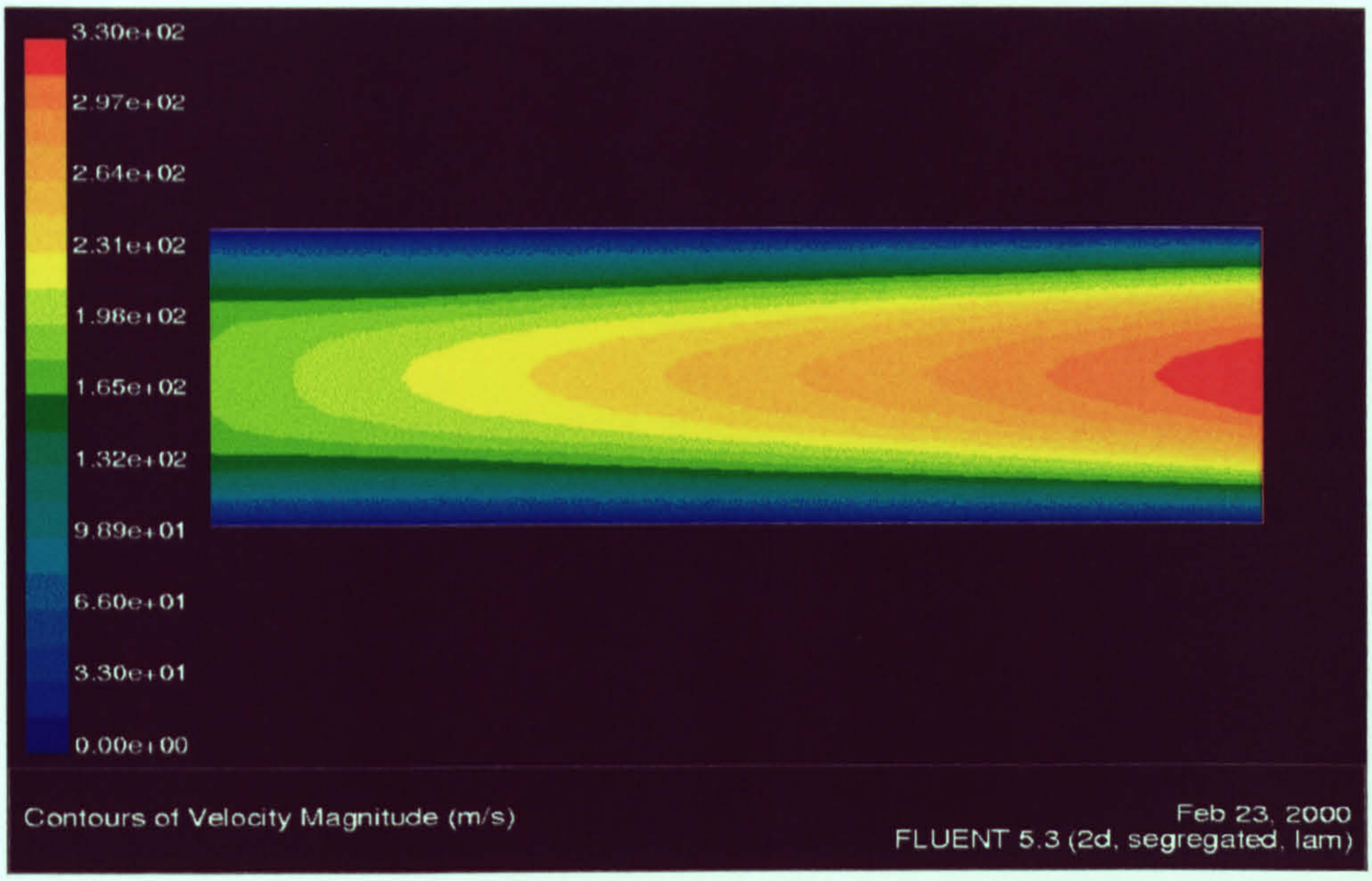
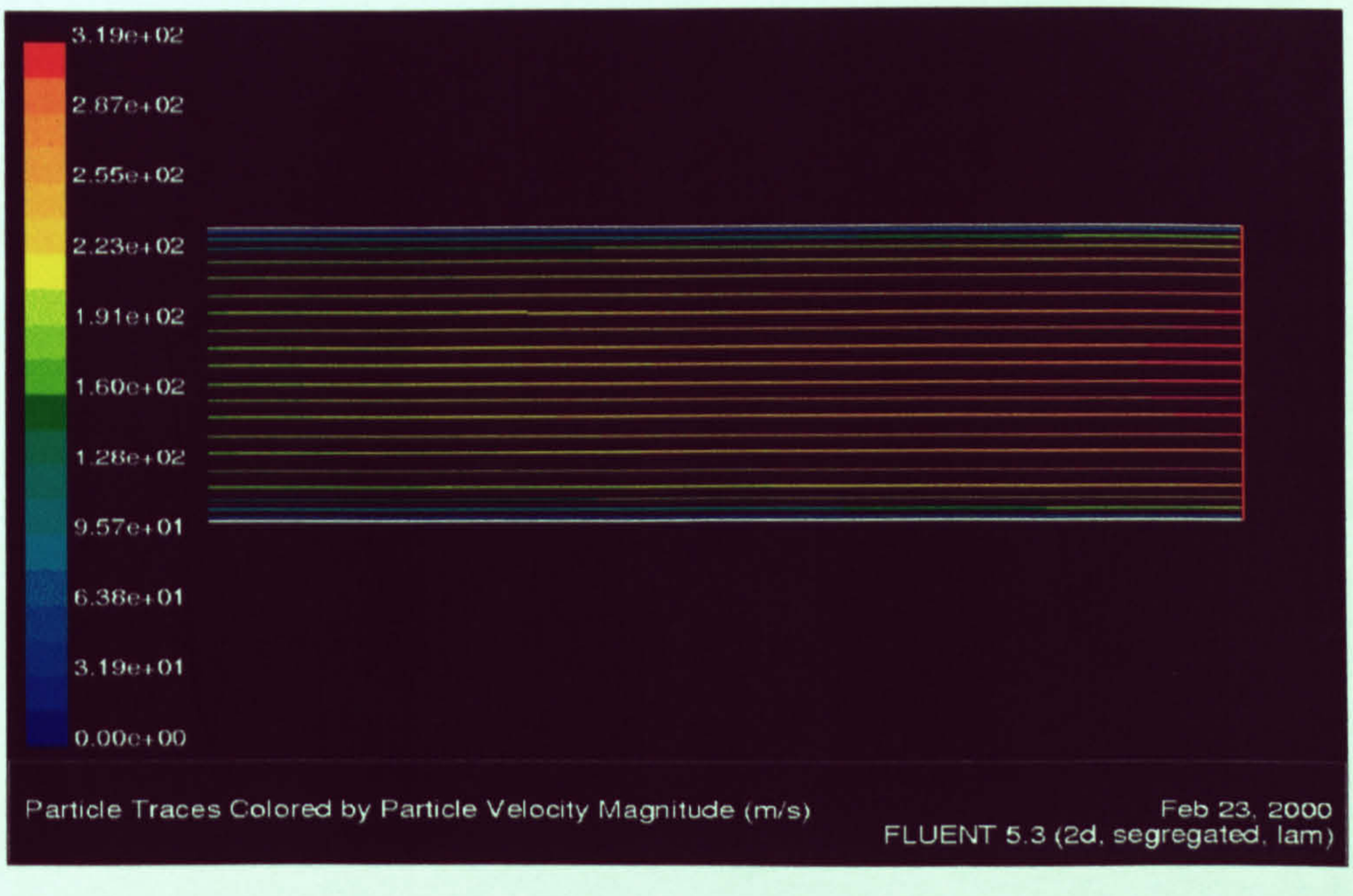


Figure 2-26. Particle velocity distribution



APPENDIX 3

3.1 Mechanical Properties of Stainless steel

Corrosion resistance is the most important criterion used to select stainless steel for a particular application. However, strength is also a significant factor in majority of elevated-temperature applications and may even be the key factor governing the choice of a stainless steel. The stainless steels used in applications in which high-temperature strength is important are sometimes referred to as *heat-resistant steel*. Many stainless steels used for elevated-temperature applications are designed for service at temperature up to 650°C. For service at elevated temperatures, the first property considered is the tensile strength during short-term exposure at elevated temperatures. Figure 3-1 represent the variation of tensile strength with sort-term temperature exposure for various type of stainless steel. The tensile strength tends to drop sharply as sort-term temperature exposure exceeds about 480°C. In addition, stainless steels hardness degrades as the short-term exposure temperature reaches about 550°C as in figure 3-2.

Figure 3-1. Typical short time tensile strength of various types of stainless steel.

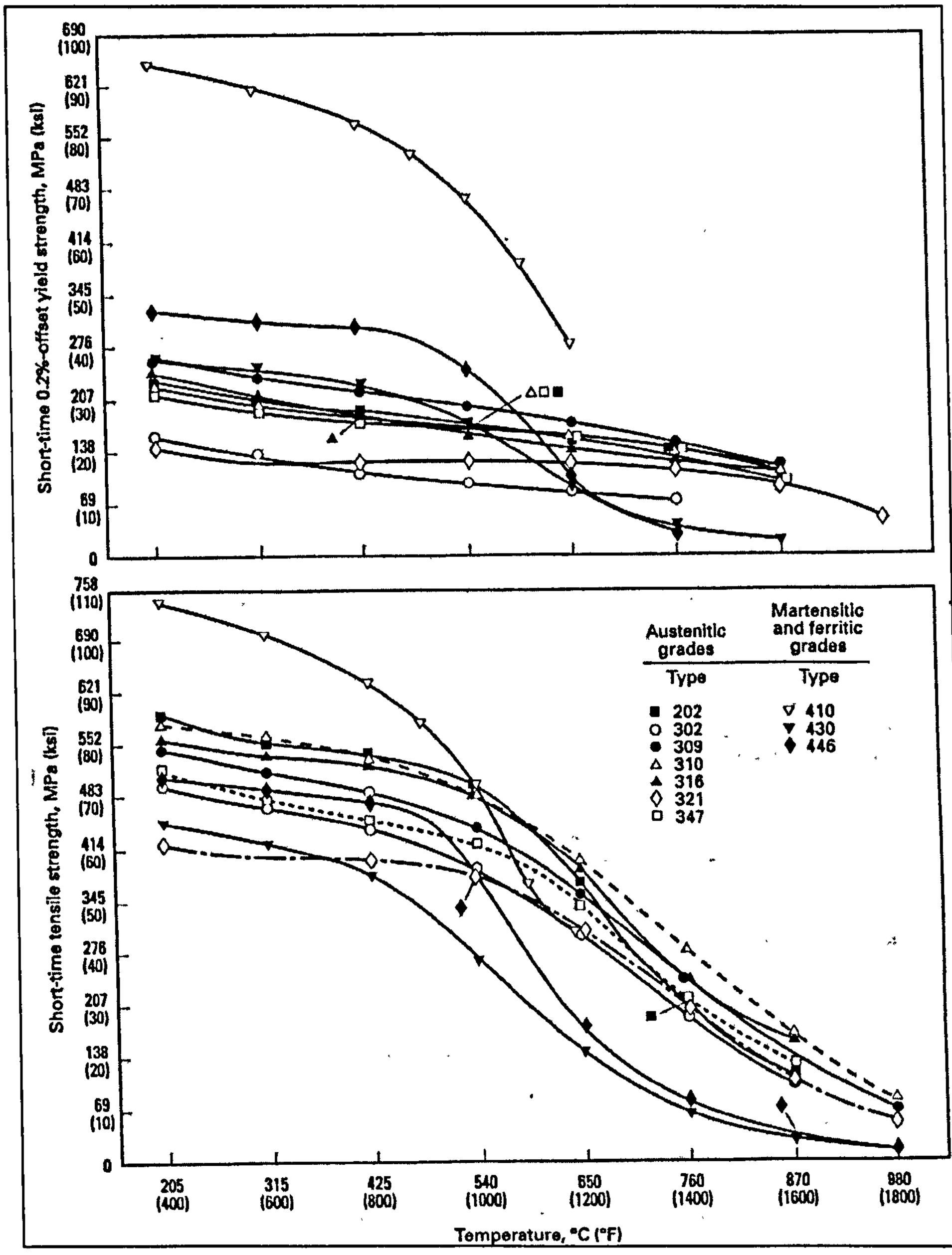


Figure 3-2. Variation of hardness of stainless steel with temperature.

